

# **Pilot Assisted and Semiblind Channel Estimation for Interleaved Frequency Division Multiple Access and the Generalization for Block-Interleaved Frequency Division Multiple Access**

Dem Fachbereich 18  
Elektrotechnik und Informationstechnik  
der Technischen Universität Darmstadt  
zur Erlangung der Würde eines  
Doktor-Ingenieurs (Dr.-Ing.)  
vorgelegte Dissertation

von  
Dipl.-Ing. Anja Sohl  
geboren am 28.11.1979 in Limburg a.d. Lahn

Referent:	Prof. Dr.-Ing. Anja Klein
Korreferent:	Prof. Dr.-Ing. Wolfgang Koch
Tag der Einreichung:	25. Mai 2010
Tag der mündlichen Prüfung:	...



---

# Kurzfassung

Interleaved Frequency Division Multiple Access (IFDMA) ist ein aussichtsreiches Vielfachzugriffsverfahren für die Aufwärtsstrecke zukünftiger Mobilfunksysteme. Im Vergleich zu anderen Vielfachzugriffsverfahren bietet es wesentliche Vorteile, die vor allem für die Aufwärtsübertragung von besonderer Bedeutung sind. Aufgrund einer Vorkodierung der zu übertragenden Datensymbole und der Verwendung von verteilten Subträgern, weist die Datenübertragung mit Hilfe von IFDMA eine hohe Frequenzdiversität auf und ist aus diesem Grund äußerst zuverlässig. Weiterhin ist das Verhältnis von Spitzen- zu Durchschnittsleistung (VSDL) des Sendesignals sehr niedrig, was die Verwendung von kosteneffizienten Leistungsverstärkern in den mobilen Endgeräten ermöglicht. Eine Verallgemeinerung des IFDMA-Verfahrens ist das sogenannte Block-Interleaved Frequency Division Multiple Access (B-IFDMA)-Verfahren. Hierbei werden die vorkodierten Datensymbole auf Blöcken von benachbarten Subträgern übertragen, die über die gesamte Bandbreite des Systems verteilt sind. B-IFDMA weist die gleichen Vorteile wie IFDMA auf und ist zudem weniger anfällig gegenüber einem Versatz der Trägerfrequenz am Empfänger. Eine wesentliche Bedingung für die zuverlässige und effiziente Datenübertragung mit IFDMA und B-IFDMA ist die Schätzung des Mobilfunkkanals mit hoher Güte und geringen Kosten. Die Kanalschätzung für IFDMA und B-IFDMA innerhalb der Aufwärtsstrecke eines Mobilfunksystems bringt neue Herausforderungen mit sich, da für IFDMA und B-IFDMA vorkodierte Datensymbole auf Subträgern übertragen werden, die über die gesamte Bandbreite des Systems verteilt sind. In dieser Arbeit werden neue Algorithmen für die Schätzung des Mobilfunkkanals bei IFDMA und B-IFDMA vorgestellt.

Zunächst wird der Kanal für das IFDMA-Verfahren geschätzt. Dafür werden Pilotsymbole in den zu übertragenden Datenstrom eingefügt und am Empfänger ausgewertet. Es werden zwei verschiedene Verfahren zum Einfügen von Pilotsymbolen und die jeweiligen Algorithmen zur Kanalschätzung vorgestellt. Beide Verfahren werden entwickelt, um das niedrige VSDL des Sendesignals beizubehalten und zuverlässige Schätzwerte des Kanals unter Verwendung von möglichst wenigen Pilotsymbolen zu liefern. Es zeigt sich, dass die pilotbasierte Kanalschätzung für IFDMA Schätzwerte mit hoher Güte liefert. Allerdings ist die Anzahl der benötigten Pilotsymbole groß, da die Übertragung auf verteilten Subträgern im Frequenzbereich die Anwendung von Interpolationsfiltern in den meisten Fällen unmöglich macht.

Um die Anzahl der Pilotsymbole dennoch zu reduzieren, wird die semiblinde Schätzung des Mobilfunkkanals für IFDMA eingeführt. Die empfangenen Datensymbole enthalten ebenso wie die Pilotsymbole Informationen über den Mobilfunkkanal. Diese zusätzliche

Information wird mit Hilfe der semiblinde Kanalschätzung genutzt, um auf diese Weise die Anzahl der verwendeten Pilotsymbole gegenüber der pilotbasierten Kanalschätzung zu reduzieren. In dieser Arbeit werden zwei verschiedene semiblinde Verfahren zur Schätzung der Veränderungen des Kanals im Frequenzbereich eingeführt. Beide Verfahren basieren auf der Nutzung der Zyklostationarität des empfangenen IFDMA Signals. Um zusätzlich die Veränderungen des Kanals im Zeitbereich zu schätzen, werden die beiden semiblinde Algorithmen mit einem sogenannten Decision-Directed Kanalschätzalgorithmus kombiniert. Dieser Algorithmus verwendet die empfangenen Datensymbole als virtuelle Pilotsymbole um der Veränderung des Kanals im Zeitbereich zu folgen. Die Auswertung der eingeführten semiblinde Kanalschätzalgorithmen bestätigt, dass die Anzahl der verwendeten Pilotsymbole im Vergleich zu pilotbasierten Kanalschätzalgorithmen reduziert werden kann. Weiterhin zeigt sich, dass die Güte der semiblinde Kanalschätzer für geringe Rauschleistungen vergleichbar mit der Güte der pilotbasierten Kanalschätzer ist.

Abschließend wird die Kanalschätzung für das B-IFDMA-Verfahren vorgestellt. Da B-IFDMA als Verallgemeinerung von IFDMA verstanden werden kann, werden die für IFDMA hergeleiteten pilotbasierten und semiblinde Kanalschätzverfahren auf ihre Anwendbarkeit bei B-IFDMA untersucht. Es zeigt sich, dass B-IFDMA aufgrund der blockweisen Übertragung im Frequenzbereich Vorteile bei der Anwendung von Interpolationsfiltern im Frequenzbereich bietet. Aufgrund dieser Eigenschaft können im Vergleich zu IFDMA neue Verfahren zur Einfügung von Pilotsymbolen und zur Kanalschätzung hergeleitet werden. Darüber hinaus bietet B-IFDMA ebenso wie IFDMA die Möglichkeit, die Anzahl der verwendeten Pilotsymbole mit Hilfe der semiblinde Kanalschätzung zu reduzieren.

---

# Abstract

For the uplink of future mobile radio systems, Interleaved Frequency Division Multiple Access (IFDMA) is a promising multiple access scheme as, in comparison to other multiple access schemes, IFDMA offers several advantageous properties that are of special interest for uplink transmission. For example, due to the precoding of the data symbols and the allocation of distributed subcarriers to a user under consideration, the IFDMA transmission is most reliable as it provides high frequency diversity. Further, the IFDMA transmit signal exhibits a low Peak-to-Average Power Ratio (PAPR) which enables the utilization of cost-efficient amplifiers in the mobile terminals. A generalization of the IFDMA scheme is the Block-Interleaved Frequency Division Multiple Access (B-IFDMA) scheme, where the precoded data symbols are transmitted on distributed blocks of neighboring subcarriers. The B-IFDMA scheme maintains the advantages of IFDMA and, at the same time, exhibits less sensitivity against carrier frequency offsets than IFDMA. One major demand in order to make use of the reliable data transmission provided by IFDMA and B-IFDMA is the estimation of the mobile radio channel with high accuracy and low pilot symbol overhead. Channel estimation for the uplink transmission with IFDMA and B-IFDMA entails new challenges as precoded data symbols are transmitted on distinct subcarriers that are distributed over the whole available bandwidth. This thesis introduces new channel estimation algorithms for IFDMA as well as B-IFDMA.

First, the channel is estimated for IFDMA with the help of pilot symbols that are inserted into the data stream and evaluated at the receiver. Two different pilot insertion methods and corresponding estimation algorithms are introduced under consideration of maintaining the low PAPR of the IFDMA transmit signal and providing reliable estimation performance while consuming a low pilot symbol overhead. It is revealed that pilot assisted channel estimation for IFDMA exhibits good estimation performance but suffers from a high pilot symbol overhead. The high pilot symbol overhead is due to the transmission on distributed subcarriers in frequency domain which prevents the application of interpolation filtering in most cases.

In order to avoid the high pilot symbol overhead for IFDMA channel estimation, in this thesis, also semiblind channel estimation is presented for IFDMA. The semiblind channel estimation exploits the information about the channel that is inherent to the received data signal. Thus, the application of semiblind channel estimation allows to reduce the pilot symbol overhead compared to pilot assisted channel estimation. For the semiblind estimation of frequency domain channel variations, two algorithms are introduced that take advantage of the cyclostationarity of the IFDMA signal. In order

to additionally estimate the channel variations in time domain, these two algorithms are combined with a so-called decision directed estimation approach which utilizes the received data symbols as virtual pilot symbols. The analysis of the proposed semiblind channel estimation algorithms confirms their benefit in terms of pilot symbol overhead reduction compared to the introduced pilot assisted channel estimation approaches. Furthermore, it is shown that the estimation performance of semiblind channel estimation is comparable to the estimation performance of pilot assisted channel estimation in case of a low noise power.

Finally, channel estimation for B-IFDMA is addressed. As B-IFDMA represents a generalization of IFDMA, the pilot assisted and semiblind channel estimation algorithms derived for IFDMA are investigated with respect to their applicability to B-IFDMA. It turns out that, due to the transmission on distributed blocks of subcarriers, B-IFDMA opens up the possibility of interpolation in frequency domain and, thus, supports the derivation of new pilot insertion methods and estimation algorithms compared to IFDMA. Further, it is revealed that semiblind channel estimation is also applicable to B-IFDMA and entails a beneficial reduction of the pilot symbol overhead.

# Contents

<b>1</b>	<b>Introduction</b>	<b>1</b>
1.1	IFDMA and Block-IFDMA . . . . .	1
1.2	Channel Estimation . . . . .	3
1.3	State of the Art . . . . .	5
1.4	Open Issues . . . . .	10
1.5	Contributions and Overview . . . . .	11
<b>2</b>	<b>IFDMA System Model</b>	<b>15</b>
2.1	Introduction . . . . .	15
2.2	IFDMA Transmitter . . . . .	16
2.2.1	Transmitter Model . . . . .	16
2.2.2	IFDMA Signal Generation in Frequency Domain . . . . .	18
2.2.3	IFDMA Signal Generation in Time Domain . . . . .	19
2.2.4	Important IFDMA Signal Properties . . . . .	21
2.2.4.1	Allocation of Subcarriers and Time Slots . . . . .	21
2.2.4.2	Peak-to-Average Power Ratio . . . . .	22
2.3	Mobile Radio Channel . . . . .	23
2.3.1	Time-Variant Multipath Propagation . . . . .	23
2.3.2	Stochastic Channel Description . . . . .	25
2.3.3	Discrete-Time Channel Model . . . . .	27
2.4	IFDMA Receiver . . . . .	28
2.4.1	Receiver Model . . . . .	28
2.4.2	IFDMA Signal Demodulation in Frequency Domain . . . . .	29
<b>3</b>	<b>Pilot Assisted Channel Estimation for IFDMA</b>	<b>35</b>
3.1	Introduction . . . . .	35
3.2	Estimation of Frequency Domain Channel Variations . . . . .	36
3.2.1	Introduction . . . . .	36
3.2.2	Symbolwise Pilot Insertion . . . . .	37
3.2.2.1	Signal Generation . . . . .	37
3.2.2.2	Estimation Algorithm . . . . .	39
3.2.3	Subcarrierwise Pilot Insertion . . . . .	40
3.2.3.1	Signal Generation . . . . .	40
3.2.3.2	Estimation Algorithm . . . . .	43
3.3	Estimation of Time Domain Channel Variations . . . . .	48
3.3.1	Introduction . . . . .	48
3.3.2	Pilot Grid . . . . .	49

3.3.3	Estimation Algorithm . . . . .	49
3.4	Performance and Complexity Analysis . . . . .	53
3.4.1	Analysis Assumptions . . . . .	53
3.4.2	Peak-to-Average Power Ratio . . . . .	54
3.4.3	Pilot Symbol Overhead . . . . .	58
3.4.4	Mean Square Error . . . . .	63
3.4.5	Complexity . . . . .	70
3.5	Conclusions . . . . .	72
<b>4</b>	<b>Semiblind Channel Estimation for IFDMA</b>	<b>75</b>
4.1	Introduction . . . . .	75
4.2	Reduced Number of Pilot Symbols in Frequency Domain . . . . .	76
4.2.1	Introduction . . . . .	76
4.2.2	Correlation Based Semiblind Channel Estimation . . . . .	77
4.2.2.1	Estimation for Channels with Small Delay Spread . . .	77
4.2.2.2	Estimation for Channels with Large Delay Spread . . .	84
4.2.2.3	Multi-User Influence . . . . .	89
4.2.3	Subspace Based Semiblind Channel Estimation . . . . .	92
4.2.3.1	Estimation for Channels with Small Delay Spread . . .	92
4.2.3.2	Estimation for Channels with Large Delay Spread . . .	98
4.2.3.3	Multi-User Influence . . . . .	104
4.3	Reduced Number of Pilot Symbols in Time Domain . . . . .	107
4.3.1	Introduction . . . . .	107
4.3.2	Decision Directed Channel Estimation . . . . .	107
4.4	Performance and Complexity Analysis . . . . .	111
4.4.1	Analysis Assumptions . . . . .	111
4.4.2	Pilot Symbol Overhead . . . . .	111
4.4.3	Mean Square Error . . . . .	114
4.4.4	Complexity . . . . .	131
4.5	Conclusions . . . . .	132
<b>5</b>	<b>Channel Estimation for Block-IFDMA</b>	<b>135</b>
5.1	Introduction . . . . .	135
5.2	System Model . . . . .	135
5.3	Pilot Assisted Channel Estimation for Block-IFDMA . . . . .	138
5.3.1	Introduction . . . . .	138
5.3.2	Subcarrierwise Pilot Insertion . . . . .	139
5.3.2.1	Signal Generation . . . . .	139
5.3.2.2	Estimation Algorithm . . . . .	141
5.3.3	Chipwise Pilot Insertion . . . . .	143



5.3.3.1	Signal Generation . . . . .	143
5.3.3.2	Estimation Algorithm . . . . .	144
5.3.4	Performance and Complexity Analysis . . . . .	145
5.3.4.1	Analysis Assumptions . . . . .	145
5.3.4.2	Peak-to-Average Power Ratio . . . . .	145
5.3.4.3	Pilot Symbol Overhead . . . . .	148
5.3.4.4	Mean Square Error . . . . .	152
5.3.4.5	Complexity . . . . .	157
5.4	Semiblink Channel Estimation for Block-IFDMA . . . . .	158
5.4.1	Introduction . . . . .	158
5.4.2	Subspace Based Semiblink Channel Estimation . . . . .	159
5.4.3	Performance Analysis . . . . .	161
5.4.3.1	Analysis Assumptions . . . . .	161
5.4.3.2	Mean Square Error . . . . .	162
5.5	Conclusions . . . . .	165
<b>6</b>	<b>Conclusions</b>	<b>169</b>
	<b>Appendix</b>	<b>173</b>
A.1	Derivation of Eq. (4.27) in Section 4.2.2.2 . . . . .	173
A.2	Derivation of the matrices $\mathcal{G}_0^{(u)}, \dots, \mathcal{G}_{Q-1}^{(u)}$ in Eq. (4.49) . . . . .	178
A.3	Derivation of Eq. (4.61) in Section 4.2.3.2 . . . . .	179
A.4	Derivation of the matrices $\hat{\mathcal{G}}_0^{(u)}, \dots, \hat{\mathcal{G}}_{Q-1}^{(u)}$ in Eq. (4.69) . . . . .	181
A.5	Derivation of Eq. (5.20) in Section 5.3.3 . . . . .	183
	<b>List of Acronyms</b>	<b>185</b>
	<b>List of Symbols</b>	<b>187</b>
	<b>Bibliography</b>	<b>193</b>
	<b>Lebenslauf</b>	<b>201</b>



# Chapter 1

## Introduction

### 1.1 IFDMA and Block-IFDMA

At present, research activities for the development of beyond third generation (B3G) or fourth generation (4G) mobile radio systems are in progress worldwide. In a mobile radio system, it is distinguished between uplink and downlink transmission. The uplink represents the transmission from a mobile terminal to a base station within a mobile radio cell, whereas the downlink represents the transmission from a base station to the mobile terminal of a certain user. For the uplink of the future mobile radio systems, several multiple access schemes are under discussion as candidate transmission schemes. One candidate is the well-known Orthogonal Frequency Division Multiple Access (OFDMA) scheme, where the total available bandwidth is divided into mutually orthogonal subcarriers [vNP00, SL05, HP03]. For each user in the system, the data symbols are transmitted on a fraction of the total available bandwidth. More precisely, this means that a certain number of subcarriers in frequency domain is allocated to a specific user and one data symbol is transmitted on a single subcarrier. The corresponding time unit for the transmission of data symbols on this user specific set of subcarriers is denoted as OFDMA symbol in the following. The distance between neighboring subcarriers is small in comparison to the total bandwidth and the frequency variations of the mobile radio channel are insignificant for each subcarrier [vNP00]. However, OFDMA suffers from high fluctuations of the signal envelope which is unfavorable especially for uplink transmission as cost-intensive highly linear power amplifiers are required for the mobile terminals [vNP00]. Other promising multiple access schemes result from the application of a Discrete Fourier Transform (DFT) precoding to OFDMA. The application of DFT precoding leads to multiple access schemes that combine most of the advantages of OFDMA with a low Peak-to-Average Power Ratio (PAPR) of the transmit signal [FCS04, GRC<sup>+</sup>02, XZG03, MG08]. Furthermore, due to the DFT precoding, the information about each data symbol is spread over all allocated subcarriers, in contrast to OFDMA where each data symbol is transmitted on one specific subcarrier. In the remainder of this thesis, the focus is on DFT precoded OFDMA schemes.

For DFT precoded OFDMA, there exist different possibilities of how to allocate subcarriers to a specific user. An allocation of blocks of neighboring subcarriers to a user

leads to a multiple access scheme that has been denoted as Localized Frequency Division Multiple Access (LFDMA) or Single Carrier Frequency Division Multiple Access (SC-FDMA) [3GP06, MG08]. Throughout this thesis, the DFT precoded OFDMA with blockwise allocation of subcarriers is denoted as LFDMA. Due to the blockwise structure, on the one hand, LFDMA provides good robustness to carrier frequency offsets as well as high multi user diversity gains in case of adaptive resource allocation [LMG06]. On the other hand, LFDMA shows low frequency diversity because the subcarriers allocated to a specific user are restricted to a localized fraction of the available bandwidth [SFK06].

A promising alternative to the blockwise subcarrier allocation is the allocation of subcarriers that are equidistantly distributed over the total available bandwidth to a user under consideration. Here, the subcarriers allocated to different users are combwise interleaved to each other. This interleaved subcarrier structure leads to the Interleaved Frequency Division Multiple Access (IFDMA) scheme which has been introduced in [SDBS98] and has attracted great interest during the last years within the research project named Wireless World Initiative New Radio (WINNER) of the European Union (EU) [WINdf]. The IFDMA transmission scheme provides high frequency diversity as the data symbols are spread over subcarriers that are distributed over the total available bandwidth and, therefore, is well suitable for non-adaptive uplink transmission [FKCS05a]. As IFDMA can be explained as DFT precoded OFDMA with equidistantly distributed subcarrier allocation, the signal generation can be described by the allocation of the DFT precoded data symbols to the user specific set of subcarriers. In analogy to OFDMA, the corresponding time unit for the transmission of the DFT precoded data symbols on the set of subcarriers is denoted as IFDMA symbol in the following. An alternative explanation of signal generation for IFDMA can be given in time domain. In time domain, the IFDMA signal can be described as a compression, repetition and subsequent user dependent phase rotation of blocks of modulated data symbols [SDBS98]. This specific signal generation is very efficient in terms of implementation issues and demonstrates the low PAPR of the IFDMA transmit signal enabling the application of low cost amplifiers [FKH08]. Nevertheless, due to the equidistant distribution of subcarriers, IFDMA is sensitive against carrier frequency offsets [FKCS04].

A generalization of the equidistantly distributed subcarrier allocation has been presented in [WINdf]. Here, blocks of subcarriers that are equidistantly distributed over the available bandwidth are allocated to each user. In contrast to IFDMA, where a block is built by a single subcarrier, for the subcarrier allocation presented in [WINdf], each block consists of a certain number larger than one of neighboring subcarriers. This

subcarrier allocation in connection with a DFT precoding leads to the so-called Block-Interleaved Frequency Division Multiple Access (B-IFDMA) scheme. B-IFDMA can be seen as a generalization of IFDMA which maintains the advantage of high frequency diversity as the blocks of subcarriers are distributed over the bandwidth and, at the same time, provides more robustness to carrier frequency offsets than IFDMA [SFE<sup>+</sup>09].

## 1.2 Channel Estimation

In this section, the principle of channel estimation in a mobile communication system is explained in general and is further related to the application to IFDMA and B-IFDMA. In a mobile communication system, a signal is transmitted over the mobile radio channel to the receiver. The signal that is transmitted by a user suffers from reflection, diffraction and scattering caused by obstacles in the propagation environment. Due to reflection, diffraction and scattering, the signal reaches the receiver over different propagation paths. This physical effect is called multipath propagation and produces constructive and destructive superpositions of attenuated, delayed and phase-shifted versions of the originally transmitted signal at the receiver. The time spread of an impulse due to multipath propagation is denoted as the delay spread of the mobile radio channel. In frequency domain, the effect of multipath propagation can be described by a frequency selective channel transfer function. This frequency selectivity is dependent on the number of received delayed versions of the transmitted signal. The higher the number of delayed paths at the receiver, i.e. the larger the delay spread, the higher the frequency selectivity of the channel. Additionally, the propagation conditions for the transmission of a signal are changing with time as the transmitter or the receiver are moving. Thus, the mobile radio channel is frequency selective as well as varying with time. Two important measures for the description of the rate of channel variations in frequency and time domain are the coherence bandwidth and the coherence time. These measures give the range in frequency and time domain where the channel characteristics are assumed to be approximately constant.

In order to identify the originally transmitted data symbols at the receiver, the influence the signal has suffered during the transmission needs to be reversed. Reversing the channel influence entails that knowledge about the mobile radio channel is required at the receiver. As this knowledge about the channel is not inherent in the receiver, an estimate for the frequency selective channel characteristic is desired. Due to the time variability of the channel characteristics, the estimation procedure needs to be repeated at least once per coherence time in order to avoid outdated channel estimates. The procedure of evaluating the frequency selective and time variant channel is called

channel estimation. The estimate of the channel is then utilized to reverse the channel influence on the received signal which is commonly denoted as equalization. After equalization, an estimate of the data symbols can be obtained. In case of downlink transmission, the mobile terminal of a certain user receives a superposed version of the signals transmitted by the base station to all users in the system. In this case, all user signals experience identical channel conditions and the receiving mobile terminal can exploit the signals of all users to estimate the channel. In case of uplink transmission, the base station receives the signals of different users where each signal is affected by different channel conditions. Therefore, for channel estimation, only the signal of a certain user can be exploited to estimate the corresponding user-specific channel. In the following, this case of uplink channel estimation is considered.

A prominent technique for channel estimation is denoted as pilot assisted channel estimation. In Figure 1.1, the principle of pilot assisted channel estimation and its relation to data estimation are illustrated in a block diagram. Pilot assisted channel estimation is based on the transmission of symbols that are known at the receiver, so-called pilot symbols. The pilot symbols are inserted into the data stream and transmitted over the mobile radio channel. At the receiver, the pilot symbols are analyzed in order to obtain a channel estimate which is utilized for equalization. Finally, the data symbols are estimated at the receiver. As already mentioned, the characteristic of a mobile radio channel is varying with time and frequency. In order to obtain estimates which provide information about the time and frequency domain channel variations, the pilot symbols need to be transmitted periodically in time domain and spread over the whole bandwidth which is provided for data transmission. For an OFDMA based transmission scheme, this means that pilot symbols are transmitted within distinct distributed OFDMA symbols in time domain and on distinct subcarriers in frequency domain [vNP00,SL05]. The channel characteristics for the remaining OFDMA symbols and subcarriers can be obtained via the application of interpolation techniques in frequency and time domain [vNP00,SL05]. The application of interpolation in frequency and time domain implies that the distance between neighboring pilot symbols fulfills the sampling theorem in frequency and time domain. This means that the distance between neighboring pilot symbols has to be chosen according to the coherence bandwidth and coherence time in order to be able to follow the channel variations in both domains with the help of interpolation. However, the transmission of pilot symbols reduces the effective data rate of each user as the subcarrier used for pilot transmission in a certain OFDMA symbol cannot be utilized for data transmission. Thus, the number of pilot symbols required for channel estimation shall be kept as low as possible. The application of pilot assisted channel estimation to IFDMA entails the insertion of pilot symbols into the IFDMA transmit signal. Nevertheless, the beneficially low

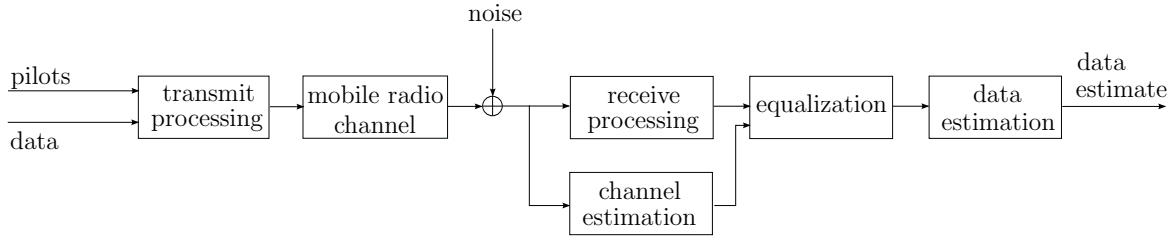


Figure 1.1. Block diagram of the pilot assisted channel estimation principle

PAPR of the IFDMA transmit signal without pilot symbols shall be maintained after pilot insertion. Furthermore, it has to be considered that for IFDMA, the data symbols are transmitted on a certain number of subcarriers which are equidistantly distributed over the available bandwidth. In general, interpolation in frequency domain between the distributed subcarriers allocated to a specific user is not feasible due to the large distance between adjacent subcarriers. Therefore, it appears that each of the subcarriers allocated to a user within certain IFDMA symbols has to be utilized for pilot transmission and is not available for the transmission of data symbols. The missing possibility of interpolation in frequency domain leads to an increased pilot symbol overhead concerning channel estimation for IFDMA in comparison to channel estimation for multiple access schemes allocating neighboring subcarriers to the users. An alternative approach to pilot assisted channel estimation is the so-called semiblind channel estimation. Here, the information about the channel which is inherent to the received data symbols is exploited and is combined with the information about the channel gained by the transmission of pilot symbols. As additional knowledge about the channel is gained from the received data symbols, the number of pilot symbols required can be reduced in comparison to pilot assisted channel estimation.

For B-IFDMA, equidistantly distributed blocks of subcarriers are allocated to a certain user. B-IFDMA enables the application of pilot assisted channel estimation with interpolation in frequency domain as, in contrast to IFDMA, interpolation can be applied within each block of neighboring subcarriers in frequency domain.

## 1.3 State of the Art

This section presents a review of the state of the art in terms of channel estimation algorithms particularly with regard to the application to IFDMA and B-IFDMA.

The pilot assisted channel estimation is a widely-used means for channel estimation in mobile communication systems utilizing OFDMA as transmission scheme and has

been considered frequently in literature. In case of pilot assisted channel estimation for the uplink of a mobile communication system, the techniques introduced for Orthogonal Frequency Division Multiplexing (OFDM), where all available subcarriers in the system are allocated to a single user, are directly applicable to OFDMA which represents the multiple access variant of OFDM. In the following, the most important literatures dealing with pilot assisted channel estimation techniques for OFDM and, thus, OFDMA which are of importance in terms of pilot assisted channel estimation for IFDMA and B-IFDMA are stated. In [vNP00, SE96, vdBES<sup>+</sup>95, HKR97b], pilot assisted channel estimation is presented for OFDM. The pilot symbols are inserted regularly on distinct subcarriers in frequency domain and within distinct OFDM symbols in time domain. Based on the pilot symbols, the channel is estimated by a two-dimensional interpolation. This two-dimensional interpolation means that a filter is applied jointly in frequency and time domain in order to estimate the channel variations in both domains. In [HKR97b], a Wiener filter is applied for the two-dimensional interpolation procedure. Based on this, [HKR97a] presents a less complex variant of interpolation in frequency and time domain for OFDM channel estimation. This two times one-dimensional Wiener filtering procedure in [HKR97a] approves that the separation of the filtering in frequency and time domain is an efficient compromise in terms of complexity and performance. The application of pilot assisted channel estimation with two times one-dimensional Wiener filtering to OFDM has been further considered in [San03, SL05]. In [TM97], the two times one-dimensional filtering is compared for different patterns of pilot allocation in frequency and time domain.

Pilot assisted channel estimation has also been considered for the application in a system using LFDMA as multiple access scheme where advantage can be taken of the allocation of neighboring subcarriers to the users. In [LFDLD06], pilot symbols are inserted at distinct points in time using IFDMA modulated pilot sequences. By doing so, the pilot symbols are inserted in frequency domain with equidistant spacing. The channel can be estimated by interpolation among the channel estimates at the pilot frequencies. In [LIC], the channel is estimated over the whole bandwidth for each user in the system. This means, pilot symbols are multiplexed over the whole bandwidth and not only within the block of subcarriers that are allocated to a certain user. In order to maintain the orthogonality in-between the pilot sequences of different users, a code division multiplexing approach is applied. [DLF08] presents a more bandwidth efficient pilot insertion technique. Here, the pilot symbols are superimposed to data symbols. By doing so, the resources used for pilot transmission are also accessible for data transmission. However, the pilot and data symbols produce mutual interferences which are reduced by an iterative receiver with joint equalization and channel estimation.

For IFDMA, new aspects arise for the insertion of pilot symbols and the channel



estimation process due to the particular structure of the IFDMA transmit signal in time domain. The insertion of pilot symbols shall meet the requirement of maintaining the low PAPR of the IFDMA transmit signal. The consideration of a low PAPR of the transmit signal while multiplexing pilot symbols in frequency domain to an OFDM signal has been addressed in [GEPB06]. In [LFDL07b], this approach has been considered for the application to the general case of single-carrier transmission. In both works, the PAPR of the transmit signal with pilot symbols is reduced by the application of a selection algorithm which searches for a pilot sequence producing a low PAPR of the transmit signal. For IFDMA, pilot assisted channel estimation has been considered in [DMO09], where a regular pilot allocation in frequency and time domain has been proposed for DFT precoded OFDMA schemes, e.g. for IFDMA and B-IFDMA. For B-IFDMA, one pilot symbol is placed within each block of neighboring subcarriers in frequency domain. This pilot symbol per block is located near the center of each block. The channel is estimated by the application of two times one-dimensional Wiener interpolation filtering. For IFDMA, a set of distributed subcarriers in frequency domain is allocated to each user and, thus, the application of interpolation is not always feasible. Nevertheless, the channel estimation algorithm shall consume a low pilot symbol overhead and the pilot insertion shall have marginal influence on the PAPR of the transmit signal.

In order to reduce the pilot symbol overhead in frequency domain, the estimation of frequency domain channel variations with the help of semiblink channel estimation is an appropriate approach. In general, semiblink channel estimation is a combination of pilot assisted channel estimation and a blind channel estimation technique. A prominent class of blind channel estimation algorithms is based on second order statistics and exploits the redundancy existent in the received signal. In [TXK94, SG98, CSLG00, TG97, MDCM95, GN07], second order statistics based blind channel estimation has been presented for general single-carrier systems where the redundancy in the received signal is introduced according to different strategies. These strategies can be roughly divided into two groups, where the first group of strategies introduces redundancy via signal processing at the receiver and the second group via signal processing at the transmitter. In [TXK94], a cyclostationary signal with inherent redundancy is obtained by an oversampling at the receiver. In [MDCM95], the redundancy is again introduced at the receiver by either an oversampling of the signal at a single receiver or considering the same signal at multiple receivers. The introduction of redundancy at the transmitter is proposed in [TG97, GN07]. Here, a specific precoding is applied to the transmit signal. Another approach for transmitter induced redundancy is presented in [SG98, CSLG00], where a new modulation scheme introduces a cyclostationarity into the transmit signal. The principle of second order statistics based blind

channel estimation has been further extended to the application in an OFDM system in [HG99, MdCD02, LP05]. For the application of second order statistics based blind channel estimation to OFDM, it has been proposed, e.g. in [HG99, MdCD02], to exploit the redundancy which is inherent due to the transmission of a cyclic prefix. In [LP05], additional linear precoding is applied to the OFDM signal at the transmitter in order to estimate the channel based on second order statistics. The second order statistics based semiblind channel estimation, i.e., the combination of pilot assisted and second order statistics based blind channel estimation, has been presented in [MdCD02, MdCDB99, MdC99, SV07a] for the application to OFDM. Most of the aforementioned works on second order statistics assume that the channel is approximately time invariant. Therefore, by applying these algorithms, only the channel variations in frequency domain can be estimated for the case that the channel variations in time domain are small. For second order statistics based blind channel estimation, time varying channel conditions are considered by the introduction of a forgetting factor or a sliding window for the evaluation of the received signal in [TG97, SV07b]. The second order statistics based semiblind channel estimation for OFDM is accommodated to time varying channel conditions in [MdCD02] by the introduction of a sliding window for the evaluation of the received signal. In [HWG04], the channel variations in time domain are tracked by the application of a Kalman filter. The parameters of the state equation which is used in the Kalman filter are estimated with the help of second order statistics.

Considering IFDMA, it is beneficial to overcome the high pilot symbol overhead in frequency domain which is caused by the distributed subcarriers. The IFDMA signal generation in time domain introduced in [SDBS98] shows that the IFDMA signal contains redundancy due to the signal generation based on compression and repetition of the blocks of data symbols. Thus, second order statistics algorithms are well suitable for the application to IFDMA as advantage can be taken of the cyclostationary structure of the received IFDMA signal without any additional introduction of redundancy at the transmitter or the receiver. The application of second order statistics based semiblind channel estimation algorithms to IFDMA for the estimation of frequency domain channel variations has not been addressed in previous works so far. Furthermore, the aforementioned works did not consider the case where the available bandwidth is shared by multiple users in the system.

In order to reduce the pilot symbol overhead in time domain, an iterative estimation of the channel variations in time domain is appropriate. This principle is known as decision directed channel estimation and utilizes an initializing channel estimate to obtain estimates of the data symbols in the succeeding points in time. Based on the estimated data symbols, which are sometimes denoted as virtual pilot symbols in the context of decision directed channel estimation, an updated channel estimate for the succeeding

points in time can be obtained. The decision directed channel estimation has been presented in various works, e.g., in [FS99] for the application to single-carrier systems and multicarrier systems like OFDM. The drawback of the iterative procedure for the estimation of channel variations in time domain is comprised in its sensitivity to error propagation and noise amplification with increasing time duration. Therefore, several strategies for the mitigation of error propagation have been presented. [MMF98] introduces Wiener filtering and Kalman filtering for estimation refinement. In [LFDL07a], a decision directed channel estimation procedure combating the noise amplification is presented for single-carrier systems. The initialization channel estimate is obtained by pilot assisted channel estimation and the application of two times one-dimensional Wiener interpolation filters. Based on this, the decision directed estimates are calculated. Then, strongly noise affected channel estimates are replaced by initializing estimates and a final Wiener filter is applied after decision directed estimation to improve the estimation performance. [RGR<sup>+</sup>03] presents a decision directed channel estimation for OFDM where a weighting factor is introduced representing the quality of the actual decision directed estimate. In order to combat error propagation, this weighting factor is used to calculate a weighted summation of the actual and a certain number of previous decision directed estimates. By doing so, an improved version of the decision directed channel estimate is obtained. In [BRN08], pilot assisted channel estimation is applied to OFDM for the estimation of channel variations in frequency and time domain. The decision directed channel estimation is applied in order to improve the pilot assisted channel estimation. For DFT precoded OFDM, [LFDL08] introduces two different pilot assisted channel estimation techniques for the initialization of decision directed channel estimation. The first one uses pilot symbols that are superimposed to data symbols on each subcarrier. The second one uses distinct subcarriers for pilot transmission. The pilot symbols are modulated according to the IFDMA scheme in order to obtain equidistantly spaced pilot subcarriers in frequency domain. Decision directed channel estimation with superimposed pilot and data symbols for the initializing estimate is also considered in [HFBC01] for the application to OFDM. In [GG08], decision directed channel estimation is introduced for IFDMA with two antennas and maximum ratio combining at the receiver. For the initialization of the decision directed channel estimation, again pilot assisted channel estimation is applied. [LTAN08] evaluates the performance of decision directed channel estimation for IFDMA for the case that an initializing channel estimate is available not only for the subcarrier allocated to the user under consideration but for all subcarriers in the system. A noise reduction of the decision directed channel estimates is obtained by the application of windowing in time domain. In [DMO09], decision directed channel estimation has also been proposed for the application to IFDMA and B-IFDMA. Here, the information about the reliability of the data symbol hypotheses at the output of the decoder is utilized in the

decision directed channel estimation. The consideration of the so-called soft-info of the data symbols helps to improve the channel estimation performance.

In [DeB04], a different approach for IFDMA channel estimation with reduced number of pilot symbols in time domain has been introduced. Here, the channel is estimated with the help of pilot assisted channel estimation for a certain IFDMA symbol. Then, the pilot sequence is extended in time domain by hypotheses for all possible transmit symbols which are used as a virtual pilot sequence in order to track the channel variations in time domain. This algorithm implies that a trellis with all data symbol hypotheses has to be evaluated with the help of a metric representing the probability for a correct path decision. In order to reduce the complexity of this trellis based channel estimation algorithm, a reduced state metric has been proposed additionally.

Each of the aforementioned algorithms for the estimation of the channel variations in time domain with a reduced number of pilot symbols is based on the assumption that an initializing channel estimate can be obtained by pilot assisted channel estimation. In this initializing estimate, the frequency domain channel variations are estimated and are used for the iterative procedure in order to follow the channel variations in time domain. To the best of the authors knowledge, the case where the number of pilot symbols is insufficient to obtain a pilot assisted initializing channel estimate has not been addressed so far.

## 1.4 Open Issues

In this section, the open issues for channel estimation in IFDMA and B-IFDMA arising from the review of the state-of-the-art channel estimation techniques in Section 1.3 are summarized:

1. How can pilot symbols for channel estimation be inserted in the IFDMA transmit signal while supporting the transmission of variable data rates, having small influence on the PAPR of the IFDMA transmit signal and consuming low pilot symbol overhead? How can the channel variations in frequency and time domain be estimated under consideration of the pilot insertion methods satisfying the aforementioned question?
2. How can the cyclostationarity of the IFDMA signal be exploited in order to reduce the pilot symbol overhead for the estimation of channel variations in frequency domain?

3. How is the semiblind estimation of channel variations in frequency domain influenced by multiple users in the system?
4. How can the channel variations in time domain be estimated while applying semiblind estimation of channel variations in frequency domain to IFDMA? How can the pilot symbol overhead for the estimation of channel variations in frequency and time domain be reduced while applying semiblind channel estimation to IFDMA?
5. What are the differences of pilot assisted channel estimation for B-IFDMA in comparison to IFDMA? In terms of pilot assisted channel estimation, how can advantage be taken of the blocks of neighboring subcarriers in case of B-IFDMA?
6. How can the pilot symbol overhead for the estimation of channel variations in frequency domain be reduced while applying semiblind channel estimation to B-IFDMA?

## 1.5 Contributions and Overview

This section gives an overview of the thesis and summarizes the main contributions addressing the open problems introduced in Section 1.4. In the following, the contents along with the main contributions of each chapter are briefly described.

In Chapter 2, a model for a communication system utilizing IFDMA as multiple access scheme is presented. The IFDMA signal generation is described in frequency as well as in time domain and the transmission of this signal over a mobile radio channel is explained. For this purpose, a model for the mathematical description of the mobile radio channel characteristics is given. The IFDMA signal demodulation is presented in frequency domain and the influence of the channel on the received signal is evaluated.

Chapter 3 presents pilot assisted channel estimation for IFDMA and gives answer to the Question 1 stated in Section 1.4:

1. Two different pilot insertion methods are introduced which assure the transmission with variable data rates and fulfill the requirements of low PAPR and low pilot symbol overhead to a different extent. For each of the two pilot insertion methods, appropriate estimation algorithms are presented in order to estimate the channel variations in frequency and time domain.

The pilot insertion methods and their appropriate estimation algorithms are investigated with respect to the influence on the PAPR of the IFDMA transmit signal, the pilot symbol overhead consumption, the Mean Square Error (MSE) performance and the computational complexity.

In Chapter 4, the application of semiblind channel estimation to IFDMA is introduced in order to estimate the channel variations in frequency and time domain with a reduced number of pilot symbols compared to the pilot assisted channel estimation introduced in Chapter 3. This Chapter answers the Questions 2, 3 and 4 of the open issues:

2. Two different semiblind channel estimation approaches are introduced for the estimation of frequency domain channel variations in an IFDMA system in case of channels with small delay spreads. The first one is based on a correlation algorithm and the second one is based on a subspace algorithm. Two further semiblind channel estimation approaches which are again based on the correlation and the subspace algorithm, respectively, are introduced for the application to IFDMA in case of channels with large delay spreads.
3. The influence of multiple users in the system on the performance of semiblind estimation of frequency domain channel variations is derived mathematically.
4. In order to estimate the channel variations in time domain while applying semiblind estimation of frequency domain channel variations to IFDMA, the combination of semiblind estimation of frequency domain channel variations and decision directed estimation of time domain channel variations is introduced. The error propagation behavior of the decision directed estimation is counteracted by the application of an iterative Wiener filtering procedure. By this means, the channel variations in frequency and time domain can be estimated with a reduced number of pilot symbols in frequency and time domain.

The introduced algorithms for the estimation of channel variations in frequency and time domain with a reduced number of pilot symbols are investigated in terms of the pilot symbol overhead consumption, the MSE performance and the computational complexity.

Chapter 5 presents channel estimation for B-IFDMA and addresses the open Questions 5 and 6 by the following contributions:

5. The differences between pilot assisted channel estimation for IFDMA and B-IFDMA are evaluated and the new aspects of pilot assisted channel estimation

for B-IFDMA are derived. In this context, two new channel estimation algorithms taking advantage of the B-IFDMA specific transmission on blocks of neighboring subcarriers are introduced.

6. The differences in the application of semiblink channel estimation to B-IFDMA in comparison to the application to IFDMA are presented and a semiblink estimation of channel variations in frequency domain is derived for B-IFDMA.

The pilot assisted and semiblink channel estimation for B-IFDMA are evaluated in terms of PAPR, pilot symbol overhead, MSE performance and computational complexity.

Finally, the main conclusions of the thesis are summarized in Chapter 6.





## Chapter 2

# IFDMA System Model

### 2.1 Introduction

In this chapter, a system model for mobile communication systems utilizing IFDMA as multiple access scheme is presented for an uplink scenario. The IFDMA system model is introduced in order to elaborate the channel influence on the transmitted IFDMA signal and to emphasize the parameters which have to be considered by the channel estimation algorithms. Any considerations throughout the thesis refer to the equivalent baseband.

First, the transmitter part of the mobile communication system is explained and a discrete-time model for the IFDMA signal generation is presented. The IFDMA signal generation is explained in frequency domain as well as in time domain because both representations are equivalent and of relevance for the remainder of this work. Moreover, the IFDMA signal properties that are important for the channel estimation and the investigations in this work are pointed out. Second, the physical properties of the mobile radio channel are described and a mathematical model for the mobile radio channel is given. Third, the receiver part of the mobile communication system is explained and a discrete-time model for the IFDMA signal demodulation at the receiver is presented. The IFDMA signal demodulation is explained in frequency domain due to the simplicity and clearness of this illustration whereas the IFDMA signal demodulation in time domain is neglected as it is irrelevant for the subsequent considerations. Finally, the influence of the mobile radio channel on the received IFDMA signal is derived mathematically.

Throughout this thesis, all signals are represented by their discrete time equivalents in the complex baseband. Further on,  $(\cdot)^*$ ,  $(\cdot)^T$ ,  $(\cdot)^H$ ,  $(\cdot)^{-1}$  and  $E\{\cdot\}$  denote the conjugate complex, the transpose, the Hermitian, the inverse and the expectation of a vector or a matrix, respectively. Vectors and matrices are denoted by lower and upper case boldface letters, respectively.

This chapter is organized as follows. In Section 2.2, the transmitter of the mobile communication system utilizing IFDMA as multiple access scheme is presented and the IFDMA signal generation in frequency and time domain, as well as the important

properties of the IFDMA signal are pointed out. Section 2.3 emphasizes selected channel properties and gives the mathematical representation of a mobile radio channel. Finally, in Section 2.4, the received IFDMA signal is described and the IFDMA signal demodulation is explained.

## 2.2 IFDMA Transmitter

### 2.2.1 Transmitter Model

This section presents a model for the transmitter of a mobile communication system utilizing IFDMA as multiple access scheme. The block diagram in Figure 2.1 gives an overview of the transmitter. The data source emits binary data that corresponds to the data stream of a certain user. After channel coding and interleaving, the resulting data bits are mapped to data symbols according to a bit mapping scheme like Phase Shift Keying (PSK) or Quadrature Amplitude Modulation (QAM) [Pro01]. The processing of the data symbols is performed blockwise. Therefore, the serial stream of data symbols is converted into parallel blocks of data symbols (S/P) which are fed into the IFDMA signal generator. Each data symbol within a block of data symbols belongs to the same IFDMA symbol and the output of the IFDMA signal generator will be denoted as an IFDMA symbol in the remainder of this thesis. After the IFDMA signal generation, a cyclic prefix with a duration that exceeds the maximum delay of the mobile radio channel is inserted at the beginning of each IFDMA symbol [vNP00]. Due to cyclic prefix insertion, interference between successively transmitted IFDMA symbols is avoided. After IFDMA signal generation and cyclic prefix insertion, each IFDMA symbol with cyclic prefix is parallel to serial (P/S) converted and fed into a windowing filter for spectral shaping of the resulting transmit signal. Afterwards, a digital to analog (D/A) converter is applied to the transmit signal. Finally, the analog transmit signal is modulated onto a radio frequency carrier, amplified and transmitted over the mobile radio channel.

In the following, the focus is on the IFDMA signal generation and cyclic prefix insertion which is highlighted by the dotted box in Figure 2.1 and is illustrated in the equivalent baseband with discrete-time input and output vectors in Figure 2.2. As already mentioned, for IFDMA signal generation,  $Q$  data symbols that are transmitted by a certain user are processed in parallel and, therefore, combined in a block of data symbols. The input of the IFDMA signal generator is given by the  $k^{\text{th}}$  block,  $k = 0, \dots, K - 1$ , which

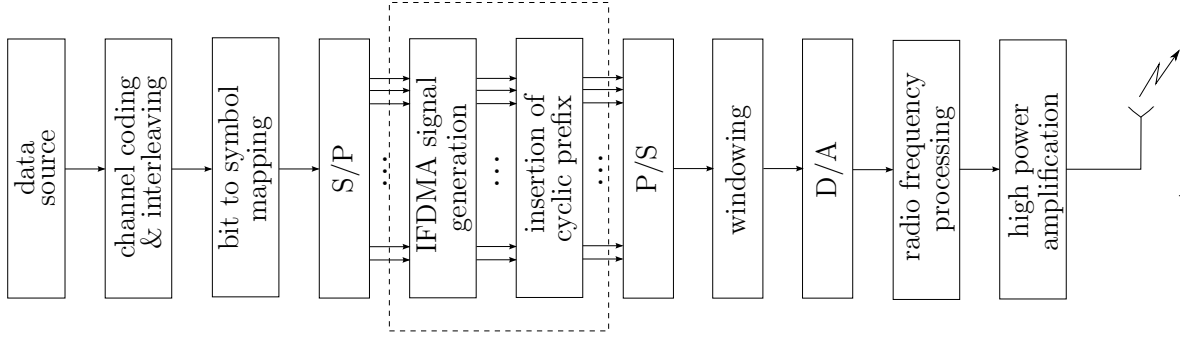


Figure 2.1. Block diagram of the transmitter in the mobile communication system

consists of  $Q$  data symbols  $d_{k,q}^{(u)}$ ,  $q = 0, \dots, Q-1$ , that are transmitted at data symbol rate  $1/T_S$  by the user with index  $u$ ,  $u = 0, \dots, U-1$ , and is denoted by

$$\mathbf{d}_k^{(u)} = [d_{k,0}^{(u)}, \dots, d_{k,Q-1}^{(u)}]^T. \quad (2.1)$$

The data symbols  $d_{k,q}^{(u)}$  result from coded and interleaved data bits that are mapped according to a bit mapping scheme like PSK or QAM. Further on, the data symbols  $d_{k,q}^{(u)}$  are assumed to be independently identically distributed (i.i.d.) with  $E\{|d_{k,q}^{(u)}|^2\} = \sigma_D^2$  and zero-mean. The output of the IFDMA signal generator which results from the  $k^{\text{th}}$  block  $\mathbf{d}_k^{(u)}$  is denoted as the  $k^{\text{th}}$  IFDMA symbol  $\mathbf{x}_k^{(u)}$ . The IFDMA symbol which is preceded by a cyclic prefix is represented by  $\tilde{\mathbf{x}}_k^{(u)}$ . The mathematical relations between the  $k^{\text{th}}$  block  $\mathbf{d}_k^{(u)}$  of data symbols and the  $k^{\text{th}}$  IFDMA symbol  $\mathbf{x}_k^{(u)}$  are derived in the following Sections 2.2.2 and 2.2.3.

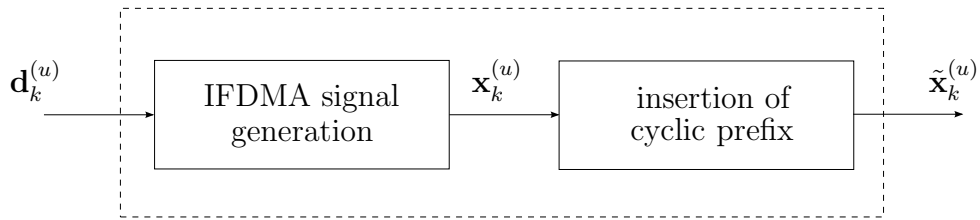


Figure 2.2. IFDMA signal generation and cyclic prefix insertion with discrete-time input and output vectors

The IFDMA signal generation in frequency domain is presented in Section 2.2.2. In time domain, an equivalent description of the signal generation can be given which is presented in Section 2.2.3.

### 2.2.2 IFDMA Signal Generation in Frequency Domain

This section presents the IFDMA signal generation in frequency domain according to [FKCS05a].

In the following, the blocks  $\mathbf{d}_k^{(u)}$  of data symbols are processed in frequency domain first and, subsequently, transformed in time domain in order to obtain the IFDMA symbols which are finally extended by a cyclic prefix. In Figure 2.3, the block diagram of the IFDMA signal generation in frequency domain and subsequent cyclic prefix insertion is illustrated. First, a DFT precoding is applied to the block  $\mathbf{d}_k^{(u)}$  of data symbols. In the following, let  $\mathbf{F}_A$  represent an  $A \times A$  DFT matrix with the elements  $[\mathbf{F}_A]_{i,m}$ ,  $i, m = 0, \dots, Q - 1$ , calculated by

$$[\mathbf{F}_A]_{i,m} = \frac{1}{\sqrt{A}} \cdot e^{-j \frac{2\pi i m}{A}}. \quad (2.2)$$

Then,  $\mathbf{F}_Q$  represents a  $Q \times Q$  DFT precoding matrix and the output of the precoder is given by

$$\bar{\mathbf{d}}_k^{(u)} = \mathbf{F}_Q \cdot \mathbf{d}_k^{(u)} = \left[ \bar{d}_{k,0}^{(u)}, \dots, \bar{d}_{k,Q-1}^{(u)} \right]^T \quad (2.3)$$

denoting the frequency domain representation of the  $k^{\text{th}}$  block of data symbols. The elements  $\bar{d}_{k,q}^{(u)}$  are assigned to a user specific set of  $Q$  subcarriers in frequency domain. These  $Q$  user specific subcarriers are equidistantly distributed over the total number  $N = L_U \cdot Q$ ,  $L_U \in \mathbb{Z}$ , of available subcarriers in the system. The subcarrier assignment can be described by an  $N \times Q$  mapping matrix  $\mathbf{M}^{(u)}$  which is characterized by its elements  $[\mathbf{M}^{(u)}]_{n,q}$ , with  $n = 0, \dots, N - 1$  and  $q = 0, \dots, Q - 1$ , that are given by

$$[\mathbf{M}^{(u)}]_{n,q} = \begin{cases} 1 & \text{for } n = q \cdot L_U + u, \\ 0 & \text{else} \end{cases} \quad (2.4)$$

[FKCS05a]. After the assignment of the elements  $\bar{d}_{k,q}^{(u)}$ ,  $q = 0, \dots, Q - 1$ , to the user specific subcarriers, an  $N$ -point Inverse Discrete Fourier Transform (IDFT) operation represented by the  $N \times N$  IDFT matrix  $\mathbf{F}_N^H$  is applied in order to get a time domain signal vector at the output of the IFDMA signal generator. Thus, the DFT-precoded, mapped and IDFT transformed block of data symbols becomes

$$\mathbf{x}_k^{(u)} = \mathbf{F}_N^H \cdot \mathbf{M}^{(u)} \cdot \mathbf{F}_Q \cdot \mathbf{d}_k^{(u)} = \left[ x_{k,0}^{(u)}, \dots, x_{k,N-1}^{(u)} \right]^T \quad (2.5)$$

[FKCS05a].  $\mathbf{x}_k^{(u)}$  represents the  $k^{\text{th}}$  IFDMA symbol of a user with index  $u$  with the elements  $x_{k,n}^{(u)}$ ,  $n = 0, \dots, N - 1$ , transmitted at chip rate  $1/T_C = L_U/T_S$ .

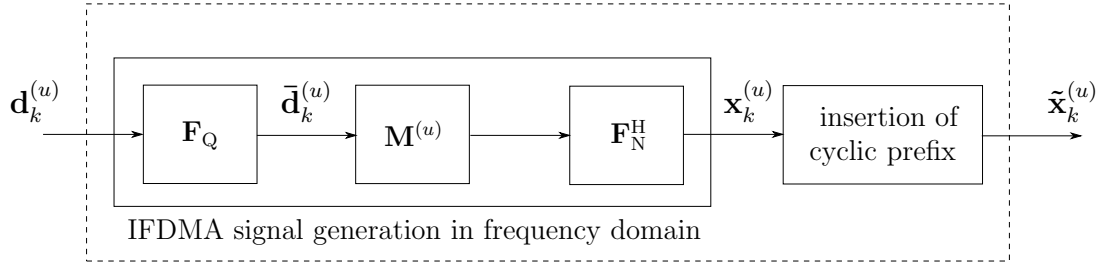


Figure 2.3. Block diagram of IFDMA signal generation in frequency domain and cyclic prefix insertion

In order to avoid intersymbol and intercarrier interference which is caused by transmission over a multipath channel, a cyclic prefix consisting of  $N_G = L_G \cdot Q$  elements is inserted in-between successive IFDMA symbols, where  $L_G$  is chosen such that  $N_G \in \mathbb{Z}$  [vNP00]. For cyclic prefix insertion, the last  $N_G$  elements of  $\mathbf{x}_k^{(u)}$  are repeated at the beginning of the same IFDMA symbol vector. Finally, the  $k^{\text{th}}$  IFDMA symbol with cyclic prefix is represented by a vector with  $(L_U + L_G) \cdot Q = L \cdot Q$  elements according to

$$\tilde{\mathbf{x}}_k^{(u)} = \underbrace{[x_{k,N-N_G}^{(u)}, \dots, x_{k,N-1}^{(u)}]_{\text{cyclic prefix}}}_{\text{cyclic prefix}}, [x_{k,0}^{(u)}, \dots, x_{k,N-1}^{(u)}]^T. \quad (2.6)$$

### 2.2.3 IFDMA Signal Generation in Time Domain

This section presents the IFDMA signal generation in time domain whose principle has been introduced in [SDBS98].

In Figure 2.4, the block diagram of the IFDMA signal generation in time domain is illustrated. First, the block  $\mathbf{d}_k^{(u)}$  of data symbols with a duration of  $Q \cdot T_S$  is compressed in time domain by the factor  $L_U = N/Q$  [SDBS98]. The resulting compressed block has a duration of  $\frac{Q T_S}{L_U}$  and is denoted by

$$\mathbf{w}_k^{(u)} = [w_{k,0}^{(u)}, \dots, w_{k,Q-1}^{(u)}]^T. \quad (2.7)$$

The elements  $w_{k,q}$ ,  $q = 0, \dots, Q - 1$ , are transmitted at chip rate  $1/T_C = L_U/T_S$  and have the average power  $\mathbb{E}\{|w_{k,q}^{(u)}|^2\} = \sigma_W^2$ . Subsequently,  $\mathbf{w}_k^{(u)}$  is repeated  $L_U$ -times. The vector consisting of the compressed and  $L_U$ -times repeated blocks of data symbols has a duration of  $Q \cdot T_S$ , which corresponds to the duration of the original block  $\mathbf{d}_k^{(u)}$  of data symbols. After compression and repetition, a user dependent phase shift is applied in order to assure the orthogonality between the signals of different users.

With  $\varphi^{(u)} = u \cdot 2\pi/N$  the user dependent phase [SDBS98], the phase shift matrices  $\Phi_i^{(u)}$ ,  $i = 0, \dots, L_U - 1$ , are defined as diagonal matrices according to

$$\Phi_i^{(u)} = \begin{bmatrix} e^{-j \cdot (i \cdot Q) \cdot \varphi^{(u)}} & 0 & \dots & 0 \\ 0 & \ddots & & \vdots \\ \vdots & & & 0 \\ 0 & \dots & 0 & e^{-j \cdot (i \cdot Q + Q - 1) \cdot \varphi^{(u)}} \end{bmatrix}. \quad (2.8)$$

Then, the  $k^{\text{th}}$  IFDMA symbol  $\mathbf{x}_k^{(u)}$  of the user with index  $u$  is calculated by

$$\mathbf{x}_k^{(u)} = \begin{bmatrix} x_{k,0}^{(u)} \\ \vdots \\ x_{k,N-1}^{(u)} \end{bmatrix} = \begin{bmatrix} \Phi_0^{(u)} \\ \vdots \\ \Phi_{L_U-1}^{(u)} \end{bmatrix} \cdot \mathbf{w}_k^{(u)}. \quad (2.9)$$

In [SDBS98] it has been shown that compressing a block  $\mathbf{d}_k^{(u)}$  of data symbols by the factor  $L_U$  in time domain is equivalent to spreading the spectrum of the original block  $\mathbf{d}_k^{(u)}$  by factor  $L_U$ . The subsequent  $L_U$ -fold repetition of the compressed block  $\mathbf{w}_k^{(u)}$  leads to a discrete spectrum whose spectral lines exhibit a distance of  $\frac{L_U}{Q \cdot T_s}$  which is the inverse of the time periodicity of the compressed and repeated blocks. The multiplication of the compressed and repeated blocks with the user-specific phase shift matrices  $\Phi_i^{(u)}$  produces a shift in frequency domain and ensures the orthogonality between the signals of different users. With these considerations and according to [FKCS05a], the IFDMA symbol  $\mathbf{x}_k^{(u)}$  in Eq. (2.9) is equivalent to the IFDMA symbol in Eq. (2.5).

Finally,  $\mathbf{x}_k^{(u)}$  is extended by a cyclic prefix as explained in Section 2.2.2 and, thus, the  $k^{\text{th}}$  IFDMA symbol of user  $u$  including cyclic prefix is again represented by

$$\tilde{\mathbf{x}}_k^{(u)} = \underbrace{[x_{k,N-N_G}^{(u)}, \dots, x_{k,N-1}^{(u)}]}_{\text{cyclic prefix}}, x_{k,0}^{(u)}, \dots, x_{k,N-1}^{(u)}]^T. \quad (2.10)$$

In analogy to Eq. (2.9), the extension of  $\mathbf{x}_k^{(u)}$  by a cyclic prefix can be expressed according to

$$\tilde{\mathbf{x}}_k^{(u)} = \begin{bmatrix} \Phi_{L_U-L_G}^{(u)} \\ \vdots \\ \Phi_{L_U-1}^{(u)} \\ \Phi_0^{(u)} \\ \vdots \\ \Phi_{L_U-1}^{(u)} \end{bmatrix} \cdot \mathbf{w}_k^{(u)}. \quad (2.11)$$

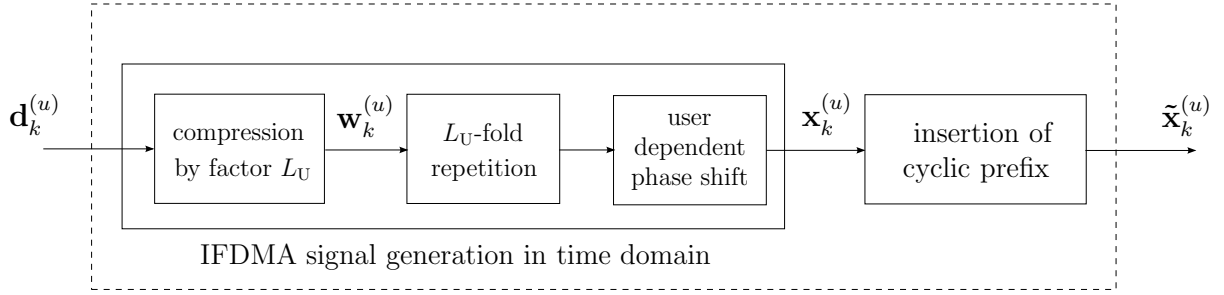


Figure 2.4. Block diagram of IFDMA signal generation in time domain and cyclic prefix insertion

## 2.2.4 Important IFDMA Signal Properties

### 2.2.4.1 Allocation of Subcarriers and Time Slots

In this section, a graphical illustration of the user specific assignment of subcarriers in frequency domain is given and the properties of this subcarrier allocation are pointed out. Furthermore, the combination of IFDMA with an additional user separation in time domain is introduced.

In Figure 2.5, the IFDMA subcarrier allocation is depicted exemplarily for a user with index  $u = 0$  and a user with index  $u = 1$  on a grid in frequency domain and time domain. The elements  $\bar{d}_{k,q}^{(u)}$ ,  $q = 0, \dots, Q - 1$ , of the precoded data vector  $\bar{\mathbf{d}}_k^{(u)}$  are transmitted on  $Q$  user-specific subcarriers that are equidistantly distributed over the total number  $N$  of subcarriers in the system. Each element  $\bar{d}_{k,q}^{(u)}$  is transmitted on a subcarrier with index  $q \cdot L_U + u$ , where the factor  $L_U = \frac{N}{Q}$  is as introduced in Section 2.2.2 and Section 2.2.3. With

$$\Delta f = \frac{1}{Q \cdot T_S} = \frac{1}{L_U \cdot Q \cdot T_C}, \quad (2.12)$$

the subcarrier spacing in the system, the spacing between neighboring subcarriers allocated to a user under consideration is given by  $L_U \cdot \Delta f$ . The smaller the number  $Q$  of transmitted data symbols per IFDMA symbol, i.e. the lower the data rate that is transmitted per user, the larger is the distance between neighboring subcarriers in frequency domain. The sets of subcarriers allocated to different users are shifted relatively to one another by  $u \cdot \Delta f$  which guarantees the orthogonality between the signals transmitted by different users. Due to this frequency shift, the sets of subcarriers allocated to different users are combwise interleaved to each other. For the example given in Figure 2.5, this means that there is no frequency shift for the set of subcarriers related to the user with index  $u = 0$  and a frequency shift of  $\Delta f$  for the set of subcarriers related to the user with index  $u = 1$ .

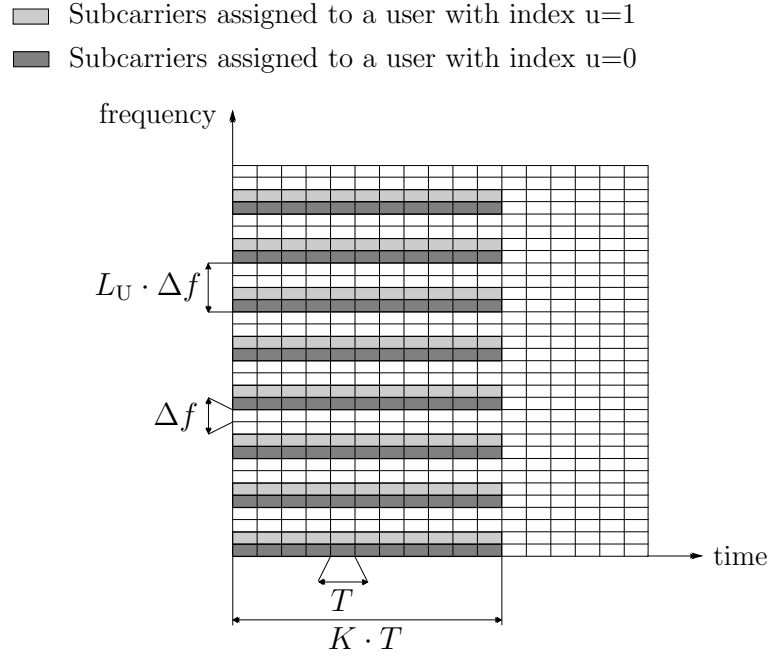


Figure 2.5. Allocation of subcarriers and time slots to two different users

In time domain, the data symbols of different users are additionally separated by the transmission within different Time Division Multiple Access (TDMA) slots. The time duration of an IFDMA symbol plus cyclic prefix is given by

$$T = (L_U + L_G) \cdot Q \cdot T_C = L \cdot Q \cdot T_C. \quad (2.13)$$

Each TDMA slot consists of  $K$  successively transmitted IFDMA symbols plus cyclic prefix and exhibits a time duration of  $K \cdot T$ . The succeeding time slots which are indicated by empty boxes in Figure 2.5 are utilized to transmit the data of other users in the system. I.e., the data of a user under consideration is transmitted on a user-specific set of  $Q$  subcarriers in frequency domain and within  $K$  successively transmitted IFDMA symbols in time domain. The introduction of the additional user separation in time domain allows the mobile terminal of a user under consideration to enter a micro sleep mode during the transmission phase of the other users. This micro sleep mode is beneficial in terms of the power consumption of the mobile terminal because, by this means, considerable energy savings can be achieved for the mobile terminal of each user [SFF<sup>+</sup>07, WINdf].

#### 2.2.4.2 Peak-to-Average Power Ratio

In this section, a definition for the PAPR per IFDMA symbol is given and evaluated qualitatively as a measure of the envelope fluctuations of the IFDMA transmit signal [vNP00].



The PAPR per IFDMA symbol represents the ratio between the peak power and the average power within one IFDMA symbol and is defined by

$$PAPR_k = \max_n \left\{ \frac{|x_{k,n}^{(u)}|^2}{E\{|x_{k,n}^{(u)}|^2\}} \right\}, \quad \text{for } n = 0, \dots, N-1, \quad (2.14)$$

[FKH08]. A qualitative conclusion about the PAPR of the IFDMA transmit signal can be drawn by considering the IFDMA signal generation in time domain as explained in Section 2.2.3. The signal is built by compression, repetition and phase shifting of blocks of data symbols in time domain and, thus, the PAPR of the data symbols remains unaffected. Therefore, it appears that the PAPR per IFDMA symbol corresponds to the PAPR of the data symbols themselves and that the IFDMA transmit signal provides a low PAPR which helps to avoid non-linearities in the signal at the output of the high power amplifier and allows the usage of low cost amplifiers [FKH08].

## 2.3 Mobile Radio Channel

### 2.3.1 Time-Variant Multipath Propagation

This section addresses the properties of multipath propagation in a mobile radio scenario.

A signal that is transmitted in a terrestrial environment suffers from reflection, diffraction and scattering at obstacles in the propagation environment. Due to reflection, diffraction and scattering, several copies of the original transmit signal are received with different delay, attenuation and phase shift. Considering a linear model of the terrestrial wave propagation, these physical effects can be represented by a multipath model as illustrated in Figure 2.6. The signal is transmitted over different propagation paths, where each path is characterized by a distinct delay, attenuation and phase shift [Pae02].

In a non-stationary scenario, where the transmitter or the receiver are moving, the received signal suffers from fluctuations of the signal amplitudes that are caused by large-scale and small-scale fading [Rap02]. The large-scale fading can be explained by shadowing effects in the propagation environment due to the moving of the transmitter or receiver over large distances. The large-scale fading leads to slow fluctuations of the signal amplitude and is assumed to be mitigated by perfect power control [Kan05].

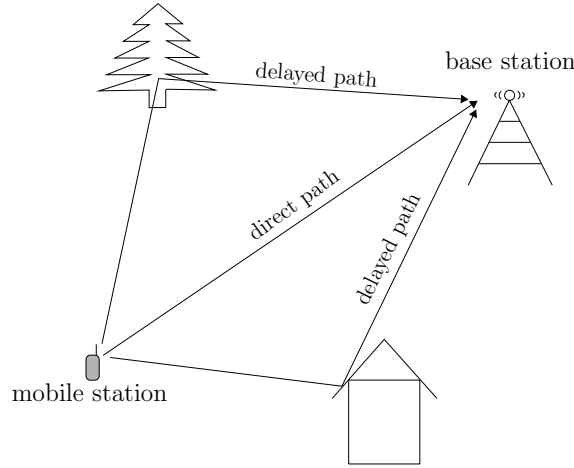


Figure 2.6. Multipath propagation in a mobile radio scenario

Thus, the large-scale fading is neglected for the following considerations. The small-scale fading can be explained by the movement of the transmitter or receiver over a distance of a few wavelength which causes timely varying interference between the different received multipath components and can result in large fluctuations of the received signal amplitude [Rap02]. Further on, in a non-stationary scenario, the Doppler-effect occurs and causes a frequency shift, the so-called Doppler shift, on each propagation path. With  $v$  the velocity of the transmitting mobile station,  $c$  the speed of light,  $f_0$  the carrier frequency of the transmit signal and  $\alpha$  the angle between the direction of arrival of the incident wave and the moving direction of the transmitter, the Doppler shift  $f_D$  is given by

$$f_D = \frac{v \cdot f_0}{c} \cdot \cos(\alpha) \quad (2.15)$$

[Pae02]. The maximum Doppler shift  $f_{D,\max} = \frac{v \cdot f_0}{c}$  occurs for  $\alpha = 0, \pi$ . In Figure 2.7, the relation between direction of arrival of the incident wave and the moving direction of the transmitter is explained graphically. The influence of the Doppler shift on the received signal can be described in time domain. Since different multipath components experience different Doppler shifts, the received signal consists of the superposition of different waveforms each shifted in frequency by a different Doppler shift. The superposition of these oscillations causes timely varying signal amplitudes at the receiver. Therefore, the Doppler shift is a measure for the time variability of the propagation conditions that a signal is exposed to [Mol05].

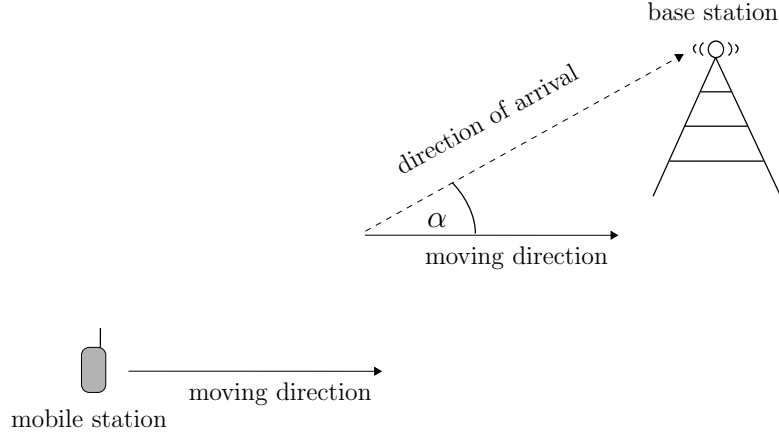


Figure 2.7. Illustration of Doppler shift

### 2.3.2 Stochastic Channel Description

In this section, a mathematical model for the mobile radio channel is presented and important stochastic measures characterizing the mobile radio channel are pointed out.

The aforementioned physical effects that occur during multipath propagation in a mobile radio scenario are denoted as the mobile radio channel which can be modeled based on a discrete, linear time-variant system in the equivalent baseband. The different delay paths are represented by  $\mathcal{L}$  time-variant channel coefficients which are user dependent because different users experience different channel conditions in the uplink of a mobile radio system. With  $\delta$  the delta-distribution,  $t$  the absolute time,  $\tau$  the relative path delay time and  $\tau_\iota$  the delay time of the  $\iota^{\text{th}}$  delay path, the time-variant impulse response of the mobile radio channel is given by

$$h(t, \tau)^{(u)} = \sum_{\iota=0}^{\mathcal{L}-1} h_{t,\iota}^{(u)} \delta(\tau - \tau_\iota) . \quad (2.16)$$

The time-variant channel transfer function is obtained by applying the Fourier transformation to the time-variant channel impulse response with respect to the delay time  $\tau$  according to

$$\bar{h}(t, f)^{(u)} = \int_{-\infty}^{+\infty} h(t, \tau)^{(u)} e^{-j2\pi f\tau} d\tau . \quad (2.17)$$

According to [Pae02], the function in Eq. (2.17) can be considered as a stochastic measure. Thus, the properties of the mobile radio channel can be described by the autocorrelation function of  $\bar{h}(t, f)^{(u)}$ . With  $t_1, t_2$  denoting certain points in time and  $f_1, f_2$  denoting certain frequencies, the autocorrelation function of  $\bar{h}(t, f)^{(u)}$  is given by

$$R_{\bar{h}}(t_1, t_2, f_1, f_2)^{(u)} = E\{\bar{h}(t_1, f_1)^{(u)*} \cdot \bar{h}(t_2, f_2)^{(u)}\} . \quad (2.18)$$

A widely used class of linear, time-variant channel models is the class of Wide-Sense Stationary Uncorrelated Scattering (WSSUS) channels. WSSUS channels exhibit a wide-sense stationarity in terms of the absolute time  $t$  and statistically uncorrelated scatterers in terms of the delay time  $\tau$ . In the following, the WSSUS assumption is demonstrated for the autocorrelation function  $R_{\bar{h}}(t_1, t_2, f_1, f_2)^{(u)}$  of the time-variant channel transfer function  $\bar{h}(t, f)^{(u)}$  as the properties of this autocorrelation function are of importance for the remainder of this thesis. The autocorrelation function of the time-variant channel impulse response  $h(t, \tau)^{(u)}$  is described in detail under consideration of the WSSUS assumption in, e.g., [Bel63, Pae02, Mol05] and is not presented in this work.

On the one hand, due to the wide-sense stationarity assumption in time domain,  $R_{\bar{h}}(t_1, t_2, f_1, f_2)^{(u)}$  depends only on the time difference  $t_2 - t_1$ , but not on the absolute point in time. On the other hand, the assumption of uncorrelated scatterers leads to stationarity in frequency domain and, thus,  $R_{\bar{h}}(t_1, t_2, f_1, f_2)^{(u)}$  depends only on the frequency difference  $f_2 - f_1$ . Consequently, the statistical properties of the channel do not change with time and frequency and, thus, the autocorrelation function of the time-variant channel transfer function can be rewritten according to

$$R_{\bar{h}}(t_1, t_2, f_1, f_2)^{(u)} = R_{\bar{h}}(t_2 - t_1, f_2 - f_1)^{(u)} = R_{\bar{h}}(t', f')^{(u)} \quad (2.19)$$

[Pae02].  $R_{\bar{h}}(t', f')^{(u)}$  is denoted as the time frequency correlation function and is a measure for the variations of the channel conditions within a time interval given by  $t' = t_2 - t_1$  and a bandwidth given by  $f' = f_2 - f_1$ .

The time correlation function of the mobile radio channel can be calculated under consideration of  $R_{\bar{h}}(t', f')^{(u)}$  for  $f' = 0$  and with the help of the Doppler power spectral density  $S_{f_D}(f_D)^{(u)}$ . According to [Pae02], the time correlation function is given by

$$R_{\bar{h},t}(t')^{(u)} = R_{\bar{h}}(t', f' = 0)^{(u)} = \int_{-\infty}^{+\infty} S_{f_D}(f_D)^{(u)} e^{j2\pi f_D t'} df_D. \quad (2.20)$$

The frequency correlation function of the mobile radio channel can be calculated under consideration of  $R_{\bar{h}}(t', f')^{(u)}$  for  $t' = 0$  and with the help of the delay power spectral density  $S_{\tau}(\tau)^{(u)}$ . According to [Pae02], the frequency correlation function is given by

$$R_{\bar{h},f}(f')^{(u)} = R_{\bar{h}}(t' = 0, f')^{(u)} = \int_{-\infty}^{+\infty} S_{\tau}(\tau)^{(u)} e^{-j2\pi f' \tau} d\tau. \quad (2.21)$$

Throughout the thesis, the Doppler power spectral density is considered as a Jakes

distribution [Hoe92] that is given by

$$S_{f_D}(f_D)^{(u)} = \begin{cases} \frac{1}{\pi f_{D,\max} \sqrt{1 - \left(\frac{f_D}{f_{D,\max}}\right)^2}} & \text{for } |f_D| \leq f_{D,\max}, \\ 0 & \text{else.} \end{cases} \quad (2.22)$$

The delay power spectral density is considered as a decaying exponential function. With  $\tau_{\max}$  the maximum delay of the channel and  $\tau_{\text{rms}} = \tau_{\max}/(3 \cdot \ln(10))$  the root mean square width [Hoe92], the delay power spectral density is given by

$$S_{\tau}(\tau)^{(u)} = \begin{cases} \frac{e^{-\frac{\tau}{\tau_{\text{rms}}}}}{\tau_{\text{rms}}(1 - e^{-\frac{\tau_{\max}}{\tau_{\text{rms}}}})} & \text{for } 0 \leq \tau \leq \tau_{\max}, \\ 0 & \text{else.} \end{cases} \quad (2.23)$$

Then, the time and frequency correlation functions can be calculated with Eq. (2.20) and (2.21) and with  $J_0(\cdot)$  the 0<sup>th</sup> order Bessel function of first kind according to

$$R_{\bar{h},t}(t')^{(u)} = J_0(2\pi f_{D,\max} t') \quad (2.24)$$

and

$$R_{\bar{h},f}(f')^{(u)} = \frac{1 - e^{-\tau_{\max}(1/\tau_{\text{rms}} + j2\pi f')}}{(1 - e^{-\tau_{\max}/\tau_{\text{rms}}})(1 + j2\pi f'\tau_{\text{rms}})}, \quad (2.25)$$

respectively. With the help of Eq. (2.24) and (2.25), the channel variations in time domain and frequency domain can be characterized.

### 2.3.3 Discrete-Time Channel Model

In this section, a discrete-time representation of the mobile radio channel is derived in order to describe the IFDMA signal at the receiver of the mobile communication system.

Due to the definition of the transmit signal in discrete-time, an equivalent discrete-time channel model of the channel impulse response specified in Eq. (2.16) is considered in the following [Hoe92]. It is assumed that the channel delay coefficients stay constant for the duration  $T$  of an IFDMA symbol including cyclic prefix and are changing for each IFDMA symbol with index  $k = 0, \dots, K - 1$ . Further, it is assumed that the delays  $\tau_l$  that are related to certain path delay times can be expressed as integer multiples of the chip duration  $T_C$ , i.e.,  $\tau_l = m_l \cdot T_C$  with  $m_l \in \mathbb{N}$ , and that no relevant copies of the signal are received with delay times larger than the maximum delay time  $\tau_{\max}$  of the channel which is given by

$$\tau_{\max} = L_C \cdot T_C. \quad (2.26)$$

Then, according to [Hoe92], the discrete-time channel impulse response can be defined as the channel impulse response  $h(t, \tau)^{(u)}$  that is sampled at time instants  $t = k \cdot T$  and  $\tau = l \cdot T_C$  with  $l = 0, \dots, L_C - 1$  and is given by

$$h(k, l)^{(u)} = h(k \cdot T, l \cdot T_C)^{(u)} = \sum_{l=0}^{L_C-1} h_{k,l}^{(u)} \delta(\tau - \tau_l) . \quad (2.27)$$

The frequency variations of the mobile radio channel are characterized with the help of the coherence bandwidth  $B_{\text{coh}}$  that determines the bandwidth for which the channel characteristics are correlated and is approximated by

$$B_{\text{coh}} \approx \frac{1}{\tau_{\text{max}}} \quad (2.28)$$

[FK03]. The time variations of the mobile radio channel are characterized with the help of the coherence time  $T_{\text{coh}}$  that determines the time duration for which the channel characteristics can be considered as time-invariant and is approximated by

$$T_{\text{coh}} \approx \frac{1}{2 \cdot f_{D,\text{max}}} \quad (2.29)$$

[FK03].

The IFDMA symbols  $\tilde{\mathbf{x}}_k^{(u)}$ ,  $k = 0, \dots, K - 1$ , each containing a cyclic prefix with a time duration  $N_G \cdot T_C$  that is larger than the maximum delay  $\tau_{\text{max}}$  of the mobile radio channel, are transmitted over the channel with impulse response  $h(k, l)^{(u)}$ . With  $N_G > L_C$  and  $N > N_G > L_C$ , an  $N \times 1$  channel impulse response vector  $\mathbf{h}_k^{(u)}$  containing the time-variant channel delay coefficients  $h_{k,l}^{(u)}$  is defined according to

$$\mathbf{h}_k^{(u)} = [h_{k,0}^{(u)}, \dots, h_{k,L_C-1}^{(u)}, \underbrace{0, \dots, 0}_{N-L_C}]^T . \quad (2.30)$$

The application of an  $N$ -point DFT to the vector  $\mathbf{h}_k^{(u)}$  according to

$$\bar{\mathbf{h}}_k^{(u)} = \mathbf{F}_N \cdot \mathbf{h}_k^{(u)} \quad (2.31)$$

leads to a vector  $\bar{\mathbf{h}}_k^{(u)} = [\bar{h}_{k,0}^{(u)}, \dots, \bar{h}_{k,N-1}^{(u)}]^T$  containing  $N$  time-variant coefficients of the channel transfer function.

## 2.4 IFDMA Receiver

### 2.4.1 Receiver Model

In this section, a model is presented for the receiver of the mobile communication system that has been introduced in Section 2.2.

In Figure 2.8, the block diagram that has already been presented in Figure 2.1 for the transmitter of the mobile communication system is expanded by the mobile radio channel and the receiver part located at a base station of the mobile communication system. The signal that has been transmitted over the mobile radio channel and distorted by Additive White Gaussian Noise (AWGN) undergoes a radio frequency processing at the receiver where the center frequency of the signal is converted from the carrier frequency to the baseband. After digital to analog (D/A) conversion, the pulse shaping window is removed and signal parts related to the same IFDMA symbol are processed in parallel afterwards. The cyclic prefix is removed and the received IFDMA symbol is demodulated. Then, the demodulated data symbols are fed into an equalizer where the channel influence is reduced. Finally, after a parallel to serial (P/S) conversion, the equalized data symbols are demapped, decoded and deinterleaved and the received data bits are fed into the data sink.

### 2.4.2 IFDMA Signal Demodulation in Frequency Domain

In this section, the influence of the mobile radio channel on the transmitted IFDMA signal is explained and the received discrete-time IFDMA signal at the base station is derived. Further, a discrete-time model for the IFDMA signal demodulation part that is highlighted by the dotted box in Figure 2.8 is presented. The IFDMA signal demodulation is given in frequency domain which represents the description corresponding to the IFDMA signal generation in Section 2.2.2.

In Figure 2.9, the IFDMA signal demodulation is embedded in the discrete-time transmission chain illustrating the IFDMA signal generation at the transmitter, cf. Section 2.2.2, the transmission over the mobile radio channel, distortion by AWGN and the IFDMA signal demodulation at the receiver. In the following, the focus is on the receiver part in Figure 2.9. Further on, optimum frequency and time synchronisation between mobile station and base station is assumed.

The IFDMA symbol  $\tilde{\mathbf{x}}_k^{(u)}$  with cyclic prefix that is received after transmission over the mobile radio channel with impulse response vector  $\mathbf{h}_k^{(u)}$  and distortion by the AWGN vector  $\tilde{\mathbf{v}}_k^{(u)} = [\nu_{k,0}^{(u)}, \dots, \nu_{k,N+N_G-1}^{(u)}]$ , whose elements have the average power  $\sigma_v^2$ , is denoted by

$$\tilde{\mathbf{r}}_k^{(u)} = \left[ r_{k,0}^{(u)}, \dots, r_{k,N+N_G-1}^{(u)} \right]^T. \quad (2.32)$$

Due to cyclic prefix insertion, the interference between successively transmitted IFDMA symbols is avoided and the transmission over the channel can be explained for a single

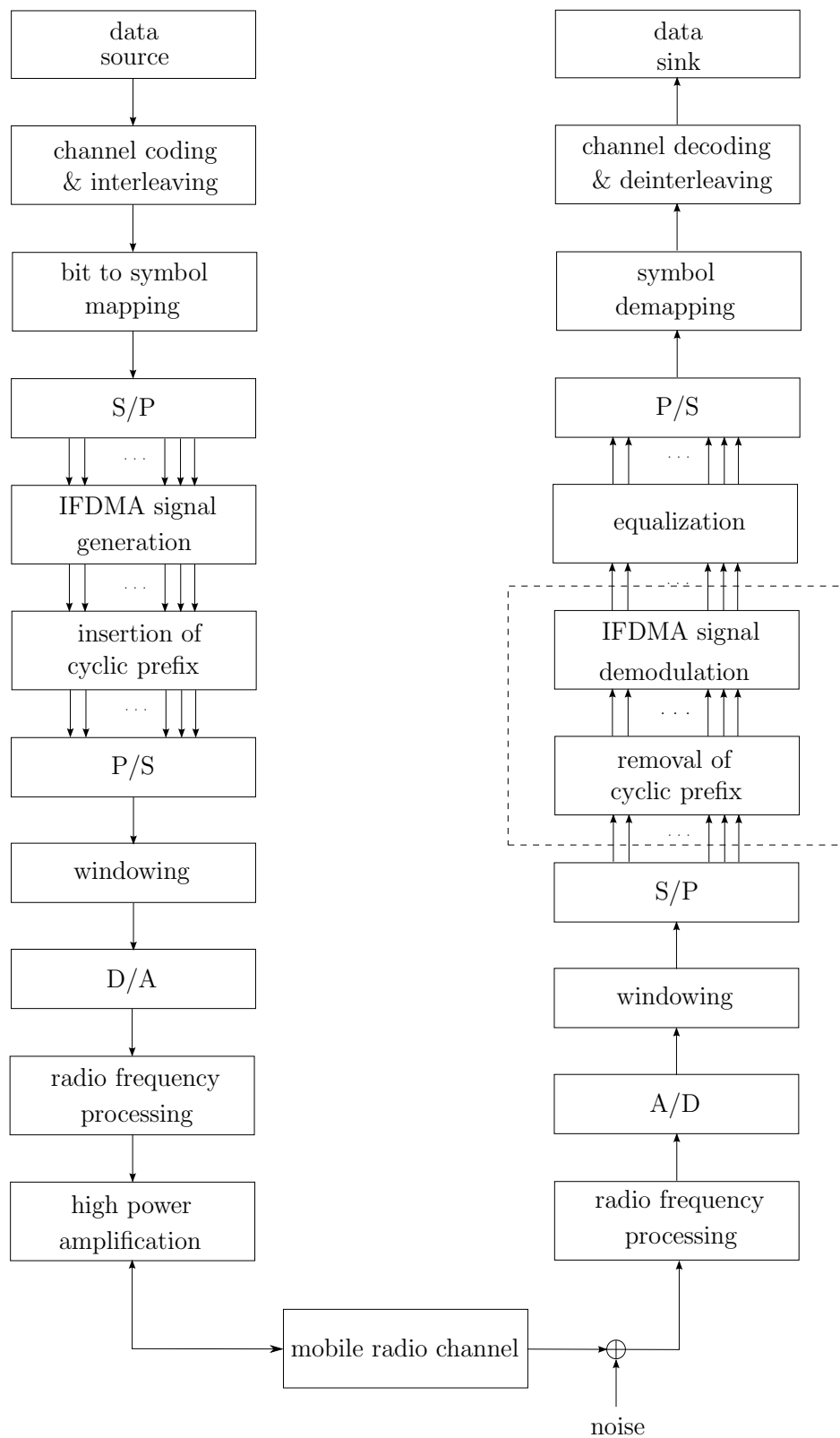


Figure 2.8. Block diagram for transmitter, channel and receiver in the mobile communication system



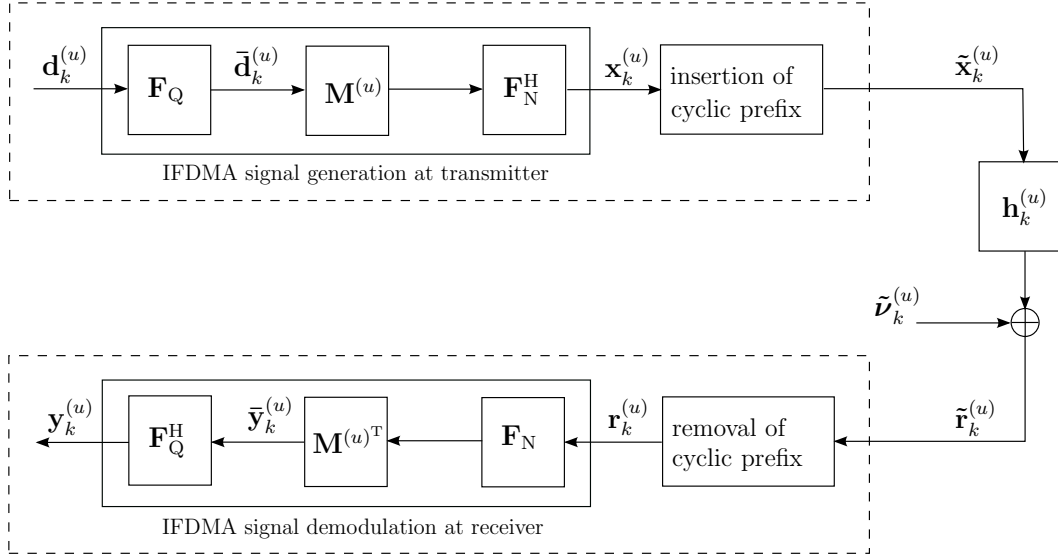


Figure 2.9. Discrete-time transmission chain

IFDMA symbol with index  $k$  independently from the other IFDMA symbols. At the receiver, the cyclic prefix part of  $\tilde{\mathbf{r}}_k^{(u)}$  is discarded and

$$\mathbf{r}_k^{(u)} = \left[ r_{k,N_G}^{(u)}, \dots, r_{k,N+N_G-1}^{(u)} \right]^T \quad (2.33)$$

denotes the received IFDMA symbol.

$\mathbf{r}_k^{(u)}$  can be described as a function of the transmitted IFDMA symbol  $\mathbf{x}_k^{(u)}$ , the mobile radio channel with impulse response vector  $\mathbf{h}_k^{(u)}$  and the AWGN vector  $\boldsymbol{\nu}_k^{(u)} = [\nu_{k,N_G}^{(u)}, \dots, \nu_{k,N+N_G-1}^{(u)}]^T$ . With  $\mathbf{H}_k^{(u)}$  the  $N \times N$  right circulant matrix having  $\mathbf{h}_k^{(u)}$  as its first column, the received IFDMA symbol  $\mathbf{r}_k^{(u)}$  is given by

$$\mathbf{r}_k^{(u)} = \mathbf{H}_k^{(u)} \cdot \mathbf{x}_k^{(u)} + \boldsymbol{\nu}_k^{(u)} \quad (2.34)$$

[WG00, FKCS05b]. With the help of Eq. (2.5),  $\mathbf{r}_k^{(u)}$  is described as a function of the transmitted data symbols  $\mathbf{d}_k^{(u)}$  according to

$$\mathbf{r}_k^{(u)} = \mathbf{H}_k^{(u)} \cdot \mathbf{F}_N^H \cdot \mathbf{M}^{(u)} \cdot \mathbf{F}_Q \cdot \mathbf{d}_k^{(u)} + \boldsymbol{\nu}_k^{(u)}. \quad (2.35)$$

The demodulation of  $\mathbf{r}_k^{(u)}$  is performed by the application of an  $N$ -point DFT matrix  $\mathbf{F}_N$ , the demapping matrix  $\mathbf{M}^{(u)T}$  and a  $Q$ -point IDFT matrix  $\mathbf{F}_Q^H$  and, thus, the demodulated IFDMA symbol  $\mathbf{y}_k^{(u)}$  is calculated by

$$\begin{aligned} \mathbf{y}_k^{(u)} &= \mathbf{F}_Q^H \cdot \mathbf{M}^{(u)T} \cdot \mathbf{F}_N \cdot \mathbf{r}_k^{(u)} \\ &= \mathbf{F}_Q^H \cdot \mathbf{M}^{(u)T} \cdot \mathbf{F}_N \cdot \mathbf{H}_k^{(u)} \cdot \mathbf{F}_N^H \cdot \mathbf{M}^{(u)} \cdot \mathbf{F}_Q \cdot \mathbf{d}_k^{(u)} + \mathbf{F}_Q^H \cdot \mathbf{M}^{(u)T} \cdot \mathbf{F}_N \cdot \boldsymbol{\nu}_k^{(u)} \end{aligned} \quad (2.36)$$

[FKCS05b]. For  $k = 0, \dots, K-1$  and  $q = 0, \dots, Q-1$ , let the elements  $c_{k,q}^{(u)}$  be calculated based on the elements  $h_{k,n}^{(u)}$ ,  $n = 0, \dots, N-1$ , of the channel impulse response vector according to

$$c_{k,q}^{(u)} = \sum_{i=0}^{L_U-1} h_{k,iQ+q}^{(u)} \cdot e^{j \cdot \frac{2\pi}{N} \cdot u \cdot (i \cdot Q + q)} \quad (2.37)$$

[SDB98]. Then, the matrix

$$\mathcal{H}_k^{(u)} = \mathbf{F}_Q^H \cdot \mathbf{M}^{(u)T} \cdot \mathbf{F}_N \cdot \mathbf{H}_k^{(u)} \cdot \mathbf{F}_N^H \cdot \mathbf{M}^{(u)} \cdot \mathbf{F}_Q \quad (2.38)$$

refers to a  $Q \times Q$  right circulant matrix having the vector  $\mathbf{c}_k^{(u)} = [c_{k,0}^{(u)}, \dots, c_{k,Q-1}^{(u)}]^T$  as its first column [FKCS05b]. The elements  $c_{k,q}^{(u)}$  are referred to as the elements of the cyclic channel impulse response in the remainder of the thesis. The noise vector after IFDMA signal demodulation is calculated by

$$\mathbf{v}_k^{(u)} = \mathbf{F}_Q^H \cdot \mathbf{M}^{(u)T} \cdot \mathbf{F}_N \cdot \boldsymbol{\nu}_k^{(u)}. \quad (2.39)$$

According to [SDB98], the elements of  $\mathbf{v}_k^{(u)}$  represent a white noise process. With Eq. (2.38) and (2.39), the demodulated IFDMA symbol  $\mathbf{y}_k^{(u)}$  is described in dependency of  $\mathbf{v}_k^{(u)}$  and the matrix  $\mathcal{H}_k^{(u)}$  containing the elements of the cyclic channel impulse response according to

$$\mathbf{y}_k^{(u)} = \mathcal{H}_k^{(u)} \cdot \mathbf{d}_k^{(u)} + \mathbf{v}_k^{(u)}. \quad (2.40)$$

For channel estimation and equalization purposes, the demodulated IFDMA symbol  $\mathbf{y}_k^{(u)}$  is considered in frequency domain. The demodulated IFDMA symbol  $\bar{\mathbf{y}}_k^{(u)}$  in frequency domain is given by

$$\begin{aligned} \bar{\mathbf{y}}_k^{(u)} &= \mathbf{F}_Q \cdot \mathbf{y}_k^{(u)} \\ &= \mathbf{F}_Q \cdot \mathcal{H}_k^{(u)} \cdot \mathbf{d}_k^{(u)} + \mathbf{F}_Q \cdot \mathbf{v}_k^{(u)}. \end{aligned} \quad (2.41)$$

In [GvL96], it has been shown that pre-multiplication with a  $Q \times Q$  DFT matrix and post-multiplication with a  $Q \times Q$  IDFT matrix of a  $Q \times Q$  circulant matrix  $\mathcal{H}_k^{(u)}$  leads to a diagonalized matrix. Thus, according to [GvL96],

$$\bar{\mathcal{H}}_k^{(u)} = \mathbf{F}_Q \cdot \mathcal{H}_k^{(u)} \cdot \mathbf{F}_Q^H \quad (2.42)$$

is a  $Q \times Q$  diagonal matrix having the vector

$$\bar{\mathbf{c}}_k^{(u)} = \mathbf{F}_Q \cdot \mathbf{c}_k^{(u)} = [\bar{c}_{k,0}^{(u)}, \dots, \bar{c}_{k,Q-1}^{(u)}]^T \quad (2.43)$$

as its main diagonal.

Under consideration of Eq. (2.42), Eq. (2.41) can be rewritten according to

$$\begin{aligned}\bar{\mathbf{y}}_k^{(u)} &= \mathbf{F}_Q \cdot \mathcal{H}_k^{(u)} \cdot \mathbf{F}_Q^H \cdot \mathbf{F}_Q \cdot \mathbf{d}_k^{(u)} + \mathbf{F}_Q \cdot \mathbf{v}_k^{(u)} \\ &= \bar{\mathcal{H}}_k^{(u)} \cdot \bar{\mathbf{d}}_k^{(u)} + \bar{\mathbf{v}}_k^{(u)}\end{aligned}\quad (2.44)$$

which shows that due to cyclic prefix insertion the transmission of an IFDMA symbol over a multipath channel can be described in frequency domain by the multiplication of the DFT elements  $\bar{d}_{k,q}$ ,  $q = 0, \dots, Q-1$ , transmitted on each allocated subcarrier with one complex channel coefficient  $\bar{c}_{k,q}^{(u)}$ . That means, in frequency domain, each subcarrier is affected by a flat fading channel that can be described by the complex factor  $\bar{c}_{k,q}^{(u)}$  which is denoted as the  $q^{\text{th}}$  channel transfer factor corresponding to the subcarrier with index  $q \cdot L_U + u$  and the IFDMA symbol with index  $k$  in the following. The  $q^{\text{th}}$  channel transfer factor is given by the  $(q \cdot L_U + u)^{\text{th}}$  element of the vector  $\bar{\mathbf{h}}_k^{(u)}$  which contains the  $N$  channel transfer factors  $\bar{h}_{k,n}^{(u)}$ ,  $n = 0, \dots, N-1$ , corresponding to all subcarriers in the system. Thus, the channel transfer factors corresponding to the  $Q$  subcarriers allocated to a user are specified according to

$$\bar{c}_{k,q}^{(u)} = \bar{h}_{k,q \cdot L_U + u}^{(u)}, \quad q = 0, \dots, Q-1. \quad (2.45)$$

Eq. (2.44) shows that due to cyclic prefix insertion, the interference between the  $Q$  subcarriers allocated to a certain user is avoided. Moreover, for  $U \leq L_U$ , the signals transmitted by different users maintain their orthogonality even for transmission over a multipath channel [SDBS98].

According to Eq. (2.44), an estimate of the transmitted data symbols  $\mathbf{d}_k^{(u)}$  can be obtained if the matrix  $\bar{\mathcal{H}}_k^{(u)}$  and, thus, the  $Q$  channel transfer factors  $\bar{c}_{k,q}^{(u)}$  are known at the receiver. Then, the equalizer compensates the channel influence on the demodulated IFDMA symbols  $\bar{\mathbf{y}}_k^{(u)}$ ,  $k = 0, \dots, K-1$ , in frequency domain and the transmitted data symbols can be estimated. In a practical system, the channel transfer factors  $\bar{c}_{k,q}^{(u)}$  are unknown and, thus, estimates have to be utilized for equalization. The estimation of the  $Q$  channel transfer factors is addressed in the remainder of this thesis.



## Chapter 3

# Pilot Assisted Channel Estimation for IFDMA

### 3.1 Introduction

In this chapter, pilot assisted channel estimation is presented for IFDMA. In order to obtain an estimate of the channel variations in frequency and time domain, pilot symbols are inserted into the data stream, transmitted over the mobile radio channel and analyzed at the receiver.

In Section 2.4, it has been explained that, due to cyclic prefix insertion, the channel influence on the IFDMA symbol can be fully described by the channel transfer factors corresponding to the  $Q$  allocated subcarriers. Therefore, in this chapter, the channel transfer factors corresponding to the  $Q$  allocated subcarriers are estimated by the application of a channel estimation algorithm in frequency domain and the channel transfer factors of the remaining subcarriers in the system are disregarded for channel estimation. The estimation of the  $Q$  channel transfer factors is preferred to the estimation of the  $L_C$  channel delay taps as the channel transfer factors are required for equalization purposes. The  $Q$  channel transfer factors, representing the frequency domain channel variations, are estimated based on a single IFDMA symbol. As the channel transfer factors are varying with time, the time variations of the channel transfer factors, representing the time domain channel variations, are estimated in a second step under consideration of multiple IFDMA symbols. This procedure is equivalent to a two times one-dimensional channel estimation [HKR97b].

In Section 3.2, the estimation of the frequency domain channel variations is presented for a single IFDMA symbol. For this purpose, assuming the mobile radio channel to be time invariant at least for the duration of an IFDMA symbol, a single IFDMA symbol is considered for the insertion of pilot symbols and the analysis of the pilot symbols at the receiver. In this context, two different possibilities of pilot insertion and the corresponding estimation algorithms are introduced where each of these two methods fulfills the requirements of a low PAPR of the transmit signal and a low pilot symbol overhead to a different extent. Thereafter, in Section 3.3, the estimation of the time domain channel variations is presented. Here, the pilot insertion methods proposed in Section 3.2 are utilized to transmit pilot symbols within multiple IFDMA symbols and

estimate the channel variations in frequency domain for multiple IFDMA symbols. By applying an interpolation filter in time domain, the channel variations in time domain are estimated in addition to the channel variations in frequency domain. In Section 3.4, the presented pilot insertion methods and estimation algorithms are compared in terms of the influence on the PAPR of the IFDMA transmit signal, the pilot symbol overhead consumption, the MSE between the true channel transfer function and the estimated channel transfer function and the computational complexity. The main conclusions of this chapter are drawn in Section 3.5. Several parts of this Chapter 3 have been originally published by the author in [SFK06,SK07].

## 3.2 Estimation of Frequency Domain Channel Variations

### 3.2.1 Introduction

In this section, the pilot assisted estimation of the channel variations in frequency domain is presented. For this purpose, pilot symbols are inserted within a single IFDMA symbol at the transmitter and a channel estimation algorithm is applied at the receiver. The insertion of pilot symbols within a single IFDMA symbol and the corresponding channel estimation algorithm is introduced under consideration of the following requirements:

- The low PAPR of the IFDMA transmit signal shall be maintained after the insertion of pilot symbols.
- The pilot insertion method and the corresponding channel estimation algorithm shall provide satisfying estimation performance while consuming low pilot symbol overhead and while supporting the transmission of variable data rates. A high pilot symbol overhead shall be avoided as the energy that is spent for the transmission of pilot symbols remains unavailable for the transmission of data symbols.

The pilot symbols used in this thesis are taken from a Constant Amplitude Zero Autocorrelation (CAZAC) sequence [BC02]. These sequences show favorable properties in terms of channel estimation purposes, such as a low PAPR in time domain and a uniformly distributed power spectral density. Due to the uniformly distributed

power in frequency domain, the estimation exhibits comparable performance for the total available bandwidth in the system and the estimation error is independent of the frequency [Pop92]. Throughout the section, the insertion of pilot symbols is explained based on the IFDMA signal generation in frequency domain presented in Section 2.2.2, due to the simplicity of this model. The inserted pilot symbols are utilized to estimate the  $Q$  channel transfer factors corresponding to the allocated subcarriers.

In the following, two pilot insertion methods are introduced. For each of these two methods, the signal generation for pilot insertion and the algorithm for estimating the channel variations in frequency domain are explained.

### 3.2.2 Symbolwise Pilot Insertion

#### 3.2.2.1 Signal Generation

In this section, the IFDMA signal generation is presented for symbolwise pilot insertion.

For symbolwise pilot insertion, the IFDMA symbol with index  $k = \kappa$  is used to transmit pilot symbols instead of data symbols. In Figure 3.1, the IFDMA signal generation with symbolwise pilot insertion is illustrated in a block diagram. For  $k \neq \kappa$ , the switch  $A$  is in the upper position and the vector  $\mathbf{d}_k^{(u)}$  containing data symbols is modulated according to Eq. (2.5) and (2.6). For  $k = \kappa$ , pilot symbols are inserted into the IFDMA signal and the switch  $A$  is in the lower position. The vector  $\boldsymbol{\rho}^{(u)}$  containing the sequence of pilot symbols in time domain is the input of the block diagram.  $\boldsymbol{\rho}^{(u)}$  is given by

$$\boldsymbol{\rho}^{(u)} = [\rho_0^{(u)}, \dots, \rho_{Q_P-1}^{(u)}]^T \quad (3.1)$$

and consists of  $Q_P = Q$  complex values which are taken from a CAZAC sequence and have an average power  $E\{|\rho_{q_P}^{(u)}|^2\} = \sigma_P^2$ ,  $q_P = 0, \dots, Q - 1$ . In order to maintain the orthogonality of the  $U$  users' signals, the sequence  $\boldsymbol{\rho}^{(u)}$  of pilot symbols is processed in analogy to the IFDMA signal generation explained in Section 2.2.2. By doing so, the elements of  $\boldsymbol{\rho}^{(u)}$  are transmitted on the  $Q$  subcarriers that are allocated to the user under consideration. With  $\mathbf{M}^{(u)}$  the mapping matrix with elements as defined in Eq. (2.4), the IFDMA modulated pilot sequence  $\mathbf{p}^{(u)}$  in discrete-time is calculated according to

$$\mathbf{p}^{(u)} = \mathbf{F}_N^H \cdot \mathbf{M}^{(u)} \cdot \mathbf{F}_Q \cdot \boldsymbol{\rho}^{(u)}. \quad (3.2)$$

The frequency domain representation of the modulated pilot sequence  $\mathbf{p}^{(u)}$  is given by the vector  $\bar{\mathbf{p}}^{(u)}$  that is calculated according to

$$\bar{\mathbf{p}}^{(u)} = \mathbf{F}_N \cdot \mathbf{p}^{(u)} = [\bar{p}_0^{(u)}, \dots, \bar{p}_{N-1}^{(u)}]^T. \quad (3.3)$$

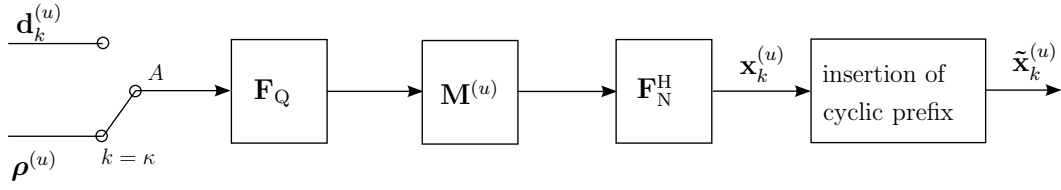


Figure 3.1. Block diagram of IFDMA signal generation with symbolwise pilot insertion and cyclic prefix insertion.

With the DFT elements  $\bar{\rho}_{q_P}^{(u)}$ ,  $q_P = 0, \dots, Q - 1$ , of  $\boldsymbol{\rho}^{(u)}$  that are calculated according to

$$\bar{\boldsymbol{\rho}}^{(u)} = \mathbf{F}_Q \cdot \boldsymbol{\rho}^{(u)} = [\bar{\rho}_0^{(u)}, \dots, \bar{\rho}_{Q-1}^{(u)}]^T, \quad (3.4)$$

the elements  $\bar{p}_n^{(u)}$ ,  $n = 0, \dots, N - 1$ , of the frequency domain vector  $\bar{\mathbf{p}}^{(u)}$  are given by

$$\bar{p}_n^{(u)} = \begin{cases} \bar{\rho}_{q_P}^{(u)} & \text{for } n = q_P \cdot L_U + u, \\ 0 & \text{else.} \end{cases} \quad (3.5)$$

That means, the elements  $\bar{\rho}_{q_P}^{(u)}$ ,  $q_P = 0, \dots, Q - 1$ , are transmitted on the allocated subcarriers with indices  $q_P \cdot L_U + u$  after IFDMA modulation.

The modulated pilot sequence  $\mathbf{p}^{(u)}$  is transmitted within the IFDMA symbol with index  $k = \kappa$  and, thus, the  $\kappa^{\text{th}}$  IFDMA symbol is given by

$$\mathbf{x}_\kappa^{(u)} = \mathbf{p}^{(u)}. \quad (3.6)$$

As explained in Eq. (2.6),  $\mathbf{x}_\kappa^{(u)}$  is preceded by a cyclic prefix with  $N_G$  elements and, finally,  $\tilde{\mathbf{x}}_\kappa^{(u)}$  denoting the  $\kappa^{\text{th}}$  IFDMA symbol with cyclic prefix is transmitted over the mobile radio channel.

Due to the described symbolwise pilot insertion, the pilot symbols are orthogonal to the data symbols of the considered user and to the IFDMA signals of other users in the system. This orthogonality is kept after transmission over a multipath channel and, thus, the channel transfer factors can be estimated without influences caused by the data symbols of the considered user or the IFDMA signals transmitted by other users in the system.

As for symbolwise pilot insertion, the sequence of pilot symbols is processed in analogy to the IFDMA signal generation explained in Section 2.2, the modulated pilot sequence  $\mathbf{p}^{(u)}$  can also be expressed by compression, repetition and phase shifting of the sequence  $\boldsymbol{\rho}^{(u)}$ . Therefore, the PAPR of  $\mathbf{p}^{(u)}$  is given by the PAPR of the sequence  $\boldsymbol{\rho}^{(u)}$  of pilot symbols itself. The sequence  $\boldsymbol{\rho}^{(u)}$  consists of elements that are taken from a CAZAC sequence and, thus, the PAPR is small for symbolwise pilot insertion. As for symbolwise pilot insertion, each allocated subcarrier of the IFDMA symbol with index  $\kappa$  is used for pilot transmission, this IFDMA symbol remains unused for data transmission.



### 3.2.2.2 Estimation Algorithm

In this section, the channel estimation algorithm for the symbolwise pilot insertion method is explained. In Figure 3.2, the block diagram presented in Figure 3.1 is extended by the receiver part containing the analysis of the transmitted pilot symbols.

The IFDMA symbol  $\tilde{\mathbf{x}}_k^{(u)}$  with cyclic prefix is transmitted over the mobile radio channel with the channel impulse response given by the vector  $\mathbf{h}_k^{(u)}$ . As already explained in Section 2.4, the cyclic prefix is removed at the receiver and, subsequently, an  $N \times N$  DFT matrix  $\mathbf{F}_N$  is applied prior to the subcarrier demapping that is realized by the application of the demapping matrix  $\mathbf{M}^{(u)\text{T}}$ . For  $k \neq \kappa$ , the switch  $B$  is in the upper position and the received IFDMA symbols containing data symbols are demodulated according to Eq. (2.36). For  $k = \kappa$ , the switch  $B$  is in the lower position and the received IFDMA symbol containing the pilot symbols is processed. With Eq. (2.36) and (2.41), the values that are received on the  $Q$  allocated subcarriers in frequency domain within the IFDMA symbol with index  $\kappa$  can be expressed by

$$\begin{aligned}\bar{\mathbf{y}}_\kappa^{(u)} &= \mathbf{M}^{(u)\text{T}} \cdot \mathbf{F}_N \cdot \mathbf{r}_\kappa^{(u)} \\ &= \mathbf{M}^{(u)\text{T}} \cdot \mathbf{F}_N \cdot \mathbf{H}_\kappa^{(u)} \cdot \mathbf{F}_N^H \cdot \mathbf{M}^{(u)} \cdot \bar{\boldsymbol{\rho}}^{(u)} + \mathbf{M}^{(u)\text{T}} \cdot \mathbf{F}_N \cdot \boldsymbol{\nu}_\kappa^{(u)}\end{aligned}\quad (3.7)$$

With Eq. (2.38) in Eq. (2.42) and under consideration of Eq. (2.39), the vector  $\bar{\mathbf{y}}_\kappa^{(u)}$  is given by

$$\bar{\mathbf{y}}_\kappa^{(u)} = \bar{\mathcal{H}}_\kappa^{(u)} \cdot \bar{\boldsymbol{\rho}}^{(u)} + \bar{\mathbf{v}}_\kappa^{(u)}. \quad (3.8)$$

Let  $\text{diag}\{\bar{\boldsymbol{\rho}}^{(u)}\}$  denote a  $Q \times Q$  diagonal matrix having the vector  $\bar{\boldsymbol{\rho}}^{(u)}$  as its main diagonal. Then, with Eq. (2.42) and (2.43), Eq. (3.8) can be rewritten according to

$$\bar{\mathbf{y}}_\kappa^{(u)} = \text{diag}\{\bar{\boldsymbol{\rho}}^{(u)}\} \cdot \bar{\mathbf{c}}_\kappa^{(u)} + \bar{\mathbf{v}}_\kappa^{(u)}. \quad (3.9)$$

Eq. (3.9) is an expression for the values that are received on the  $Q$  allocated subcarriers in frequency domain within the IFDMA symbol with index  $\kappa$  in dependency of the vector  $\bar{\mathbf{c}}_\kappa^{(u)}$  containing the channel transfer factors corresponding to the subcarriers with indices  $q_P \cdot L_U + u$ ,  $q_P = 0, \dots, Q - 1$ . The vector  $\bar{\mathbf{v}}_\kappa^{(u)}$  is given by

$$\bar{\mathbf{v}}_\kappa^{(u)} = \mathbf{M}^{(u)\text{T}} \cdot \mathbf{F}_N \cdot \boldsymbol{\nu}_\kappa^{(u)} \quad (3.10)$$

and contains the AWGN in frequency domain since  $\mathbf{M}^{(u)\text{T}}$  and  $\mathbf{F}_N$  are linear operations. Then, the Minimum Variance Unbiased (MVU) estimate  $\hat{\bar{\mathbf{c}}}_\kappa^{(u)}$  of the vector  $\bar{\mathbf{c}}_\kappa^{(u)}$  is calculated by a Least Square (LS) estimator [Kay93] and is given by

$$\hat{\bar{\mathbf{c}}}_\kappa^{(u)} = \text{diag}\{\bar{\boldsymbol{\rho}}^{(u)}\}^{-1} \cdot \bar{\mathbf{y}}_\kappa^{(u)}. \quad (3.11)$$

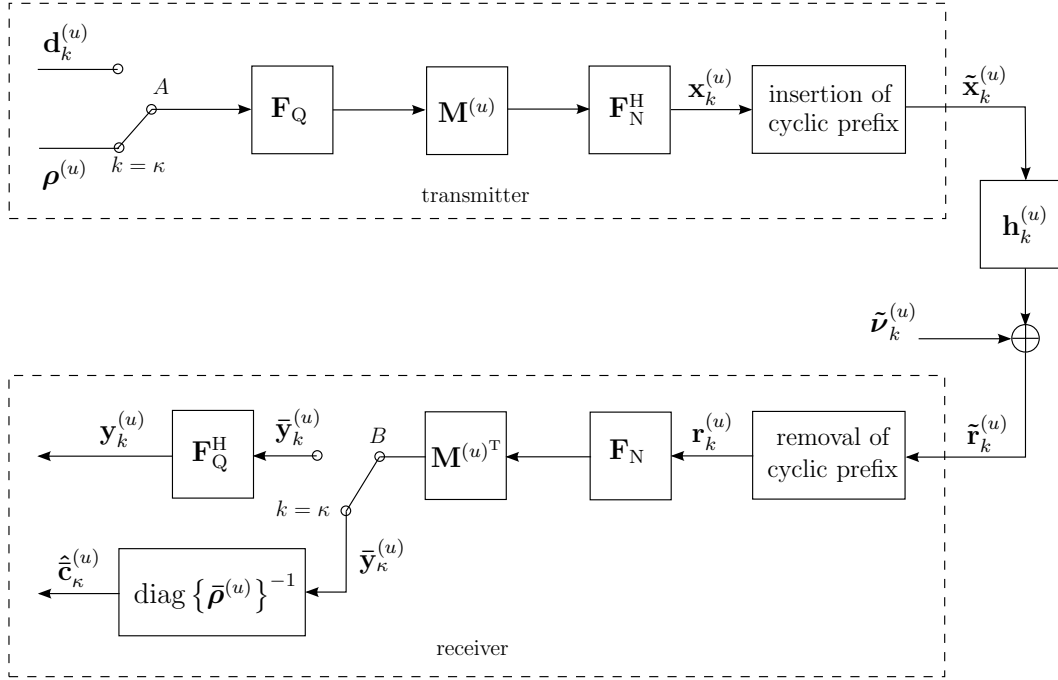


Figure 3.2. Block diagram of transmission chain with symbolwise pilot insertion at the transmitter and LS channel estimation for each allocated subcarrier at the receiver.

Thus, for symbolwise pilot insertion, the  $Q$  channel transfer factors are estimated by an LS estimation for each allocated subcarrier. With Eq. (3.9) in Eq. (3.11), it can be stated that the estimated vector  $\hat{\mathbf{c}}_\kappa^{(u)}$  is composed of the true vector  $\bar{\mathbf{c}}_\kappa^{(u)}$  and a noise term according to

$$\hat{\mathbf{c}}_\kappa^{(u)} = \bar{\mathbf{c}}_\kappa^{(u)} + \text{diag}\{\bar{\rho}^{(u)}\}^{-1} \cdot \bar{\mathbf{v}}_\kappa^{(u)}. \quad (3.12)$$

In the remainder of the thesis, the symbolwise pilot insertion with LS estimation on each allocated subcarrier is shortly denoted as symbolwise LS.

### 3.2.3 Subcarrierwise Pilot Insertion

#### 3.2.3.1 Signal Generation

In this section, the IFDMA signal generation is presented for subcarrierwise pilot insertion.

For subcarrierwise pilot insertion, a subset of  $Q_P$  subcarriers out of the total number  $Q$  of subcarriers allocated to a certain user in the IFDMA symbol with index  $k = \kappa$  is utilized for pilot transmission. The remaining  $Q_D = Q - Q_P$  subcarriers are exploited for

transmitting data symbols within the  $\kappa^{\text{th}}$  IFDMA symbol. That means, pilot and data symbols are multiplexed within the IFDMA symbol with index  $k = \kappa$ . In Figure 3.3, the IFDMA signal generation with subcarrierwise pilot insertion is presented in a block diagram. For  $k \neq \kappa$ , the switch  $A$  is in the upper position and the vector  $\mathbf{d}_k^{(u)}$  containing data symbols is modulated according to Eq. (2.5) and (2.6). For  $k = \kappa$ , switch  $A$  is in the lower position. Then, the sequence  $\boldsymbol{\rho}^{(u)} = [\rho_0^{(u)}, \dots, \rho_{Q_P-1}^{(u)}]^T$  of  $Q_P$  pilot symbols which are taken from a CAZAC sequence and have an average power  $E\{|\rho_{q_P}^{(u)}|^2\} = \sigma_P^2$ ,  $q_P = 0, \dots, Q_P - 1$ , and the sequence  $\boldsymbol{\delta}_\kappa^{(u)} = [d_{\kappa,0}^{(u)}, \dots, d_{\kappa,Q_D-1}^{(u)}]^T$  of data symbols with average power  $E\{|d_{\kappa,q_D}^{(u)}|^2\} = \sigma_D^2$ ,  $q_D = 0, \dots, Q_D - 1$ , are processed in parallel.

The vector  $\boldsymbol{\rho}^{(u)}$  containing the sequence of pilot symbols in time domain is multiplied by a  $Q_P \times Q_P$  DFT matrix  $\mathbf{F}_{Q_P}$ . The resulting vector  $\bar{\boldsymbol{\rho}}^{(u)}$  containing the frequency domain representation of the pilot symbols is given by

$$\bar{\boldsymbol{\rho}}^{(u)} = \mathbf{F}_{Q_P} \cdot \boldsymbol{\rho}^{(u)} = [\bar{\rho}_0^{(u)}, \dots, \bar{\rho}_{Q_P-1}^{(u)}]^T. \quad (3.13)$$

The elements  $\bar{\rho}_{q_P}^{(u)}$ ,  $q_P = 0, \dots, Q_P - 1$ , are mapped onto a subset consisting of  $Q_P$  equidistantly spaced subcarriers out of the total number  $Q$  of subcarriers allocated to the user. The number  $Q_P$  of subcarriers that are used for pilot transmission is calculated by

$$Q_P = \frac{Q}{I}, \quad (3.14)$$

where  $I$  denotes the interpolation depth in frequency domain and is chosen such that  $Q_P \in \mathbb{Z}$ . That means, e.g. for  $I = 2$ , every second subcarrier that is allocated to a specific user is utilized for pilot transmission. The elements  $\bar{\rho}_{q_P}^{(u)}$ , with  $q_P = 0, \dots, Q_P - 1$ , are transmitted on subcarriers with indices

$$\eta(q_P) = q_P \cdot L_U \cdot I + u. \quad (3.15)$$

The subcarriers with indices  $\eta(q_P)$  for  $q_P = 0, \dots, Q_P - 1$  are denoted as the pilot carrying subcarriers in the following. The allocation of the elements  $\bar{\rho}_{q_P}^{(u)}$  to the  $Q_P$  pilot carrying subcarriers is performed by the application of the pilot mapping matrix  $\mathbf{M}_P^{(u)}$  whose elements  $[\mathbf{M}_P^{(u)}]_{n,q_P}$  for  $n = 0, \dots, N - 1$  and  $q_P = 0, \dots, Q_P - 1$  are given by

$$[\mathbf{M}_P^{(u)}]_{n,q_P} = \begin{cases} 1 & \text{for } n = \eta(q_P), \\ 0 & \text{else.} \end{cases} \quad (3.16)$$

Simultaneously, the vector  $\boldsymbol{\delta}_\kappa^{(u)}$  containing the data symbols is multiplied by a  $Q_D \times Q_D$  DFT matrix  $\mathbf{F}_{Q_D}$ . The resulting sequence  $\bar{\boldsymbol{\delta}}_\kappa^{(u)}$  of data symbols in frequency domain is given by

$$\bar{\boldsymbol{\delta}}_\kappa^{(u)} = \mathbf{F}_{Q_D} \cdot \boldsymbol{\delta}_\kappa^{(u)} = [\bar{d}_{\kappa,0}^{(u)}, \dots, \bar{d}_{\kappa,Q_D-1}^{(u)}]^T. \quad (3.17)$$

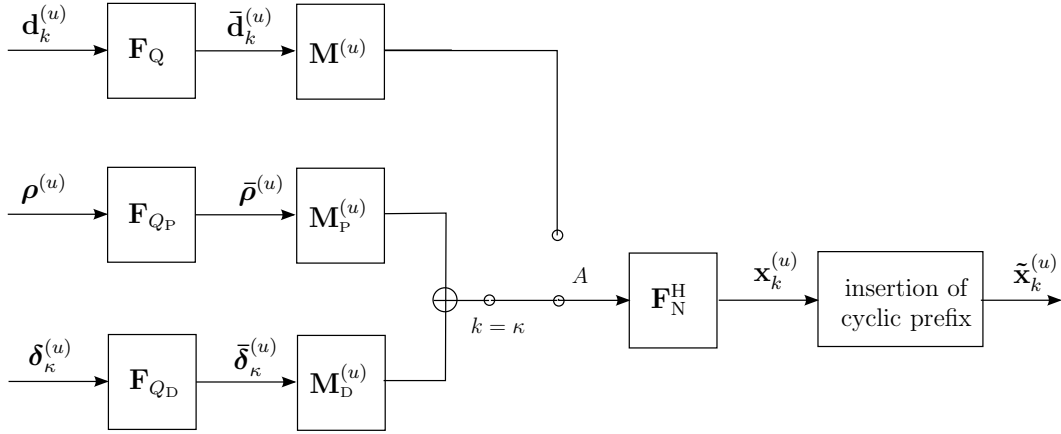


Figure 3.3. Block diagram of IFDMA signal generation with subcarrierwise pilot insertion and cyclic prefix insertion.

The elements  $\bar{d}_{\kappa,0}^{(u)}$ ,  $q_D = 0, \dots, Q_D - 1$ , are transmitted on the remaining  $Q_D$  subcarriers with indices

$$\zeta(q_D) = \left\lfloor \frac{q_D}{I-1} \right\rfloor \cdot L_U + L_U \cdot (q_D + 1) + u, \quad (3.18)$$

where  $\left\lfloor \frac{q_D}{I-1} \right\rfloor$  denotes the nearest integer which is smaller than or equal to  $\frac{q_D}{I-1}$ . The subcarriers with indices  $\zeta(q_D)$  for  $q_D = 0, \dots, Q_D - 1$  are denoted as the non-pilot carrying subcarriers in the following. The allocation of the elements  $\bar{d}_{\kappa,0}^{(u)}$ ,  $q_D = 0, \dots, Q_D - 1$ , to the remaining  $Q_D$  non-pilot carrying subcarriers is realized by the data mapping matrix  $\mathbf{M}_D^{(u)}$ . The elements  $[\mathbf{M}_D^{(u)}]_{n,q_D}$  for  $n = 0, \dots, N - 1$  and  $q_D = 0, \dots, Q_D - 1$  of the data mapping matrix  $\mathbf{M}_D^{(u)}$  are given by

$$[\mathbf{M}_D^{(u)}]_{n,q_D} = \begin{cases} 1 & \text{for } n = \zeta(q_D), \\ 0 & \text{else.} \end{cases} \quad (3.19)$$

The superposition of the mapped pilot and mapped data symbols is multiplied by an  $N \times N$  IDFT matrix  $\mathbf{F}_N^H$ . Then, the IFDMA symbol  $\mathbf{x}_\kappa^{(u)}$  containing pilot and data symbols is given by

$$\mathbf{x}_\kappa^{(u)} = \mathbf{F}_N^H \cdot \left( \mathbf{M}_P^{(u)} \cdot \mathbf{F}_{Q_P} \cdot \boldsymbol{\rho}^{(u)} + \mathbf{M}_D^{(u)} \cdot \mathbf{F}_{Q_D} \cdot \boldsymbol{\delta}_\kappa^{(u)} \right). \quad (3.20)$$

Finally,  $\mathbf{x}_\kappa^{(u)}$  is expanded by a cyclic prefix with  $N_G$  elements and the resulting IFDMA symbol with cyclic prefix  $\tilde{\mathbf{x}}_\kappa^{(u)}$  is transmitted over the mobile radio channel.

The described subcarrierwise pilot insertion allows the transmission of a variable number  $Q_P \leq Q$  of pilot symbols while maintaining mutual orthogonality between pilot and data symbols transmitted within the same IFDMA symbol as well as between the IFDMA signals transmitted by different users. This orthogonality is kept after

transmission over a multipath channel and, thus, the channel transfer factors can be estimated without influences caused by the data symbols transmitted within the same IFDMA symbol or the IFDMA signals transmitted by other users in the system.

According to Eq. (3.20), the transmitted IFDMA symbol  $\tilde{\mathbf{x}}_\kappa^{(u)}$  with cyclic prefix contains a superposition of the mapped pilot and the mapped data symbols. This superposition leads to an increase of the PAPR of the transmit symbol due to subcarrierwise pilot insertion. Therefore, the subcarrierwise pilot insertion method complies less with the requirement of a low PAPR than the symbolwise pilot insertion method. Based on the subcarrierwise pilot insertion method introduced by the author, further development with respect to PAPR reduction has been recently considered in [TYU09]. However, in terms of the pilot symbol overhead requirement, the subcarrierwise pilot insertion method entails the advantage of transmitting pilot and data symbols within the same IFDMA symbol which opens up the possibility to reduce the pilot symbol overhead compared to the symbolwise pilot insertion method.

### 3.2.3.2 Estimation Algorithm

In this section, the channel estimation algorithm is explained for the subcarrierwise pilot insertion method.

In Figure 3.4, the block diagram presented in Figure 3.3 is extended by the receiver part including the analysis of the received pilot symbols. At the receiver, the cyclic prefix is removed and the received IFDMA symbol  $\mathbf{r}_k^{(u)}$  is transformed into frequency domain by multiplication with the  $N \times N$  DFT matrix  $\mathbf{F}_N$ . For  $k \neq \kappa$ , the switch  $B$  is in the upper position and the demodulation of the received IFDMA symbols containing data symbols only is performed as explained in Eq. (2.36). At the output the demodulated IFDMA symbol  $\mathbf{y}_k^{(u)}$  is obtained. For  $k = \kappa$ , the switch  $B$  is in the lower position and the frequency domain representation of the received IFDMA symbol is processed in parallel for data demodulation and channel estimation. The data demodulation is performed by the multiplication with the transpose  $\mathbf{M}_D^{(u)\text{T}}$  of the data mapping matrix and subsequent multiplication with the  $Q_D \times Q_D$  IDFT matrix  $\mathbf{F}_{Q_D}^H$ . Let  $\mathbf{0}_{Q_D \times Q_P}$  denote a  $Q_D \times Q_P$  matrix containing all zero entries. Then in analogy to Eq. (2.36) and with

$$\mathbf{M}_D^{(u)\text{T}} \cdot \mathbf{M}_P^{(u)} = \mathbf{0}_{Q_D \times Q_P}, \quad (3.21)$$

the vector  $\mathbf{y}_\kappa^{(u)}$  containing the  $Q_D$  demodulated data symbols in the  $\kappa^{\text{th}}$  IFDMA symbol is calculated by

$$\mathbf{y}_\kappa^{(u)} = \mathbf{F}_{Q_D}^H \cdot \mathbf{M}_D^{(u)\text{T}} \cdot \mathbf{F}_N \cdot \mathbf{r}_\kappa^{(u)} \quad (3.22)$$

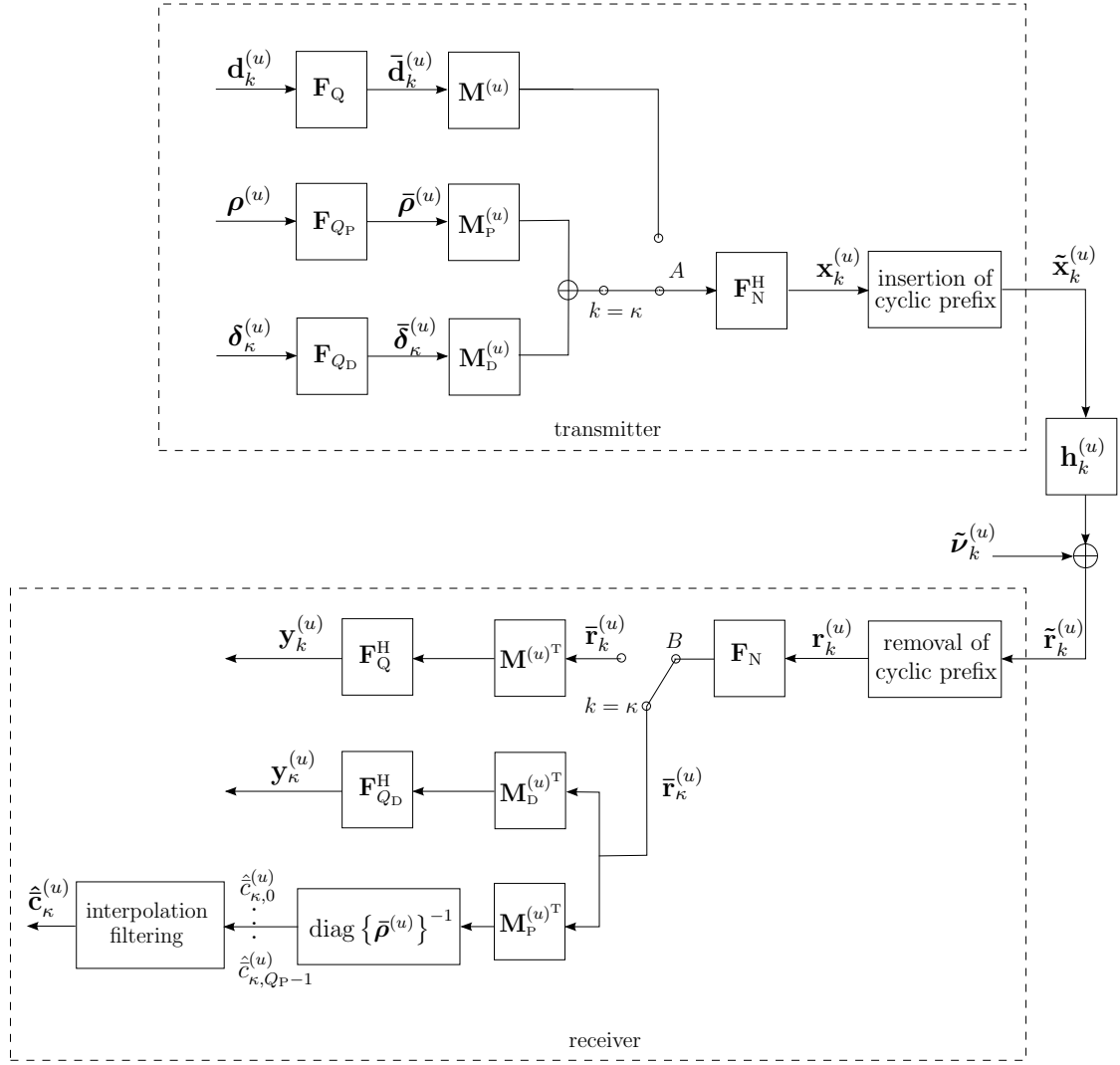


Figure 3.4. Block diagram of transmission chain with subcarrierwise pilot insertion at the transmitter and LS channel estimation with interpolation filtering at the receiver.

For channel estimation, the frequency domain representation of the received IFDMA symbol is multiplied by the transpose  $\mathbf{M}_P^{(u)T}$  of the pilot mapping matrix. Let  $\mathbf{0}_{Q_P \times Q_D}$  denote a  $Q_P \times Q_D$  matrix containing all zero entries. Then, with

$$\mathbf{M}_P^{(u)T} \cdot \mathbf{M}_D^{(u)} = \mathbf{0}_{Q_P \times Q_D} \quad (3.23)$$

and

$$\mathbf{r}_\kappa^{(u)} = \mathbf{H}_\kappa^{(u)} \cdot \mathbf{F}_N^H \cdot \left( \mathbf{M}_P^{(u)} \cdot \mathbf{F}_{Q_P} \cdot \boldsymbol{\rho}^{(u)} + \mathbf{M}_D^{(u)} \cdot \mathbf{F}_{Q_D} \cdot \boldsymbol{\delta}_\kappa^{(u)} \right) + \boldsymbol{\nu}_\kappa, \quad (3.24)$$

the channel transfer factors of the pilot carrying subcarriers with indices  $\eta(q_P)$ ,  $q_P = 0, \dots, Q_P - 1$ , in the IFDMA symbol with index  $\kappa$  are estimated by an LS estimation according to

$$\begin{bmatrix} \hat{c}_{\kappa,0}^{(u)} \\ \vdots \\ \hat{c}_{\kappa,Q_P-1}^{(u)} \end{bmatrix}^T = \text{diag} \{ \bar{\boldsymbol{\rho}}^{(u)} \}^{-1} \cdot \mathbf{M}_P^{(u)T} \cdot \mathbf{F}_N \cdot \mathbf{r}_\kappa^{(u)}. \quad (3.25)$$

With  $[\bar{v}_{\kappa,0}^{(u)}, \dots, \bar{v}_{\kappa,Q_P-1}^{(u)}]^T$  a vector containing the AWGN on each pilot carrying subcarrier in frequency domain, the vector of LS estimates in Eq. (3.25) can be expressed by

$$\begin{bmatrix} \hat{\bar{c}}_{\kappa,0}^{(u)}, \dots, \hat{\bar{c}}_{\kappa,Q_P-1}^{(u)} \end{bmatrix}^T = \begin{bmatrix} \bar{c}_{\kappa,0}^{(u)}, \dots, \bar{c}_{\kappa,Q_P-1}^{(u)} \end{bmatrix}^T + \text{diag} \{ \bar{\rho}^{(u)} \}^{-1} \cdot \begin{bmatrix} \bar{v}_{\kappa,0}^{(u)}, \dots, \bar{v}_{\kappa,Q_P-1}^{(u)} \end{bmatrix}^T. \quad (3.26)$$

The LS estimates  $\hat{\bar{c}}_{\kappa,q_P}^{(u)}$ ,  $q_P = 0, \dots, Q_P - 1$ , which correspond to the channel transfer factors of the pilot carrying subcarriers with the indices  $\eta(q_P)$  are exploited to get estimates  $\hat{\bar{c}}_{\kappa,q_D}^{(u)}$ ,  $q_D = 0, \dots, Q_D - 1$ , of the channel transfer factors of the remaining, non-pilot carrying subcarriers with indices  $\zeta(q_D)$ . For this purpose, a Wiener interpolation filter or a DFT interpolation filter can be utilized whose applications is explained in the following.

**Wiener interpolation filter** The Wiener interpolation filter is a Finite Impulse Response (FIR) filter with  $W$  filter coefficients that is applied to the LS estimates  $\hat{\bar{c}}_{\kappa,q_P}^{(u)}$ ,  $q_P = 0, \dots, Q_P - 1$ , in order to obtain estimates for the channel transfer factors corresponding to the non-pilot carrying subcarriers. The LS estimates obtained for the pilot carrying subcarriers are utilized as supporting points for the filtering process in frequency domain and, thus, the number  $W$  of filter coefficients is smaller than or equal to the number  $Q_P$  of pilot carrying subcarriers, i.e.  $W \leq Q_P$ . Let

$$\mathbf{b}_{q_D} = [b_{q_D,0}, \dots, b_{q_D,W-1}]^T \quad (3.27)$$

denote a vector containing  $W$  Wiener filter coefficients for filtering in frequency domain in order to obtain an estimate for the channel transfer factor corresponding to the non-pilot carrying subcarrier with index  $\zeta(q_D)$ . Let further  $[\hat{\bar{c}}_{\kappa,q_{D1}}^{(u)}, \dots, \hat{\bar{c}}_{\kappa,q_{DW}}^{(u)}]^T$  denote a vector containing  $W$  estimated channel transfer factors with indices  $q_{D1}, \dots, q_{DW}$ . These estimated channel transfer factors correspond to the pilot carrying subcarriers with indices  $\eta(q_{D1}), \dots, \eta(q_{DW})$  which specify the  $W$  nearest pilot carrying subcarriers with respect to the non-pilot carrying subcarrier with index  $\zeta(q_D)$  [San03]. Then, the channel transfer factor  $\bar{c}_{\kappa,q_D}^{(u)}$  of the subcarrier with index  $\zeta(q_D)$  is estimated by

$$\hat{\bar{c}}_{\kappa,q_D}^{(u)} = \mathbf{b}_{q_D}^T \cdot [\hat{\bar{c}}_{\kappa,q_{D1}}^{(u)}, \dots, \hat{\bar{c}}_{\kappa,q_{DW}}^{(u)}]^T \quad (3.28)$$

[HKR97b]. That means, an estimate of the channel transfer factor of the non-pilot carrying subcarrier with index  $\zeta(q_D)$  is obtained by filtering the estimated channel transfer factors of the  $W$  nearest pilot carrying subcarriers with respect to  $\zeta(q_D)$  [San03].

The vector  $\mathbf{b}_{q_D}$  of Wiener filter coefficients is derived such that

$$\mathbf{b}_{q_D} = \underset{\mathbf{b}_{q_D}}{\text{argmin}} \left\{ \mathbb{E} \left\{ \left\| \mathbf{b}_{q_D}^T \cdot [\hat{\bar{c}}_{\kappa,q_{D1}}^{(u)}, \dots, \hat{\bar{c}}_{\kappa,q_{DW}}^{(u)}]^T - \bar{c}_{\kappa,q_D}^{(u)} \right\|_2^2 \right\} \right\}. \quad (3.29)$$

That means, the mean square error between the estimated channel transfer factor and the true channel transfer factor corresponding to a non-pilot carrying subcarrier with index  $\zeta(q_D)$  in the IFDMA symbol with index  $\kappa$  is minimized by filtering with the elements of  $\mathbf{b}_{q_D}$ . The derivation of the Wiener filter coefficients can be found in literature as, e.g., in [Hay96]. Therefore, in this thesis, the result of minimizing is given without further derivation.

The minimization of the mean square error leads to the Wiener-Hopf equation that is given by

$$\mathbb{E} \left\{ \left[ \hat{\bar{c}}_{\kappa, q_{D1}}^{(u)}, \dots, \hat{\bar{c}}_{\kappa, q_{DW}}^{(u)} \right]^H \cdot \left[ \hat{\bar{c}}_{\kappa, q_{D1}}^{(u)}, \dots, \hat{\bar{c}}_{\kappa, q_{DW}}^{(u)} \right] \right\} \cdot \mathbf{b}_{q_D} = \mathbb{E} \left\{ \bar{c}_{\kappa, q_D}^{(u)*} \cdot \left[ \hat{\bar{c}}_{\kappa, q_{D1}}^{(u)}, \dots, \hat{\bar{c}}_{\kappa, q_{DW}}^{(u)} \right]^T \right\}. \quad (3.30)$$

Based on Eq. (3.30), the vector  $\mathbf{b}_{q_D}^T$  containing the Wiener filter coefficients is calculated by

$$\begin{aligned} \mathbf{b}_{q_D}^T &= \mathbb{E} \left\{ \bar{c}_{\kappa, q_D}^{(u)*} \cdot \left[ \hat{\bar{c}}_{\kappa, q_{D1}}^{(u)}, \dots, \hat{\bar{c}}_{\kappa, q_{DW}}^{(u)} \right] \right\} \\ &\quad \cdot \left( \mathbb{E} \left\{ \left[ \hat{\bar{c}}_{\kappa, q_{D1}}^{(u)}, \dots, \hat{\bar{c}}_{\kappa, q_{DW}}^{(u)} \right]^H \cdot \left[ \hat{\bar{c}}_{\kappa, q_{D1}}^{(u)}, \dots, \hat{\bar{c}}_{\kappa, q_{DW}}^{(u)} \right] \right\} \right)^{-1}. \end{aligned} \quad (3.31)$$

For the calculation of the Wiener filter coefficients, the expectation values in Eq. (3.31) are expressed with the help of the frequency correlation function of the channel which is given in Eq. (2.21). With  $\bar{v}_{\kappa, q_{D1}}^{(u)}, \dots, \bar{v}_{\kappa, q_{DW}}^{(u)}$  the AWGN on the  $W$  nearest pilot carrying subcarriers and Eq. (2.21), the first term of the product of expectation values in Eq. (3.31) is calculated by

$$\begin{aligned} \mathbb{E} \left\{ \bar{c}_{\kappa, q_D}^{(u)*} \cdot \left[ \hat{\bar{c}}_{\kappa, q_{D1}}^{(u)}, \dots, \hat{\bar{c}}_{\kappa, q_{DW}}^{(u)} \right] \right\} &= \mathbb{E} \left\{ \bar{c}_{\kappa, q_D}^{(u)*} \cdot \left[ \bar{c}_{\kappa, q_{D1}}^{(u)} + \frac{\bar{v}_{\kappa, q_{D1}}^{(u)}}{\bar{p}_{q_{D1}}^{(u)}}, \dots, \bar{c}_{\kappa, q_{DW}}^{(u)} + \frac{\bar{v}_{\kappa, q_{DW}}^{(u)}}{\bar{p}_{q_{DW}}^{(u)}} \right] \right\} \\ &= \left[ R_{\bar{h}, f}^{(u)}((\eta(q_{D1}) - \zeta(q_D)) \cdot \Delta f), \dots, R_{\bar{h}, f}^{(u)}((\eta(q_{DW}) - \zeta(q_D)) \cdot \Delta f) \right], \end{aligned} \quad (3.32)$$

where  $\eta(q_{D1}) - \zeta(q_D)$  describes the number of subcarriers between the pilot carrying subcarrier with index  $\eta(q_{D1})$  and the non-pilot carrying subcarrier with index  $\zeta(q_D)$ .

Let the inverse of the Signal-to-Noise Ratio (SNR) on each pilot carrying subcarrier be defined by

$$\gamma = \mathbb{E} \left\{ \frac{\bar{v}_{\kappa, q_P}^{(u)*} \cdot \bar{v}_{\kappa, q_P}^{(u)}}{\bar{p}_{q_P}^{(u)*} \cdot \bar{p}_{q_P}^{(u)}} \right\}. \quad (3.33)$$



Then, with Eq. (2.21) and Eq. (3.33), the second term of expectation values in Eq. (3.31) is expressed by

$$\begin{aligned}
& \mathbb{E} \left\{ \left[ \hat{\bar{c}}_{\kappa, q_{D_1}}^{(u)}, \dots, \hat{\bar{c}}_{\kappa, q_{D_W}}^{(u)} \right]^H \cdot \left[ \hat{\bar{c}}_{\kappa, q_{D_1}}^{(u)}, \dots, \hat{\bar{c}}_{\kappa, q_{D_W}}^{(u)} \right] \right\} \\
&= \mathbb{E} \left\{ \left[ \bar{c}_{\kappa, q_{D_1}}^{(u)} + \frac{\bar{v}_{\kappa, q_{D_1}}^{(u)}}{\bar{p}_{q_{D_1}}^{(u)}}, \dots, \bar{c}_{\kappa, q_{D_W}}^{(u)} + \frac{\bar{v}_{\kappa, q_{D_W}}^{(u)}}{\bar{p}_{q_{D_W}}^{(u)}} \right]^H \cdot \left[ \bar{c}_{\kappa, q_{D_1}}^{(u)} + \frac{\bar{v}_{\kappa, q_{D_1}}^{(u)}}{\bar{p}_{q_{D_1}}^{(u)}}, \dots, \bar{c}_{\kappa, q_{D_W}}^{(u)} + \frac{\bar{v}_{\kappa, q_{D_W}}^{(u)}}{\bar{p}_{q_{D_W}}^{(u)}} \right] \right\} \\
&= \begin{bmatrix} R_{\bar{h}, f}^{(u)}(0) + \gamma & R_{\bar{h}, f}^{(u)}((\eta(q_{D_2}) - \eta(q_{D_1})) \cdot \Delta f) & \dots & R_{\bar{h}, f}^{(u)}((\eta(q_{D_W}) - \eta(q_{D_1})) \cdot \Delta f) \\ R_{\bar{h}, f}^{(u)}((\eta(q_{D_1}) - \eta(q_{D_2})) \cdot \Delta f) & R_{\bar{h}, f}^{(u)}(0) + \gamma & & \vdots \\ \vdots & & \ddots & \\ R_{\bar{h}, f}^{(u)}((\eta(q_{D_1}) - \eta(q_{D_W})) \cdot \Delta f) & \dots & & R_{\bar{h}, f}^{(u)}(0) + \gamma \end{bmatrix}, \tag{3.34}
\end{aligned}$$

with  $\eta(q_{D_1}) - \eta(q_{D_2})$  describing the number of subcarriers between the pilot carrying subcarrier with index  $\eta(q_{D_1})$  and the pilot carrying subcarrier with index  $\eta(q_{D_2})$ .

For each non-pilot carrying subcarrier with index  $\zeta(q_D)$ ,  $q_D = 0, \dots, Q_D - 1$ , the vector  $\mathbf{b}_{q_D}$  of Wiener filter coefficients is computed and the estimate of the channel transfer factor is calculated according to Eq. (3.31). Finally, the LS estimates of the pilot carrying subcarriers and the Wiener filter estimates of the non-pilot carrying subcarriers are combined in the vector  $\hat{\bar{\mathbf{c}}}_{\kappa}^{(u)}$ . In the remainder of the thesis, the subcarrierwise pilot insertion with LS estimation and Wiener interpolation is shortly denoted as subcarrier Wiener.

**DFT interpolation filter** For IFDMA, the characteristic equidistant distribution of subcarriers over the total available bandwidth allows to estimate the channel transfer factors of the non-pilot carrying subcarriers with the help of DFT interpolation. The DFT interpolation is applied for the case that the number  $Q_P$  of pilot carrying subcarriers is larger than or equal to the number  $L_C$  of channel delay taps. Then, due to the equidistant distribution of the pilot carrying subcarriers over the total available bandwidth which is achieved by subcarrierwise pilot insertion, the vector  $[\hat{\bar{c}}_{\kappa, 0}^{(u)}, \dots, \hat{\bar{c}}_{\kappa, Q_P - 1}^{(u)}]$  containing the LS estimates of the channel transfer factors comprises all information about the  $L_C$  channel delay taps. Thus, the channel transfer factors of the non-pilot carrying subcarriers can be determined by calculating the  $L_C$  channel delay taps first.

The estimated channel impulse response vector  $\hat{\bar{\mathbf{c}}}_{\kappa}^{(u)}$  which contains the  $L_C$  channel

delay taps is calculated according to

$$\begin{aligned}\hat{\mathbf{c}}_{\kappa}^{(u)} &= \begin{bmatrix} \mathbf{F}_{Q_P}^H \\ \mathbf{0}_{Q_D \times Q_P} \end{bmatrix} \cdot \left[ \hat{c}_{\kappa,0}^{(u)}, \dots, \hat{c}_{\kappa,Q_P-1}^{(u)} \right]^T \\ &= \left[ \hat{c}_{\kappa,0}^{(u)}, \dots, \hat{c}_{\kappa,Q-1}^{(u)} \right]^T,\end{aligned}\tag{3.35}$$

where the last  $Q_D$  elements of  $\hat{\mathbf{c}}_{\kappa}^{(u)}$  can be set to zero if the condition  $Q_P \geq L_C$  is fulfilled. An estimate of the channel transfer factors for each of the  $Q$  allocated subcarriers is obtained by the application of a  $Q$ -point DFT with respect to  $\hat{\mathbf{c}}_{\kappa}^{(u)}$ . Thus, the vector  $\hat{\mathbf{c}}_{\kappa}^{(u)}$  containing estimates of the channel transfer factors corresponding to the pilot carrying and the non-pilot carrying subcarriers is calculated by

$$\hat{\hat{\mathbf{c}}}_{\kappa}^{(u)} = \mathbf{F}_Q \cdot \hat{\mathbf{c}}_{\kappa}^{(u)}.\tag{3.36}$$

The channel estimates obtained by DFT interpolation differ from the channel estimates obtained by Wiener interpolation. In contrast to the Wiener interpolation, the DFT interpolation is not optimum with respect to MSE performance. However, in case of zero noise power, the channel transfer factors corresponding to the non-pilot carrying subcarriers can be ideally reconstructed by applying DFT interpolation as the pilot carrying subcarriers are equidistantly distributed over the available bandwidth and represent an ideal sampling in frequency domain. In the remainder of the thesis, the subcarrierwise pilot insertion with LS estimation and DFT interpolation is shortly denoted as subcarrier DFT.

## 3.3 Estimation of Time Domain Channel Variations

### 3.3.1 Introduction

In this section, the channel variations in time domain are estimated with the help of pilot assisted channel estimation. For this purpose, the pilot insertion methods with regard to a single IFDMA symbol that have been presented in Section 3.2 are utilized to transmit pilot symbols within several IFDMA symbols out of the  $K$  successively transmitted IFDMA symbols in time domain. By this means, in the first step, the channel variations in frequency domain are estimated for distinct and individual IFDMA symbols as explained in Section 3.2. In the second step, the variations in time domain between the channel transfer factors identified for the individual IFDMA symbols are

estimated. This refers to the two times one-dimensional interpolation procedure which has been introduced for the application to OFDM in [HKR97b]. In this section, the interpolation in time domain is explained for the combination with the symbolwise and subcarrierwise pilot insertion method, respectively.

### 3.3.2 Pilot Grid

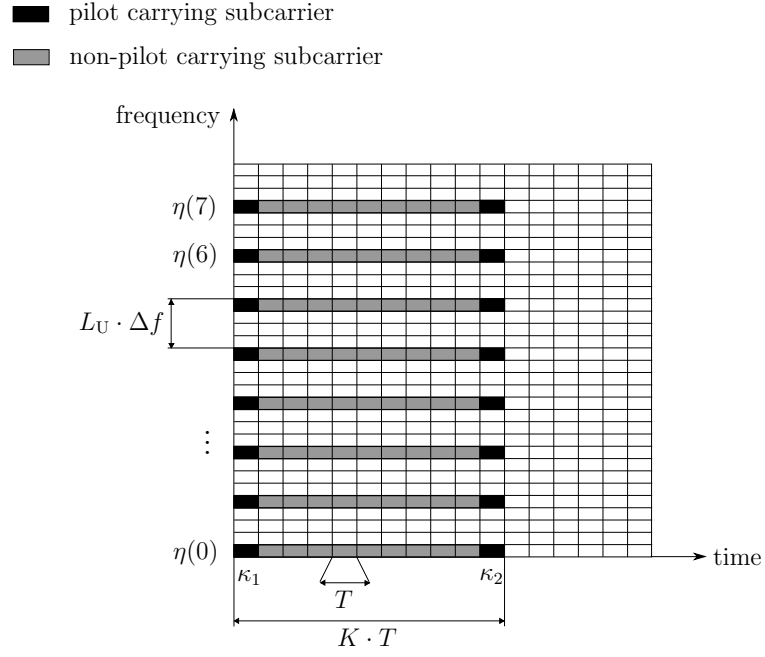
In this section, the pilot insertion for the estimation of the channel variations in time domain is explained.

In Section 3.2, the symbolwise and subcarrierwise pilot insertion have been introduced considering a single IFDMA symbol. In general,  $P$  IFDMA symbols with indices  $k = \kappa_1, \dots, \kappa_P$  are utilized for pilot transmission. Within these distinct IFDMA symbols, the pilot symbols are inserted applying symbolwise or subcarrierwise pilot insertion. In the following, the IFDMA symbols with indices  $k = \kappa_1, \dots, \kappa_P$  are referred to as pilot carrying IFDMA symbols, whereas the IFDMA symbols with indices  $k \neq \kappa_1, \dots, \kappa_P$  are referred to as non-pilot carrying IFDMA symbols.

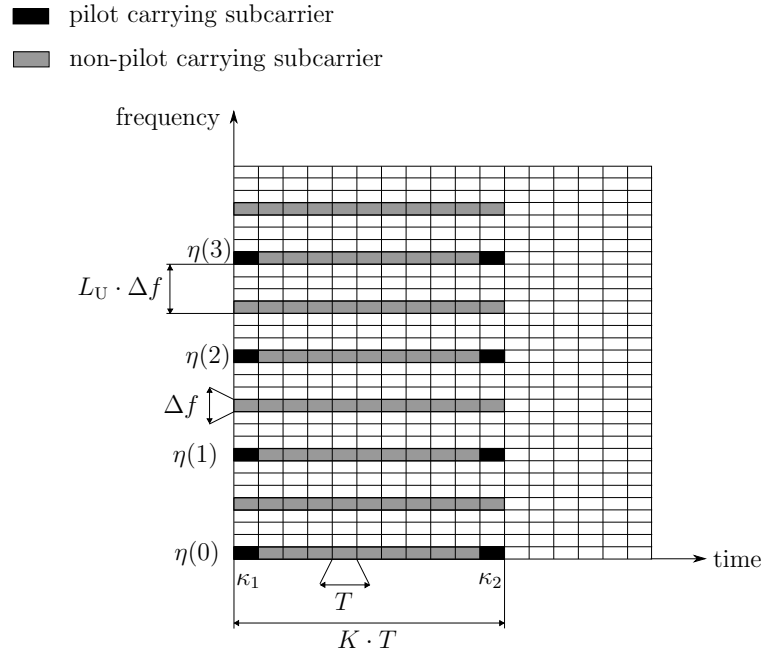
In the following, the pilot insertion is explained based on the graphical illustration of the IFDMA signal shown in Figure 2.5. In Figure 3.5(a), the IFDMA signal transmitted by a certain user is illustrated on a grid in frequency and time domain for the case that the IFDMA symbols with indices  $k = \kappa_1, \kappa_2$  are utilized to insert pilot symbols with the symbolwise pilot insertion method. In this example,  $Q_P = 8$  allocated subcarriers are used for pilot transmission in the first and last IFDMA symbol of the TDMA slot consisting of  $K$  IFDMA symbols. Thus,  $P = 2$  IFDMA symbols are used for pilot transmission and, therefore, no data symbols are transmitted in these pilot carrying IFDMA symbols. Figure 3.5(b) visualizes the case for subcarrierwise pilot insertion in the IFDMA symbols with indices  $k = \kappa_1, \kappa_2$ . For the present example, the interpolation depth is chosen as  $I = 2$  and, thus,  $Q_P = 4$  subcarriers within  $P = 2$  IFDMA symbols are used for pilot transmission. The remaining  $Q_D = 4$  non-pilot carrying subcarriers in the pilot carrying IFDMA symbols are exploited for the transmission of data symbols.

### 3.3.3 Estimation Algorithm

In this section, the estimation of the channel variations in time domain is explained for the case that multiple IFDMA symbols are utilized for pilot transmission.



(a) symbolwise pilot insertion



(b) subcarrierwise pilot insertion

Figure 3.5. Pilot and non-pilot carrying subcarriers for symbolwise and subcarrierwise pilot insertion within multiple IFDMA symbols

A reasonable assumption for the distance between two successive TDMA slots transmitted by a certain user is that this distance is much larger than the coherence bandwidth of the channel [SFE<sup>+</sup>09]. Therefore, it can be assumed that interpolation in time domain is only feasible within a single TDMA slot and the following explanations are based on the consideration of  $K$  successively transmitted IFDMA symbols.

For the pilot carrying IFDMA symbols with indices  $k = \kappa_1, \dots, \kappa_P$ , the vectors  $\hat{\mathbf{c}}_{\kappa_1}^{(u)}, \dots, \hat{\mathbf{c}}_{\kappa_P}^{(u)}$  are available which contain the channel transfer factors that are estimated according to symbolwise LS, subcarrierwise Wiener or subcarrierwise DFT, respectively. These estimates are utilized to calculate the vectors of estimated channel transfer factors for the remaining non-pilot carrying IFDMA symbols. For this purpose, a Wiener interpolation filter is applied in time domain which is explained in the following.

Let us assume that the vector

$$\mathbf{a}_k = [a_{k,0}, \dots, a_{k,V-1}]^T \quad (3.37)$$

contains the  $V$  Wiener filter coefficients  $a_{k,0}, \dots, a_{k,V-1}$  for the interpolation filtering in time domain in order to obtain a channel estimate for the non-pilot carrying IFDMA symbol with index  $k$ . The channel estimates obtained for the pilot carrying IFDMA symbols are utilized as supporting points for the filtering process in time domain and, thus, the number  $V$  of filter coefficients is smaller than or equal to the number  $P$  of pilot carrying IFDMA symbols, i.e.  $V \leq P$ . Let further  $\hat{c}_{k_1,q}^{(u)}, \dots, \hat{c}_{k_V,q}^{(u)}$  denote the estimates of the  $q^{\text{th}}$  channel transfer factor within the IFDMA symbols with indices  $k = k_1, \dots, k_V$ . The indices  $k_1, \dots, k_V$  describe the indices of the  $V$  nearest pilot carrying IFDMA symbols with respect to the non-pilot carrying IFDMA symbol with index  $k$  [San03].

Then, an estimate for the  $q^{\text{th}}$  channel transfer factor within the non-pilot carrying IFDMA symbol with index  $k$  is obtained by

$$\hat{c}_{k,q}^{(u)} = \mathbf{a}_k^T \cdot [\hat{c}_{k_1,q}^{(u)}, \dots, \hat{c}_{k_V,q}^{(u)}]^T. \quad (3.38)$$

That means, an estimate for the  $q^{\text{th}}$  channel transfer factor within the non-pilot carrying symbols with index  $k$  is obtained by filtering the estimates of the  $q^{\text{th}}$  channel transfer factor within the  $V$  nearest pilot carrying symbols with respect to  $k$ .

The elements of  $\mathbf{a}_k$  are calculated according to

$$\mathbf{a}_k = \underset{\mathbf{a}_k}{\operatorname{argmin}} \left\{ \mathbb{E} \left\{ \left\| \mathbf{a}_k^T \cdot [\hat{c}_{k_1,q}^{(u)}, \dots, \hat{c}_{k_V,q}^{(u)}]^T - \bar{c}_{k,q}^{(u)} \right\|_2^2 \right\} \right\}. \quad (3.39)$$

Eq. (3.39) is derived, e.g., in [Hay96] and leads to the Wiener-Hopf equation that is given by

$$\mathbb{E} \left\{ \left[ \hat{\bar{c}}_{k_1,q}^{(u)}, \dots, \hat{\bar{c}}_{k_V,q}^{(u)} \right]^H \cdot \left[ \hat{\bar{c}}_{k_1,q}^{(u)}, \dots, \hat{\bar{c}}_{k_V,q}^{(u)} \right] \right\} \cdot \mathbf{a}_k = \mathbb{E} \left\{ \bar{c}_{k,q}^{(u)*} \cdot \left[ \hat{\bar{c}}_{k_1,q}^{(u)}, \dots, \hat{\bar{c}}_{k_V,q}^{(u)} \right]^T \right\} . \quad (3.40)$$

With Eq. (3.40), the vector  $\mathbf{a}_k^T$  containing the Wiener filter coefficients for interpolation filtering in time domain is obtained by

$$\mathbf{a}_k^T = \mathbb{E} \left\{ \bar{c}_{k,q}^{(u)*} \cdot \left[ \hat{\bar{c}}_{k_1,q}^{(u)}, \dots, \hat{\bar{c}}_{k_V,q}^{(u)} \right] \right\} \cdot \left( \mathbb{E} \left\{ \left[ \hat{\bar{c}}_{k_1,q}^{(u)}, \dots, \hat{\bar{c}}_{k_V,q}^{(u)} \right]^H \cdot \left[ \hat{\bar{c}}_{k_1,q}^{(u)}, \dots, \hat{\bar{c}}_{k_V,q}^{(u)} \right] \right\} \right)^{-1} . \quad (3.41)$$

The expectation values in Eq. (3.41) are expressed with the help of the time correlation function of the channel which is given in Eq. (2.20).

Thus, with Eq. (2.20), the first term of the product of expectation values in Eq. (3.41) is calculated according to

$$\begin{aligned} \mathbb{E} \left\{ \bar{c}_{k,q}^{(u)*} \cdot \left[ \hat{\bar{c}}_{k_1,q}^{(u)}, \dots, \hat{\bar{c}}_{k_V,q}^{(u)} \right] \right\} &= \mathbb{E} \left\{ \bar{c}_{k,q}^{(u)*} \cdot \left[ \bar{c}_{k_1,q}^{(u)} + \frac{\bar{v}_{k_1,q}^{(u)}}{\bar{p}_q^{(u)}}, \dots, \bar{c}_{k_V,q}^{(u)} + \frac{\bar{v}_{k_V,q}^{(u)}}{\bar{p}_q^{(u)}} \right] \right\} \\ &= \left[ R_{\bar{h},t}^{(u)}((k_1 - k) \cdot T), \dots, R_{\bar{h},t}^{(u)}((k_V - k) \cdot T) \right] , \end{aligned} \quad (3.42)$$

where  $k_1 - k$  describes the number of IFDMA symbols between the pilot carrying IFDMA symbol with index  $k_1$  and the non-pilot carrying IFDMA symbol with index  $k$ .

With Eq. (2.20), the second term of expectation values in Eq. (3.41) is expressed by

$$\begin{aligned} &\mathbb{E} \left\{ \left[ \hat{\bar{c}}_{k_1,q}^{(u)}, \dots, \hat{\bar{c}}_{k_V,q}^{(u)} \right]^H \cdot \left[ \hat{\bar{c}}_{k_1,q}^{(u)}, \dots, \hat{\bar{c}}_{k_V,q}^{(u)} \right] \right\} \\ &= \mathbb{E} \left\{ \left[ \bar{c}_{k_1,q}^{(u)} + \frac{\bar{v}_{k_1,q}^{(u)}}{\bar{p}_q^{(u)}}, \dots, \bar{c}_{k_V,q}^{(u)} + \frac{\bar{v}_{k_V,q}^{(u)}}{\bar{p}_q^{(u)}} \right]^H \cdot \left[ \bar{c}_{k_1,q}^{(u)} + \frac{\bar{v}_{k_1,q}^{(u)}}{\bar{p}_q^{(u)}}, \dots, \bar{c}_{k_V,q}^{(u)} + \frac{\bar{v}_{k_V,q}^{(u)}}{\bar{p}_q^{(u)}} \right] \right\} \\ &= \begin{bmatrix} R_{\bar{h},t}^{(u)}(0) + \gamma & R_{\bar{h},t}^{(u)}((k_2 - k_1) \cdot T) & \dots & R_{\bar{h},t}^{(u)}((k_V - k_1) \cdot T) \\ R_{\bar{h},t}^{(u)}((k_1 - k_2) \cdot T) & R_{\bar{h},t}^{(u)}(0) + \gamma & & \vdots \\ \vdots & & \ddots & \\ R_{\bar{h},t}^{(u)}((k_1 - k_V) \cdot T) & \dots & & R_{\bar{h},t}^{(u)}(0) + \gamma \end{bmatrix} , \end{aligned} \quad (3.43)$$

with  $k_1 - k_2$  describing the distance between the pilot carrying IFDMA symbol with index  $k_1$  and the pilot carrying IFDMA symbol with index  $k_2$ .

For each non-pilot carrying IFDMA symbol, the vector  $\mathbf{a}_k$  of Wiener filter coefficients is computed and the estimates of the channel transfer factors are calculated according to Eq. (3.38).

## 3.4 Performance and Complexity Analysis

### 3.4.1 Analysis Assumptions

In this Section 3.4, the symbolwise and subcarrierwise pilot insertion and the corresponding algorithms for the estimation of channel variations in frequency and time domain presented in Section 3.2 and Section 3.3 are analyzed with respect to their influence on the PAPR of the transmit signal, their pilot symbol overhead consumption, their MSE performance and their computational complexity in Sections 3.4.2, 3.4.3, 3.4.4 and 3.4.5, respectively. In the following, the assumptions which are valid for the performance analysis are presented.

For the performance analysis, the transmission from the mobile station of a single user to the base station in a cellular scenario is considered. The consideration of a single user in the system is reasonable because, for all the pilot insertion methods presented in Section 3.2, the pilot symbols transmitted by different users maintain their orthogonality after transmission over a multipath channel. The results for the aforementioned performance measures are obtained by computer simulations. To give an overview of the introduced system and channel parameters, a summary is presented in Table 3.1.

For the data symbols, a convolutional code of rate  $1/2$  and constraint length 6 is used for channel coding. Afterwards, a random interleaver with an interleaving depth of 0.8 ms is applied. The coded and interleaved data bits are QPSK modulated and the modulated data symbols are transmitted with an average power of  $\sigma_D^2 = 1$ . For transmission, a system bandwidth of  $B = 40$  MHz which is divided into  $N = 1024$  subcarriers is available at a carrier frequency of  $f_0 = 3.7$  GHz. The spacing between neighboring subcarriers is equal to  $\Delta f = 39.1$  kHz. Each IFDMA symbol is preceded by a cyclic prefix of length  $T_G = 3.2 \mu\text{s}$  which results in the overall duration of an IFDMA symbol of  $T = 28.8 \mu\text{s}$ . The aforementioned system parameters are based on the WINNER system model that has been defined in [WINdf]. The TDMA slot is assumed to consist of  $K = 30$  successively transmitted IFDMA symbols which results in a TDMA slot duration of 86.4 ms. The pilot symbols that are used for channel estimation are taken from a CAZAC sequence and are transmitted with an average power of  $\sigma_p^2 = 1$ . The channel is modeled by the WINNER SCM urban macro-cell channel that is implemented according to [WINdf, DMO09]. For this channel model, the channel delay paths which contain 95 % of the total energy of all delay paths are comprised within a delay time of  $1.845 \mu\text{s}$ . The remaining delay paths representing 5 %

Table 3.1. System and channel parameters

System parameters	
Error Correction Coding	Convolutional coding
Code rate	1/2
Constraint length	6
Interleaving	Random
Interleaving depth	0.8 ms
Modulation	QPSK
Bandwidth	$B = 40$ MHz
Number of subcarriers	$N = 1024$
Carrier frequency	$f_0 = 3.7$ GHz
Subcarrier spacing	$\Delta f = 39.1$ kHz
Guard interval duration	$T_G = 3.2$ $\mu$ s
Number of IFDMA symbols per TDMA slot	$K = 30$
Decoder	Max-Log-MAP [KB90, RVH95]
Equalizer	Linear MMSE FDE [SKJ94]

Channel parameters	
Channel	WINNER SCM [WINdf]
Channel scenario	urban macro-cell
Coherence bandwidth	$B_{\text{coh}} \approx 290$ kHz

of the total energy can be received with delays up to  $3.5 \mu\text{s}$ . With the definitions in Section 2.3, the coherence bandwidth of the channel results in  $B_{\text{coh}} \approx 290$  kHz. The channel conditions are assumed to be constant for the duration  $T$  of an IFDMA symbol including cyclic prefix and are assumed to be varying for different IFDMA symbols. At the receiver, the channel influence is combated by a linear Minimum Mean Square Error (MMSE) Frequency Domain Equalizer (FDE) [SKJ94]. For decoding purposes, a Max-Log-MAP decoder is applied [KB90, RVH95]. The equalizer and decoder have no relevance for the investigations throughout this section and are mentioned for the sake of completeness.

### 3.4.2 Peak-to-Average Power Ratio

In this section, the symbolwise and subcarrierwise pilot insertion methods are investigated in terms of their respective influence on the PAPR of the pilot carrying IFDMA symbol.

The PAPR per pilot carrying IFDMA symbol is defined as introduced in Eq. (2.14) and represents the ratio between the peak power and the average power within one



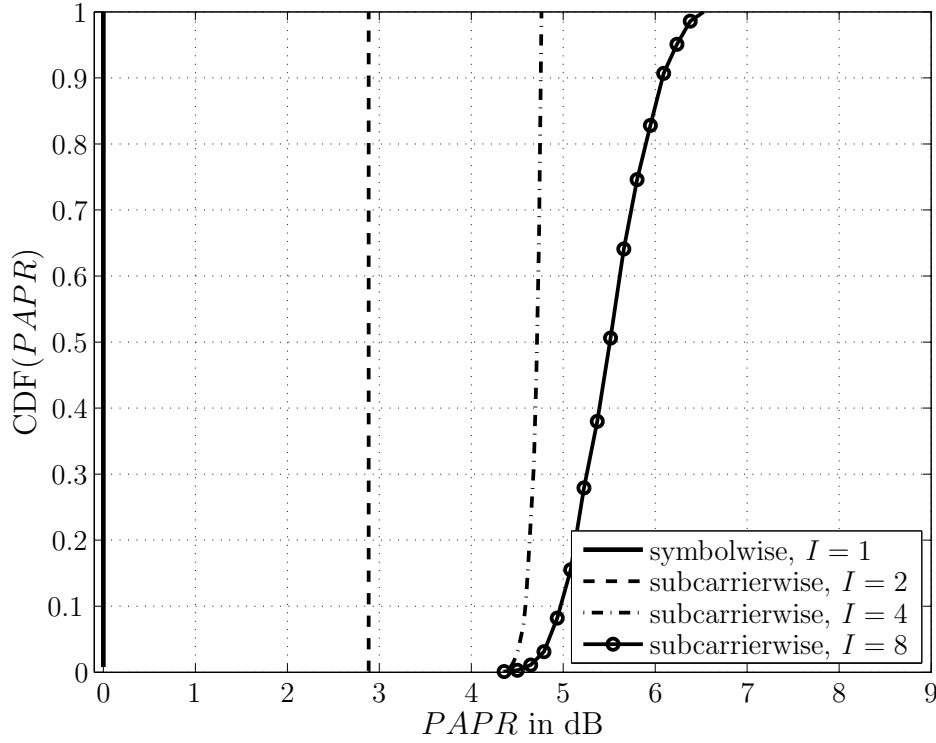


Figure 3.6. CDF of the PAPR in dB in case of symbolwise pilot insertion with  $I = 1$  and subcarrierwise pilot insertion with  $I = 2, 4, 8$  for  $Q = 512$  allocated subcarriers per user.

pilot carrying IFDMA symbol. The investigations that are carried out in this section are based on the definition of the PAPR given by

$$PAPR = \max_n \left\{ \frac{\|x_{\kappa,n}^{(u)}\|_2^2}{E\{\|x_{\kappa,n}^{(u)}\|_2^2\}} \right\}, \quad \text{for } n = 0, \dots, N-1, \quad (3.44)$$

[FKH08] with  $x_{\kappa,n}^{(u)}$  the elements of the vector  $\mathbf{x}_{\kappa}^{(u)}$  as defined in Eq. (3.6) and (3.20), respectively. In the following, the Cumulative Distribution Function (CDF) of the PAPR in dB per pilot carrying IFDMA symbol is presented [Pap84]. The simulation results are obtained from 1000 Monte-Carlo runs in order to provide converging results for the PAPR which represents a random variable.

Figure 3.6 shows the CDF of the PAPR in case of symbolwise pilot insertion with the interpolation depth  $I = 1$  and subcarrierwise pilot insertion with the interpolation depths  $I = 2, 4, 8$ . The results are valid for  $Q = 512$  allocated subcarriers per user. It can be seen that for symbolwise pilot insertion, the PAPR is the lowest and equals 0 dB which means that the peak power is equal to the mean power within the pilot carrying IFDMA symbol. The reason for that can be found in the generation of the

pilot signal for symbolwise pilot insertion. According to Section 2.2.3, the generation of the pilot signal can be described alternatively by compression, repetition and user dependent phase shifting of a CAZAC sequence. As the CAZAC sequence exhibits constant amplitudes in time domain and this amplitude remains unaffected by the compression, repetition and phase shift operations, the modulated pilot signal exhibits a PAPR in time domain which is identical to the PAPR of the CAZAC sequence itself. For subcarrierwise pilot insertion, the PAPR increases compared to symbolwise pilot insertion and exhibits a dependency on the interpolation depth  $I$ . In other words, for subcarrierwise pilot insertion, the PAPR is dependent on the number  $Q_P$  of pilot carrying subcarriers. The PAPR increases with an increasing interpolation depth  $I$ , i.e., a decreasing number  $Q_P$  of pilot carrying subcarriers. This can be substantiated with the allocation of the non-pilot carrying subcarriers in frequency domain. For  $I = 2$ , the  $Q_P = Q/2$  pilot carrying and  $Q_D = Q/2$  non-pilot carrying subcarriers are equidistantly distributed over the available bandwidth. The transmitted IFDMA symbol consists of a superposition of pilot and data symbols. As both, the pilot and the data symbols, are transmitted on equidistant subcarriers in frequency domain, both contributions to the total transmit signal exhibit the same structure as an IFDMA symbol. The increase of the PAPR compared to symbolwise pilot insertion is due to the superposition of the mapped pilot symbols and the mapped data symbols. For  $I > 2$ , the non-pilot carrying subcarriers exhibit a non-equidistant allocation in frequency domain. With increasing interpolation depth  $I$ , the non-pilot carrying subcarriers exhibit a subcarrier allocation that differs considerably from the equidistant subcarrier allocation of an IFDMA symbol and, therefore, the PAPR increases with increasing interpolation depth  $I$ .

In Figure 3.7(a) and Figure 3.7(b), the CDF of the PAPR is shown for the same cases as in Figure 3.6, but for  $Q = 128$  and  $Q = 32$  allocated subcarriers per user, respectively. It can be seen that the maximum PAPR value of each curve is the same as in Figure 3.6, but the distribution of the PAPR changes for the cases where  $I > 2$ . For  $Q = 32$  and  $I > 2$ , the probability that the PAPR has a value smaller than or equal to 4 dB is 0.4, whereas, for  $Q = 128$ , it is approximately 0.05 and for  $Q = 512$ , it is zero. In general, it can be seen that for  $Q = 128$  and  $Q = 32$  with  $I > 2$ , small PAPR values are more likely than for  $Q = 512$ , but the maximum PAPR values remain unaffected. The increasing probability of small PAPR values with decreasing value of  $Q$  can be explained as follows. For  $I > 2$ , neither the pilot nor the non-pilot carrying subcarriers are equidistantly distributed over the available bandwidth and the PAPR of the IFDMA symbol containing pilot and data symbols is increased compared to  $I = 2$  where the pilot and non-pilot carrying subcarriers are equidistantly distributed. As explained in Section 2.2, due to the DFT precoding, each IFDMA symbol contains  $L_U$

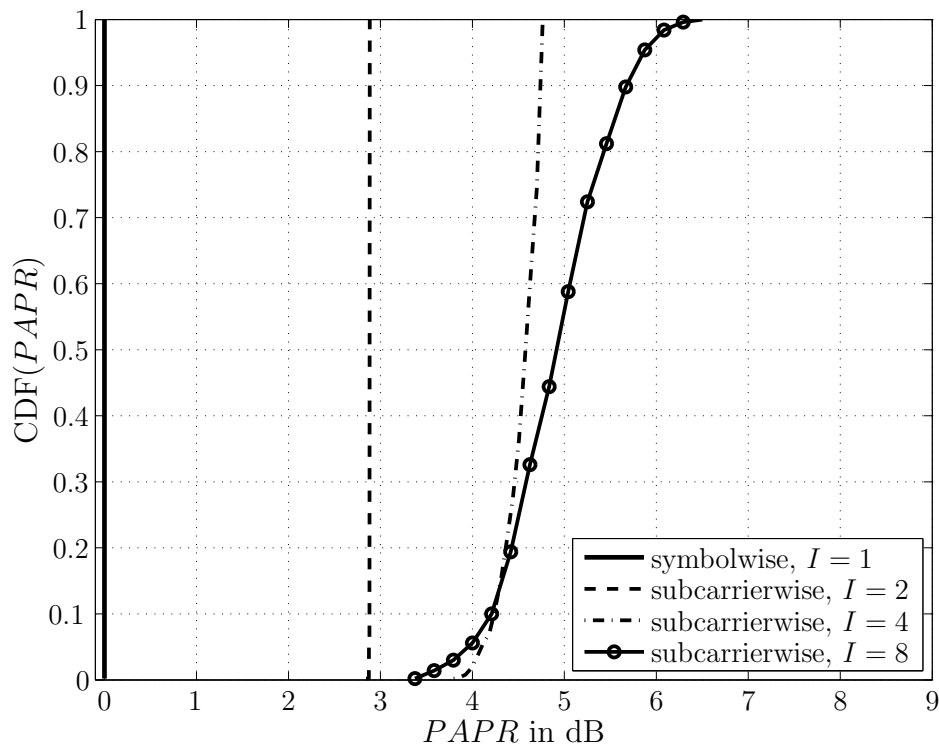
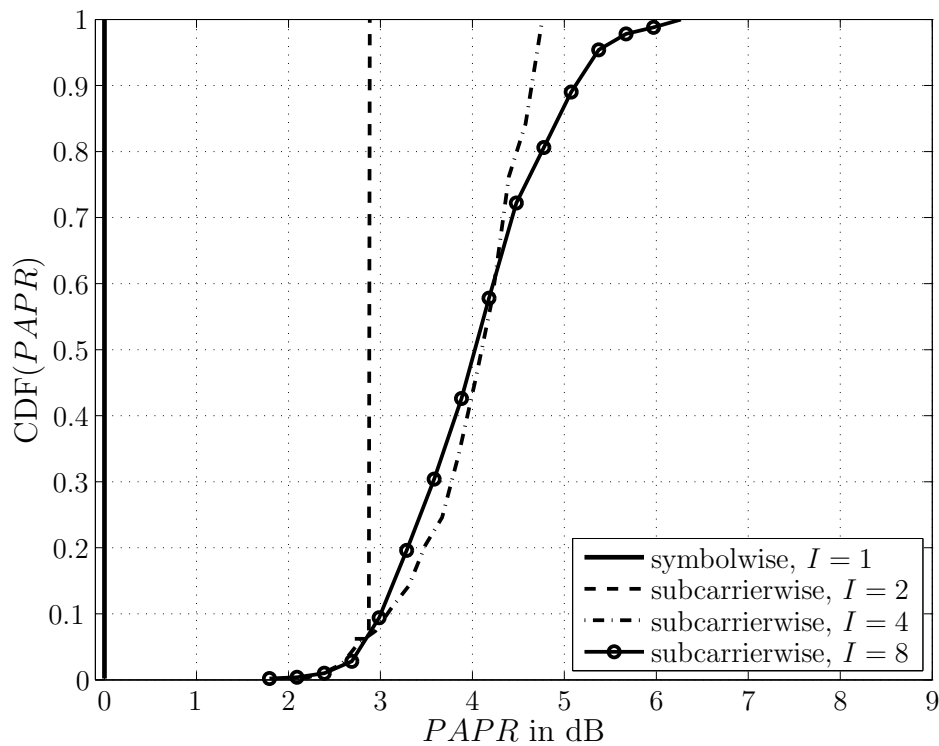
(a)  $Q = 128$ (b)  $Q = 32$ 

Figure 3.7. CDF of the PAPR in dB in case of symbolwise pilot insertion with  $I = 1$  and subcarrierwise pilot insertion with  $I = 2, 4, 8$ .

times each of the  $Q$  data symbols that shall be transmitted. With decreasing number  $Q$  of allocated subcarriers,  $L_U$  increases and the IFDMA symbol contains less differing data symbols. These considerations can be transferred to the  $Q_P$  pilot and  $Q_D$  data symbols.  $Q_P$  and  $Q_D$  decrease with decreasing  $Q$  and, thus, for  $I > 2$ , the probability of small PAPR values increases with decreasing  $Q$  because each IFDMA symbol contains less differing pilot and data symbols.

### 3.4.3 Pilot Symbol Overhead

In this section, symbolwise LS, subcarrierwise Wiener and subcarrierwise DFT are investigated in terms of their respective pilot symbol overhead consumption. In the following, the average power  $\sigma_P^2$  of the pilot symbols is assumed to be equal to the average power  $\sigma_D^2$  of the data symbols. First, the number  $Q_P$  of pilot carrying subcarriers which is equivalent to the number of pilot symbols transmitted per pilot carrying IFDMA symbol is derived.

For symbolwise pilot insertion, an LS estimation is performed in frequency domain for each allocated subcarrier. Thus, each of the  $Q$  allocated subcarriers is used for pilot transmission which leads to  $Q_P = Q$  pilot carrying subcarriers, where  $Q_P$  is independent of the channel variations in frequency domain.

For subcarrierwise pilot insertion, an interpolation filter is applied in frequency domain. Therefore, the distance between neighboring pilot carrying subcarriers has to fulfill the sampling theorem in frequency domain. In order to estimate the channel variations in frequency domain, at least one pilot carrying subcarrier per coherence bandwidth  $B_{\text{coh}}$  is required and the number  $D_F$  of subcarriers between two neighboring pilot carrying subcarriers has to fulfill

$$D_F \leq \frac{B_{\text{coh}}}{\Delta f} = \frac{1}{\tau_{\text{max}} \cdot \Delta f} = \frac{L_U \cdot Q}{L_C} \quad (3.45)$$

[FK03]. That means, at least every  $D_F^{\text{th}}$  subcarrier in the system has to be used for pilot transmission and, therefore,  $D_F$  is denoted as the pilot distance in frequency domain in the following. The estimation performance can be improved by choosing  $D_F$  under consideration of an oversampling in frequency domain. For that purpose, the oversampling factor  $O_F \in \mathbb{Z}$ , representing the number of pilot carrying subcarriers per coherence bandwidth, is introduced. The pilot distance with oversampling in frequency domain is given by

$$D_F = \frac{B_{\text{coh}}}{O_F \cdot \Delta f} = \frac{L_U \cdot Q}{O_F \cdot L_C}. \quad (3.46)$$

$D_F$  describes the distance between neighboring pilot carrying subcarriers for the case that each of the  $N$  subcarriers in the system can be used for pilot transmission. However, for IFDMA, only the  $Q$  equidistantly spaced subcarriers that are allocated to a certain user can be utilized for pilot transmission. Therefore, in order to calculate the number  $Q_P$  of transmitted pilot symbols per pilot carrying IFDMA symbol, the pilot distance  $D_F$  and the distance  $L_U$  between neighboring allocated subcarriers is considered. The interpolation depth  $I$  introduced in Section 3.2.3 is chosen under consideration of the pilot distance in frequency domain and is calculated according to

$$I = \left\lfloor \frac{D_F}{L_U} \right\rfloor. \quad (3.47)$$

For  $B_{\text{coh}} < 2 \cdot L_U \cdot \Delta f$ , the interpolation depth equals  $I = 1$  and, thus,  $Q_P = Q$  pilot symbols are transmitted per pilot carrying IFDMA symbol which corresponds to  $Q$  pilot carrying subcarriers. For the case that  $B_{\text{coh}} \geq 2 \cdot L_U \cdot \Delta f$ , the interpolation depth fulfills  $I > 1$  which means that interpolation is possible in frequency domain and

$$Q_P = \left\lceil \frac{Q}{I} \right\rceil \quad (3.48)$$

subcarriers with an equidistant spacing of  $I \cdot L_U$  are used for pilot transmission. Provided that the sampling theorem in frequency domain is fulfilled,  $Q_P$  is calculated by using Eq. (3.46) and (3.47) in Eq. (3.48) according to

$$Q_P = \left\lceil \frac{Q}{\left\lfloor \frac{Q}{O_F \cdot L_C} \right\rfloor} \right\rceil \quad (3.49)$$

which shows that the number  $Q_P$  of pilot carrying subcarriers is always larger than or equal to the number  $L_C$  of channel delay taps. I.e.,  $Q_P \geq L_C$  is fulfilled and, thus, the requirement for the application of DFT interpolation is met, cf. Section 3.2.3.

In the following, the number  $P$  of pilot carrying IFDMA symbols is derived as a function of the coherence time of the channel for the case of pilot insertion for multiple IFDMA symbols. In case of pilot insertion for multiple IFDMA symbols, an interpolation filter is applied in time domain and the distance between neighboring pilot carrying IFDMA symbols has to fulfill the sampling theorem in time domain. Therefore, the channel variations in time domain can be estimated if at least one IFDMA symbol per coherence time  $T_{\text{coh}}$  is utilized for pilot transmission. The number  $D_T$  of IFDMA symbols between two neighboring pilot carrying IFDMA symbols is given by

$$D_T \leq \frac{T_{\text{coh}}}{T} = \frac{1}{2 \cdot f_{D,\text{max}} \cdot T} = \frac{c}{2 \cdot f_0 \cdot v \cdot T} \quad (3.50)$$

[FK03]. That means, at least every  $D_T^{\text{th}}$  IFDMA symbol is used for pilot transmission

and therefore,  $D_T$  is denoted as the pilot distance in time domain in the following. Again, the estimation performance can be improved by choosing  $D_T$  under consideration of an oversampling in time domain that is realized by the oversampling factor  $O_T \in \mathbb{Z}$ , representing the number of pilot carrying IFDMA symbol per coherence time. The pilot distance with oversampling in time domain is given by

$$D_T = \frac{T_{\text{coh}}}{O_T \cdot T}. \quad (3.51)$$

That means, for  $K$  successively transmitted IFDMA symbols,  $P = \left\lceil \frac{K}{D_T} \right\rceil$  pilot carrying IFDMA symbols are necessary to estimate the channel variations in time domain. In the following, it is assumed that the distance between two successive TDMA slots that are transmitted by a certain user is larger than the coherence time of the channel and, thus, interpolation in time domain is only feasible within one TDMA slot containing  $K$  successively transmitted IFDMA symbols. Under this assumption and for the case that  $K \leq D_T$ , i.e. the pilot distance in time domain is smaller than the total number  $K$  of transmitted IFDMA symbols, at least  $P = 2$  pilot carrying IFDMA symbols are necessary for each TDMA slot consisting of  $K$  IFDMA symbols with cyclic prefix in order to apply an interpolation filter in time domain. Based on these considerations, the number  $Q_P$  of pilot symbols per IFDMA symbol and the number  $P$  of pilot carrying IFDMA symbols are summarized in Table 3.2. In Table 3.2 and in the remainder of this section, it is assumed that symbolwise LS, subcarrierwise Wiener and subcarrierwise DFT are combined with Wiener interpolation in time domain, respectively.

In the following, the number  $Q_P$  of pilot carrying subcarriers and the number  $P$  of pilot carrying IFDMA symbols are used to derive an expression for the pilot symbol overhead as an SNR degradation.

The overall energy that is available for the transmission of  $K$  IFDMA symbols is split up for the transmission of pilot symbols and the transmission of data symbols. The energy that has to be spent for the transmission of the  $Q_P \cdot P$  pilot symbols remains unused for the transmission of data symbols and, therefore, reduces the overall energy that is allocated for data transmission. This energy reduction is equivalent to an SNR degradation and, thus, the overall pilot symbol overhead  $\Lambda$  is expressed as an SNR degradation and calculated by

$$\Lambda = 10 \cdot \log_{10} \left( \frac{Q \cdot K}{Q \cdot K - Q_P \cdot P} \right) \quad (3.52)$$

[BC02]. The numerator in Eq. (3.52) describes the overall number of transmitted data and pilot symbols, whereas the denominator describes the number of transmitted

Table 3.2. Number  $Q_P$  of pilot carrying subcarriers and number  $P$  of pilot carrying IFDMA symbols required for pilot assisted channel estimation.

Number of pilot symbols	Symbolwise LS	Subcarrierwise Wiener / DFT
No. $Q_P$ of pilot carrying subcarriers	$Q_P = Q$	for $D_F < 2 \cdot L_U$ : $Q_P = Q$  for $D_F \geq 2 \cdot L_U$ : $Q_P = Q \cdot \left( \left\lfloor \frac{D_F}{L_U} \right\rfloor \right)^{-1}$
No. $P$ of pilot carrying IFDMA symbols	for $K \leq D_T$ : $P = 2$  for $K > D_T$ : $P = \left\lceil \frac{K}{D_T} \right\rceil$	

payload symbols. With Table 3.2 and Eq. (3.52), the pilot symbol overhead  $\Lambda$  can be calculated according to Table 3.3.

According to Table 3.3, the pilot symbol overhead  $\Lambda$  is dependent on the oversampling factors  $O_F, O_T$ , the velocity  $v$  of the mobile terminal and the number  $L_C$  of channel delay taps.

In Figure 3.8, the overhead  $\Lambda$  is depicted as a function of the number  $Q$  of allocated subcarriers for the case of symbolwise pilot insertion and subcarrierwise pilot insertion with the oversampling factor  $O_F$  in frequency domain as parameter. The results are valid for  $K = 30$  successively transmitted IFDMA symbols and a velocity of  $v = 50$  km/h which corresponds to the case where  $K < D_T$ . Therefore,  $P = 2$  pilot carrying IFDMA symbols are utilized for channel estimation which complies with the application of an oversampling factor of  $O_T \approx 3$  in time domain. The three curves on the right hand side correspond to  $L_C = 128$  channel delay taps. The three curves on the left hand side correspond to  $L_C = 8$  channel delay taps. It can be seen, that for symbolwise pilot insertion, the pilot symbol overhead is equal to  $\Lambda = 0.3$  dB for each number  $Q$  of allocated subcarriers. It is also independent of the channel characteristic in frequency domain and, thus, the number  $L_C$  of channel delay taps. For subcarrierwise pilot

Table 3.3. Pilot symbol overhead  $\Lambda$  for symbolwise and subcarrierwise pilot insertion.

Number $K$ of IFDMA symbols	Symbolwise LS	Subcarrierwise Wiener / DFT
$K \leq D_T$	$10 \cdot \log_{10} \left( \frac{K}{K-2} \right)$	for $D_F < 2 \cdot L_U$ : $10 \cdot \log_{10} \left( \frac{K}{K-2} \right)$ for $D_F \geq 2 \cdot L_U$ : $10 \cdot \log_{10} \left( \frac{K}{K - \frac{1}{\lfloor \frac{D_F}{L_U} \rfloor} \cdot 2} \right)$
$K > D_T$	$10 \cdot \log_{10} \left( 1 - \left\lceil \frac{2 \cdot f_0 \cdot v \cdot T \cdot O_T}{c} \right\rceil \right)^{-1}$	for $D_F < 2 \cdot L_U$ : $10 \cdot \log_{10} \left( 1 - \left\lceil \frac{2 \cdot f_0 \cdot v \cdot T \cdot O_T}{c} \right\rceil \right)^{-1}$ for $D_F \geq 2 \cdot L_U$ : $10 \cdot \log_{10} \left( 1 - \frac{1}{\lfloor \frac{D_F}{L_U} \rfloor} \left\lceil \frac{2 \cdot f_0 \cdot v \cdot T \cdot O_T}{c} \right\rceil \right)^{-1}$

insertion, the pilot symbol overhead decreases if interpolation in frequency domain is feasible.

The coherence bandwidth is proportional to the inverse of the number  $L_C$  of channel delay taps and, thus, the interpolation depth  $I$  in frequency domain increases with decreasing  $L_C$ . That means, for  $L_C = 8$ , interpolation in frequency domain is possible for smaller numbers  $Q$  of allocated subcarriers in comparison to  $L_C = 128$ . With the previous considerations, it can be stated that interpolation in frequency domain is possible if the relation between the number  $Q$  of allocated subcarriers and the number  $L_C$  of channel delay taps fulfills

$$Q > 2 \cdot O_F \cdot L_C \quad (3.53)$$

and that the pilot symbol overhead  $\Lambda$  is reduced in these cases.



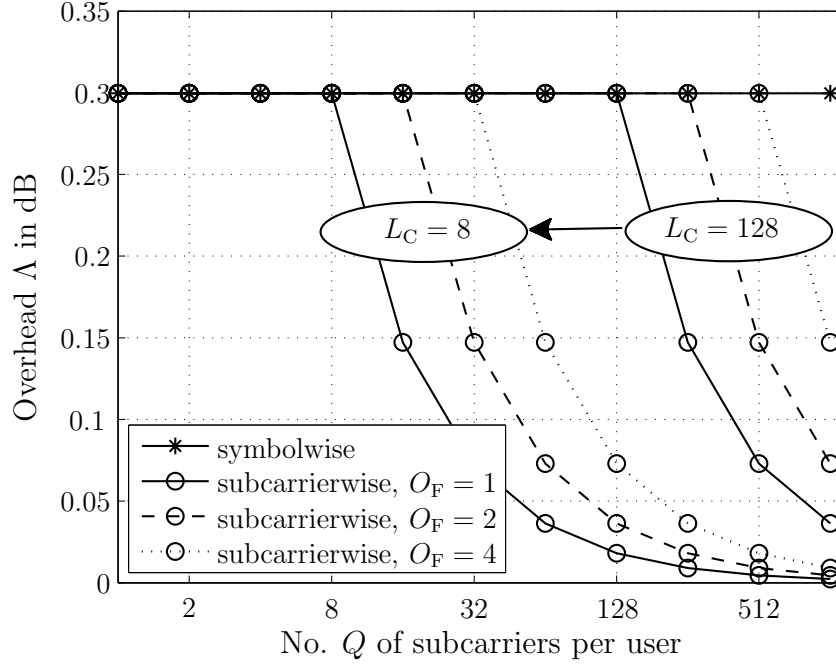


Figure 3.8. Overhead  $\Lambda$  as a function of the number  $Q$  of allocated subcarriers with the oversampling factor  $O_F = 1, 2, 4$  as parameter and a velocity  $v = 50$  km/h and  $L_C = 8, 128$  channel delay taps.

### 3.4.4 Mean Square Error

In this section, the MSE performance is investigated for the estimation algorithms introduced in Section 3.2 and in Section 3.3. The MSE is defined as

$$MSE = \frac{1}{K} \sum_{k=0}^{K-1} \frac{\left\| \hat{\mathbf{c}}_k^{(u)} - \bar{\mathbf{c}}_k^{(u)} \right\|_2^2}{\left\| \bar{\mathbf{c}}_k^{(u)} \right\|_2^2}. \quad (3.54)$$

and gives the squared error averaged over  $K$  IFDMA symbols between the estimated channel transfer factors and the true channel transfer factors which is normalized to the energy of the true channel transfer factors corresponding to the  $Q$  allocated subcarriers. The MSE is chosen as performance measure because it describes the estimation accuracy of the algorithm itself without influences that can be reduced to channel coding or equalizer performance. In the following, the MSE is presented as a function of the SNR which is given as a logarithmic value of the ratio between the energy  $E_B$  that is spent per useful data bit and the noise power  $N_0$ . The calculation of the SNR takes into account the overhead due to channel coding and insertion of the cyclic prefix. Additionally, the SNR degradation due to pilot symbol insertion according to

Section 3.4.3 is included in the SNR. The presented curves are obtained from Monte-Carlo simulations whose results are averaged over 1000 simulation runs in order to obtain converging results.

First, the focus is on the estimation of the channel variations in frequency domain. For this reason, the performance for the estimation of the channel variations in frequency domain is investigated under consideration of a time invariant channel. The channel variations in frequency domain are estimated for a single IFDMA symbol while the channel variations in time domain are assumed to be negligible. Second, the overall performance for the estimation of the channel variations in frequency and time domain is considered. For this reason, the MSE is presented for the two times one-dimensional channel estimation algorithms that have been introduced in Section 3.3. For purposes of clarity, Table 3.4 gives an overview of the results that are presented in this section.

Table 3.4. Overview of presented MSE results.

ESTIMATION APPROACH FOR CHANNEL VARIATIONS IN FREQUENCY DOMAIN	ESTIMATION APPROACH FOR CHANNEL VARIATIONS IN TIME DOMAIN	
	single IFDMA symbol + no estimation	multiple IFDMA symbols + Wiener interpolation
symbolwise LS	Figure 3.9	Figure 3.10, Figure 3.11 Figure 3.12
subcarrierwise Wiener	Figure 3.9	Figure 3.11, Figure 3.12
subcarrierwise DFT	Figure 3.9	Figure 3.11, Figure 3.12

The presented results are valid for the following parameters:

- In Section 3.4.3, it has been shown that for a coherence bandwidth  $B_{\text{coh}} \leq 8 \cdot \Delta f$  of the WINNER SCM urban macro-cell channel, interpolation in frequency domain is applicable only for a large number  $Q$  of allocated subcarriers. In order to

present results for different oversampling factors  $O_F$  in frequency domain,  $Q = 512$  is chosen in the following.

- For Wiener interpolation in frequency domain, a filter with  $W = 4$  coefficients is applied. The application of a filter with more filter coefficients is not required because the distance between the pilot carrying subcarrier which serve as supporting points is much larger than the coherence bandwidth for  $W > 4$ .

Figure 3.9 shows the MSE as a function of  $E_B/N_0$  in dB with the interpolation depth  $I$  in frequency domain as parameter for the estimation of channel variations in frequency domain according to Section 3.2. In Figure 3.9, the MSE for the estimation of the channel variations in frequency domain is observable without influences due to channel variability in time domain. Results are presented for symbolwise LS, subcarrierwise Wiener and subcarrierwise DFT under consideration of a single IFDMA symbol. According to Eq. (3.47), the maximum interpolation depth equals  $I = 4$  for the oversampling factor  $O_F = 1$  in frequency domain. That means, for  $Q = 512$ , at least every 4<sup>th</sup> allocated subcarrier has to be used for pilot transmission in order to fulfill the sampling theorem in frequency domain.

For symbolwise LS, the interpolation depth is  $I = 1$  and, thus,  $Q_P = Q$  subcarriers are used for pilot transmission which allows to perform an LS estimation for each allocated subcarrier. It can be seen that the MSE decreases linearly with increasing SNR and is unbiased as the LS estimation provides the MVU estimate for each allocated subcarrier. For subcarrierwise pilot insertion, different interpolation depths  $I$  are investigated. For subcarrierwise pilot insertion with  $I = 4$ , the MSE runs into an error floor due to large interpolation errors that are observable for large SNR values. For  $E_B/N_0 < 10$  dB, the DFT interpolation exhibits the same performance as the symbolwise LS. The results for Wiener interpolation show even better performance than the results for symbolwise LS because the Wiener interpolation minimizes the errors that are caused by AWGN. This noise reduction has an effect if the interpolation error is smaller than the errors due to AWGN and, thus, occurs only for low SNR values. For large SNR values, the results for DFT interpolation show slightly better performance than the results for Wiener interpolation. This can be explained as follows. For DFT interpolation, the spectrum of the IFDMA signal is ideally sampled by the pilot carrying subcarriers if the number of channel delay taps  $L_C$  is equal to or smaller than the number  $Q_P$  of pilot carrying subcarriers. Assuming negligible small noise power, the channel impulse response can be ideally reconstructed as the channel transfer function is sampled at  $Q_P \geq L_C$  equidistantly spaced subcarriers in frequency domain. As for the WINNER SCM urban macro-cell channel, the number  $L_C$  of channel delay taps differs for each

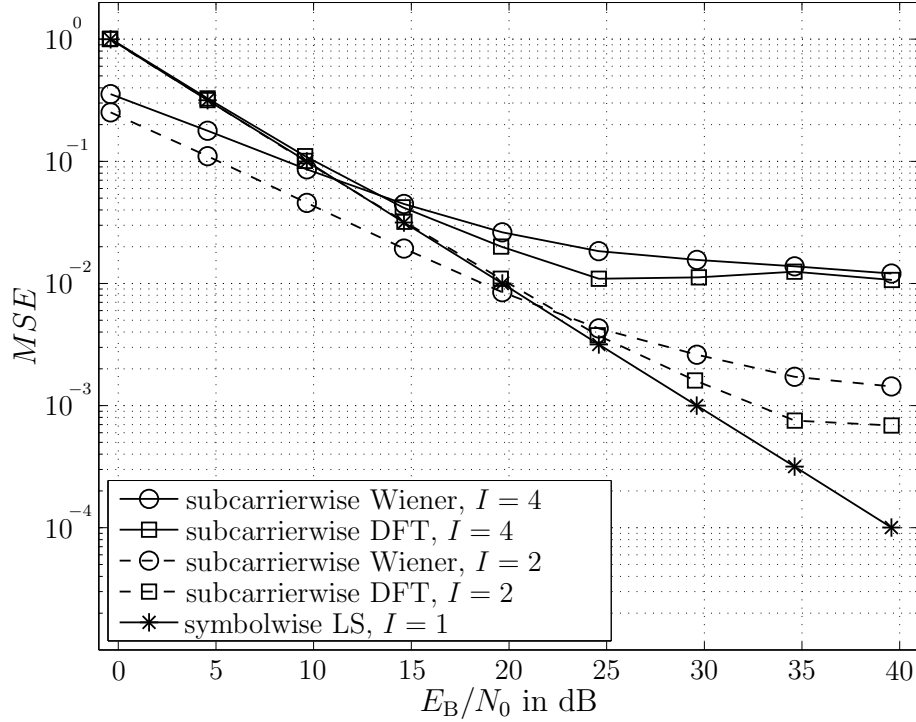


Figure 3.9. MSE as a function of  $E_B/N_0$  in dB for the estimation of channel variations in frequency domain with symbolwise and subcarrierwise pilot insertion with the interpolation depth  $I$  as parameter and under consideration of a single IFDMA symbol with  $Q = 512$ .

Monte-Carlo run, the condition for the ideal reconstruction by DFT interpolation is not always satisfied. Therefore, the DFT interpolation outperforms the Wiener interpolation for large SNR values but shows worse performance than the symbolwise LS. For subcarrierwise pilot insertion with  $I = 2$ , again, the DFT interpolation exhibits the same performance as the symbolwise LS for  $E_B/N_0 < 25$  dB. In comparison to  $I = 4$ , the performance of the DFT interpolation is improved for  $E_B/N_0 \geq 10$  dB. However, for large SNR values, the MSE for DFT interpolation still exhibits an error floor. In case of Wiener interpolation with  $I = 2$ , the performance is improved noticeably for all SNR values compared to Wiener interpolation with  $I = 4$ . For  $E_B/N_0 < 20$  dB, the results for Wiener interpolation show better performance than the results for DFT interpolation. For  $E_B/N_0 \geq 20$  dB, the results for DFT interpolation show a lower error floor than the results for Wiener interpolation. Again, this can be reduced to the property of the DFT interpolation to ideally reconstruct the channel impulse response if the number  $L_C$  of channel delay taps is equal to the number  $Q_P$  of pilot carrying subcarriers.

In the following, the MSE performance of two times one-dimensional channel estimation considering the channel variations in frequency and time domain is investigated. For the estimation of channel variations in time domain, the following parameters are utilized:

- $P = 2$  IFDMA symbols with the indices  $\kappa_1 = 0$  and  $\kappa_2 = 29$  are utilized for pilot transmission.
- The channel variations in time domain are estimated by Wiener interpolation with a filter of length  $V = 2$  as there are only two pilot carrying IFDMA symbols serving as supporting points.

In Figure 3.10, the MSE is presented as a function of  $E_B/N_0$  in dB with the oversampling factor  $O_T$  in time domain as parameter. In this figure, the influence of the oversampling factor  $O_T$  in time domain is investigated and, therefore, the results are presented for symbolwise LS within  $P = 2$  pilot carrying IFDMA symbols in order to eliminate the influence of interpolation errors in frequency domain on the overall estimation performance. The number  $P$  and the indices  $\kappa$  of the pilot carrying IFDMA symbols are chosen as fixed numbers, therefore, different velocities  $v$  of the mobile terminal lead to different oversampling factors  $O_T$  in time domain. For  $v \approx 84$  km/h, the coherence time results in  $T_{\text{coh}} \approx 60 \cdot T$  and, therefore, a mobile terminal velocity of  $v \approx 84$  km/h is equivalent to an oversampling factor  $O_T = 2$  in time domain. In Figure 3.10, results are shown for oversampling factors  $O_T = 2, \dots, 10$ . The relation between the velocity  $v$  of the mobile terminal and the oversampling factor  $O_T$  in time domain is given in Table 3.5.

Table 3.5. Relation between  $O_T$  and  $v$ .

$v$ in km/h	17	19	21	24	28	34	42	56	84
$O_T$	10	9	8	7	6	5	4	3	2

It can be seen that for  $E_B/N_0 < 20$  dB, the MSE performance is improved compared to the results for symbolwise LS in Figure 3.9. This is due to the application of the Wiener interpolation in time domain which enables to reduce the estimation errors that are caused by AWGN. The reduction of the estimation errors that are caused by AWGN is observable in the low SNR region where the AWGN can be assumed as the primary source of estimation errors. However, for  $E_B/N_0 > 20$  dB, the MSE performance is strongly degraded for  $O_T = 2$  due to interpolation errors in time domain. The performance in the high SNR region is improved by increasing the oversampling factor  $O_T$  which reduces the influence of interpolation errors in time domain. For  $O_T \geq 6$  the

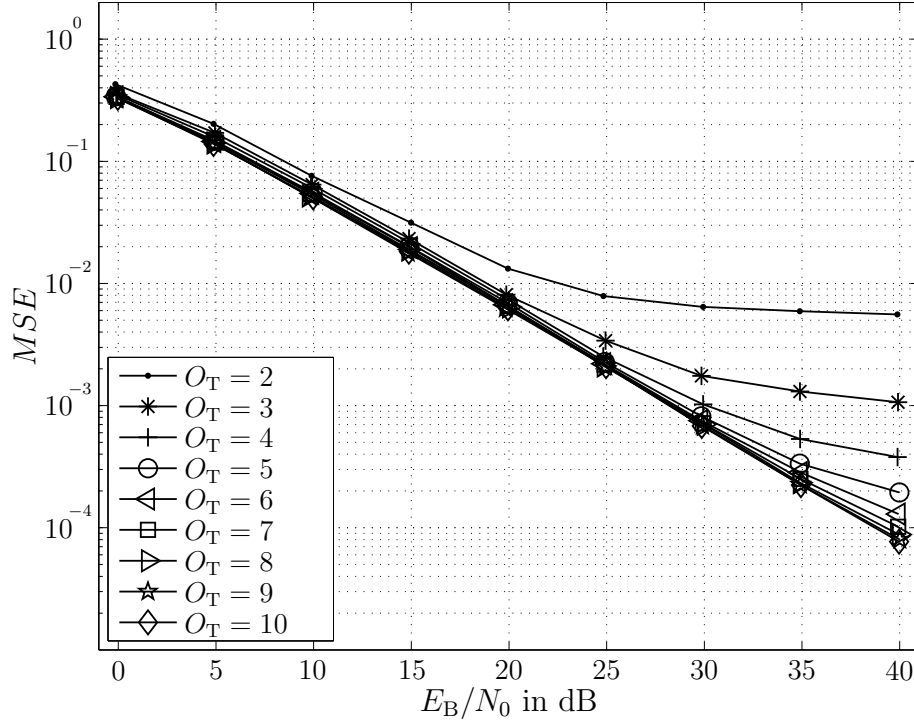


Figure 3.10. MSE as a function of  $E_B/N_0$  in dB for the estimation of channel variations in frequency and time domain with different mobile terminal velocities corresponding to different oversampling factors  $O_T$  in time domain as parameter.

influence of interpolation errors in time domain becomes insignificantly small. It can be stated that for Wiener interpolation in time domain, oversampling factors  $O_T \geq 5$  are reasonable choices in order to reduce the influence of interpolation errors in time domain. In other words, for increasing velocities of the mobile terminal, the number of pilot carrying IFDMA symbols per TDMA slot has to be increased in order to avoid a MSE performance degradation due to interpolation errors in time domain. The number  $P$  of pilot carrying IFDMA symbols can be calculated as a function of the oversampling factor  $O_T$ , the number  $K$  of IFDMA symbols per TDMA slot and the velocity  $v$  in m/s of the mobile terminal according to

$$P = \left\lceil \frac{2 \cdot K \cdot 2 \cdot v \cdot f_0 \cdot T \cdot O_T}{c} \right\rceil. \quad (3.55)$$

In the following, the interaction between interpolation errors in frequency and time domain is investigated and the influence of both errors on the MSE performance is presented.

In Figure 3.11, the MSE is presented as a function of  $E_B/N_0$  in dB with the interpolation depth  $I$  as parameter. The results are valid for an oversampling factor  $O_T = 6$  in

time domain which corresponds to a velocity  $v = 28$  km/h of the mobile terminal. The channel variations in frequency domain are estimated by symbolwise LS, subcarrierwise Wiener and subcarrierwise DFT.

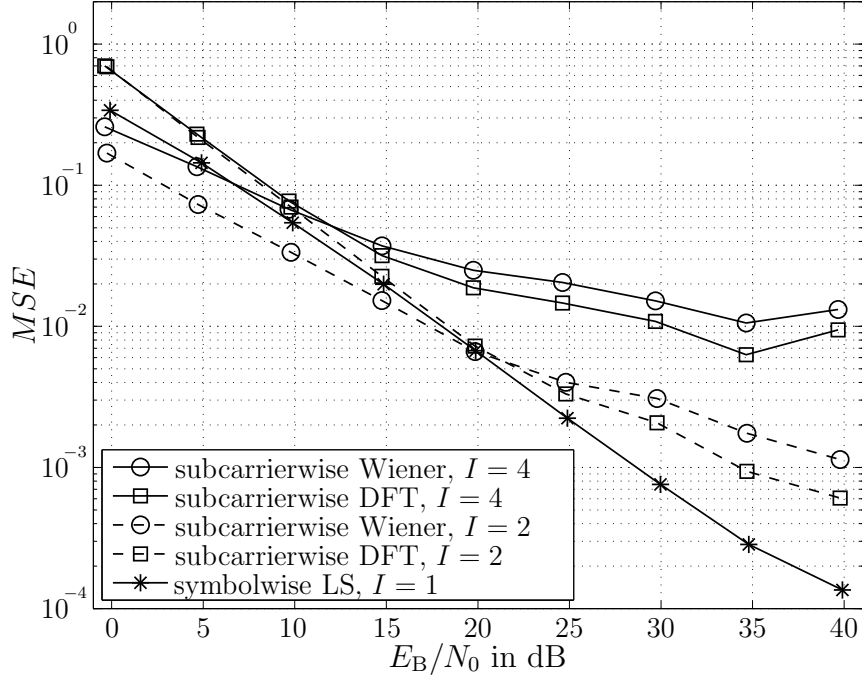


Figure 3.11. MSE as a function of  $E_B/N_0$  in dB for the estimation of channel variations in frequency and time domain with the interpolation depth  $I$  as parameter and under consideration of an oversampling factor  $O_T = 6$  in time domain for  $Q = 512$ .

Figure 3.11 shows that for an oversampling factor  $O_T = 6$  in time domain, the MSE performance can be improved by Wiener interpolation compared to the results in Figure 3.9 where a single IFDMA symbol and, thus, no interpolation in time domain, is considered. Additionally, for  $E_B/N_0 < 20$  dB, the subcarrierwise Wiener shows the best MSE performance in case of the interpolation depth  $I = 2$ . It can be stated that for an oversampling factor  $O_T = 6$  in time domain, interpolation errors in time domain are avoided and the noise reduction due to Wiener interpolation improves the estimation performance compared to the case where no interpolation in time domain is applied. Further on, for  $I = 2$ , i.e. an oversampling factor  $O_F = 2$  in frequency domain, and for  $E_B/N_0 > 20$  dB, the estimation performance can be improved by the application of Wiener interpolation compared to the case where an LS estimation is applied to each allocated subcarrier.

In Figure 3.12, the MSE is presented as a function of  $E_B/N_0$  in dB with the interpolation depth  $I$  as parameter. The results are valid for the same assumptions as in

Figure 3.11, except the oversampling factor that is chosen as  $O_T = 2$  which corresponds to a velocity  $v = 84$  km/h of the mobile terminal. Figure 3.12 shows, that for  $E_B/N_0 < 20$  dB, again the subcarrierwise Wiener shows the best MSE performance in case of the interpolation depth  $I = 2$ . However, for  $E_B/N_0 > 20$  dB, the MSE performance is clearly degraded for each of the estimation algorithms and the curves run into error floors. This performance degradation is due to the oversampling factor  $O_T = 2$  in time domain. For a velocity of  $v = 84$  km/h, the Wiener interpolation in time domain causes interpolation errors for the chosen distance between the pilot carrying IFDMA symbols.

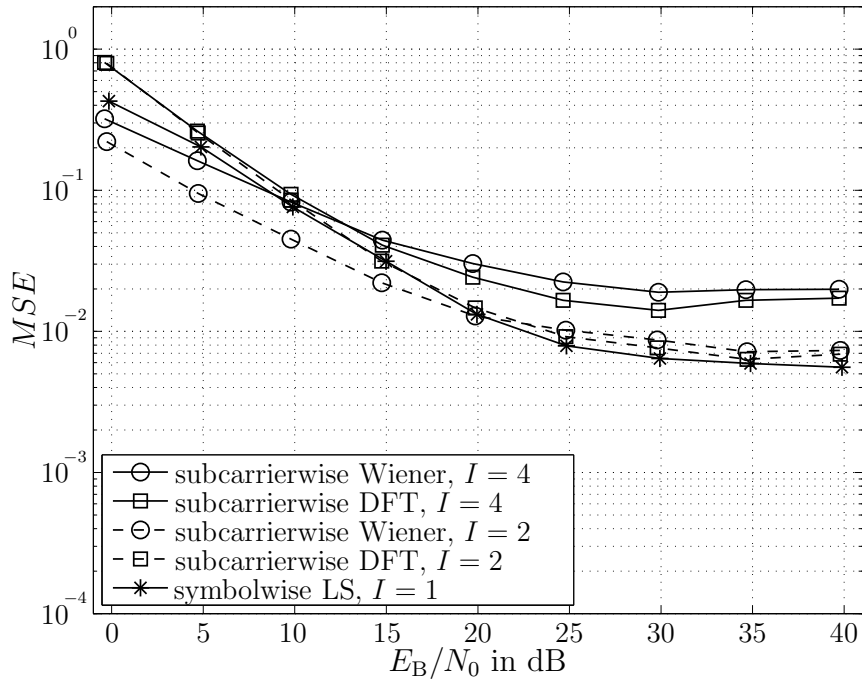


Figure 3.12. MSE as a function of  $E_B/N_0$  in dB for the estimation of channel variations in frequency and time domain with the interpolation depth  $I$  as parameter and under consideration of an oversampling factor  $O_T = 2$  in time domain for  $Q = 512$ .

### 3.4.5 Complexity

In this section, the estimation algorithms for symbolwise LS, subcarrierwise Wiener and subcarrierwise DFT are investigated in terms of their computational complexity. In the following, the computational complexity is measured based on the required number of complex multiplications. For that purpose, the complex multiplications



that are required for the aforementioned channel estimation approaches are calculated and compared. Further on, the complexity of the Wiener interpolation in time domain which is used to estimate the channel transfer factors of the non-pilot carrying IFDMA symbols is considered which is identical for each of the aforementioned pilot insertion methods. In the following, divisions are assumed to have the same computational complexity as multiplications and repeated operations are assumed to contribute only once to the computational complexity as the result of these operations can be stored and reused [Sil08]. Further on, the calculation of the Wiener filter coefficients can be realized once in an offline process and the result can be stored in memory and retrieved for the filtering operations. Therefore, the calculation of the Wiener filter coefficients is discounted within the complexity considerations and only the filtering operations themselves are counted. Further on, the application of the DFT and IDFT is assumed to be realized by a Fast Fourier Transform (FFT) and Inverse Fast Fourier Transform (IFFT) algorithm according to [KK98], respectively.

In Table 3.6, the number of complex multiplications is given for the respective estimation algorithm. It can be seen that the second part is identical for each of the three algorithms as it refers to the Wiener interpolation in time domain. In time domain, each of the  $Q$  channel transfer factors within the  $K - P$  non-pilot carrying IFDMA symbols is obtained by the multiplication of  $V$  supporting channel transfer factors with one Wiener filter coefficient, respectively. The first part of the complex multiplications differs for each of the algorithms. The estimation algorithm for symbolwise LS exhibits the least complexity as the estimation is performed by an LS estimation whose complexity increases linearly with increasing number  $Q$  of allocated subcarriers. For subcarrierwise Wiener, the complexity increases because a Wiener filter with  $W$  coefficients is applied for the  $Q_D$  non-pilot carrying subcarriers additionally to the LS estimation for the  $Q_P$  pilot carrying subcarriers. For subcarrierwise DFT, the DFT and IDFT operations which are applied to the  $Q_P$  LS estimates of the channel transfer factors are realized by FFT and IFFT operations and lead to an increasing complexity with  $Q_P \cdot \log_2(Q_P)$  which corresponds to the IFFT size and  $Q \cdot \log_2(Q)$  which corresponds to the FFT size. For symbolwise LS and subcarrierwise Wiener, the first part of the number of complex multiplications is clear less than the second part representing the Wiener interpolation in time domain under the assumption of practical parameters. Therefore, the complexity of both algorithms is comparable as it is mainly determined by the Wiener interpolation in time domain. For subcarrierwise DFT, the contributions of the FFT and IFFT operations to the overall computational complexity cannot be neglected.

Table 3.6. Number of complex multiplications

Algorithm	Complex multiplications
symbolwise LS	$P \cdot Q + (K - P) \cdot Q \cdot V$
subcarrierwise Wiener	$P \cdot (Q_P + Q_D \cdot W) + (K - P) \cdot Q \cdot V$
subcarrierwise DFT	$P \cdot (Q_P + Q_P \cdot \log_2(Q_P) + Q \cdot \log_2(Q)) + (K - P) \cdot Q \cdot V$

### 3.5 Conclusions

In this chapter, different methods for the insertion of pilot symbols into the IFDMA transmit signal have been presented. The pilot insertion methods have been combined with different algorithms for the estimation of the channel variations in frequency and time domain. Further on, the pilot insertion methods have been investigated in terms of their respective influence on the PAPR of the IFDMA transmit signal. For the introduced pilot assisted channel estimation algorithms, the pilot symbol overhead has been derived as an SNR degradation and the MSE performance has been presented. Finally, the algorithms have been compared in terms of their computational complexity. The main conclusions of this chapter can be summarized as follows:

- For symbolwise pilot insertion, the modulation process leaves the PAPR unaffected and, thus, the modulated pilot sequence exhibits the same PAPR as the unmodulated pilot sequence. For the usage of CAZAC sequences as pilot sequence, the PAPR of symbolwise pilot insertion is the same as for an IFDMA signal without pilot transmission. For subcarrierwise pilot insertion, the PAPR increases with increasing interpolation depth  $I$ .
- The sampling theorem in frequency and time domain has to be fulfilled in order to estimate the channel variations in frequency and time domain by pilot assisted channel estimation. That means, at least one subcarrier per coherence bandwidth of the channel and one IFDMA symbol per coherence time of the channel has to be used for pilot transmission. For IFDMA, the fulfillment of the sampling

theorem in frequency and time domain entails the usage of each of the  $Q$  allocated subcarriers for pilot transmission in frequency domain if the number  $L_C$  of channel delay taps is larger than  $\frac{Q}{2}$ . That means, for IFDMA, interpolation in frequency domain is solely feasible if  $Q$  is large, i.e., the transmitted data rate is high.

- The application of oversampling in frequency and time domain reduces interpolation errors and, thus, improves the channel estimation performance. For the considered WINNER SCM urban macro-cell channel, an oversampling factor  $O_F = 2$  in frequency domain and an oversampling factor  $O_T = 5$  in time domain leads to reasonable performance results.
- The application of subcarrierwise pilot insertion with Wiener interpolation in frequency and time domain leads to the best MSE performance in comparison to the other presented algorithms for  $E_B/N_0 < 20$  dB because due to the application of Wiener filtering, the estimation errors caused by AWGN are reduced. For  $E_B/N_0 > 20$  dB, the application of symbolwise pilot insertion with LS estimation for each allocated subcarrier in frequency domain and Wiener interpolation in time domain shows the best MSE performance because interpolation errors in frequency domain are avoided.



## Chapter 4

# Semiblink Channel Estimation for IFDMA

### 4.1 Introduction

In this chapter, semiblink channel estimation is presented for IFDMA.

For pilot assisted channel estimation, it has been shown that at least one subcarrier per coherence bandwidth and one IFDMA symbol per coherence time has to be used for pilot transmission in order to get a reliable estimate of the time varying channel transfer factors. In frequency domain, for IFDMA, the distance between adjacent subcarriers allocated to a user is often larger than the coherence bandwidth of the channel. This means, if the number  $Q$  of allocated subcarriers is smaller than twice the number  $L_C$  of channel delay taps, interpolation in frequency domain between the distributed subcarriers allocated to a specific user is not possible due to the large distance between adjacent subcarriers. Therefore, especially for a small number  $Q$  of allocated subcarriers, i.e., for low data rates, each allocated subcarrier has to be used for pilot transmission to fulfill the sampling theorem in frequency domain. The missing possibility of interpolation in frequency domain even for channels with low frequency selectivity, i.e., a small delay spread in time domain, leads to an increasing pilot symbol overhead for IFDMA. In time domain, the data of a certain user is transmitted within TDMA slots each consisting of  $K$  successively transmitted IFDMA symbols with cyclic prefix. The distance between the TDMA slots allocated to a certain user is much larger than the coherence time of the channel [WINDf]. The application of pilot assisted channel estimation with interpolation in time domain entails the transmission of pilot symbols within at least two pilot carrying IFDMA symbols for each allocated TDMA slot. This means, the pilot symbol overhead increases for a small number  $K$  of IFDMA symbols per TDMA slot.

To overcome the aforementioned high pilot symbol overhead for IFDMA, the application of semiblink channel estimation is introduced in this chapter. By applying semiblink channel estimation, the sampling theorem in frequency and time domain can be violated and the number  $Q_P$  of pilot carrying subcarriers and the number  $P$  of pilot carrying IFDMA symbols can be reduced compared to pilot assisted channel estimation. In frequency domain, the channel transfer factors of the non-pilot carrying subcarriers can be estimated by evaluating the second order statistics of the

received IFDMA signal to obtain information about the channel. For this second order statistics analysis, the redundancy within the IFDMA signal which is introduced by the signal generation in time domain through compression and repetition is exploited. In Section 4.2, the application of two different second order statistics based channel estimation algorithms is introduced for IFDMA. The algorithms are derived for the application in an IFDMA system and special features arising due to the application to a multiple access scheme are pointed out. In time domain, the data symbols transmitted within the non-pilot carrying IFDMA symbols can be exploited to obtain an estimate of the channel transfer factors for each of the  $K$  IFDMA symbols transmitted within the TDMA slot. In Section 4.3, the second order statistics based channel estimation algorithms introduced in Section 4.2 are combined with a decision directed channel estimation approach. By this means, the channel can be estimated even if the sampling theorem in frequency and time domain is not fulfilled and current channel estimation approaches fail. In order to mitigate error propagation in time domain, the application of an iterative Wiener filter to the decision directed estimates in time domain is proposed which improves the estimation performance. Section 4.4 presents the pilot symbol overhead, the MSE performance and the computational complexity of the introduced semiblind channel estimation algorithms. The main conclusions of this chapter are drawn in Section 4.5. Parts of this chapter have been originally published by the author in [SK08, SK09b].

## 4.2 Reduced Number of Pilot Symbols in Frequency Domain

### 4.2.1 Introduction

In this section, two second order statistics based channel estimation algorithms are presented for IFDMA. The number of pilot symbols in frequency domain is reduced such that the sampling theorem in frequency domain is no longer fulfilled and the channel variations in frequency domain cannot be estimated with the help of interpolation filters. The pilot symbols are inserted by the subcarrierwise pilot insertion according to Section 3.2.3 and the LS estimates  $\hat{c}_{\kappa, q_P}^{(u)}$ ,  $q_P = 0, \dots, Q_P - 1$ , of the channel transfer factors corresponding to the  $Q_P$  pilot carrying subcarriers are obtained according to Eq. (3.25). The number  $Q_P$  of pilot carrying subcarriers is assumed to be smaller than the number  $L_C$  of channel delay taps and, thus, the application of interpolation in frequency domain as explained in Section 3.2.3 is not feasible for the estimation of the channel transfer factors corresponding to the non-pilot carrying subcarriers. The LS

estimates of the channel transfer factors corresponding to the pilot carrying subcarriers are combined with two different second order statistics approaches leading to two semi-blind channel estimation approaches for the estimation of frequency domain channel variations. The first one that is introduced in Section 4.2.2 is the correlation based semiblind channel estimation. It is based on [TG97] and exploits the information about the channel impulse response vector that is inherent to the autocorrelation matrix of the received IFDMA symbols. The second one introduced in Section 4.2.3 is the subspace based semiblind channel estimation which is based on [MDCM95] and [MdCD02] and takes advantage of the orthogonality between signal and noise subspace.

In the following,  $\mathbf{0}_a$  and  $\mathbf{0}_{a \times b}$  denote an  $a \times a$  and an  $a \times b$  matrix, respectively, which contains all zero elements. Further on,  $\mathbf{I}_a$  represents an  $a \times a$  identity matrix and  $\square$  stands for matrix or vector entries which are not calculated explicitly as they are of no relevance for the subsequent derivations.

## 4.2.2 Correlation Based Semiblind Channel Estimation

### 4.2.2.1 Estimation for Channels with Small Delay Spread

In this section, the correlation based semiblind channel estimation is derived for the case of small channel delay spreads which means that the number  $L_C$  of channel delay taps is assumed to fulfill the condition

$$L_C \leq Q. \quad (4.1)$$

For this case, the cyclic prefix consists of  $N_G = L_G \cdot Q$  elements with  $L_G = 1$  and interpolation for pilot assisted channel estimation is not feasible if  $L_C > Q/2$ . The restriction according to Eq. (4.1) is made as each received IFDMA symbol exhibits a cyclostationarity with  $Q$  due to the signal generation by compression and repetition. Thus, a maximum number of  $L_C = Q$  channel delay taps can be estimated. For the application of correlation based semiblind channel estimation to IFDMA, each received IFDMA symbol with cyclic prefix is analyzed at the receiver. As the cyclic prefix parts of different users cannot assumed to be orthogonal to each other, the influence of multiple users in the system shall be considered. In order to derive the principle of correlation based semiblind channel estimation at first,  $U = 1$  user in the system is considered in this section.

In Figure 4.1, the principle of the correlation based semiblind channel estimation for IFDMA is illustrated in a block diagram. This figure depicts the transmitter and the

receiver part for subcarrierwise pilot insertion as introduced in Section 3.2.3. The receiver part is extended by the correlation based estimation, which is combined with the LS estimation at the pilot carrying subcarriers. In the following, the principle of correlation based estimation for IFDMA is deduced at first. Then, the combination of correlation based estimation with the pilot based LS estimation is explained.

For correlation based channel estimation, the received signal is analyzed before cyclic prefix removal. As defined in Section 2.4, the  $k^{\text{th}}$  IFDMA symbol with cyclic prefix  $\tilde{\mathbf{x}}_k^{(u)}$  of user  $u$  after transmission over the channel with impulse response vector  $\mathbf{h}_k^{(u)}$  and distortion by the AWGN vector  $\tilde{\mathbf{v}}_k^{(u)}(k) = [\nu_{k,0}^{(u)}, \dots, \nu_{k,LQ-1}^{(u)}]$  is denoted by  $\tilde{\mathbf{r}}_k^{(u)} = [r_{k,0}^{(u)}, \dots, r_{k,LQ-1}^{(u)}]^T$ . The vector  $\tilde{\mathbf{r}}_k^{(u)}$  includes the received cyclic prefix part and consists of  $LQ = (L_U + L_G)Q$  elements. Due to the IFDMA signal generation by compression, repetition and phase shifting, it is known that the received vector  $\tilde{\mathbf{r}}_k^{(u)}$  comprises  $L$  blocks each containing identical data symbols which are compressed in time and phase shifted. Thus, the received vector  $\tilde{\mathbf{r}}_k^{(u)}$  can be split into  $L$  blocks  $\mathbf{r}_{k,j}^{(u)} = [r_{k,jQ}^{(u)}, \dots, r_{k,jQ+Q-1}^{(u)}]^T$ ,  $j = 0, \dots, L-1$ , each containing the  $Q$  transmitted data symbols. With this, the received vector  $\tilde{\mathbf{r}}_k^{(u)}$  including the received cyclic prefix part can be represented by  $L$  blocks according to

$$\tilde{\mathbf{r}}_k^{(u)} = \left[ \mathbf{r}_{k,0}^{(u)T}, \dots, \mathbf{r}_{k,L-1}^{(u)T} \right]^T. \quad (4.2)$$

Due to the transmission over a multipath channel, the received vector  $\tilde{\mathbf{r}}_k^{(u)}$  with index  $k$  is influenced by the transmitted IFDMA symbol with index  $k$ , the cyclic prefix of the IFDMA symbol with index  $k$  and the last block of the IFDMA symbol with index  $k-1$ . This influence is illustrated in Figure 4.2.

Let  $\mathbf{H}_{k,0}^{(u)}$  denote the  $Q \times Q$  Toeplitz matrix given by

$$\mathbf{H}_{k,0}^{(u)} = \begin{bmatrix} h_{k,0}^{(u)} & 0 & \dots & \dots & 0 \\ h_{k,1}^{(u)} & h_{k,0}^{(u)} & 0 & \dots & \vdots \\ \vdots & & \ddots & & 0 \\ h_{k,L_C-1}^{(u)} & \dots & h_{k,0}^{(u)} & 0 & \vdots \\ & \ddots & & \ddots & \\ 0 & \dots & 0 & h_{k,L_C-1}^{(u)} & \dots & h_{k,0}^{(u)} \end{bmatrix}, \quad (4.3)$$



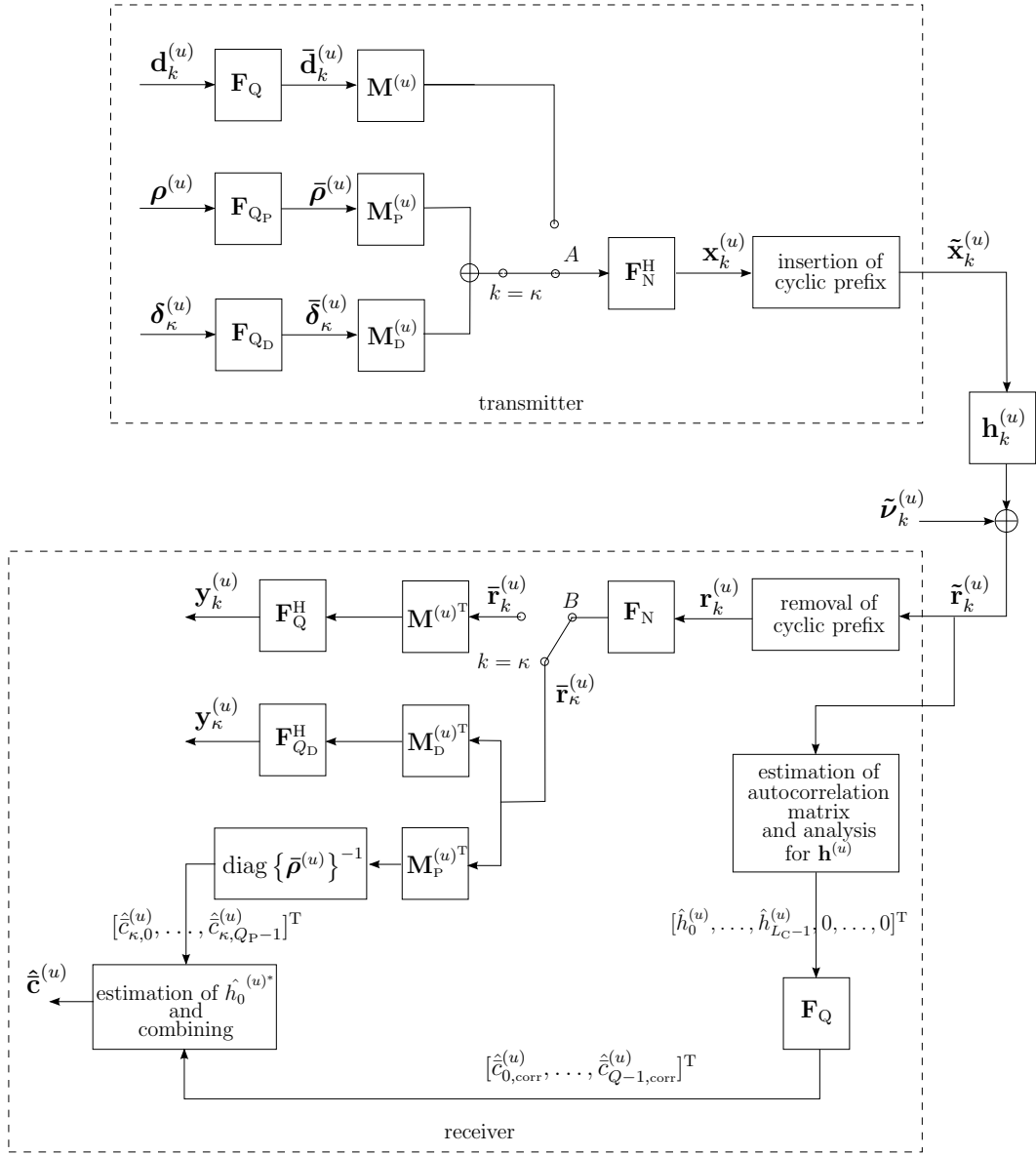


Figure 4.1. Block diagram of transmission chain with subcarrierwise pilot insertion at the transmitter and correlation based semiblind channel estimation at the receiver.

let further  $\mathbf{H}_{k,1}^{(u)}$  denote the  $Q \times Q$  Toeplitz matrix given by

$$\mathbf{H}_{k,1}^{(u)} = \begin{bmatrix} 0 & \cdots & 0 & h_{k,L_C-1}^{(u)} & \cdots & h_{k,1}^{(u)} \\ \vdots & & & \ddots & \ddots & \vdots \\ 0 & \cdots & & 0 & h_{k,L_C-1}^{(u)} & \\ 0 & \cdots & & & 0 & \\ \vdots & & & & & \vdots \\ 0 & \cdots & & & & 0 \end{bmatrix}. \quad (4.4)$$

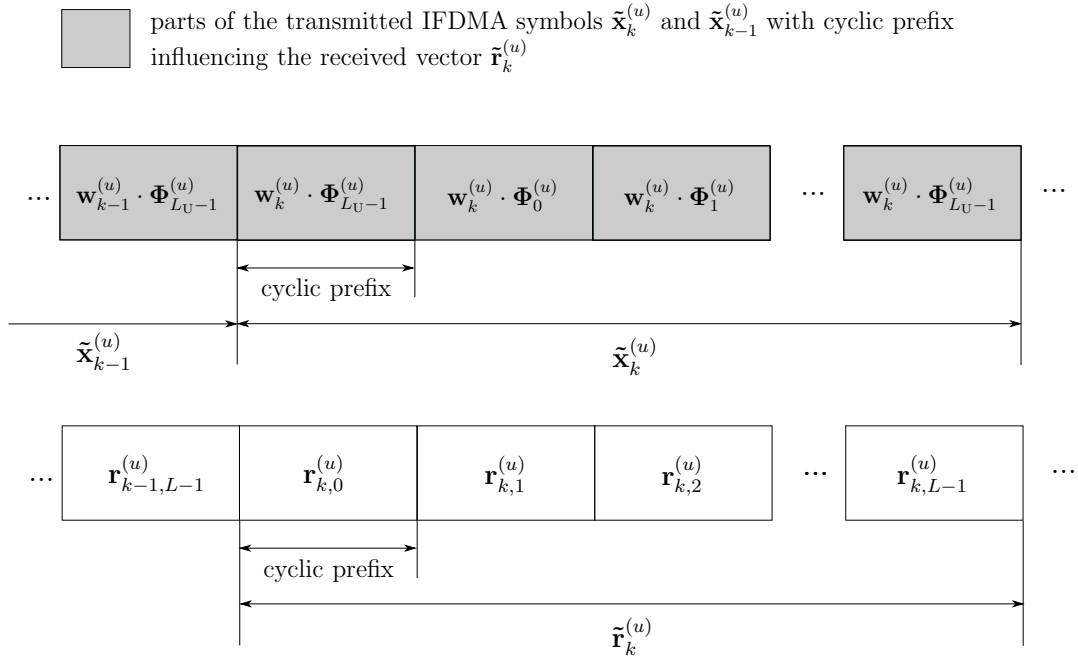


Figure 4.2. Influence of the transmitted IFDMA symbols  $\tilde{\mathbf{x}}_k^{(u)}$  and  $\tilde{\mathbf{x}}_{k-1}^{(u)}$  with cyclic prefix on the received vector  $\tilde{\mathbf{r}}_k^{(u)}$  due to transmission over a multipath channel with  $L_C \leq Q$  delay taps.

Then, the  $LQ \times (L+1)Q$  matrix  $\mathbf{H}_{k,\text{corr}}^{(u)}$  is defined by

$$\mathbf{H}_{k,\text{corr}}^{(u)} = \begin{bmatrix} \mathbf{H}_{k,1}^{(u)} & \mathbf{H}_{k,0}^{(u)} & \mathbf{0}_Q & \cdots & \mathbf{0}_Q \\ \mathbf{0}_Q & \mathbf{H}_{k,1}^{(u)} & \mathbf{H}_{k,0}^{(u)} & \cdots & \mathbf{0}_Q \\ \vdots & & \ddots & \ddots & \mathbf{0}_Q \\ \mathbf{0}_Q & \cdots & \mathbf{0}_Q & \mathbf{H}_{k,1}^{(u)} & \mathbf{H}_{k,0}^{(u)} \end{bmatrix}. \quad (4.5)$$

With  $\Phi_i^{(u)}$ ,  $i = 0, \dots, L_U - 1$ , according to Eq. (2.8), let the  $(L+1)Q \times 2Q$  matrix  $\Theta_{\text{corr}}^{(u)}$  contain the user dependent phase shift and be defined according to

$$\Theta_{\text{corr}}^{(u)} = \begin{bmatrix} \Phi_{L_U-1}^{(u)} & \mathbf{0}_Q \\ \mathbf{0}_Q & \Phi_{L_U-1}^{(u)} \\ \mathbf{0}_Q & \Phi_0^{(u)} \\ \mathbf{0}_Q & \Phi_1^{(u)} \\ \vdots & \vdots \\ \mathbf{0}_Q & \Phi_{L_U-1}^{(u)} \end{bmatrix}. \quad (4.6)$$

Then, the received vector  $\tilde{\mathbf{r}}_k^{(u)}$  is specified based on Eqs. (4.2), (4.5), (4.6), the vector

$\mathbf{w}_k^{(u)}$  defined in Eq. (2.7) and the AWGN vector  $\tilde{\mathbf{v}}_k^{(u)}$  according to

$$\tilde{\mathbf{r}}_k^{(u)} = \mathbf{H}_{k,\text{corr}}^{(u)} \cdot \boldsymbol{\Theta}_{\text{corr}}^{(u)} \cdot \begin{bmatrix} \mathbf{w}_{k-1}^{(u)} \\ \mathbf{w}_k^{(u)} \end{bmatrix} + \tilde{\mathbf{v}}_k^{(u)}. \quad (4.7)$$

With  $\mathbb{E}\{\mathbf{w}_k^{(u)} \cdot \mathbf{w}_k^{(u)\text{H}}\} = \sigma_W^2 \cdot \mathbf{I}_Q$ ,  $\mathbb{E}\{\mathbf{w}_k^{(u)} \cdot \mathbf{w}_{k-1}^{(u)\text{H}}\} = \mathbf{0}_Q$  and  $\mathbb{E}\{\tilde{\mathbf{v}}_k^{(u)} \cdot \tilde{\mathbf{v}}_k^{(u)\text{H}}\} = \sigma_\nu^2 \cdot \mathbf{I}_{LQ}$ , the autocorrelation matrix  $\mathbb{E}\{\tilde{\mathbf{r}}_k^{(u)} \cdot \tilde{\mathbf{r}}_k^{(u)\text{H}}\}$  of the received vector  $\tilde{\mathbf{r}}_k^{(u)}$  is given by

$$\mathbb{E}\{\tilde{\mathbf{r}}_k^{(u)} \cdot \tilde{\mathbf{r}}_k^{(u)\text{H}}\} = \mathbf{H}_{k,\text{corr}}^{(u)} \cdot \boldsymbol{\Theta}_{\text{corr}}^{(u)} \cdot \sigma_W^2 \cdot \mathbf{I}_{2Q} \cdot \boldsymbol{\Theta}_{\text{corr}}^{(u)\text{H}} \cdot \mathbf{H}_{k,\text{corr}}^{(u)\text{H}} + \sigma_\nu^2 \cdot \mathbf{I}_{LQ}. \quad (4.8)$$

Considering the definition of  $\mathbf{H}_{k,\text{corr}}^{(u)}$  in Eq. (4.5) and the definition of  $\boldsymbol{\Theta}_{\text{corr}}^{(u)}$  in Eq. (4.6), the calculation of the first  $Q$  columns of the autocorrelation matrix in Eq. (4.8) equals

$$\mathbb{E}\{\tilde{\mathbf{r}}_k^{(u)} \cdot \tilde{\mathbf{r}}_k^{(u)\text{H}}\} = \sigma_W^2 \cdot \begin{bmatrix} \mathbf{H}_{k,0}^{(u)} \cdot \mathbf{H}_{k,0}^{(u)\text{H}} + \mathbf{H}_{k,1}^{(u)} \cdot \mathbf{H}_{k,1}^{(u)\text{H}} & \square & \dots & \square \\ (\mathbf{H}_{k,0}^{(u)} \cdot \boldsymbol{\Phi}_0^{(u)} + \mathbf{H}_{k,1}^{(u)} \cdot \boldsymbol{\Phi}_{L_U-1}^{(u)}) \cdot \boldsymbol{\Phi}_{L_U-1}^{(u)\text{H}} \cdot \mathbf{H}_{k,0}^{(u)\text{H}} & \square & \dots & \square \\ (\mathbf{H}_{k,0}^{(u)} \cdot \boldsymbol{\Phi}_1^{(u)} + \mathbf{H}_{k,1}^{(u)} \cdot \boldsymbol{\Phi}_0^{(u)}) \cdot \boldsymbol{\Phi}_{L_U-1}^{(u)\text{H}} \cdot \mathbf{H}_{k,0}^{(u)\text{H}} & \square & \dots & \square \\ \vdots & \vdots & \ddots & \vdots \\ (\mathbf{H}_{k,0}^{(u)} \cdot \boldsymbol{\Phi}_{L_U-1}^{(u)} + \mathbf{H}_{k,1}^{(u)} \cdot \boldsymbol{\Phi}_{L_U-2}^{(u)}) \cdot \boldsymbol{\Phi}_{L_U-1}^{(u)\text{H}} \cdot \mathbf{H}_{k,0}^{(u)\text{H}} & \square & \dots & \square \end{bmatrix} + \sigma_\nu^2 \cdot \mathbf{I}_{LQ}. \quad (4.9)$$

Eq. (4.9) shows that the autocorrelation matrix contains the  $Q \times Q$  matrix

$$(\mathbf{H}_{k,0}^{(u)} \cdot \boldsymbol{\Phi}_0^{(u)} + \mathbf{H}_{k,1}^{(u)} \cdot \boldsymbol{\Phi}_{L_U-1}^{(u)}) \cdot \boldsymbol{\Phi}_{L_U-1}^{(u)\text{H}} \cdot \mathbf{H}_{k,0}^{(u)\text{H}}, \quad (4.10)$$

whose first column entry can be derived under consideration of the Toeplitz structure of  $\mathbf{H}_{k,0}^{(u)}$  and  $\mathbf{H}_{k,1}^{(u)}$  according to

$$(\mathbf{H}_{k,0}^{(u)} \cdot \boldsymbol{\Phi}_0^{(u)} + \mathbf{H}_{k,1}^{(u)} \cdot \boldsymbol{\Phi}_{L_U-1}^{(u)}) \cdot \boldsymbol{\Phi}_{L_U-1}^{(u)\text{H}} \cdot \mathbf{H}_{k,0}^{(u)\text{H}} = \begin{bmatrix} h_{k,0}^{(u)} & \cdot & h_{k,0}^{(u)*} & \cdot & e^{-j \cdot 0 \cdot Q \cdot \varphi^{(u)}} & \cdot & e^{j \cdot (L_U-1) \cdot Q \cdot \varphi^{(u)}} & \square & \dots & \square \\ h_{k,1}^{(u)} & \cdot & h_{k,0}^{(u)*} & \cdot & e^{-j \cdot 0 \cdot Q \cdot \varphi^{(u)}} & \cdot & e^{j \cdot (L_U-1) \cdot Q \cdot \varphi^{(u)}} & \square & \dots & \square \\ \vdots & & \vdots & & \vdots & & \vdots & \vdots & \dots & \vdots \\ h_{k,L_C-1}^{(u)} & \cdot & h_{k,0}^{(u)*} & \cdot & e^{-j \cdot 0 \cdot Q \cdot \varphi^{(u)}} & \cdot & e^{j \cdot (L_U-1) \cdot Q \cdot \varphi^{(u)}} & \square & \dots & \square \\ & & 0 & & \vdots & & \vdots & \vdots & \dots & \vdots \\ & & \vdots & & 0 & & \vdots & \vdots & \dots & \vdots \\ & & & & & & \square & \dots & \square \end{bmatrix}. \quad (4.11)$$

Accordingly, the  $L_U - 1$  matrices  $(\mathbf{H}_{k,0}^{(u)}\Phi_i + \mathbf{H}_{k,1}^{(u)}\Phi_{i-1}) \cdot \Phi_{L_U-1}^H \mathbf{H}_{k,0}^{(u)H}$ ,  $i = 1, \dots, L_U - 1$ , in Eq. (4.9) result in

$$(\mathbf{H}_{k,0}^{(u)}\Phi_i + \mathbf{H}_{k,1}^{(u)}\Phi_{i-1}) \cdot \Phi_{L_U-1}^H \mathbf{H}_{k,0}^{(u)H} = \begin{bmatrix} h_{k,0}^{(u)} & \cdot & h_{k,0}^{(u)*} & \cdot & e^{-j \cdot i \cdot Q \cdot \varphi^{(u)}} & \cdot & e^{j \cdot (L_U-1) \cdot Q \cdot \varphi^{(u)}} & \square & \dots & \square \\ h_{k,1}^{(u)} & \cdot & h_{k,0}^{(u)*} & \cdot & e^{-j \cdot i \cdot Q \cdot \varphi^{(u)}} & \cdot & e^{j \cdot (L_U-1) \cdot Q \cdot \varphi^{(u)}} & \square & \dots & \square \\ & & & \vdots & & & & \vdots & \dots & \vdots \\ h_{k,L_C-1}^{(u)} & \cdot & h_{k,0}^{(u)*} & \cdot & e^{-j \cdot i \cdot Q \cdot \varphi^{(u)}} & \cdot & e^{j \cdot (L_U-1) \cdot Q \cdot \varphi^{(u)}} & \square & \dots & \square \\ & & & 0 & & & & \square & \dots & \square \\ & & & \vdots & & & & \vdots & \dots & \vdots \\ & & & 0 & & & & \square & \dots & \square \end{bmatrix}. \quad (4.12)$$

Eq. (4.11) and (4.12) show that the autocorrelation matrix of the received vector  $\tilde{\mathbf{r}}_k^{(u)}$  contains  $L_U$ -times the information about each channel delay tap  $h_{k,l}^{(u)}$ ,  $l = 0, \dots, L_C - 1$ . Based on the observations in Eqs. (4.9), (4.11) and (4.12), the  $Q \times 1$  vector  $[h_{k,0}^{(u)}, \dots, h_{k,L_C-1}^{(u)}, 0, \dots, 0]^T$  containing the  $L_C$  channel delay taps can be calculated by

$$\begin{aligned} [h_{k,0}^{(u)}, \dots, h_{k,L_C-1}^{(u)}, 0, \dots, 0]^T &= \\ & \frac{1}{L_U \cdot \sigma_W^2 \cdot h_{k,0}^{(u)*}} \cdot \mathbb{E} \left\{ \sum_{i=0}^{L_U-1} e^{j \cdot i \cdot Q \cdot \varphi^{(u)}} \cdot e^{-j \cdot (L_U-1) \cdot Q \cdot \varphi^{(u)}} \cdot r_{k,0}^{(u)*} \cdot \mathbf{r}_{k,i+1}^{(u)} \right\}. \end{aligned} \quad (4.13)$$

For practical implementations, the expectation value in Eq. (4.13) is approximated by the arithmetic mean over  $K$  received vectors [Hän01]. This approximation is valid for small channel variations in time domain implying that the channel delay taps  $h_{k,l}^{(u)}$  are approximately constant within the time duration  $K \cdot T$ , i.e.,

$$h_l^{(u)} \approx h_{k,l}^{(u)}, \quad \text{for } k = 0, \dots, K-1 \text{ and } l = 0, \dots, L_C-1. \quad (4.14)$$

Thus, a joint estimate  $[\hat{h}_0^{(u)}, \dots, \hat{h}_{L_C-1}^{(u)}, 0, \dots, 0]^T$  for all  $k = 0, \dots, K-1$  is given by

$$\begin{aligned} [\hat{h}_0^{(u)}, \dots, \hat{h}_{L_C-1}^{(u)}, 0, \dots, 0]^T &= \\ & \frac{1}{L_U \cdot K \cdot \sigma_W^2 \cdot h_0^{(u)*}} \cdot \sum_{k=0}^{K-1} \sum_{i=0}^{L_U-1} e^{j \cdot i \cdot Q \cdot \varphi^{(u)}} \cdot e^{-j \cdot (L_U-1) \cdot Q \cdot \varphi^{(u)}} \cdot r_{k,0}^{(u)*} \cdot \mathbf{r}_{k,i+1}^{(u)}, \end{aligned} \quad (4.15)$$

with  $K$  the number of received vectors used to estimate the expectation value at the receiver.

As the factor  $h_0^{(u)*}$  is unknown at the receiver, the channel delay taps can only be estimated within this complex scalar ambiguity if no further information about the channel is available [TG97]. The ambiguity in Eq. (4.15) can be resolved by taking into account the pilot assisted channel estimates of the channel transfer factors corresponding to the  $Q_P$  pilot carrying subcarriers. For this purpose, the vector  $[\hat{h}_0^{(u)}, \dots, \hat{h}_{L_C-1}^{(u)}, 0, \dots, 0]^T$  estimated by the correlation based estimation according to Eq. (4.15) is considered in frequency domain. The frequency domain representation of the correlation based estimate is calculated according to

$$\left[ \hat{c}_{0,\text{corr}}^{(u)}, \dots, \hat{c}_{Q-1,\text{corr}}^{(u)} \right]^T = \mathbf{F}_Q \cdot \left[ \hat{h}_0^{(u)}, \dots, \hat{h}_{L_C-1}^{(u)}, 0, \dots, 0 \right]^T. \quad (4.16)$$

Due to the assumption  $L_C \leq Q$ , the elements  $\hat{c}_{q,\text{corr}}^{(u)}$ ,  $q = 0, \dots, Q-1$ , of the resulting vector correspond to the channel transfer factors of the  $Q$  allocated subcarriers as it has been defined in Eq. (2.43) and (2.45). The additional index 'corr' is applied to distinguish the correlation based estimate from the LS estimate. The elements  $\hat{c}_{q,\text{corr}}^{(u)}$ ,  $q = 0, \dots, Q-1$ , exhibit the same factor  $h_0^{(u)*}$  of ambiguity as the elements  $\hat{h}_l^{(u)}$ ,  $l = 0, \dots, L_C-1$ , because this constant factor remains unaffected by the application of the DFT operation in Eq. (4.16). The factor of ambiguity is estimated by taking the average over the ratio between the LS estimates and the correlation based estimates at the pilot carrying subcarriers. Thus, the factor of ambiguity is estimated by

$$\hat{h}_0^{(u)*} = \frac{1}{Q_P} \sum_{q_P=0}^{Q_P-1} \frac{\hat{c}_{\kappa,q_P}^{(u)}}{\hat{c}_{q_P,\text{corr}}^{(u)}}. \quad (4.17)$$

Then, the complex scalar ambiguity can be resolved and the estimates of the channel transfer factors for the non-pilot carrying subcarriers are obtained by

$$\hat{c}_{q_D}^{(u)} = \frac{\hat{c}_{q_D,\text{corr}}^{(u)}}{\hat{h}_0^{(u)*}} \quad \text{for } q_D = 0, \dots, Q_D-1, \quad (4.18)$$

which are valid for all IFDMA symbols with indices  $k = 0, \dots, K-1$ . Finally, the estimates  $\hat{c}_{q_D}^{(u)}$ ,  $q_D = 0, \dots, Q_D-1$ , and the LS estimates  $\hat{c}_{\kappa,q_P}^{(u)}$ ,  $q_P = 0, \dots, Q_P-1$ , are combined in the vector  $\hat{\mathbf{c}}^{(u)}$ .

In this section, it has been shown that the channel transfer factors corresponding to the non-pilot carrying subcarriers can be estimated by analyzing the autocorrelation matrix of the received vectors  $\tilde{\mathbf{r}}_k^{(u)}$ ,  $k = 0, \dots, K-1$ , if the number  $L_C$  of channel delay taps is smaller than or equal to the number  $Q$  of elements per IFDMA block. This condition applies to the introduced correlation based semiblind channel estimation because each IFDMA symbol with cyclic prefix contains blocks of  $Q$  differing data symbols. As the correlation of these blocks is used to estimate the channel delay taps, the number of unknown elements is restricted to  $Q$ .

#### 4.2.2.2 Estimation for Channels with Large Delay Spread

In this section, the correlation based semiblink channel estimation that has been explained in Section 4.2.2.1 is derived for the case of large channel delay spreads which means that the number  $L_C$  of channel delay taps is assumed to fulfill the condition

$$L_C > Q. \quad (4.19)$$

For this case, the cyclic prefix consists of  $N_G = L_C \cdot Q$  elements with

$$L_G = \left\lceil \frac{L_C}{Q} \right\rceil. \quad (4.20)$$

For large channel delay spreads, the estimation of the channel delay taps  $h_{k,0}^{(u)}, \dots, h_{k,L_C-1}^{(u)}$  is not feasible while applying the correlation based semiblink channel estimation introduced in Section 4.2.2.1. However, for IFDMA, the knowledge of the  $Q$  channel transfer coefficients corresponding to the allocated subcarriers is sufficient to describe the channel influence on the received IFDMA symbol. Therefore, in the following, a correlation based semiblink channel estimation is derived which provides estimates of the elements  $c_{k,q}^{(u)}$ ,  $q = 0, \dots, Q - 1$  of the cyclic channel impulse response which are the time domain representations of the  $Q$  channel transfer factors corresponding to the allocated subcarriers. By doing so, the number of unknown elements to be estimated reduces from  $L_C$  to  $Q$  and the correlation based semiblink channel estimation is feasible. In the following, the principle of correlation based semiblink channel estimation for channels with large delay spread is again presented for  $U = 1$  user in the system. Again, the principle of correlation based estimation for large channel delay spreads is deduced at first. Then, the combination of correlation based estimation with the pilot based LS estimation is explained.

For the correlation based channel estimation, the vector  $\tilde{\mathbf{r}}_k^{(u)}$  containing the received IFDMA symbol with index  $k$  and the corresponding cyclic prefix is considered as explained in Section 4.2.2.1. Due to the assumption that the number  $L_C$  of channel delay taps is larger than the number  $Q$  of elements per IFDMA block, the received vector  $\tilde{\mathbf{r}}_k^{(u)}$  is influenced by the transmitted IFDMA symbol with index  $k$ , the cyclic prefix of the IFDMA symbol with index  $k$  and the last  $L_G$  blocks of the transmitted IFDMA symbol with index  $k - 1$  as it is illustrated in Figure 4.3.

In order to describe the vector  $\tilde{\mathbf{r}}_k^{(u)}$  in dependency of the channel delay taps  $h_{k,l}^{(u)}$ ,  $l = 0, \dots, L_C - 1$ , the  $Q \times Q$  matrices  $\mathbf{H}_{k,0}^{(u)}, \dots, \mathbf{H}_{k,L_G}^{(u)}$  are defined in the following.

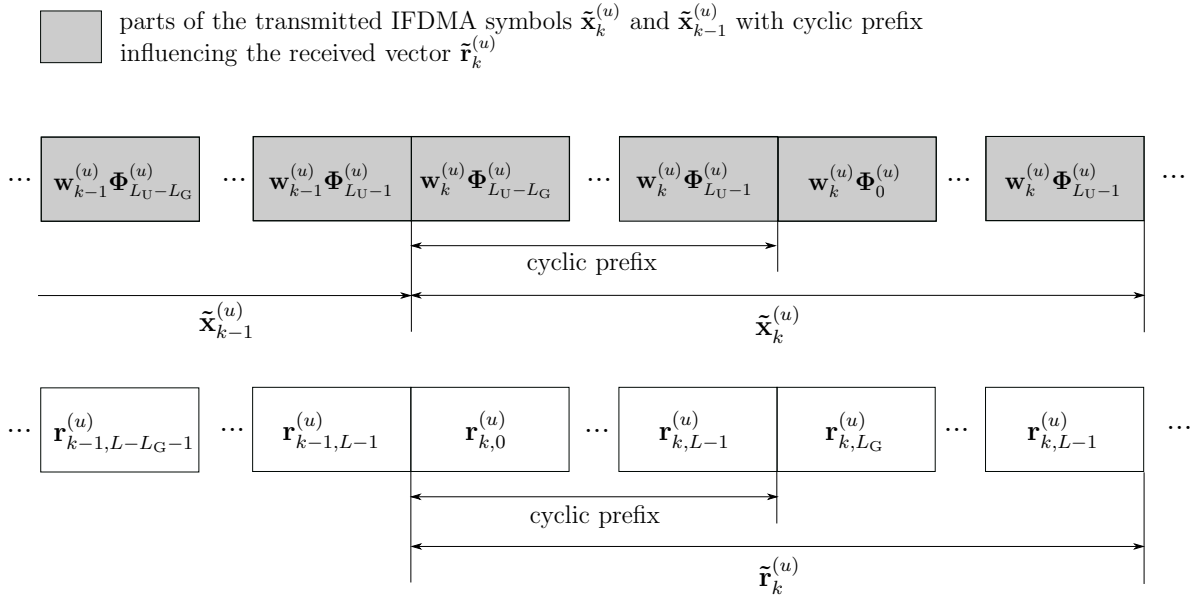


Figure 4.3. Influence of the transmitted IFDMA symbols  $\tilde{\mathbf{x}}_k^{(u)}$  and  $\tilde{\mathbf{x}}_{k-1}^{(u)}$  with cyclic prefix on the received vector  $\tilde{\mathbf{r}}_k^{(u)}$  due to transmission over a multipath channel with  $L_C > Q$  delay taps.

Let  $\mathbf{H}_{k,0}^{(u)}$  denote the Toeplitz matrix that is given by

$$\mathbf{H}_{k,0}^{(u)} = \begin{bmatrix} h_{k,0}^{(u)} & 0 & \cdots & \cdots & 0 \\ h_{k,1}^{(u)} & h_{k,0}^{(u)} & 0 & \cdots & \vdots \\ \vdots & & \ddots & & 0 \\ h_{k,Q-1}^{(u)} & \cdots & & h_{k,0}^{(u)} \end{bmatrix}. \quad (4.21)$$

The Toeplitz matrices  $\mathbf{H}_{k,j}^{(u)}$ ,  $j = 1, \dots, L_G - 2$ , are defined according to

$$\mathbf{H}_{k,j}^{(u)} = \begin{bmatrix} h_{k,jQ}^{(u)} & h_{k,jQ-1}^{(u)} & \cdots & h_{k,(j-1)Q+1}^{(u)} \\ h_{k,jQ+1}^{(u)} & h_{k,jQ}^{(u)} & \cdots & \vdots \\ \vdots & & \ddots & \\ h_{k,(j+1)Q-1}^{(u)} & \cdots & h_{k,jQ}^{(u)} \end{bmatrix}. \quad (4.22)$$

Further, let  $\mathbf{H}_{k,L_G-1}^{(u)}$  and  $\mathbf{H}_{k,L_G}^{(u)}$  be defined according to

$$\mathbf{H}_{k,L_G-1}^{(u)} = \begin{bmatrix} h_{k,(L_G-1)Q}^{(u)} & \cdots & & h_{k,(L_G-2)Q+1}^{(u)} \\ \vdots & \ddots & & \vdots \\ h_{k,L_G-1}^{(u)} & & & \vdots \\ 0 & \ddots & \ddots & \\ \vdots & & & \\ 0 & \cdots & 0 & h_{k,L_G-1}^{(u)} & \cdots & h_{k,(L_G-1)Q}^{(u)} \end{bmatrix} \quad (4.23)$$

and

$$\mathbf{H}_{k,L_G}^{(u)} = \begin{bmatrix} 0 & \cdots & 0 & h_{k,L_G-1}^{(u)} & \cdots & h_{k,(L_G-1)Q+1}^{(u)} \\ \vdots & & & \ddots & \ddots & \vdots \\ 0 & \cdots & & 0 & h_{k,L_G-1}^{(u)} & \\ 0 & \cdots & & & 0 & \\ \vdots & & & & \vdots & \\ 0 & \cdots & & & 0 & \end{bmatrix}, \quad (4.24)$$

respectively.

With the aforementioned definitions, the received vector  $\tilde{\mathbf{r}}_k^{(u)}$  can be represented by

$$\tilde{\mathbf{r}}_k^{(u)} = \begin{bmatrix} \mathbf{H}_{k,L_G}^{(u)} & \cdots & \mathbf{H}_{k,0}^{(u)} & \mathbf{0}_Q & \cdots & \mathbf{0}_Q \\ \mathbf{0}_Q & \mathbf{H}_{k,L_G}^{(u)} & \cdots & \mathbf{H}_{k,0}^{(u)} & \mathbf{0}_Q & \cdots & \mathbf{0}_Q \\ \vdots & & & & & & \\ \mathbf{0}_Q & & \cdots & \mathbf{0}_Q & \mathbf{H}_{k,L_G}^{(u)} & \cdots & \mathbf{H}_{k,0}^{(u)} \end{bmatrix} \cdot \begin{bmatrix} \Phi_{L_U-L_G}^{(u)} & \mathbf{0}_Q \\ \vdots & \vdots \\ \Phi_{L_U-1}^{(u)} & \mathbf{0}_Q \\ \mathbf{0}_Q & \Phi_{L_U-L_G}^{(u)} \\ \vdots & \vdots \\ \mathbf{0}_Q & \Phi_{L_U-1}^{(u)} \\ & \Phi_0^{(u)} \\ \vdots & \vdots \\ \mathbf{0}_Q & \Phi_{L_U-1}^{(u)} \end{bmatrix} + \begin{bmatrix} \mathbf{w}_{k-1}^{(u)} \\ \mathbf{w}_k^{(u)} \end{bmatrix} + \tilde{\mathbf{v}}_k^{(u)}. \quad (4.25)$$

Now, the blocks  $\mathbf{r}_{k,0}^{(u)}, \dots, \mathbf{r}_{k,L-1}^{(u)}$  of the vector  $\tilde{\mathbf{r}}_k^{(u)}$  are inverse phase shifted which leads



to the vector  $\tilde{\mathbf{r}}_k^{(u)}$  that is calculated according to

$$\begin{aligned} \tilde{\mathbf{r}}_k^{(u)} &= \begin{bmatrix} \mathbf{r}_{k,0}^{(u)} \\ \vdots \\ \mathbf{r}_{k,L-1}^{(u)} \end{bmatrix} \\ &= \begin{bmatrix} \Phi_{L_U-L_G}^{(u)H} & 0 & \dots & 0 \\ 0 & \ddots & 0 & 0 \\ & 0 & \Phi_{L_U-1}^{(u)H} & 0 & \dots & 0 \\ \vdots & & 0 & \Phi_0^{(u)H} & 0 & \vdots \\ & & & & \ddots & 0 \\ 0 & \dots & & 0 & \Phi_{L_U-1}^{(u)H} \end{bmatrix} \cdot \mathbf{r}_k^{(u)}. \end{aligned} \quad (4.26)$$

The vector  $\tilde{\mathbf{r}}_k^{(u)}$  exhibits a dependency on the matrix  $\mathcal{H}_k^{(u)}$  which contains the elements  $c_{k,q}^{(u)}$  of the cyclic channel impulse response as defined in Eq. (2.38). A detailed derivation of the vector  $\tilde{\mathbf{r}}_k^{(u)}$  can be found in the Appendix A.1. At this point, only the crucial relation between  $\tilde{\mathbf{r}}_k^{(u)}$  and the matrix  $\mathcal{H}_k^{(u)}$  is stated which is given by

$$\begin{aligned} \tilde{\mathbf{r}}_k^{(u)} &= \left\{ \begin{array}{l} L_G \\ \\ L_U \end{array} \right\} \begin{bmatrix} \square & \Phi_{L_U-L_G}^{(u)H} \cdot \mathbf{H}_{k,0}^{(u)} \cdot \Phi_{L_U-L_G}^{(u)} \\ \vdots & \square \\ & \vdots \\ \square & \square \\ \mathbf{0}_Q & \mathcal{H}_k^{(u)} \\ \vdots & \vdots \\ \mathbf{0}_Q & \mathcal{H}_k^{(u)} \end{bmatrix} \cdot \begin{bmatrix} \mathbf{w}_{k-1}^{(u)} \\ \mathbf{w}_k^{(u)} \end{bmatrix} \\ &+ \begin{bmatrix} \Phi_{L_U-L_G}^{(u)H} & 0 & \dots & 0 \\ 0 & \ddots & 0 & 0 \\ & 0 & \Phi_{L_U-1}^{(u)H} & 0 & \dots & 0 \\ \vdots & & 0 & \Phi_0^{(u)H} & 0 & \vdots \\ & & & & \ddots & 0 \\ 0 & \dots & & 0 & \Phi_{L_U-1}^{(u)H} \end{bmatrix} \cdot \tilde{\mathbf{v}}_k^{(u)}. \end{aligned} \quad (4.27)$$

The autocorrelation matrix of  $\tilde{\mathbf{r}}_k^{(u)}$  is specified by

$$\mathbb{E} \left\{ \tilde{\mathbf{r}}_k^{(u)} \cdot \tilde{\mathbf{r}}_k^{(u)\text{H}} \right\} = \begin{matrix} & & L_G & & \\ & & \left\{ \begin{matrix} \left[ \begin{array}{cccc} & \square & & \dots & \square \\ & \vdots & & & \vdots \\ & \square & & \square & \\ \mathcal{H}_k^{(u)} \cdot \Phi_{L_U-L_G}^{(u)\text{H}} \cdot \mathbf{H}_{k,0}^{(u)} \cdot \Phi_{L_U-L_G}^{(u)} & \square & \dots & \square \\ & \vdots & & \vdots & \vdots \\ \mathcal{H}_k^{(u)} \cdot \Phi_{L_U-L_G}^{(u)\text{H}} \cdot \mathbf{H}_{k,0}^{(u)} \cdot \Phi_{L_U-L_G}^{(u)} & \square & \dots & \square \end{array} \right] \cdot \sigma_W^2 + \sigma_\nu^2 \cdot \mathbf{I}_{L_Q} \end{matrix} \right. & & \\ & & L_U & & \end{matrix} \quad (4.28)$$

and contains  $L_U$  times the matrix multiplication  $\mathcal{H}_k^{(u)} \cdot \Phi_{L_U-L_G}^{(u)\text{H}} \cdot \mathbf{H}_{k,0}^{(u)} \cdot \Phi_{L_U-L_G}^{(u)}$ .

The calculation of  $\mathcal{H}_k^{(u)} \cdot \Phi_{L_U-L_G}^{(u)\text{H}} \cdot \mathbf{H}_{k,0}^{(u)} \cdot \Phi_{L_U-L_G}^{(u)}$  leads to the  $Q \times Q$  matrix that is given by

$$\begin{aligned} & \mathcal{H}_k^{(u)} \cdot \Phi_{L_U-L_G}^{(u)\text{H}} \cdot \mathbf{H}_{k,0}^{(u)} \cdot \Phi_{L_U-L_G}^{(u)} \\ &= \begin{bmatrix} c_{k,0}^{(u)} & c_{k,Q-1}^{(u)} & \dots & c_{k,1}^{(u)} \\ c_{k,1}^{(u)} & c_{k,0}^{(u)} & \dots & c_{k,Q-2}^{(u)} \\ \vdots & \dots & \ddots & \vdots \\ c_{k,Q-1}^{(u)} & c_{k,Q-2}^{(u)} & \dots & c_{k,0}^{(u)} \end{bmatrix} \cdot \begin{bmatrix} h_0^{(u)} & 0 & \dots & \dots & 0 \\ h_1^{(u)} \cdot e^{j \cdot \varphi^{(u)}} & h_0^{(u)} & 0 & \dots & \vdots \\ \vdots & & \ddots & & 0 \\ h_{Q-1}^{(u)} \cdot e^{j \cdot (Q-1) \cdot \varphi^{(u)}} & \dots & \dots & & h_0^{(u)} \end{bmatrix}^{\text{H}} \\ &= \begin{bmatrix} c_{k,0}^{(u)} \cdot h_{k,0}^{(u)*} & \square & \dots & \square \\ \vdots & \vdots & & \vdots \\ c_{k,Q-1}^{(u)} \cdot h_{k,0}^{(u)*} & \square & \dots & \square \end{bmatrix}. \end{aligned} \quad (4.29)$$

Thus, the first column of the autocorrelation matrix in Eq. (4.28) contains  $L_U$  times the cyclic channel impulse response vector  $\mathbf{c}_k^{(u)} = [c_{k,0}^{(u)}, \dots, c_{k,Q-1}^{(u)}]^{\text{T}}$ . Considering the derivations in Section 4.2.2.1 and assuming that there are only small channel variations in time domain, i.e.,  $c_{k,q}^{(u)} \approx c_q^{(u)}$  for  $k = 0, \dots, K-1$  and  $q = 0, \dots, Q-1$  the vector  $\mathbf{c}^{(u)} = [c_0^{(u)}, \dots, c_{Q-1}^{(u)}]^{\text{T}}$  can be estimated by

$$\left[ \hat{c}_0^{(u)}, \dots, \hat{c}_{Q-1}^{(u)} \right]^{\text{T}} = \frac{1}{L_U \cdot K \cdot \sigma_W^2 \cdot h_0^{(u)*}} \sum_{k=0}^{K-1} \sum_{i=0}^{L_U-1} \tilde{\mathbf{r}}_{k,i+L_G}^{(u)} \cdot \tilde{r}_{k,0}^{(u)*}. \quad (4.30)$$

The cyclic channel impulse response vector is estimated within the complex scalar ambiguity represented by the factor  $h_0^{(u)*}$ . An estimate of the factor  $h_0^{(u)*}$  is obtained

as explained in Section 4.2.2.1. The vector  $[\hat{c}_0^{(u)}, \dots, \hat{c}_{Q-1}^{(u)}]^T$  is transformed in frequency domain according to

$$\left[ \hat{c}_{0,\text{corr}}^{(u)}, \dots, \hat{c}_{Q-1,\text{corr}}^{(u)} \right]^T = \mathbf{F}_Q \cdot \left[ \hat{c}_0^{(u)}, \dots, \hat{c}_{Q-1}^{(u)} \right]^T. \quad (4.31)$$

The elements  $\hat{c}_{q,\text{corr}}^{(u)}$ ,  $q = 0, \dots, Q-1$ , of the resulting vector correspond to the channel transfer factors of the  $Q$  allocated subcarriers as it has been defined in Eq. (2.43) and (2.45). Then, the factor of ambiguity is estimated according to Eq. (4.17) and the estimates  $\hat{c}_{q_D}^{(u)}$ ,  $q_D = 0, \dots, Q_D-1$ , with resolved complex scalar ambiguity are calculated as shown in Eq. (4.18). Finally, the estimates  $\hat{c}_{q_D}^{(u)}$ ,  $q_D = 0, \dots, Q_D-1$ , and the LS estimates  $\hat{c}_{\kappa,q_P}^{(u)}$ ,  $q_P = 0, \dots, Q_P-1$ , are combined in the vector  $\hat{\mathbf{c}}^{(u)}$ .

### 4.2.2.3 Multi-User Influence

In this section, the correlation based semiblink channel estimation that has been derived in Section 4.2.2.1 is investigated for the case that the signals of multiple users are transmitted within the same TDMA slot. As for correlation based semiblink channel estimation, the received IFDMA signals are analyzed with the cyclic prefix parts inclusively, the impact of the signals transmitted by multiple users on the estimation algorithm needs to be investigated. The LS estimates of the channel transfer factors corresponding to the  $Q_P$  pilot carrying subcarriers remain unaffected by the transmission of multiple users within the same TDMA slot as it has been shown in Section 3.2.3. Therefore, this section concentrates on the influence of multiple users on the correlation based channel estimation. For this purpose, the received IFDMA signal at a base station is considered and the correlation based channel estimation is derived for a certain user with index  $u_1$  in case of uplink transmission. For the sake of completeness, the influence of multiple users allocated to the same TDMA slot on the correlation based channel estimation is further investigated for downlink transmission. For clarity reasons, the investigations are performed under the assumption of small channel delay spreads, i.e.,  $L_C \leq Q$ . However, the conclusions are applicable to the case of large channel delay spreads as well.

**Uplink** For uplink transmission, the received signal is considered at a base station of the system. During uplink transmission, the signals transmitted within the same TDMA slot by each of the  $U$  users experience user-specific channel conditions. At the base station the superposition of the  $U$  users' signals disturbed by AWGN is received. The total received vector with index  $k$  at the base station is represented by

$$\tilde{\mathbf{r}}_k = \sum_{u=0}^{U-1} \left( \mathbf{H}_{k,\text{corr}}^{(u)} \cdot \boldsymbol{\Theta}_{\text{corr}}^{(u)} \cdot \begin{bmatrix} \mathbf{w}_{k-1}^{(u)} \\ \mathbf{w}_k^{(u)} \end{bmatrix} \right) + \tilde{\mathbf{v}}_k. \quad (4.32)$$

The total received vectors  $\tilde{\mathbf{r}}_k$  with  $k = 0, \dots, K-1$  are utilized to derive a correlation based channel estimate for the user with index  $u_1$ . Due to cyclic prefix insertion, the IFDMA symbols transmitted by different users maintain their orthogonality after transmission over a multipath channel. Therefore, the IFDMA symbol transmitted by the user with index  $u_1$  can be separated from the IFDMA symbols transmitted by other users. However, the cyclic prefixes transmitted by different users are not orthogonal to each other and the cyclic prefix transmitted by the user with index  $u_1$  cannot be separated from the cyclic prefixes transmitted by other users at the base station.

The received vector  $\tilde{\mathbf{r}}_k^{(u_1)}$  of the considered user with index  $u_1$  can thus be represented by the received vector defined in Eq. (4.7) that is superposed by the cyclic prefix parts transmitted by other users.  $\tilde{\mathbf{r}}_k^{(u_1)}$  is given by

$$\begin{aligned} \tilde{\mathbf{r}}_k^{(u_1)} &= \mathbf{H}_{k,\text{corr}}^{(u_1)} \cdot \boldsymbol{\Theta}_{\text{corr}}^{(u_1)} \cdot \begin{bmatrix} \mathbf{w}_{k-1}^{(u_1)} \\ \mathbf{w}_k^{(u_1)} \end{bmatrix} + \tilde{\mathbf{v}}_k^{(u_1)} \\ &+ \sum_{\substack{u=0 \\ u \neq u_1}}^{U-1} \left( \begin{bmatrix} \mathbf{H}_{k,1}^{(u)} & \mathbf{H}_{k,0}^{(u)} & \mathbf{0}_Q & \cdots & \mathbf{0}_Q \\ \mathbf{0}_Q & \mathbf{0}_Q & \mathbf{0}_Q & \cdots & \mathbf{0}_Q \\ \vdots & & \ddots & \ddots & \vdots \\ \mathbf{0}_Q & \cdots & \mathbf{0}_Q & \mathbf{0}_Q & \mathbf{0}_Q \end{bmatrix} \cdot \boldsymbol{\Theta}_{\text{corr}}^{(u)} \cdot \begin{bmatrix} \mathbf{w}_{k-1}^{(u)} \\ \mathbf{w}_k^{(u)} \end{bmatrix} \right). \quad (4.33) \end{aligned}$$

With  $\mathbb{E}\{\mathbf{w}_k^{(u_1)} \cdot \mathbf{w}_k^{(u_2)\text{H}}\} = \mathbf{0}_Q$ , for  $u_1 \neq u_2$ , the autocorrelation matrix of  $\tilde{\mathbf{r}}_k^{(u_1)}$  yields

$$\begin{aligned} \mathbb{E}\left\{\tilde{\mathbf{r}}_k^{(u_1)} \cdot \tilde{\mathbf{r}}_k^{(u_1)\text{H}}\right\} &= \mathbf{H}_{k,\text{corr}}^{(u_1)} \cdot \boldsymbol{\Theta}_{\text{corr}}^{(u_1)} \cdot \sigma_W^2 \cdot \mathbf{I}_{2Q} \cdot \boldsymbol{\Theta}_{\text{corr}}^{(u_1)\text{H}} \cdot \mathbf{H}_{k,\text{corr}}^{(u_1)\text{H}} + \sigma_V^2 \cdot \mathbf{I}_{LQ} \\ &+ \sum_{\substack{u=0 \\ u \neq u_1}}^{U-1} \begin{bmatrix} \sigma_W^2 \cdot (\mathbf{H}_{k,0}^{(u)} \cdot \mathbf{H}_{k,0}^{(u)\text{H}} + \mathbf{H}_{k,1}^{(u)} \cdot \mathbf{H}_{k,1}^{(u)\text{H}}) & \mathbf{0}_Q & \cdots & \mathbf{0}_Q \\ \mathbf{0}_Q & \mathbf{0}_Q & \cdots & \mathbf{0}_Q \\ \vdots & \vdots & \ddots & \vdots \\ \mathbf{0}_Q & \mathbf{0}_Q & \cdots & \mathbf{0}_Q \end{bmatrix}. \quad (4.34) \end{aligned}$$

The additive sum term in Eq. (4.34) that is caused by the interfering cyclic prefixes transmitted by the users with indices  $u \neq u_1$  has impact on the first  $Q$  elements of the first  $Q$  columns of the autocorrelation matrix. The derivations in Section 4.2.2.1 show that this part of the autocorrelation matrix remains unused for the correlation based channel estimation and, thus, the correlation based channel estimate is not disturbed by multi-user transmission in the uplink. Therefore, the correlation based semiblind channel estimation is performed as explained in Section 4.2.2.1 at a base station if the signals of multiple users are received.

**Downlink** For downlink transmission, the received signal is considered at the mobile terminal of the user with index  $u_1$ . The superposition of the  $U$  users' signals is transmitted by a base station and experiences identical channel conditions for the case of downlink transmission. At the mobile terminal, the received signal is distorted by AWGN.

The received vector with index  $k$  at the mobile terminal of the user with index  $u_1$  is given by

$$\tilde{\mathbf{r}}_k^{(u_1)} = \mathbf{H}_{k,\text{corr}}^{(u_1)} \cdot \sum_{u=0}^{U-1} \left( \boldsymbol{\Theta}_{\text{corr}}^{(u)} \cdot \begin{bmatrix} \mathbf{w}_{k-1}^{(u)} \\ \mathbf{w}_k^{(u)} \end{bmatrix} \right) + \tilde{\mathbf{v}}_k^{(u_1)}. \quad (4.35)$$

The autocorrelation matrix of the received vector  $\tilde{\mathbf{r}}_k^{(u_1)}$  contains the superposition of the  $U$  matrices  $\boldsymbol{\Theta}_{\text{corr}}^{(u)} \cdot \boldsymbol{\Theta}_{\text{corr}}^{(u)\text{H}}$  for  $u = 0, \dots, U-1$  and is given by

$$\mathbb{E} \left\{ \tilde{\mathbf{r}}_k^{(u_1)} \cdot \tilde{\mathbf{r}}_k^{(u_1)\text{H}} \right\} = \mathbf{H}_{k,\text{corr}}^{(u_1)} \cdot \sum_{u=0}^{U-1} \left( \boldsymbol{\Theta}_{\text{corr}}^{(u)} \cdot \sigma_{\text{W}}^2 \cdot \mathbf{I}_{2Q} \cdot \boldsymbol{\Theta}_{\text{corr}}^{(u)\text{H}} \right) \cdot \mathbf{H}_{k,\text{corr}}^{(u_1)\text{H}} + \sigma_{\nu}^2 \cdot \mathbf{I}_{LQ}. \quad (4.36)$$

The calculation of the first  $Q$  columns of the autocorrelation matrix which are important for the correlation based channel estimation yields

$$\mathbb{E} \left\{ \tilde{\mathbf{r}}_k^{(u_1)} \cdot \tilde{\mathbf{r}}_k^{(u_1)\text{H}} \right\} = \sigma_{\text{W}}^2 \cdot \begin{bmatrix} \mathbf{H}_{k,0}^{(u)} \cdot \mathbf{H}_{k,0}^{(u)\text{H}} + \mathbf{H}_{k,1}^{(u)} \cdot \mathbf{H}_{k,1}^{(u)\text{H}} & \square & \dots & \square \\ \left( \mathbf{H}_{k,0}^{(u)} \cdot \sum_{u=0}^{U-1} \boldsymbol{\Phi}_0^{(u)} + \mathbf{H}_{k,1}^{(u)} \cdot \sum_{u=0}^{U-1} \boldsymbol{\Phi}_{L_U-1}^{(u)} \right) \cdot \sum_{u=0}^{U-1} \boldsymbol{\Phi}_{L_U-1}^{(u)\text{H}} \cdot \mathbf{H}_{k,0}^{(u)\text{H}} & \square & \dots & \square \\ \left( \mathbf{H}_{k,0}^{(u)} \cdot \sum_{u=0}^{U-1} \boldsymbol{\Phi}_1^{(u)} + \mathbf{H}_{k,1}^{(u)} \cdot \sum_{u=0}^{U-1} \boldsymbol{\Phi}_0^{(u)} \right) \cdot \sum_{u=0}^{U-1} \boldsymbol{\Phi}_{L_U-1}^{(u)\text{H}} \cdot \mathbf{H}_{k,0}^{(u)\text{H}} & \square & \dots & \square \\ \vdots & \vdots & \ddots & \vdots \\ \left( \mathbf{H}_{k,0}^{(u)} \cdot \sum_{u=0}^{U-1} \boldsymbol{\Phi}_{L_U-1}^{(u)} + \mathbf{H}_{k,1}^{(u)} \cdot \sum_{u=0}^{U-1} \boldsymbol{\Phi}_{L_U-2}^{(u)} \right) \cdot \sum_{u=0}^{U-1} \boldsymbol{\Phi}_{L_U-1}^{(u)\text{H}} \cdot \mathbf{H}_{k,0}^{(u)\text{H}} & \square & \dots & \square \end{bmatrix} + \sigma_{\nu}^2 \mathbf{I}_{LQ}. \quad (4.37)$$

Eq. (4.37) and the derivations in Section 4.2.2.1 lead to the calculation of the correlation based channel estimate according to

$$\begin{bmatrix} \hat{h}_0^{(u_1)}, \dots, \hat{h}_{L_C-1}^{(u_1)}, 0, \dots, 0 \end{bmatrix}^{\text{T}} = \frac{1}{L_U \cdot K \cdot \sigma_{\text{W}}^2 \cdot h_0^{(u_1)*}} \cdot \sum_{k=0}^{K-1} \sum_{i=0}^{L_u} \left\{ \sum_{u=0}^{U-1} e^{j \cdot i \cdot Q \cdot \varphi^{(u)}} \cdot \sum_{u=0}^{U-1} e^{-j \cdot (L_U-1) \cdot Q \cdot \varphi^{(u)}} \cdot r_{k,0}^{(u_1)*} \cdot \mathbf{r}_{k,i}^{(u_1)} \right\}. \quad (4.38)$$

Based on the correlation based estimate in Eq. (4.38), the factor  $h_0^{(u_1)*}$  is estimated and the correlation based semiblind channel estimate is obtained as explained in Section 4.2.2.1. Thus, for multi-user downlink transmission, the channel is estimated according to Eq. (4.38) and the influence of the  $U - 1$  signals transmitted by other users in the system on the correlation based semiblind channel estimate is eliminated.

### 4.2.3 Subspace Based Semiblind Channel Estimation

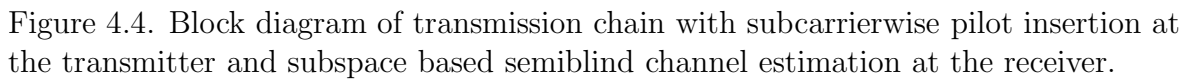
#### 4.2.3.1 Estimation for Channels with Small Delay Spread

In this section, the subspace based semiblind channel estimation is derived for the case of small channel delay spreads which means that Eq. (4.1) is fulfilled and that the cyclic prefix consists of  $N_G = Q$  elements. This restriction is reasonable as the subspace based semiblind channel estimation, like the correlation based semiblind channel estimation, is based on the cyclostationarity with  $Q$  of the received IFDMA signal. According to the correlation based semiblind channel estimation, the cyclic prefix part of each received IFDMA symbol is also analyzed for the subspace based semiblind channel estimation and, thus, the influence of multiple users in the system shall be considered. In this section, the estimation principle is presented for  $U = 1$  user in the system first.

In Figure 4.4, the principle of the subspace based semiblind channel estimation for IFDMA is illustrated in a block diagram. This figure depicts the transmitter and the receiver part for subcarrierwise pilot insertion as introduced in Section 3.2.3. The receiver part is extended by the subspace based estimation, which is combined with the LS estimation at the pilot carrying subcarriers.

In the following, the principle of subspace based estimation for IFDMA is deduced at first. Then, the combination of subspace based estimation with the pilot based LS estimation is explained.

In order to apply the subspace based channel estimation to the IFDMA signal of a user under consideration, three blocks of length  $Q$  of the received signal are considered. The last block  $\mathbf{r}_{k-1,L-1}^{(u)}$  of the IFDMA symbol with index  $k - 1$ , the cyclic prefix  $\mathbf{r}_{k,0}^{(u)}$  of the IFDMA symbol with index  $k$  and the first block  $\mathbf{r}_{k,1}^{(u)}$  of the IFDMA symbol with index  $k$  are comprised in one vector. Due to transmission over a channel with  $L_C \leq Q$  delay taps, this vector is influenced by the last two blocks of the transmitted IFDMA symbol with index  $k - 1$ , the cyclic prefix related to the transmitted IFDMA symbol



Let the matrices  $\mathbf{H}_{k,0}^{(u)}$ ,  $\mathbf{H}_{k,1}^{(u)}$  and  $\Phi_i^{(u)}$ ,  $i = 0, \dots, L_U - 1$ , be as defined in Eqs. (4.3), (4.4) and (2.8), respectively. Further on, it is assumed that there are only small channel variations in time domain, implying that the matrices  $\mathbf{H}_{k,0}^{(u)}$  and  $\mathbf{H}_{k,1}^{(u)}$  are approximately

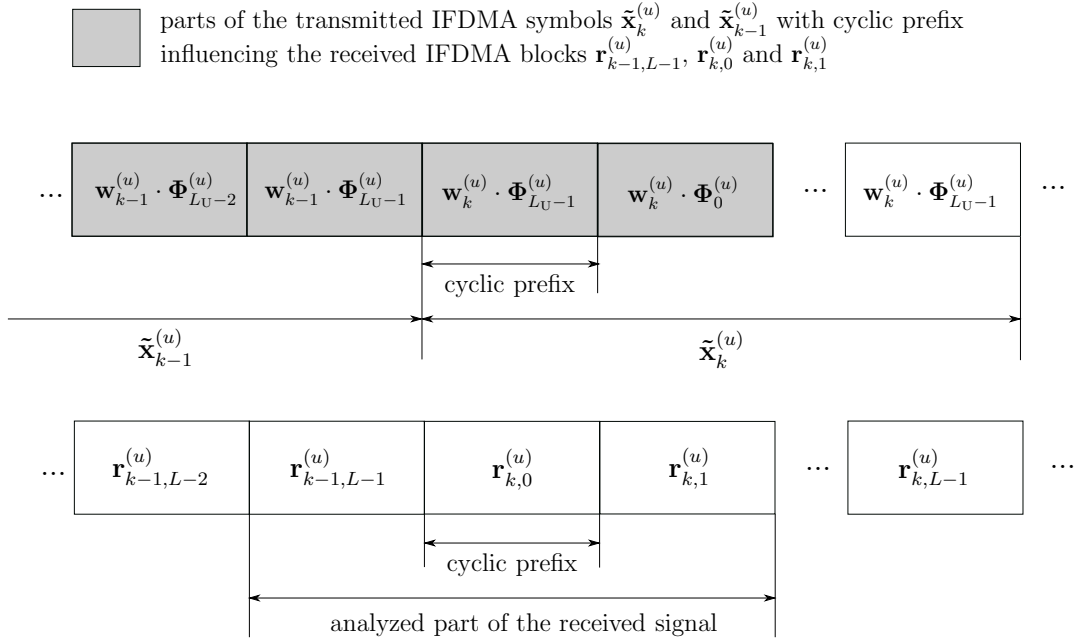


Figure 4.5. Illustration of the channel influence on the received IFDMA blocks  $\mathbf{r}_{k-1,L-1}^{(u)}$ ,  $\mathbf{r}_{k,0}^{(u)}$  and  $\mathbf{r}_{k,1}^{(u)}$ .

constant for the IFDMA symbols with indices  $k = 0, \dots, K - 1$ , i.e.,

$$\mathbf{H}_0^{(u)} \approx \mathbf{H}_{k,0}^{(u)} \text{ and } \mathbf{H}_1^{(u)} \approx \mathbf{H}_{k,1}^{(u)}, \quad \text{for } k = 0, \dots, K - 1. \quad (4.39)$$

Let  $\boldsymbol{\nu}_{k,j}^{(u)} = [\nu_{k,jQ}^{(u)}, \dots, \nu_{k,jQ+Q-1}^{(u)}]^T$  for  $j = 0, \dots, L - 1$  denote  $L$  vectors containing  $Q$  AWGN samples each.

Let further  $\mathbf{H}_{\text{sub}}^{(u)}$  denote a  $3Q \times 4Q$  matrix that is defined according to

$$\mathbf{H}_{\text{sub}}^{(u)} = \begin{bmatrix} \mathbf{H}_1^{(u)} & \mathbf{H}_0^{(u)} & \mathbf{0}_Q & \mathbf{0}_Q \\ \mathbf{0}_Q & \mathbf{H}_1^{(u)} & \mathbf{H}_0^{(u)} & \mathbf{0}_Q \\ \mathbf{0}_Q & \mathbf{0}_Q & \mathbf{H}_1^{(u)} & \mathbf{H}_0^{(u)} \end{bmatrix} \quad (4.40)$$

and  $\boldsymbol{\Theta}_{\text{sub}}^{(u)}$  denote a  $4Q \times 2Q$  matrix that is defined according to

$$\boldsymbol{\Theta}_{\text{sub}}^{(u)} = \begin{bmatrix} \boldsymbol{\Phi}_{L_U-2}^{(u)} & \mathbf{0}_Q \\ \boldsymbol{\Phi}_{L_U-1}^{(u)} & \mathbf{0}_Q \\ \mathbf{0}_Q & \boldsymbol{\Phi}_{L_U-1}^{(u)} \\ \mathbf{0}_Q & \boldsymbol{\Phi}_0^{(u)} \end{bmatrix}. \quad (4.41)$$

Then, the vector of length  $3Q$  containing the three received IFDMA blocks  $\mathbf{r}_{k-1,L-1}^{(u)}$ ,



$\mathbf{r}_{k,0}^{(u)}$  and  $\mathbf{r}_{k,1}^{(u)}$  is represented by

$$\begin{bmatrix} \mathbf{r}_{k-1,L-1}^{(u)} \\ \mathbf{r}_{k,0}^{(u)} \\ \mathbf{r}_{k,1}^{(u)} \end{bmatrix} = \mathbf{H}_{\text{sub}}^{(u)} \cdot \boldsymbol{\Theta}_{\text{sub}}^{(u)} \cdot \begin{bmatrix} \mathbf{w}_{k-1}^{(u)} \\ \mathbf{w}_k^{(u)} \end{bmatrix} + \begin{bmatrix} \boldsymbol{\nu}_{k-1,L-1}^{(u)} \\ \boldsymbol{\nu}_{k,0}^{(u)} \\ \boldsymbol{\nu}_{k,1}^{(u)} \end{bmatrix}. \quad (4.42)$$

Eq. (4.42) shows that three received IFDMA blocks are dependent on two transmitted IFDMA blocks  $\mathbf{w}_{k-1}^{(u)}$  and  $\mathbf{w}_k^{(u)}$  due to the redundancy in the transmit signal. The  $3Q \times 3Q$  autocorrelation matrix of the vector defined in Eq. (4.42) is given by

$$\begin{aligned} \mathcal{A}^{(u)} &= \mathbb{E} \left\{ \begin{bmatrix} \mathbf{r}_{k-1,L-1}^{(u)} \\ \mathbf{r}_{k,0}^{(u)} \\ \mathbf{r}_{k,1}^{(u)} \end{bmatrix} \cdot \begin{bmatrix} \mathbf{r}_{k-1,L-1}^{(u)} \\ \mathbf{r}_{k,0}^{(u)} \\ \mathbf{r}_{k,1}^{(u)} \end{bmatrix}^H \right\} \\ &= \mathbf{H}_{\text{sub}}^{(u)} \cdot \boldsymbol{\Theta}_{\text{sub}}^{(u)} \cdot \sigma_W^2 \cdot \mathbf{I}_{2Q} \cdot \boldsymbol{\Theta}_{\text{sub}}^{(u)H} \cdot \mathbf{H}_{\text{sub}}^{(u)H} + \sigma_\nu^2 \cdot \mathbf{I}_{3Q}. \end{aligned} \quad (4.43)$$

The  $3Q \times 2Q$  matrix  $\mathbf{H}_{\text{sub}}^{(u)} \cdot \boldsymbol{\Theta}_{\text{sub}}^{(u)}$  has full column rank if there is no channel zero located at the  $Q$  allocated subcarriers in frequency domain [MDCM95]. Provided this, the first part of the autocorrelation matrix  $\mathcal{A}^{(u)}$  which is represented by

$$\mathbf{H}_{\text{sub}}^{(u)} \cdot \boldsymbol{\Theta}_{\text{sub}}^{(u)} \cdot \sigma_W^2 \cdot \mathbf{I}_{2Q} \cdot \boldsymbol{\Theta}_{\text{sub}}^{(u)H} \cdot \mathbf{H}_{\text{sub}}^{(u)H} \quad (4.44)$$

has rank  $2Q$  and describes the noise-free case. Thus, the signal subspace is spanned by its eigenvectors which are the columns of the matrix  $\mathbf{H}_{\text{sub}}^{(u)} \cdot \boldsymbol{\Theta}_{\text{sub}}^{(u)}$  with the signal subspace eigenvalues represented by  $\sigma_W^2$ . Eq. (4.44) shows that the  $3Q \times 3Q$  autocorrelation matrix  $\mathcal{A}^{(u)}$  is not full rank in the noise-free case. That means for the noisy case, signal and noise subspace are separable by an eigenvalue decomposition of  $\mathcal{A}^{(u)}$  [MdCDB99]. Assuming the noise power to be smaller than the signal power, the  $Q$  eigenvectors corresponding to the  $Q$  smallest eigenvalues span the noise subspace. A detailed derivation of the identification of signal and noise subspace can be found in [MDCM95] and is not derived in detail in this work.

Let  $\mathbf{g}_0^{(u)}, \dots, \mathbf{g}_{Q-1}^{(u)}$  denote the  $3Q \times 1$  eigenvectors corresponding to the  $Q$  smallest eigenvalues of the autocorrelation matrix  $\mathcal{A}^{(u)}$  that span the noise subspace. Then, with the signal subspace spanned by  $\mathbf{H}_{\text{sub}}^{(u)} \cdot \boldsymbol{\Theta}_{\text{sub}}^{(u)}$  the orthogonality constraint

$$\mathbf{g}_q^{(u)H} \cdot \mathbf{H}_{\text{sub}}^{(u)} \cdot \boldsymbol{\Theta}_{\text{sub}}^{(u)} = \mathbf{0}_{1 \times 2Q}, \quad 0 \leq q \leq Q-1, \quad (4.45)$$

must hold as signal and noise subspace are orthogonal to each other [MdCDB99]. In the following, the  $L_C$  channel delay taps are estimated with the help of Eq. (4.45).

In order to explicitly represent Eq. (4.45) as a function of the  $Q \times 1$  vector  $[h_0^{(u)}, \dots, h_{L_C-1}^{(u)}, 0, \dots, 0]^T$ , the noise subspace eigenvectors  $\mathbf{g}_q^{(u)\text{H}}$  are transformed into the  $Q \times 4Q$  matrices  $\mathcal{G}_q^{(u)}$ . For this transformation, the  $3Q \times 1$  vector  $\mathbf{g}_q^{(u)}$  is split up in three  $Q \times 1$  vectors  $\mathbf{g}_{q,j}^{(u)}$ ,  $j = 0, 1, 2$ . With  $[\mathbf{z}]_i$  denoting the  $i^{\text{th}}$  element of a vector  $\mathbf{z}$ , the vectors  $\mathbf{g}_{q,j}^{(u)}$ ,  $j = 0, 1, 2$ , are defined according to

$$\mathbf{g}_{q,j}^{(u)} = \left[ [\mathbf{g}_q^{(u)}]_{jQ}, \dots, [\mathbf{g}_q^{(u)}]_{jQ+Q-1} \right]^T. \quad (4.46)$$

Let  $\mathbf{A}_{q,j}^{(u)}$  denote a  $Q \times Q$  matrix that is defined by

$$\mathbf{A}_{q,j}^{(u)} = \begin{bmatrix} 0 & \dots & 0 \\ & & [\mathbf{g}_{q,j}^{(u)}]_0 \\ \vdots & & \vdots \\ 0 & [\mathbf{g}_{q,j}^{(u)}]_0 & \dots & [\mathbf{g}_{q,j}^{(u)}]_{Q-2} \end{bmatrix}. \quad (4.47)$$

Further, let  $\mathbf{B}_{q,j}^{(u)}$  denote a  $Q \times Q$  matrix that is given by

$$\mathbf{B}_{q,j}^{(u)} = \begin{bmatrix} [\mathbf{g}_{q,j}^{(u)}]_0 & \dots & [\mathbf{g}_{q,j}^{(u)}]_{Q-1} \\ \vdots & \ddots & 0 \\ [\mathbf{g}_{q,j}^{(u)}]_{Q-1} & 0 & \dots & 0 \end{bmatrix}. \quad (4.48)$$

Then, the  $Q \times 4Q$  matrices  $\mathcal{G}_q^{(u)}$ ,  $q = 0, \dots, Q-1$ , are given by

$$\mathcal{G}_q^{(u)} = \left[ \mathbf{A}_{q,0}^{(u)}, \mathbf{B}_{q,0}^{(u)} + \mathbf{A}_{q,1}^{(u)}, \mathbf{B}_{q,1}^{(u)} + \mathbf{A}_{q,2}^{(u)}, \mathbf{B}_{q,2}^{(u)} \right]. \quad (4.49)$$

The transformation of  $\mathbf{g}_q^{(u)\text{H}}$  into the matrix  $\mathcal{G}_q^{(u)}$  follows the principle that is explained in [MDCM95] or [MdCD02] and is derived for the application in an IFDMA system in Appendix A.2.

With the matrices  $\mathcal{G}_q^{(u)}$ ,  $q = 0, \dots, Q-1$ , the orthogonality constraint in Eq. (4.45) can be rewritten according to

$$\left[ h_0^{(u)}, \dots, h_{L_C-1}^{(u)}, 0, \dots, 0 \right]^* \cdot \mathcal{G}_q^{(u)} \cdot \boldsymbol{\Theta}_{\text{sub}}^{(u)} = \mathbf{0}_{1 \times 2Q}, \quad 0 \leq q \leq Q-1. \quad (4.50)$$

For practical implementations, the autocorrelation matrix  $\mathcal{A}^{(u)}$  is estimated by the arithmetic mean over  $K$  received IFDMA symbols [Hän01]. This approximation is valid

for small channel variations in time domain as it has been assumed at the beginning of this section. Thus, the estimate  $\hat{\mathcal{A}}^{(u)}$  is obtained by

$$\hat{\mathcal{A}}^{(u)} = \frac{1}{K} \sum_{k=0}^{K-1} \begin{bmatrix} \mathbf{r}_{k-1,L-1}^{(u)} \\ \mathbf{r}_{k,0}^{(u)} \\ \mathbf{r}_{k,1}^{(u)} \end{bmatrix} \cdot \begin{bmatrix} \mathbf{r}_{k-1,L-1}^{(u)} \\ \mathbf{r}_{k,0}^{(u)} \\ \mathbf{r}_{k,1}^{(u)} \end{bmatrix}^H. \quad (4.51)$$

Since there is only an estimate  $\hat{\mathcal{A}}^{(u)}$  of the autocorrelation matrix  $\mathcal{A}^{(u)}$  available, the estimated versions  $\hat{\mathbf{g}}_q^{(u)}$  and  $\hat{\mathcal{G}}_q^{(u)}$ ,  $q = 0 \dots, Q-1$ , of the noise subspace eigenvectors  $\mathbf{g}_q^{(u)}$  and the matrices  $\mathcal{G}_q^{(u)}$  are utilized to estimate the channel via the orthogonality constraint

$$\left[ h_0^{(u)}, \dots, h_{L_C-1}^{(u)}, 0, \dots, 0 \right]^* \cdot \hat{\mathcal{G}}_q^{(u)} \cdot \Theta_{\text{sub}}^{(u)} = \mathbf{0}_{1 \times 2Q}, \quad 0 \leq q \leq Q-1. \quad (4.52)$$

Additionally, with the help of the vector  $[\hat{c}_{\kappa,0}^{(u)}, \dots, \hat{c}_{\kappa,Q_P-1}^{(u)}]^T$  containing the LS estimates of the pilot assisted channel estimation, a second equation in dependency of the unknown vector  $[h_0^{(u)}, \dots, h_{L_C-1}^{(u)}, 0, \dots, 0]$  can be given. Let

$$\mathcal{F} = [\mathbf{F}_Q]_{q_P \cdot I, :} \quad \text{for } q_P = 0, \dots, Q_P - 1, \quad (4.53)$$

denote a  $Q_P \times Q$  matrix containing the  $Q_P$  rows of the  $Q \times Q$  DFT matrix  $\mathbf{F}_Q$  that correspond to the pilot carrying subcarriers. Then, the relation

$$\mathcal{F} \cdot \left[ h_0^{(u)}, \dots, h_{L_C-1}^{(u)}, 0, \dots, 0 \right]^T = \left[ \hat{c}_{\kappa,0}^{(u)}, \dots, \hat{c}_{\kappa,Q_P-1}^{(u)} \right]^T \quad (4.54)$$

is valid for the pilot assisted channel estimates.

In compliance with [MdCD02], Eq. (4.52) and (4.54) are combined in a system of equations that is given by

$$\left\{ \begin{array}{l} \left[ h_0^{(u)}, \dots, h_{L_C-1}^{(u)}, 0, \dots, 0 \right]^* \cdot \hat{\mathcal{G}}_q^{(u)} \cdot \Theta_{\text{sub}}^{(u)} = \mathbf{0}_{1 \times 2Q}, \quad 0 \leq q \leq Q-1 \\ \mathcal{F} \cdot \left[ h_0^{(u)}, \dots, h_{L_C-1}^{(u)}, 0, \dots, 0 \right]^T = \left[ \hat{c}_{\kappa,0}^{(u)}, \dots, \hat{c}_{\kappa,Q_P-1}^{(u)} \right]^T \end{array} \right. \quad (4.55)$$

The system of equations in Eq. (4.55) is solved for  $[h_0^{(u)}, \dots, h_{L_C-1}^{(u)}, 0, \dots, 0]^T$ . The solution is obtained by minimizing the function  $\Upsilon^{(u)}$  that is defined as

$$\begin{aligned} \Upsilon^{(u)} = & \sum_{q=0}^{Q-1} \left\| \left[ h_0^{(u)}, \dots, h_{L_C-1}^{(u)}, 0, \dots, 0 \right]^* \cdot \hat{\mathcal{G}}_q^{(u)} \cdot \Theta_{\text{sub}}^{(u)} \right\|_2^2 \\ & + \left\| \mathcal{F} \cdot \left[ h_0^{(u)}, \dots, h_{L_C-1}^{(u)}, 0, \dots, 0 \right]^T - \left[ \hat{c}_{\kappa,0}^{(u)}, \dots, \hat{c}_{\kappa,Q_P-1}^{(u)} \right]^T \right\|_2^2 \end{aligned} \quad (4.56)$$

[MdCD02]. The derivative of  $\Upsilon^{(u)}$  with respect to  $[h_0^{(u)}, \dots, h_{L_C-1}^{(u)}, 0, \dots, 0]^*$  is set to zero and solved for the vector  $[h_0^{(u)}, \dots, h_{L_C-1}^{(u)}, 0, \dots, 0]^T$  which leads to its estimate  $[\hat{h}_0^{(u)}, \dots, \hat{h}_{L_C-1}^{(u)}, 0, \dots, 0]^T$  that is given by

$$\begin{aligned} & [\hat{h}_0^{(u)}, \dots, \hat{h}_{L_C-1}^{(u)}, 0, \dots, 0]^T = \\ & \left( \sum_{q=0}^{Q-1} \hat{\mathcal{G}}_q^{(u)} \cdot \Theta_{\text{sub}}^{(u)} \cdot \Theta_{\text{sub}}^{(u)\text{H}} \cdot \hat{\mathcal{G}}_q^{(u)\text{H}} + \mathcal{F}^{\text{H}} \cdot \mathcal{F} \right)^{-1} \cdot \mathcal{F}^{\text{H}} \cdot \left[ \hat{c}_{\kappa,0}^{(u)}, \dots, \hat{c}_{\kappa,Q_P-1}^{(u)} \right]^T. \end{aligned} \quad (4.57)$$

The subspace based semiblind channel estimate vector  $[\hat{h}_0^{(u)}, \dots, \hat{h}_{L_C-1}^{(u)}, 0, \dots, 0]^T$  is based on the estimate of the autocorrelation matrix via the arithmetic mean in Eq. (4.51) and, therefore, it represents a joint estimate for all IFDMA symbols with indices  $k = 0, \dots, K-1$ . By applying the  $Q \times Q$  DFT matrix  $\mathbf{F}_Q$  to  $[\hat{h}_0^{(u)}, \dots, \hat{h}_{L_C-1}^{(u)}, 0, \dots, 0]^T$ , the vector  $\hat{\mathbf{c}}^{(u)}$  containing the estimates for each allocated subcarrier which are valid for the IFDMA symbols with indices  $k = 0, \dots, K-1$  is obtained by

$$\hat{\mathbf{c}}^{(u)} = \mathbf{F}_Q \cdot [\hat{h}_0^{(u)}, \dots, \hat{h}_{L_C-1}^{(u)}, 0, \dots, 0]^T. \quad (4.58)$$

#### 4.2.3.2 Estimation for Channels with Large Delay Spread

In this section, the subspace based semiblind channel estimation that has been explained in Section 4.2.3.1 is derived for the case of large channel delay spreads. Assuming large channel delay spreads means that Eq. (4.19) and (4.20) are fulfilled. In order to estimate the channel variations in frequency domain for channels with large delay spreads, a subspace based semiblind channel estimation is introduced which estimates the elements  $c_{k,q}^{(u)}$ ,  $q = 0, \dots, Q-1$ , of the cyclic channel impulse response. By doing so, the number of unknown elements to be estimated reduces from  $L_C$  to  $Q$  and the subspace based semiblind channel estimation is applicable without any restriction concerning the number of channel delay taps.

In the following, the principle of subspace based semiblind channel estimation for channels with large delay spreads is again presented for  $U = 1$  user in the system. In accordance to Section 4.2.3.1, the principle of subspace based estimation for large channel delay spreads is deduced at first. Then, the combination of subspace based estimation with the pilot based LS estimation is explained.

In order to estimate the elements  $c_{k,q}^{(u)}$ ,  $q = 0, \dots, Q-1$ , of the cyclic channel impulse response with the subspace based channel estimation, the parts of the received IFDMA

signal shall be evaluated that can be expressed in dependency of the elements  $c_{k,q}^{(u)}$ ,  $q = 0, \dots, Q - 1$ . Therefore, the last block  $\mathbf{r}_{k-1,L-1}^{(u)}$  of the IFDMA symbol with index  $k - 1$ , the first block  $\mathbf{r}_{k,0}^{(u)}$  of the cyclic prefix related to the IFDMA symbol with index  $k$  and the first block  $\mathbf{r}_{k,L_G}^{(u)}$  after cyclic prefix of the IFDMA symbol with index  $k$  are considered in the following. These three received blocks are influenced by the last  $L_G$  blocks of the transmitted IFDMA symbol with index  $k - 1$  and the first  $L_G + 1$  blocks of the transmitted IFDMA symbol with index  $k$  as it is illustrated in Figure 4.6.

Let the matrices  $\mathbf{H}_{k,0}^{(u)}, \dots, \mathbf{H}_{k,L_G}^{(u)}$  and  $\Phi_i^{(u)}$ ,  $i = 0, \dots, L_U - 1$ , be as defined in Eqs. (4.21)–(4.24) and (2.8), respectively. Further on, the assumption for small channel variations in time domain holds which means that

$$\mathbf{H}_j^{(u)} \approx \mathbf{H}_{k,j}^{(u)}, \quad \text{for } j = 0, \dots, L_G \text{ and } k = 0, \dots, K - 1. \quad (4.59)$$

Then, the three received blocks are summarized in a vector that is represented by

$$\begin{bmatrix} \mathbf{r}_{k-1,L-1}^{(u)} \\ \mathbf{r}_{k,0}^{(u)} \\ \mathbf{r}_{k,L_G}^{(u)} \end{bmatrix} = \begin{bmatrix} \mathbf{H}_{L_G}^{(u)} & \dots & \mathbf{H}_0^{(u)} & \mathbf{0}_Q & \dots & \mathbf{0}_Q \\ \mathbf{0}_Q & \mathbf{H}_{L_G}^{(u)} & \dots & \mathbf{H}_0^{(u)} & \dots & \mathbf{0}_Q \\ \mathbf{0}_Q & \dots & \mathbf{0}_Q & \mathbf{H}_{L_G}^{(u)} & \dots & \mathbf{H}_0^{(u)} \end{bmatrix} \cdot \begin{bmatrix} \Phi_{L_U-L_G-1}^{(u)} & \mathbf{0}_Q \\ \vdots & \vdots \\ \Phi_{L_U-1}^{(u)} & \mathbf{0}_Q \\ \mathbf{0}_Q & \Phi_{L_U-L_G}^{(u)} \\ \vdots & \vdots \\ & \Phi_{L_U-1}^{(u)} \\ \mathbf{0}_Q & \Phi_0^{(u)} \end{bmatrix} \\ + \begin{bmatrix} \mathbf{w}_{k-1}^{(u)} \\ \mathbf{w}_k^{(u)} \end{bmatrix} + \begin{bmatrix} \boldsymbol{\nu}_{k-1,L-1}^{(u)} \\ \boldsymbol{\nu}_{k,0}^{(u)} \\ \boldsymbol{\nu}_{k,L_G}^{(u)} \end{bmatrix}. \quad (4.60)$$

The application of the inverse phase shift to the vector containing the three received blocks in Eq. (4.60) leads to a vector containing the three inverse phase shifted received blocks that is given by

$$\begin{bmatrix} \check{\mathbf{r}}_{k-1,L-1}^{(u)} \\ \check{\mathbf{r}}_{k,0}^{(u)} \\ \check{\mathbf{r}}_{k,L_G}^{(u)} \end{bmatrix} = \begin{bmatrix} \Phi_{L_U-1}^{(u)\text{H}} & \mathbf{0}_Q & \mathbf{0}_Q \\ \mathbf{0}_Q & \Phi_0^{(u)\text{H}} & \mathbf{0}_Q \\ \mathbf{0}_Q & \mathbf{0}_Q & \Phi_0^{(u)\text{H}} \end{bmatrix} \cdot \begin{bmatrix} \mathbf{r}_{k-1,L-1}^{(u)} \\ \mathbf{r}_{k,0}^{(u)} \\ \mathbf{r}_{k,L_G}^{(u)} \end{bmatrix}. \quad (4.61)$$

Eq. (4.61) can be represented in dependency of the matrix  $\mathcal{H}^{(u)}$  defined in Eq. (2.38)

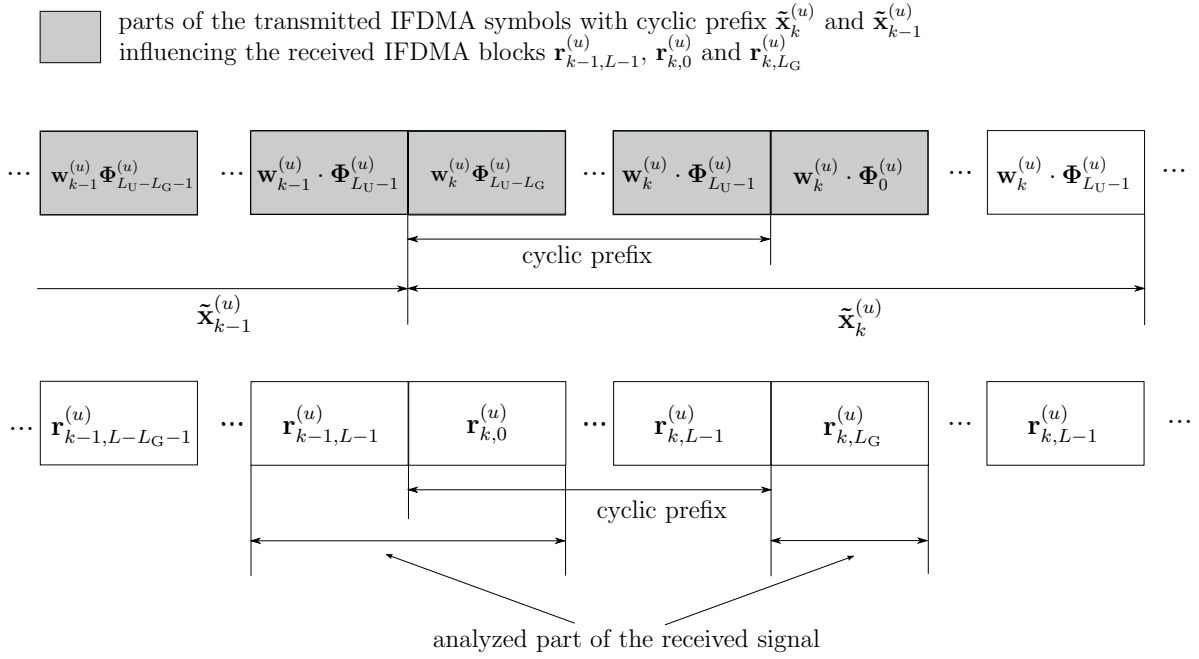


Figure 4.6. Illustration of the channel influence on the received IFDMA blocks  $\mathbf{r}_{k-1,L-1}^{(u)}$ ,  $\mathbf{r}_{k,0}^{(u)}$  and  $\mathbf{r}_{k,L_G}^{(u)}$ .

and the matrix  $\mathbf{H}_0^{(u)}$  according to

$$\begin{aligned}
 \begin{bmatrix} \tilde{\mathbf{r}}_{k-1,L-1}^{(u)} \\ \tilde{\mathbf{r}}_{k,0}^{(u)} \\ \tilde{\mathbf{r}}_{k,L_G}^{(u)} \end{bmatrix} &= \begin{bmatrix} \mathcal{H}^{(u)} & \mathbf{0}_Q \\ \left( \mathcal{H}^{(u)} - \Phi_0^{(u)\text{H}} \cdot \mathbf{H}_0^{(u)} \cdot \Phi_0^{(u)} \right) & \left( \Phi_0^{(u)\text{H}} \cdot \mathbf{H}_0^{(u)} \cdot \Phi_{L_U-L_G}^{(u)} \right) \\ \mathbf{0}_Q & \mathcal{H}^{(u)} \end{bmatrix} \cdot \begin{bmatrix} \mathbf{w}_{k-1}^{(u)} \\ \mathbf{w}_k^{(u)} \end{bmatrix} \\
 &+ \begin{bmatrix} \Phi_{L_U-1}^{(u)\text{H}} & \mathbf{0}_Q & \mathbf{0}_Q \\ \mathbf{0}_Q & \Phi_0^{(u)\text{H}} & \mathbf{0}_Q \\ \mathbf{0}_Q & \mathbf{0}_Q & \Phi_0^{(u)\text{H}} \end{bmatrix} \cdot \begin{bmatrix} \nu_{k-1,L-1}^{(u)} \\ \nu_{k,0}^{(u)} \\ \nu_{k,L_G}^{(u)} \end{bmatrix}.
 \end{aligned} \tag{4.62}$$

The derivation of Eq. (4.62) can be found in Appendix A.3.

Due to the dependency of Eq. (4.62) on the matrices  $\mathcal{H}^{(u)}$  and  $\mathbf{H}_0^{(u)}$ , it can be seen with Eq. (2.38) and (4.21) that the system matrix contains the elements  $c_0^{(u)}, \dots, c_{Q-1}^{(u)}, h_0^{(u)}, \dots, h_{Q-1}^{(u)}$ . The autocorrelation matrix of the vector containing the

three received blocks is given by

$$\begin{aligned}
\mathcal{A}^{(u)} &= \mathbb{E} \left\{ \begin{bmatrix} \tilde{\mathbf{r}}_{k-1,L-1}^{(u)} \\ \tilde{\mathbf{r}}_{k,0}^{(u)} \\ \tilde{\mathbf{r}}_{k,L_G}^{(u)} \end{bmatrix} \cdot \begin{bmatrix} \tilde{\mathbf{r}}_{k-1,L-1}^{(u)} \\ \tilde{\mathbf{r}}_{k,0}^{(u)} \\ \tilde{\mathbf{r}}_{k,L_G}^{(u)} \end{bmatrix}^H \right\} \\
&= \begin{bmatrix} \mathcal{H}^{(u)} & \mathbf{0}_Q \\ \left( \mathcal{H}^{(u)} - \Phi_0^{(u)H} \cdot \mathbf{H}_0^{(u)} \cdot \Phi_0^{(u)} \right) & \left( \Phi_0^{(u)H} \cdot \mathbf{H}_0^{(u)} \cdot \Phi_{L_U-L_G}^{(u)} \right) \\ \mathbf{0}_Q & \mathcal{H}^{(u)} \end{bmatrix} \cdot \sigma_W^2 \cdot \mathbf{I}_{2Q} \\
&\quad \cdot \begin{bmatrix} \mathcal{H}^{(u)} & \mathbf{0}_Q \\ \left( \mathcal{H}^{(u)} - \Phi_0^{(u)H} \cdot \mathbf{H}_0^{(u)} \cdot \Phi_0^{(u)} \right) & \left( \Phi_0^{(u)H} \cdot \mathbf{H}_0^{(u)} \cdot \Phi_{L_U-L_G}^{(u)} \right) \\ \mathbf{0}_Q & \mathcal{H}^{(u)} \end{bmatrix}^H + \sigma_\nu^2 \cdot \mathbf{I}_{3Q}. \tag{4.63}
\end{aligned}$$

The autocorrelation matrix  $\mathcal{A}^{(u)}$  is estimated by the arithmetic mean over  $K$  received IFDMA symbols according to

$$\hat{\mathcal{A}}^{(u)} = \frac{1}{K} \sum_{k=0}^{K-1} \begin{bmatrix} \tilde{\mathbf{r}}_{k-1,L-1}^{(u)} \\ \tilde{\mathbf{r}}_{k,0}^{(u)} \\ \tilde{\mathbf{r}}_{k,L_G}^{(u)} \end{bmatrix} \cdot \begin{bmatrix} \tilde{\mathbf{r}}_{k-1,L-1}^{(u)} \\ \tilde{\mathbf{r}}_{k,0}^{(u)} \\ \tilde{\mathbf{r}}_{k,L_G}^{(u)} \end{bmatrix}^H. \tag{4.64}$$

The estimate  $\hat{\mathcal{A}}^{(u)}$  is utilized for the identification of the noise subspace eigenvectors  $\hat{\mathbf{g}}_q^{(u)}$ ,  $q = 0, \dots, Q-1$ . Again, the noise subspace eigenvectors are orthogonal to the signal subspace that is spanned by the columns of the system matrix. The orthogonality constraint is represented by

$$\hat{\mathbf{g}}_q^{(u)H} \cdot \begin{bmatrix} \mathcal{H}^{(u)} & \mathbf{0}_Q \\ \left( \mathcal{H}^{(u)} - \Phi_0^{(u)H} \cdot \mathbf{H}_0^{(u)} \cdot \Phi_0^{(u)} \right) & \left( \Phi_0^{(u)H} \cdot \mathbf{H}_0^{(u)} \cdot \Phi_{L_U-L_G}^{(u)} \right) \\ \mathbf{0}_Q & \mathcal{H}^{(u)} \end{bmatrix} = \mathbf{0}_{1 \times 2Q} \tag{4.65}$$

for  $q = 0, \dots, Q-1$ .

In the following, the vector  $[c_0^{(u)}, \dots, c_{Q-1}^{(u)}, h_0^{(u)}, \dots, h_{Q-1}^{(u)}]^T$  of unknowns shall be estimated. The vector matrix multiplication in Eq. (4.65) shows that for each noise

subspace eigenvector  $\mathbf{g}_q^{(u)\text{H}}$ ,  $2Q$  equations are available for the estimation of the  $2Q$  unknown elements. The estimation of the elements  $h_q^{(u)}$ ,  $q = 0, \dots, Q-1$ , is performed as the system matrix depends on these elements. The desired elements  $c_q^{(u)}$ ,  $q = 0, \dots, Q-1$ , are estimated via the estimation of the vector  $[c_0^{(u)}, \dots, c_{Q-1}^{(u)}, h_0^{(u)}, \dots, h_{Q-1}^{(u)}]^\text{T}$  containing the desired and the undesired elements. For the estimation, the noise subspace eigenvectors  $\hat{\mathbf{g}}_q^{(u)}$ ,  $q = 0, \dots, Q-1$ , are transformed into the  $2Q \times 2Q$  matrices  $\hat{\mathbf{G}}_q^{(u)}$ ,  $q = 0, \dots, Q-1$ .

With  $\hat{\mathbf{g}}_{q,j}^{(u)}$ ,  $j = 0, 1, 2$ , according to the definition in Eq. (4.46), let  $\mathbf{C}_{q,j}^{(u)}$  denote a  $2Q \times Q$  matrix that is defined by

$$\mathbf{C}_{q,j}^{(u)} = \begin{bmatrix} 0 & \dots & 0 \\ \vdots & \dots & \vdots \\ 0 & \dots & 0 \\ \left[\hat{\mathbf{g}}_{q,j}^{(u)}\right]_0 \cdot e^{j0\varphi^{(u)}} & \dots & \left[\hat{\mathbf{g}}_{q,j}^{(u)}\right]_{Q-1} \cdot e^{j(Q-1)\varphi^{(u)}} \\ \vdots & & 0 \\ \vdots & \ddots & \vdots \\ \left[\hat{\mathbf{g}}_{q,j}^{(u)}\right]_{Q-1} \cdot e^{j(Q-1)\varphi^{(u)}} & 0 & \dots & 0 \end{bmatrix} \cdot \Phi_0^{(u)}. \quad (4.66)$$

Further, let  $\mathbf{D}_{q,j}^{(u)}$  denote a  $2Q \times Q$  matrix that is defined by

$$\mathbf{D}_{q,j}^{(u)} = \begin{bmatrix} \left[\hat{\mathbf{g}}_{q,j}^{(u)}\right]_0 & \left[\hat{\mathbf{g}}_{q,j}^{(u)}\right]_1 & \dots & \left[\hat{\mathbf{g}}_{q,j}^{(u)}\right]_{Q-1} \\ \vdots & & \ddots & \left[\hat{\mathbf{g}}_{q,j}^{(u)}\right]_0 \\ \vdots & & & \vdots \\ \left[\hat{\mathbf{g}}_{q,j}^{(u)}\right]_{Q-2} & \left[\hat{\mathbf{g}}_{q,j}^{(u)}\right]_{Q-1} & \dots & \\ \left[\hat{\mathbf{g}}_{q,j}^{(u)}\right]_{Q-1} & \left[\hat{\mathbf{g}}_{q,j}^{(u)}\right]_0 & \dots & \left[\hat{\mathbf{g}}_{q,j}^{(u)}\right]_{Q-2} \\ 0 & \dots & & 0 \\ \vdots & \dots & & \vdots \\ 0 & \dots & & 0 \end{bmatrix} \quad (4.67)$$



and  $\mathbf{E}_{q,j}^{(u)}$  denote a  $2Q \times Q$  matrix that is defined by

$$\mathbf{E}_{q,j}^{(u)} = \begin{bmatrix} 0 & \cdots & 0 \\ \vdots & \cdots & \vdots \\ 0 & \cdots & 0 \\ \left[\hat{\mathbf{g}}_{q,j}^{(u)}\right]_0 \cdot e^{j0\varphi^{(u)}} & \cdots & \left[\hat{\mathbf{g}}_{q,j}^{(u)}\right]_{Q-1} \cdot e^{j(Q-1)\varphi^{(u)}} \\ \vdots & & 0 \\ \vdots & \ddots & \vdots \\ \left[\hat{\mathbf{g}}_{q,j}^{(u)}\right]_{Q-1} \cdot e^{j(Q-1)\varphi^{(u)}} & 0 & \cdots & 0 \end{bmatrix} \cdot \Phi_{L_U-L_G}^{(u)}. \quad (4.68)$$

Then, the  $2Q \times 2Q$  matrices  $\hat{\mathcal{G}}_q^{(u)}$ ,  $q = 0, \dots, Q-1$ , are given by

$$\hat{\mathcal{G}}_q^{(u)} = \left[ \mathbf{D}_{q,0}^{(u)} + \mathbf{D}_{q,1}^{(u)} - \mathbf{C}_{q,1}^{(u)}, \mathbf{E}_{q,1}^{(u)} + \mathbf{D}_{q,2}^{(u)} \right]. \quad (4.69)$$

The derivation of Eq. (4.69) can be found in Appendix A.4.

With Eq. (4.69), the orthogonality constraint can be given in dependency of the vector  $[c_0^{(u)}, \dots, c_{Q-1}^{(u)}, h_0^{(u)}, \dots, h_{Q-1}^{(u)}]^T$  by

$$\left[ c_0^{(u)}, \dots, c_{Q-1}^{(u)}, h_0^{(u)}, \dots, h_{Q-1}^{(u)} \right]^* \cdot \hat{\mathcal{G}}_q^{(u)} = \mathbf{0}_{1 \times 2Q}. \quad (4.70)$$

The vector  $[c_0^{(u)}, \dots, c_{Q-1}^{(u)}, h_0^{(u)}, \dots, h_{Q-1}^{(u)}]^T$  can additionally be represented in dependency of the vector  $[\hat{c}_{\kappa,0}^{(u)}, \dots, \hat{c}_{\kappa,Q_P-1}^{(u)}]^T$  containing the pilot assisted channel estimates. Let

$$\tilde{\mathcal{F}} = [\mathcal{F} \quad \mathbf{0}_{Q_P \times Q}] \quad (4.71)$$

denote a  $Q_P \times 2Q$  matrix containing the  $Q_P \times Q$  matrix  $\mathcal{F}$  and zero elements.

Then, the relation

$$\tilde{\mathcal{F}} \cdot \left[ c_0^{(u)}, \dots, c_{Q-1}^{(u)}, h_0^{(u)}, \dots, h_{Q-1}^{(u)} \right]^T = \left[ \hat{c}_{\kappa,0}^{(u)}, \dots, \hat{c}_{\kappa,Q_P-1}^{(u)} \right]^T \quad (4.72)$$

is valid for the pilot assisted channel estimates.

As explained in Section 4.2.3.1, Eq. (4.70) and (4.72) are combined in a system of equations and an estimate  $[\hat{c}_0^{(u)}, \dots, \hat{c}_{Q-1}^{(u)}, \hat{h}_0^{(u)}, \dots, \hat{h}_{Q-1}^{(u)}]^T$  of  $[c_0^{(u)}, \dots, c_{Q-1}^{(u)}, h_0^{(u)}, \dots, h_{Q-1}^{(u)}]^T$

is found by minimizing the function

$$\begin{aligned} \Upsilon^{(u)} = & \sum_{q=0}^{Q-1} \left\| \left[ c_0^{(u)}, \dots, c_{Q-1}^{(u)}, h_0^{(u)}, \dots, h_{Q-1}^{(u)} \right]^* \cdot \hat{\mathbf{g}}_q^{(u)} \right\|_2^2 \\ & + \left\| \tilde{\mathbf{F}} \cdot \left[ c_0^{(u)}, \dots, c_{Q-1}^{(u)}, h_0^{(u)}, \dots, h_{Q-1}^{(u)} \right]^T - \left[ \hat{c}_{\kappa,0}^{(u)}, \dots, \hat{c}_{\kappa,Q_P-1}^{(u)} \right]^T \right\|_2^2. \end{aligned} \quad (4.73)$$

The solution is calculated according to Section 4.2.3.1 and the estimate results in

$$\begin{aligned} \left[ \hat{c}_0^{(u)}, \dots, \hat{c}_{Q-1}^{(u)}, \hat{h}_0^{(u)}, \dots, \hat{h}_{Q-1}^{(u)} \right]^T = \\ \left( \sum_{q=0}^{Q-1} \hat{\mathbf{g}}_q^{(u)} \cdot \hat{\mathbf{g}}_q^{(u)H} + \tilde{\mathbf{F}}^H \cdot \tilde{\mathbf{F}} \right)^{-1} \cdot \tilde{\mathbf{F}}^H \cdot \left[ \hat{c}_{\kappa,0}^{(u)}, \dots, \hat{c}_{\kappa,Q_P-1}^{(u)} \right]^T. \end{aligned} \quad (4.74)$$

The subspace based semiblind channel estimate vector  $[\hat{c}_0^{(u)}, \dots, \hat{c}_{Q-1}^{(u)}, \hat{h}_0^{(u)}, \dots, \hat{h}_{Q-1}^{(u)}]^T$  is based on the estimate of the autocorrelation matrix via the arithmetic mean in Eq. (4.64) and, therefore, it represents a joint estimate for all IFDMA symbols with indices  $k = 0, \dots, K - 1$ . For equalization purposes, only the first  $Q$  elements  $\hat{c}_q^{(u)}$ ,  $q = 0, \dots, Q - 1$ , of the estimated vector are necessary and, thus, the application of the  $Q \times Q$  DFT matrix  $\mathbf{F}_Q$  to the vector  $[\hat{c}_0^{(u)}, \dots, \hat{c}_{Q-1}^{(u)}]^T$  leads to the vector  $\hat{\mathbf{c}}^{(u)}$  containing the estimates for each allocated subcarrier which are valid for the IFDMA symbols with indices  $k = 0, \dots, K - 1$  and are obtained by

$$\hat{\mathbf{c}}^{(u)} = \mathbf{F}_Q \cdot \left[ \hat{c}_0^{(u)}, \dots, \hat{c}_{Q-1}^{(u)} \right]^T. \quad (4.75)$$

#### 4.2.3.3 Multi-User Influence

In this section, the subspace based semiblind channel estimation that has been derived in Section 4.2.3.1 is investigated for the case that the signals of multiple users are transmitted within the same TDMA slot. For clarity reasons, the investigations are performed under the assumption of small channel delay spreads, i.e.,  $L_C \leq Q$ . However, the conclusions are applicable to the case of large channel delay spreads as well.

According to the investigations of the multi-user influence on the correlation based semiblind channel estimation, this section concentrates on the influence of multiple users allocated to the same TDMA slot on the subspace based channel estimation as the pilot assisted estimation remains unaffected by multiple users in the system.

In the following, the assumption of small channel variations in time domain according to Eq. (4.39) holds. Thus, the matrix  $\mathbf{H}_{k,\text{sub}}^{(u)}$  can be represented independently from the index  $k$  by defining

$$\mathbf{H}_{\text{sub}}^{(u)} \approx \mathbf{H}_{k,\text{sub}}^{(u)}, \quad \text{for } k = 0, \dots, K-1. \quad (4.76)$$

**Uplink** For subspace based channel estimation in a multi-user uplink scenario, the vector containing three blocks of two neighboring received IFDMA symbols is considered at a base station for a user with index  $u_1$ . The vector containing the superposition of the signals transmitted by the  $U$  users in the system is expressed by

$$\begin{bmatrix} \mathbf{r}_{k-1,L-1} \\ \mathbf{r}_{k,0} \\ \mathbf{r}_{k,1} \end{bmatrix} = \sum_{u=0}^{U-1} \left( \mathbf{H}_{\text{sub}}^{(u)} \cdot \boldsymbol{\Theta}_{\text{sub}}^{(u)} \cdot \begin{bmatrix} \mathbf{w}_{k-1}^{(u)} \\ \mathbf{w}_k^{(u)} \end{bmatrix} \right) + \begin{bmatrix} \boldsymbol{\nu}_{k-1,L-1} \\ \boldsymbol{\nu}_{k,0} \\ \boldsymbol{\nu}_{k,1} \end{bmatrix}. \quad (4.77)$$

Due to cyclic prefix insertion, the IFDMA symbols without cyclic prefix that have been transmitted by different users maintain their orthogonality at the base station. Thus, the received blocks  $\mathbf{r}_{k-1,L-1}^{(u_1)}$  and  $\mathbf{r}_{k,1}^{(u_1)}$  of the user with index  $u_1$  are separated from the received blocks corresponding to other users. Nevertheless, the received block  $\mathbf{r}_{k,0}^{(u_1)}$  representing the cyclic prefix of the IFDMA symbol with index  $k$  of the user with index  $u_1$  is received within the superposition of the  $U-1$  users' cyclic prefixes and cannot be separated. Thus, the vector containing three blocks of the received signal of the user with index  $u_1$  is represented by

$$\begin{aligned} \begin{bmatrix} \mathbf{r}_{k-1,L-1}^{(u_1)} \\ \mathbf{r}_{k,0}^{(u_1)} \\ \mathbf{r}_{k,1}^{(u_1)} \end{bmatrix} &= \mathbf{H}_{\text{sub}}^{(u_1)} \cdot \boldsymbol{\Theta}_{\text{sub}}^{(u_1)} \cdot \begin{bmatrix} \mathbf{w}_{k-1}^{(u_1)} \\ \mathbf{w}_k^{(u_1)} \end{bmatrix} + \begin{bmatrix} \boldsymbol{\nu}_{k-1,L-1} \\ \boldsymbol{\nu}_{k,0} \\ \boldsymbol{\nu}_{k,1} \end{bmatrix} \\ &+ \sum_{\substack{u=0 \\ u \neq u_1}}^{U-1} \left( \begin{bmatrix} \mathbf{0}_Q & \mathbf{0}_Q & \mathbf{0}_Q & \mathbf{0}_Q \\ \mathbf{0}_Q & \mathbf{H}_1^{(u)} & \mathbf{H}_0^{(u)} & \mathbf{0}_Q \\ \mathbf{0}_Q & \mathbf{0}_Q & \mathbf{0}_Q & \mathbf{0}_Q \end{bmatrix} \cdot \begin{bmatrix} \mathbf{0}_Q & \mathbf{0}_Q \\ \boldsymbol{\Phi}_{L-1}^{(u)} & \mathbf{0}_Q \\ \mathbf{0}_Q & \boldsymbol{\Phi}_{L-1}^{(u)} \\ \mathbf{0}_Q & \mathbf{0}_Q \end{bmatrix} \cdot \begin{bmatrix} \mathbf{w}_{k-1}^{(u)} \\ \mathbf{w}_k^{(u)} \end{bmatrix} \right). \end{aligned} \quad (4.78)$$

The autocorrelation matrix

$$\mathcal{A}^{(u_1)} = \mathbb{E} \left\{ \begin{bmatrix} \mathbf{r}_{k-1,L-1}^{(u_1)} \\ \mathbf{r}_{k,0}^{(u_1)} \\ \mathbf{r}_{k,1}^{(u_1)} \end{bmatrix} \cdot \begin{bmatrix} \mathbf{r}_{k-1,L-1}^{(u_1)} \\ \mathbf{r}_{k,0}^{(u_1)} \\ \mathbf{r}_{k,1}^{(u_1)} \end{bmatrix}^H \right\} \quad (4.79)$$

is given by

$$\begin{aligned} \mathcal{A}^{(u_1)} &= \mathbf{H}_{\text{sub}}^{(u)} \cdot \boldsymbol{\Theta}_{\text{sub}}^{(u)} \cdot \sigma_W^2 \cdot \mathbf{I}_{2Q} \cdot \boldsymbol{\Theta}_{\text{sub}}^{(u)\text{H}} \cdot \mathbf{H}_{\text{sub}}^{(u)\text{H}} + \sigma_\nu^2 \cdot \mathbf{I}_{3Q} \\ &\quad + \sigma_W^2 \cdot \sum_{\substack{u=0 \\ u \neq u_1}}^{U-1} \begin{bmatrix} \mathbf{0}_Q & & \mathbf{0}_Q \\ \mathbf{0}_Q & \mathbf{H}_1^{(u)} \cdot \mathbf{H}_1^{(u)\text{H}} + \mathbf{H}_0^{(u)} \cdot \mathbf{H}_0^{(u)\text{H}} & \mathbf{0}_Q \\ \mathbf{0}_Q & & \mathbf{0}_Q \end{bmatrix}. \end{aligned} \quad (4.80)$$

It becomes clear, that the signal subspace is no longer exclusively spanned by the matrix  $\mathbf{H}_{\text{sub}}^{(u_1)} \cdot \boldsymbol{\Theta}_{\text{sub}}^{(u_1)}$  as in Eq. (4.43), but additionally by the sum of the  $U$  users cyclic prefix parts of the signal. That means, the orthogonality constraint in Eq. (4.45) or Eq. (4.52) is fulfilled only approximately because the cyclic prefix of the user with indices  $u = 0, \dots, U-1, u \neq u_1$ , have to be taken into account for the signal subspace. Thus, the estimation of  $[h_0^{(u)}, \dots, h_{L_C-1}^{(u)}, 0, \dots, 0]^T$  with the help of Eq. (4.52) is affected by the signals of the additional users in the system.

**Downlink** For subspace based channel estimation in a multi-user downlink scenario, again, the vector containing three blocks of neighboring received IFDMA symbols is considered at the mobile terminal of a user with index  $u_1$ . The received signal of user  $u_1$  prior to user separation can be expressed as

$$\begin{bmatrix} \mathbf{r}_{k-1,L-1}^{(u_1)} \\ \mathbf{r}_{k,0}^{(u_1)} \\ \mathbf{r}_{k,1}^{(u_1)} \end{bmatrix} = \mathbf{H}_{\text{sub}}^{(u_1)} \cdot \sum_{u=0}^{U-1} \left( \boldsymbol{\Theta}_{\text{sub}}^{(u)} \cdot \begin{bmatrix} \mathbf{w}_{k-1}^{(u)} \\ \mathbf{w}_k^{(u)} \end{bmatrix} \right) + \begin{bmatrix} \boldsymbol{\nu}_{k-1,L-1}^{(u_1)} \\ \boldsymbol{\nu}_{k,0}^{(u_1)} \\ \boldsymbol{\nu}_{k,1}^{(u_1)} \end{bmatrix}. \quad (4.81)$$

The autocorrelation matrix

$$\mathcal{A}^{(u_1)} = \mathbb{E} \left\{ \begin{bmatrix} \mathbf{r}_{k-1,L-1}^{(u_1)} \\ \mathbf{r}_{k,0}^{(u_1)} \\ \mathbf{r}_{k,1}^{(u_1)} \end{bmatrix} \cdot \begin{bmatrix} \mathbf{r}_{k-1,L-1}^{(u_1)} \\ \mathbf{r}_{k,0}^{(u_1)} \\ \mathbf{r}_{k,1}^{(u_1)} \end{bmatrix}^H \right\} \quad (4.82)$$

is given by

$$\begin{aligned} \mathcal{A}^{(u_1)} &= \mathbb{E} \left\{ \mathbf{H}_{\text{sub}}^{(u_1)} \cdot \left( \sum_{u=0}^{U-1} \boldsymbol{\Theta}_{\text{sub}}^{(u)} \cdot \begin{bmatrix} \mathbf{w}_{k-1}^{(u)} \\ \mathbf{w}_k^{(u)} \end{bmatrix} \right) \cdot \left( \sum_{u=0}^{U-1} \boldsymbol{\Theta}_{\text{sub}}^{(u)} \cdot \begin{bmatrix} \mathbf{w}_{k-1}^{(u)} \\ \mathbf{w}_k^{(u)} \end{bmatrix} \right)^H \cdot \mathbf{H}_{\text{sub}}^{(u_1)\text{H}} \right\} \\ &\quad + \sigma_\nu^2 \cdot \mathbf{I}_{3Q} \\ &= \mathbf{H}_{\text{sub}}^{(u_1)} \cdot \sigma_W^2 \cdot \sum_{u=0}^{U-1} \left( \boldsymbol{\Theta}_{\text{sub}}^{(u)} \cdot \boldsymbol{\Theta}_{\text{sub}}^{(u)\text{H}} \right) \cdot \mathbf{H}_{\text{sub}}^{(u_1)\text{H}} + \sigma_\nu^2 \mathbf{I}_{3Q}. \end{aligned} \quad (4.83)$$

From Eq. (4.81) and (4.83) it can be seen that the signal subspace is spanned by

$$\mathbf{H}_{\text{sub}}^{(u_1)} \cdot \sum_{u=0}^{U-1} \mathbf{\Theta}_{\text{sub}}^{(u)}. \quad (4.84)$$

Thus, in a multi-user downlink scenario, the vector  $[h_0^{(u)}, \dots, h_{L_C-1}^{(u)}, 0, \dots, 0]^T$  can be estimated as described in Section 4.2.3.1 by considering the received signal prior to user separation and replacing  $\mathbf{\Theta}_{\text{sub}}^{(u_1)}$  by the sum of user dependent phase shift matrices  $\sum_{u=0}^{U-1} \mathbf{\Theta}_{\text{sub}}^{(u)}$ .

## 4.3 Reduced Number of Pilot Symbols in Time Domain

### 4.3.1 Introduction

In this section, a channel estimation algorithm is presented for the case of a reduced number of pilot symbols in time domain.

In the following, a decision directed channel estimation algorithm is presented which aims at minimizing the error propagation with the help of an iterative Wiener filtering within each estimation step that is applied jointly to the decision directed channel estimates corresponding to a certain number of neighboring IFDMA symbols. The filtered output is used iteratively for the decision directed channel estimation again. Further on, the proposed decision directed channel estimation algorithm is initialized with the channel estimates which are provided by the correlation and subspace based semiblind channel estimation presented in Section 4.2.2 and Section 4.2.3, respectively. By this means, the channel variations in frequency and time domain can be estimated even if the sampling theorem in frequency and time domain is not fulfilled and current channel estimation approaches fail.

### 4.3.2 Decision Directed Channel Estimation

In this section, the estimation of the channel variations in time domain is explained for the Decision Directed Channel Estimation with iterative Wiener Filtering (DDCE+WF). In the following, the proposed algorithm will be denoted as DDCE+WF



mapped onto data symbols, interleaved and coded again. With the index  $e_1$  defined as

$$e_1 = \begin{cases} V & \text{for } k \leq V/2, \\ K - 1 & \text{for } k > K - V/2 - 1, \\ k + V/2 - 1 & \text{else,} \end{cases} \quad (4.85)$$

the IFDMA symbols  $\mathbf{d}_{k+1}^{(u)}, \dots, \mathbf{d}_{e_1}^{(u)}$  are estimated in the 0<sup>th</sup> iteration step. With  $k = 0$  for the 0<sup>th</sup> iteration step, the estimated IFDMA symbols are denoted by  $\hat{\mathbf{d}}_1^{(u,0)}, \dots, \hat{\mathbf{d}}_V^{(u,0)}$  in the 0<sup>th</sup> iteration step. The decision directed estimates are obtained by the LS estimates according to

$$\hat{\mathbf{c}}_k^{(u,0)} = \frac{\bar{\mathbf{y}}_k^{(u)}}{\hat{\mathbf{d}}_k^{(u,0)}}, \quad \text{for } k = 1, \dots, V. \quad (4.86)$$

The vectors  $\hat{\mathbf{c}}_1^{(u,0)}, \dots, \hat{\mathbf{c}}_V^{(u,0)}$  containing the estimates of the channel transfer factors of the 0<sup>th</sup> iteration step are fed into a Wiener filter with  $V$  coefficients in order to obtain the filtered update estimate  $\tilde{\mathbf{c}}_1^{(u)}$  with index  $k = 1$ .  $\tilde{\mathbf{c}}_1^{(u)}$  is used in the equalizer to obtain new estimates  $\hat{\mathbf{d}}_2^{(u,1)}, \dots, \hat{\mathbf{d}}_V^{(u,1)}$  in the first iteration step. In total there are  $K - 1$  iteration steps because a filtered update estimate is obtained for the channel transfer factors corresponding to each IFDMA symbol with index  $k = 1, \dots, K - 1$ . In each iteration step with index  $k$ , the already filtered update estimates as well as the unfiltered decision directed estimates of the channel transfer factors corresponding to the nearest  $V$  IFDMA symbols are used for Wiener filtering with a filter of length  $V$  to obtain the filtered update estimate  $\tilde{\mathbf{c}}_k^{(u)}$  of the current iteration step.

The iterative procedure of the DDCE+WF is presented in Table 4.1. Let  $e_2$  and  $e_3$  denote indices that are defined according to

$$e_2 = \begin{cases} k - V & \text{for } k \leq V/2, \\ k + 1 - K & \text{for } k > K - V/2 - 1, \\ -V/2 + 1 & \text{else,} \end{cases} \quad (4.87)$$

and

$$e_3 = \begin{cases} k - 1 & \text{for } k \leq V/2, \\ V - K + k & \text{for } k > K - V/2 - 1, \\ V/2 & \text{else,} \end{cases} \quad (4.88)$$

respectively.

The Wiener filter coefficients  $a_v$  with  $v = e_2, \dots, 0, \dots, e_3$  for the application to DDCE+WF are derived such that  $E\{|\tilde{\mathbf{c}}_k^{(u)} - \hat{\mathbf{c}}_k^{(u)}|\}$  becomes minimum. With the time correlation function of the channel defined in Eq. (2.20) and the calculation of the

Wiener filter coefficients in Eqs. (3.41), (3.42) and (3.43), the Wiener filter coefficients for the DDCE+WF are calculated by

$$[a_{e_2}, \dots, a_0, \dots, a_{e_3}] = [R_{\bar{h},t}^{(u)}(e_2), \dots, R_{\bar{h},t}^{(u)}(0), \dots, R_{\bar{h},t}^{(u)}(e_3)] \cdot \begin{bmatrix} R_{\bar{h},t}^{(u)}(0) + \gamma & R_{\bar{h},t}^{(u)}(1) & \dots & R_{\bar{h},t}^{(u)}(e_3 - e_2) \\ R_{\bar{h},t}^{(u)}(-1) & R_{\bar{h},t}^{(u)}(0) + \gamma & & \vdots \\ \vdots & & & R_{\bar{h},t}^{(u)}(-e_2) \\ R_{\bar{h},t}^{(u)}(e_2) & & \ddots & \vdots \\ \vdots & & & \ddots & R_{\bar{h},t}^{(u)}(1) \\ R_{\bar{h},t}^{(u)}(e_2 - e_3) & \dots & R_{\bar{h},t}^{(u)}(-1) & R_{\bar{h},t}^{(u)}(0) + \gamma \end{bmatrix}. \quad (4.89)$$

Table 4.1. Decision directed channel estimation with iterative Wiener filtering.

### 1. Initialization

Equalization with  $\hat{\mathbf{c}}^{(u)} = [\hat{c}_0^{(u)}, \dots, \hat{c}_{Q-1}^{(u)}]^T$

Estimation of the IFDMA symbols:  $\hat{\mathbf{d}}_1^{(u,0)}, \dots, \hat{\mathbf{d}}_V^{(u,0)}$

Frequency domain representation:  $\hat{\mathbf{d}}_1^{(u,0)}, \dots, \hat{\mathbf{d}}_V^{(u,0)}$

Initialize:  $\tilde{\mathbf{c}}_0^{(u)} = \hat{\mathbf{c}}^{(u)}$

For  $k = 1, \dots, K - 1$

### 2. Decision directed channel estimation

$$\hat{\mathbf{c}}_k^{(u,k)} = \frac{\bar{\mathbf{y}}_k^{(u)}}{\hat{\mathbf{d}}_k^{(u,k-1)}}, \dots, \hat{\mathbf{c}}_{e_1}^{(u,k)} = \frac{\bar{\mathbf{y}}_{e_1}^{(u)}}{\hat{\mathbf{d}}_{e_1}^{(u,k-1)}}$$

### 3. Wiener filtering with $V$ filter coefficients

$$\tilde{\mathbf{c}}_k^{(u)} = \sum_{v=e_2}^0 a_v \cdot \hat{\mathbf{c}}_{k-v}^{(u,k)} + \sum_{v=1}^{e_3} a_v \cdot \tilde{\mathbf{c}}_{k-v}^{(u)}$$

### 4. Equalization with $\tilde{\mathbf{c}}_k^{(u)}$

Estimation of the IFDMA symbols:  $\hat{\mathbf{d}}_{k+1}^{(u,k)}, \dots, \hat{\mathbf{d}}_{e_1}^{(u,k)}$

Frequency domain representation:  $\hat{\mathbf{d}}_{k+1}^{(u,k)}, \dots, \hat{\mathbf{d}}_{e_1}^{(u,k)}$

end



## 4.4 Performance and Complexity Analysis

### 4.4.1 Analysis Assumptions

In this Section 4.4, the presented semiblink channel estimation algorithms are investigated with regard to their pilot symbol overhead consumption, their MSE performance and their computational complexity. The results for the aforementioned performance measures are obtained by computer simulations. For the simulations, the system setup is identical to the one explained in Section 3.4.1 for pilot assisted channel estimation. A summary of the considered system parameters has been presented in Table 3.1.

Besides the WINNER SCM urban macro-cell channel, in this Section 4.4, a second channel model is used for the simulations. Here, the time variant multipath channel is modeled by  $L_C$  Rayleigh-fading coefficients that exhibit a decaying power with the delay time  $\tau$  according to the delay power spectral density for typical urban channels or rural area channels defined in the European working group COST 207 [Pae02]. This second channel model is utilized because the channel estimation performance shall be investigated for different numbers  $L_C$  of channel delay taps. The usage of this second channel model allows a variable adjustment of the parameter  $L_C$  and, thus, this channel model will be referred to as Typical Urban VarDelay channel or Rural Area VarDelay channel in the following.

First, the pilot symbol overhead is calculated for the semiblink channel estimation algorithms and is compared to the pilot symbol overhead results for pure pilot assisted channel estimation. Second, MSE results are presented. Third, the semiblink channel estimation algorithms are analyzed in terms of their computational complexity. The investigations with regard to the PAPR of the IFDMA transmit signal are omitted as the pilot symbols are inserted according to subcarrierwise pilot insertion whose influence on the PAPR has been presented in Section 3.4.2.

In the following, the correlation and the subspace based semiblink channel estimation are denoted as correlation SCE and subspace SCE, respectively. The DDCE+WF with correlation SCE or subspace SCE as initializing channel estimation is denoted as correlation SCE+DDCE+WF or subspace SCE+DDCE+WF for simplicity reasons.

### 4.4.2 Pilot Symbol Overhead

In this section, the pilot symbol overhead is calculated for the semiblink channel estimation algorithms correlation and subspace SCE+DDCE+WF. The results are compared

to the pilot symbol overhead results for pure pilot assisted channel estimation which have been presented in Section 3.4.3.

For pure pilot assisted channel estimation, at least one pilot symbol is transmitted per coherence bandwidth and per coherence time of the mobile radio channel which is represented by the oversampling factor  $O_F = 1$  in frequency domain and the oversampling factor  $O_T = 1$  in time domain. As explained in Section 4.2 and in Section 4.3, for semiblind channel estimation, the sampling theorems in frequency and time domain can be violated. This means that oversampling factors  $O_F < 1$  in frequency domain and  $O_T < 1$  in time domain are feasible while applying the channel estimation algorithm introduced in Section 4.3.

In Figure 4.8, the pilot symbol overhead  $\Lambda$  as defined in Eq. (3.52) is depicted as a function of the number  $Q$  of allocated subcarriers per user with the oversampling factor  $O_F$  in frequency domain as parameter. The results are valid for the following parameters:

- The mobile terminal is assumed to move with a velocity of  $v = 50$  km/h. For  $K = 30$  IFDMA symbols per TDMA slot this corresponds to the case where  $K$  is smaller than the pilot distance  $D_T$  in time domain.
- For pilot assisted channel estimation,  $P = 2$  pilot carrying IFDMA symbols are utilized at the margin of the TDMA slot, respectively, which complies with the application of an oversampling factor of  $O_T \approx 3$  in time domain.
- For semiblind channel estimation,  $P = 1$  pilot carrying IFDMA symbol is utilized.

In Figure 4.8(a),  $L_C = 128$  channel delay taps are considered. For  $Q \leq 32$ , the pilot symbol overhead of semiblind channel estimation is reduced by factor 2 compared to the pilot symbol overhead of pilot assisted channel estimation due to the reduction of the number  $P$  of pilot carrying IFDMA symbols by a factor of 2. For  $Q \leq 32$ , the pilot symbol overhead depends directly on the difference of the number  $P$  of pilot carrying IFDMA symbols as interpolation in frequency domain is neither possible for semiblind channel estimation nor for pilot assisted channel estimation. For  $Q \geq L_C \cdot O_F$ , interpolation in frequency domain is possible and, thus, the semiblind channel estimation enables the interpolation in frequency domain for  $32 \leq Q < 128$  where interpolation in frequency domain is not feasible applying pure pilot assisted channel estimation. Therefore, the pilot symbol overhead is reduced significantly compared to pilot assisted channel estimation due to the possibility of violating the sampling

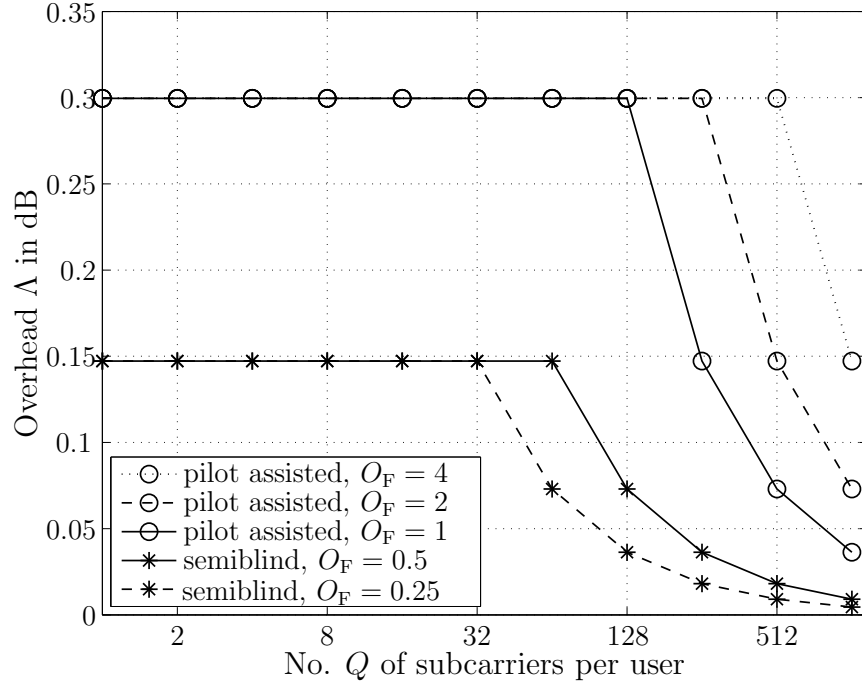
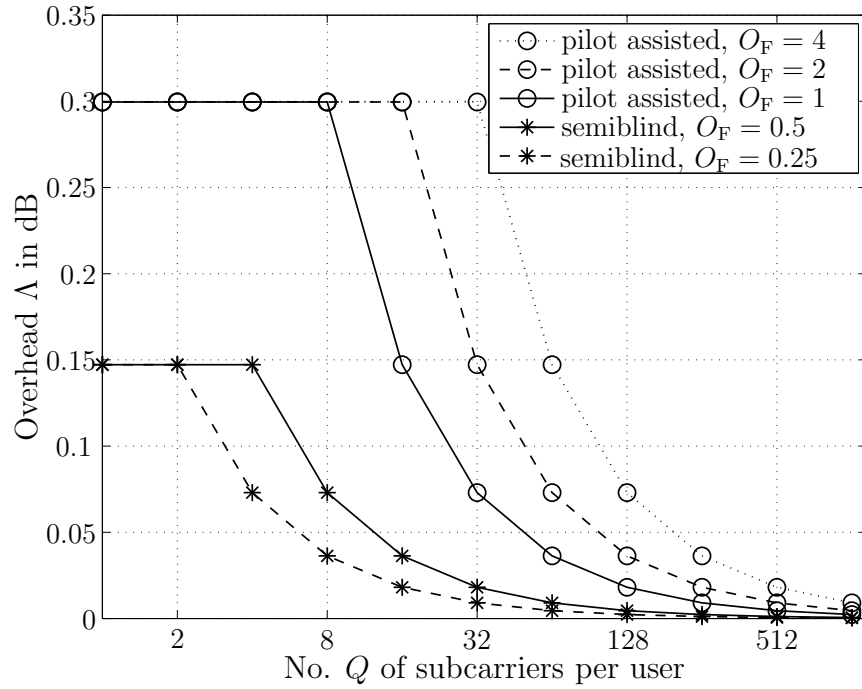
(a)  $L_C = 128$ (b)  $L_C = 8$ 

Figure 4.8. Overhead  $\Lambda$  as a function of the number  $Q$  of allocated subcarriers per user with the oversampling factor  $O_F$  in frequency domain as parameter for pilot assisted channel estimation and semiblind channel estimation and a velocity of  $v = 50$  km/h.

theorem in frequency domain, i.e., applying oversampling factors  $O_F < 1$  in frequency domain. Figure 4.8(b) shows the pilot symbol overhead for channels with  $L_C = 8$  delay taps. In analogy to the results for  $L_C = 128$ , the pilot symbol overhead can be significantly decreased due to semiblind channel estimation. Due to the small channel delay spread, interpolation in frequency domain is possible for a lower number  $Q$  of allocated subcarriers compared to the results in Figure 4.8(a).

### 4.4.3 Mean Square Error

In this section, the channel estimation algorithms introduced in Section 4.2 and Section 4.3 are investigated in terms of their MSE performance. The MSE is defined in analogy to Section 3.4.4 by

$$MSE = \frac{1}{K} \sum_{k=0}^{K-1} \left\| \frac{\hat{\mathbf{c}}_k^{(u)} - \bar{\mathbf{c}}_k^{(u)}}{\bar{\mathbf{c}}_k^{(u)}} \right\|_2^2. \quad (4.90)$$

In Figures 4.9-4.14, the correlation SCE presented in Section 4.2.2 and the subspace SCE presented in Section 4.2.3 are analyzed in terms of their MSE performance for the case of time invariant mobile radio channels. Then, Figure 4.15(a) and Figure 4.15(b) present the influence of time varying channel conditions on the correlation SCE and the subspace SCE. As these two algorithms are utilized for the initialization of the DDCE+WF in case of time varying channels, the performance of both algorithms in case of time varying channels directly influences the estimation performance of correlation SCE+DDCE+WF and subspace SCE+DDCE+WF. Finally, in Figures 4.16-4.17, the MSE results are presented for correlation SCE+DDCE+WF and subspace SCE+DDCE+WF as introduced in Section 4.3 in case of time varying channel conditions. As a reference, the MSE is also presented for DDCE+WF with symbolwise LS according to Section 3.2.2 as initializing channel estimate. For reasons of clarity, Table 3.4 gives an overview of the presented MSE results.

In the following, the MSE performance of the correlation SCE and the subspace SCE is presented under the assumption of time invariant channels, i.e., a user velocity of  $v = 0$  km/h.

In Figure 4.9, the influence of the ratio between the number  $K$  of IFDMA symbols transmitted within the TDMA slot and the number  $Q$  of data symbols per IFDMA symbol on the estimation performance is investigated. The MSE is given as a function of  $E_B/N_0$  in dB with the ratio  $K/Q$  as parameter. Further parameters are chosen as follows:

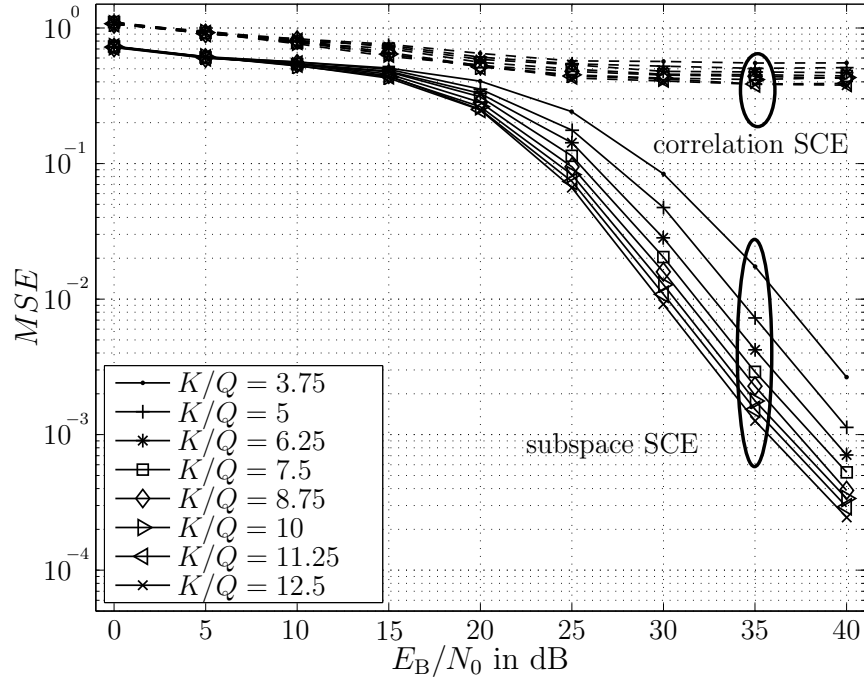
Table 4.2. Overview of presented MSE results.

ESTIMATION APPROACH FOR CHANNEL VARIATIONS IN FREQUENCY DOMAIN	ESTIMATION APPROACH FOR CHANNEL VARIATIONS IN TIME DOMAIN	
	no estimation	DDCE+WF
symbolwise LS	—	Figure 4.16(b)
correlation SCE	Figure 4.9(a), Figure 4.9(b), Figure 4.11(a), Figure 4.11(b), Figure 4.12, Figure 4.13, Figure 4.14, Figure 4.15(a), Figure 4.15(b)	Figure 4.16(a)
subspace SCE	Figure 4.9(a), Figure 4.9(b), Figure 4.10, Figure 4.11(a), Figure 4.11(b), Figure 4.12, Figure 4.13, Figure 4.14, Figure 4.15(a), Figure 4.15(b)	Figure 4.16(a) Figure 4.16(b) Figure 4.17(a) Figure 4.17(b)

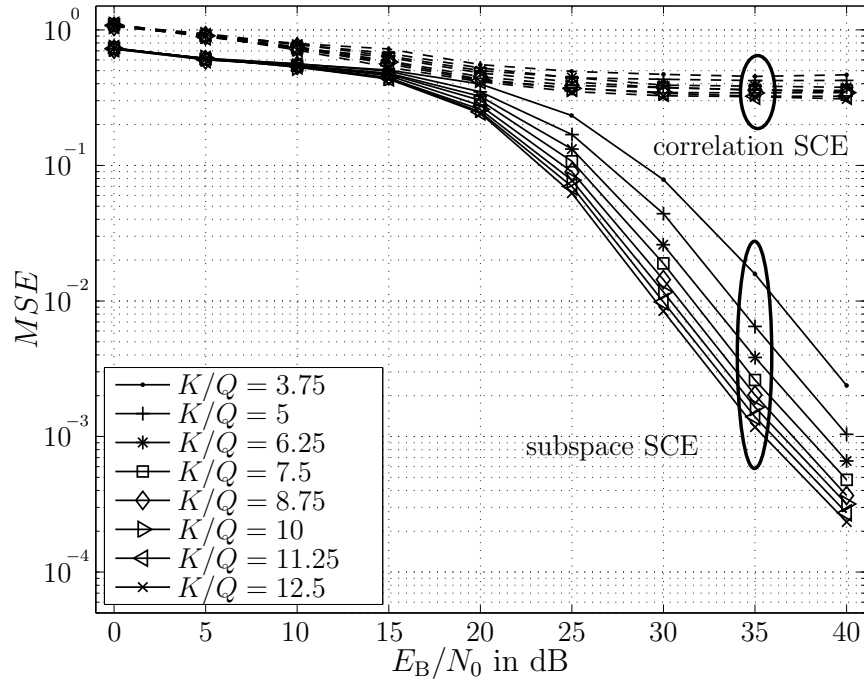
- In order to observe the influence of the ratio  $K/Q$  independently from the influences introduced by large channel delay spreads, the results are presented for small channel delay spreads, i.e.,  $L_C = Q$  channel delay taps.
- For the present results, the influence of multiple users in the system is neglected and, thus,  $U = 1$ .
- $Q_P = \frac{Q}{2}$  pilot symbols are transmitted in the IFDMA symbol with index  $k = 0$  which corresponds to an interpolation depth  $I = 2$  meaning that every second subcarrier in the IFDMA symbol with index  $k = 0$  is used for pilot transmission. In order to fulfill the sampling theorem with an oversampling factor  $D_F = 1$  in frequency domain, an interpolation depth  $I = 1$  had to be applied meaning that each allocated subcarrier has to be used for pilot transmission. Thus, the presented results are valid for a two times extended sampling theorem in frequency domain, i.e.,  $D_F = 0.5$ , as only every second subcarrier is used for pilot transmission.

In Figure 4.9(a), the considered channel corresponds to the Typical Urban VarDelay channel. It can be seen that the increase of the ratio  $K/Q$  from  $K/Q = 3.75$  up to  $K/Q = 12.5$  leads to a reduction of the MSE for both, the correlation SCE and the subspace SCE. For the correlation SCE, the MSE depends only slightly on the  $E_B/N_0$  and exhibits an error floor for the noise power tending to zero. This shows, that the correlation SCE is a biased estimator and can provide only poor estimation performances even for high  $E_B/N_0$  and large  $K/Q$ . The correlation SCE is based on the correlation between different parts of the received signal which is approximated by the arithmetic mean of the product between the received signal parts, cf. Eq. (4.15). The arithmetic mean converges towards the true value of the correlation for the ratio  $K/Q$  tending to infinity and, thus, the estimation performances is improved for increasing values of the ratio  $K/Q$ . However, an increasing ratio  $K/Q$  cannot counteract the occurrence of the error floor. The results for subspace SCE show that it performs significantly better than the correlation SCE. Moreover, for subspace SCE, it can be observed that the MSE performance is only hardly influenced by the SNR for  $E_B/N_0 \leq 15$  dB and tends to zero for an increasing  $E_B/N_0$ . This can be explained by the estimation principle of the subspace SCE which is based on the separation of the signal and the noise subspace. For this separation, it is assumed that the signal power is larger than the noise power, cf. Section 4.2.3.1. For low  $E_B/N_0$ , this assumption is fulfilled only approximately which entails an erroneous separation of the signal and the noise subspace and leads to a poor estimation performance. For high  $E_B/N_0$ , the assumption is fulfilled and the signal and the noise subspace are almost ideally separable. Therefore, the subspace SCE is an unbiased estimator which is also approved by the results in Figure 4.9(a). Similar to the correlation SCE, the subspace SCE is based on the evaluation of the autocorrelation matrix of the received signal vector. The autocorrelation matrix is approximated by an arithmetic mean which converges to the true autocorrelation matrix for the ratio  $K/Q$  tending to infinity. The estimation performance is improved for increasing values of the ratio  $K/Q$  if the assumption that the signal power is larger than the noise power is fulfilled. Thus, the performance improvement is observable for  $E_B/N_0 > 15$  dB.

In Figure 4.9(b), the results are valid for the same assumptions as in Figure 4.9(a) but for the Rural Area VarDelay channel. It can be seen that the MSE performance is slightly improved for the case of correlation SCE and all considered ratios  $K/Q$  compared to the results for the typical urban propagation scenario. For subspace SCE, the performance improvement in case of the rural area propagation scenario is very small and marginal. The rural area propagation scenario differs from the typical urban propagation scenario in the power distribution of the delay paths. Obviously, the subspace SCE copes better with strong delay paths than the correlation SCE.



(a) Typical Urban VarDelay channel



(b) Rural Area VarDelay channel

Figure 4.9. MSE as a function of  $E_B/N_0$  in dB with the ratio  $K/Q$  as parameter assuming  $U = 1$ ,  $v = 0$  km/h,  $I = 2$  and  $L_C = Q = 8$ .

In Figure 4.10, results are shown for subspace SCE with the ratio  $K/Q$  and the interpolation depth  $I$  as parameters. The Typical Urban VarDelay is considered as channel model. Results for correlation SCE are omitted as the correlation SCE provides only poor performance for  $I = 2$  as shown in Figure 4.9 and fails to estimate the channel if the interpolation depth is further increased. For  $I = 4$ ,  $Q_P = \frac{Q}{4}$  pilot symbols are transmitted on every 4<sup>th</sup> subcarrier in the IFDMA symbol with index  $k = 0$ . The interpolation depth  $I = 4$  corresponds to an oversampling factor  $O_F = 0.25$  in frequency domain which means that the sampling theorem in frequency domain is extended by factor 4.

In Figure 4.10, it can be seen that the estimation performance decreases clearly if the interpolation depth increases from  $I = 2$  to  $I = 4$ . However, for  $I = 4$ , increasing the ratio  $K/Q$  produces a performance gain that is comparable to the performance gain for  $I = 2$  if  $K/Q$  is increased. For large SNR values and large ratios  $K/Q$ , the estimation performance of subspace SCE with  $I = 4$  is quite acceptable. Thus, it can be stated that the application of subspace SCE allows the violation of the sampling theorem in frequency domain by factor 4 in case of large SNR values and large ratios  $K/Q$ .

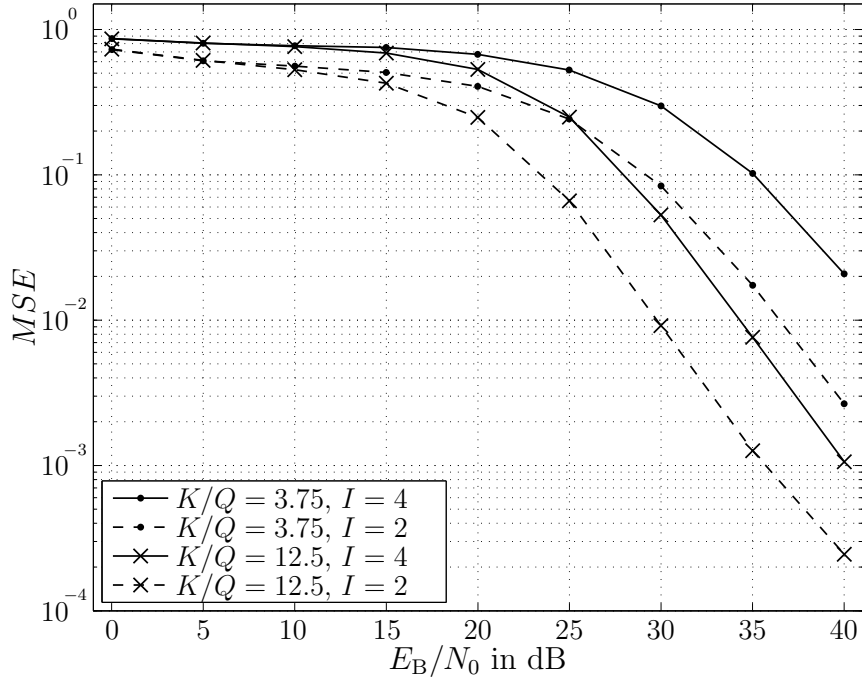


Figure 4.10. MSE as a function of  $E_B/N_0$  in dB with the ratio  $K/Q$  and the interpolation depth  $I$  as parameter assuming that  $U = 1$ ,  $v = 0$  km/h and  $L_C = Q = 8$  for the Typical Urban VarDelay channel.

For the remainder of this section, the following parameters are valid:

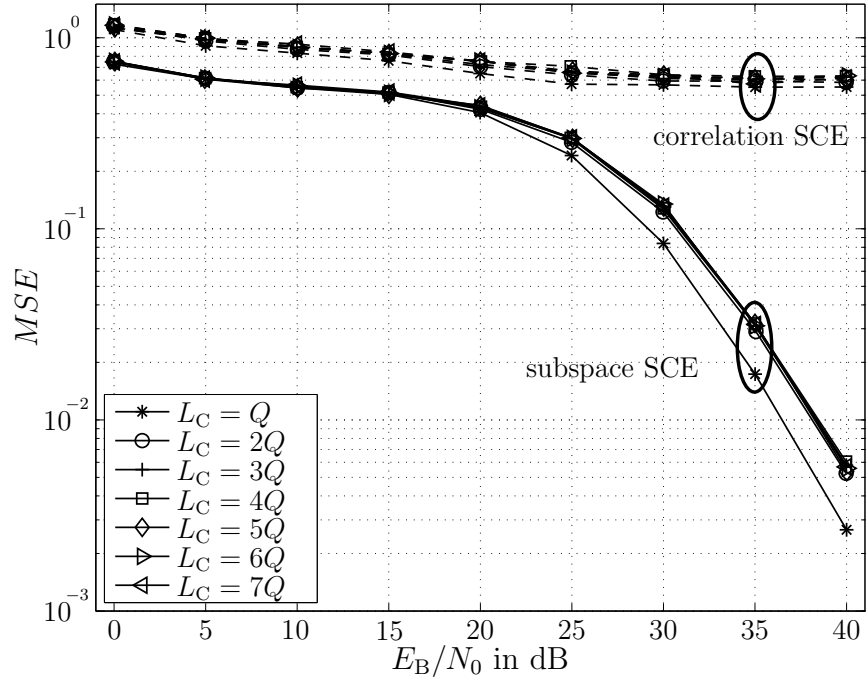


- The ratio between the number  $K$  of IFDMA symbols transmitted within the TDMA slot and the number  $Q$  of data symbols per IFDMA symbol is chosen as  $K/Q = 3.75$ . As the semiblind channel estimation approaches shall support a reduction of the number of pilot carrying subcarriers even for a small number  $Q$  of allocated subcarriers, the following results are presented for  $Q = 8$  and  $K = 30$ .
- $Q_P = \frac{Q}{2}$  pilot symbols are transmitted in the IFDMA symbol with index  $k = 0$  which corresponds to an interpolation depth of  $I = 2$ .

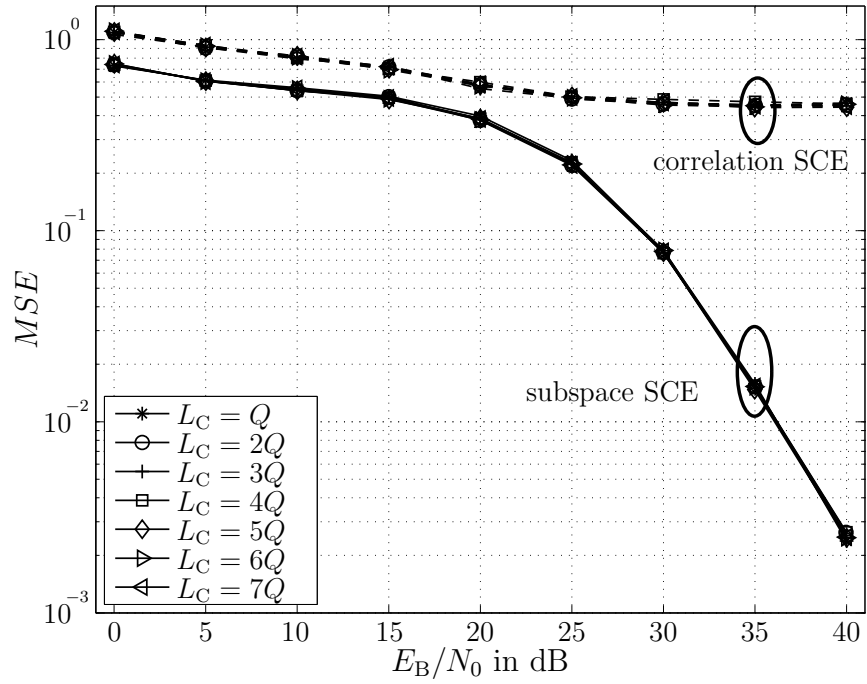
In the following, the influence of the number  $L_C$  of channel delay taps on the estimation performance of the correlation and the subspace based semiblind channel estimation is investigated. In Figure 4.11, the MSE is given as a function of  $E_B/N_0$  in dB with the number  $L_C$  of channel delay taps as parameter. The results are presented for  $U = 1$  user in the system.

In Figure 4.11(a), the Typical Urban VarDelay channel is considered. For correlation SCE, the results are obtained by applying the algorithm introduced in Section 4.2.2.1 for  $L_C = Q$  and the algorithm introduced in Section 4.2.2.2 for  $L_C > Q$ . For correlation SCE, the results in Figure 4.11(a) show that the MSE is only marginally increased due to large channel delay spreads. For  $L_C > Q$ , the MSE is independent of the specific value for  $L_C$ . This approves that the correlation SCE can cope with large channel delay spreads by means of estimating the cyclic channel impulse response as explained in Section 4.2.2.2. For subspace SCE, the results in Figure 4.11(a) are obtained by applying the algorithm introduced in Section 4.2.3.1 for  $L_C = Q$  and the algorithm introduced in Section 4.2.3.2 for  $L_C > Q$ . Comparable to the results for correlation SCE, it can be seen that the estimation of channels with  $L_C > Q$  for subspace SCE leads to a slightly increased MSE compared to the estimation for  $L_C = Q$ . The increase of the MSE can be reduced to the fact that for  $L_C > Q$ ,  $2Q$  unknown elements of the channel impulse response and the cyclic channel impulse response have to be estimated instead of  $Q$  unknowns for the case where  $L_C = Q$ . For  $L_C > Q$ , the MSE is independent of the specific value for  $L_C$  and, thus, it can be stated that due to estimating the cyclic channel impulse response according to the algorithm presented in Section 4.2.3.2 the estimation performance is independent of the channel delay spread.

In Figure 4.11(b), results are presented for the Rural Area VarDelay channel. It can be seen that for both, the correlation SCE and the subspace SCE, there is no performance degradation for the case where  $L_C > Q$  compared to  $L_C = Q$ . This can be explained by the power distribution of channel delay taps for the case of a rural area propagation



(a) Typical Urban VarDelay channel



(b) Rural Area VarDelay channel

Figure 4.11. MSE as a function of  $E_B/N_0$  in dB with the number  $L_C$  of channel delay taps as parameter for  $Q = 8$ ,  $K = 30$ ,  $U = 1$ ,  $v = 0$  km/h and  $I = 2$ .

scenario. The amount of power that is accumulated in the first channel delay taps is larger than for the typical urban propagation scenario. As the correlation SCE and the subspace SCE take advantage of the interference that is introduced by the preceding IFDMA symbol into the cyclic prefix of the current IFDMA symbol, both algorithms perform better if a larger amount of power is accumulated in the first channel delay taps.

In Figure 4.12, the influence of the considered channel model on the estimation performance of the correlation SCE and the subspace SCE is investigated for the case of channels with large delay spreads. The results are valid for the same parameters as presented for Figure 4.11. For comparison, the WINNER SCM urban macro-cell channel, the Typical Urban VarDelay channel and the Rural Area VarDelay channel are investigated. It can be seen that both, the correlation SCE and the subspace SCE perform best in case of the rural area propagation scenario. This can be deduced to the fact that a large amount of the total power of the channel delay paths is accumulated in the first delay taps. For correlation SCE, the WINNER SCM urban macro-cell channel entails better performance compared to the Typical Urban VarDelay channel. The WINNER SCM urban macro-cell channel, in contrast to the Typical Urban VarDelay channel, exhibits clustered delay paths and a power delay profile which is not continuously decaying with the delay time. Obviously, the correlation SCE copes better with this distribution of delay paths than with a continuously decaying power delay profile where each of the  $L_C$  delay paths exhibits a power larger than zero. For subspace SCE, the comparison between the WINNER SCM urban macro-cell channel and the Typical Urban VarDelay channel shows that the subspace SCE copes slightly better with the Typical Urban VarDelay channel. Although there is only slight difference in the MSE performance, it can be deduced that the subspace SCE performs better in case of a continuously decaying power delay profile.

In the following, the influence of the number  $U$  of users allocated to the same TDMA slot on the estimation performance of the correlation SCE and the subspace SCE is investigated. Results are presented for the following parameters:

- The Typical Urban VarDelay channel is used in the simulations.
- In order to observe the influence of multiple users in the system independently from the influences introduced by large channel delay spreads, the results are presented for  $L_C = Q$  channel delay taps.

In Figure 4.13, the MSE is presented as a function of  $E_B/N_0$  in dB for an uplink scenario with the number  $U$  of users as parameter. It can be seen that the performance

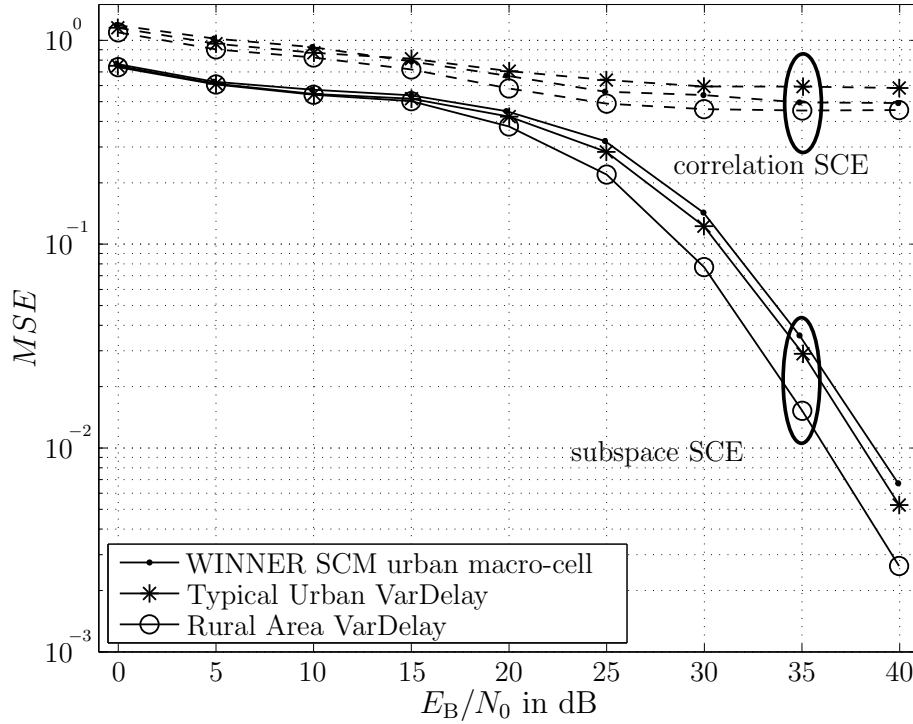


Figure 4.12. MSE as a function of  $E_B/N_0$  in dB with the considered channel model as parameter assuming that  $Q = 8$ ,  $K = 30$ ,  $U = 1$ ,  $v = 0$  km/h and  $I = 2$ .

of the correlation SCE remains unaffected by data transmission of multiple users in the system. This corresponds to the results that have been derived in Section 4.2.2.3. In contrast to this, the performance of the subspace SCE is strongly degraded due to multiple users in the system and the performance degradation depends directly on the number  $U$  of users in the system. This performance degradation is caused by superimposing cyclic prefixes that have been transmitted by the  $U$  users and cannot be separated as the cyclic prefixes of different users are not designed under consideration of mutual orthogonality.

In Figure 4.14, the influence of the number  $U$  of users allocated to the same TDMA slot on the channel estimation performance is investigated for the case of downlink transmission. For correlation SCE, it can be observed that for a downlink scenario, the data transmission of multiple users slightly improves the MSE performance. This can be explained by the increasing number of received signals that are available for channel estimation if  $U > 1$ . In a downlink scenario, the  $U$  received signals are affected by the same channel conditions and, thus, the received signal provides an increasing power for the estimation of the channel which leads to performance improvements. For subspace SCE, the MSE performance is significantly improved if the signals of multiple users are

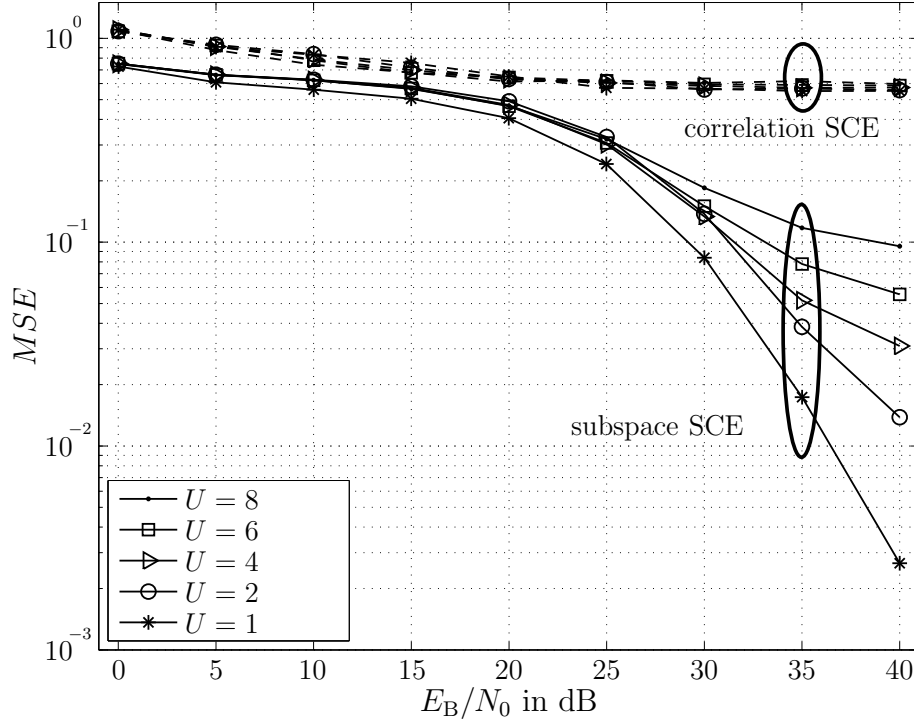


Figure 4.13. MSE as a function of  $E_B/N_0$  in dB with the number  $U$  of users as parameter assuming that  $L_C = Q = 8$ ,  $v = 0$  km/h and  $I = 2$  in an uplink scenario.

received at the mobile terminal. This can again be accounted for the increasing received power due to the superposition of the  $U$  users' signals at the receiver. However, for an increasing number  $U$  of users, the MSE degrades for large SNR. This can be explained under consideration of Eq. (4.78) which shows that the received vector consists of the superposition of  $U$  different transmit vectors of length  $2Q$ . The autocorrelation matrix of this received vector has to be estimated and the autocorrelation of  $U \times 2Q$  data symbols is approximated by the arithmetic mean. With an increasing number  $U$  of users in the system, an increasing number  $K$  of received IFDMA symbols is needed to estimate the autocorrelation matrix and to obtain a converging channel estimate.

In the following, the influence of the time variability of the channel, which is represented by the user velocity  $v$ , on the estimation performance of the correlation SCE and the subspace SCE is investigated for

- the Typical Urban VarDelay channel,
- $L_C = Q$  channel delay taps and
- $U = 1$  user in the system

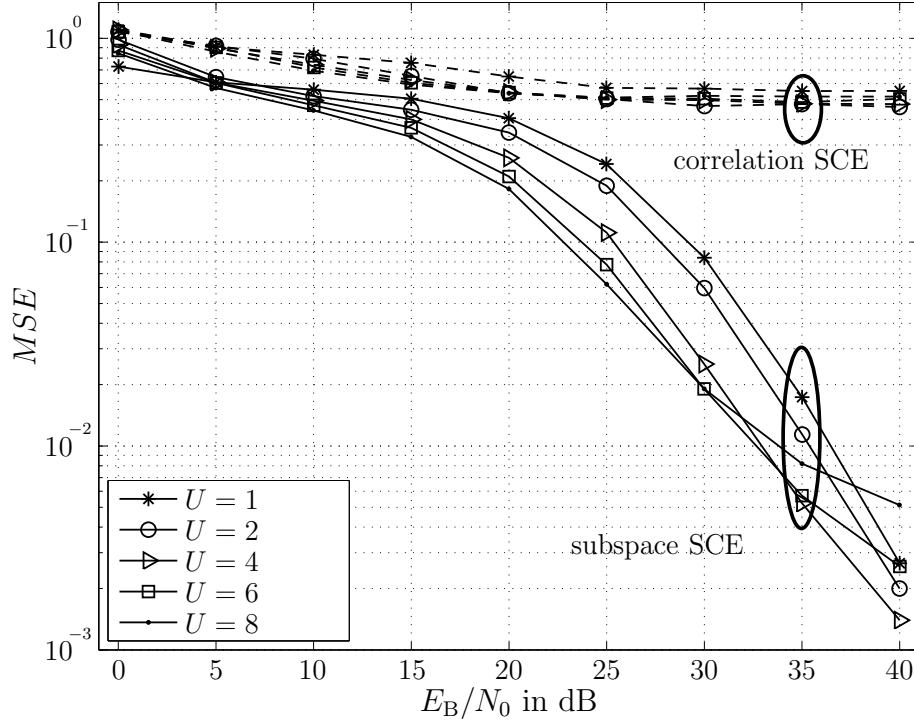
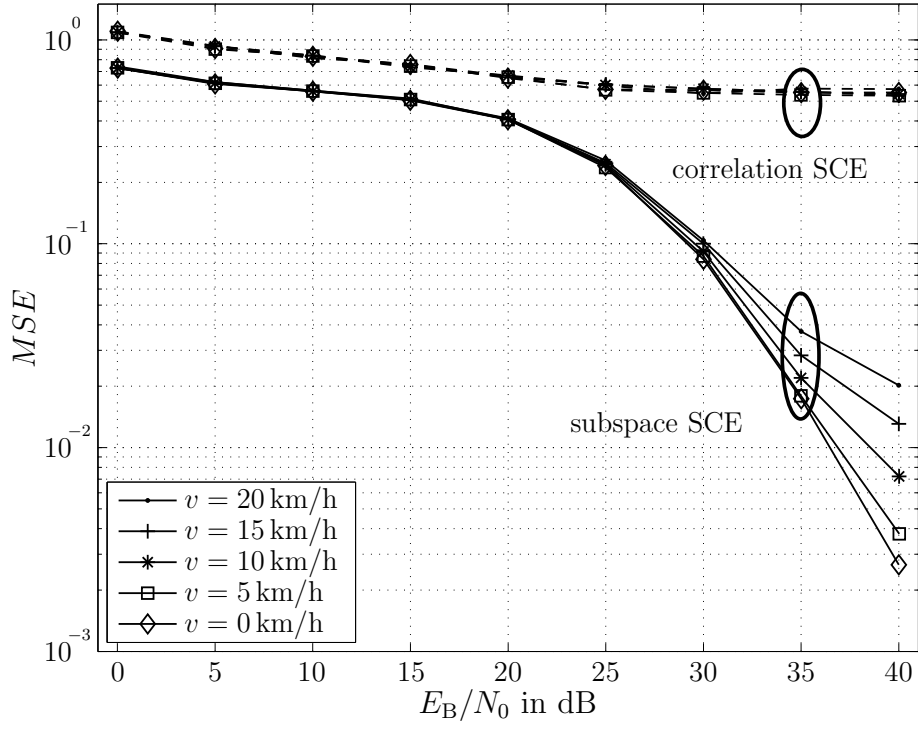


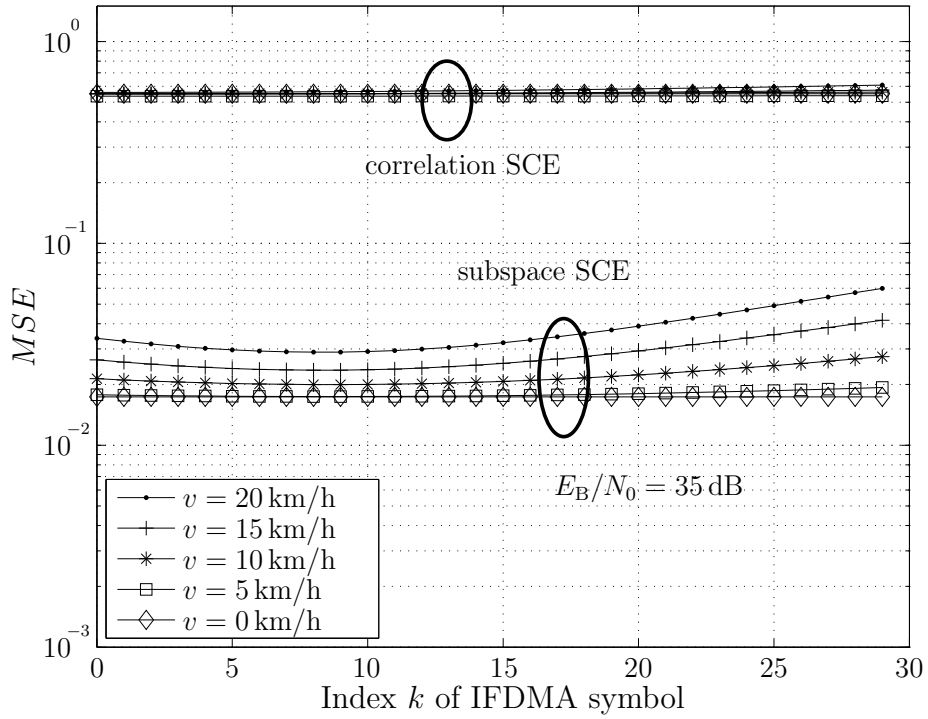
Figure 4.14. MSE as a function of  $E_B/N_0$  in dB with the number  $U$  of users as parameter assuming that  $L_C = Q = 8$ ,  $v = 0$  km/h and  $I = 2$  in a downlink scenario.

In Figure 4.15(a), the MSE is given as a function of  $E_B/N_0$  in dB with the user velocity  $v$  as parameter. For correlation SCE, the results in Figure 4.15(a) show that increasing the velocity from  $v = 0$  km/h up to  $v = 20$  km/h has no observable impact on the MSE performance. The performance degradation due to time variant channel conditions is negligible as the correlation SCE suffers already from a high error floor. For subspace SCE, the increasing velocity leads to obvious performance degradations for  $E_B/N_0 > 25$  dB. The higher the velocity, the higher the performance loss. This effect is accounted for the erroneous assumption that the channel conditions are invariant during the transmission of  $K$  IFDMA symbols. As this assumption is the basis for the calculation of the arithmetic mean in Eq. (4.51) and, thus, the basis for the subspace SCE, the violation of this assumption due to moving mobile stations leads to the performance degradations shown in Figure 4.15(a).

In Figure 4.15(b), the MSE is given as a function of the IFDMA symbol index  $k$  with the user velocity  $v$  as parameter. The results are valid for the same assumptions as in Figure 4.15(a) and are presented for  $E_B/N_0 = 35$  dB. It can be seen that for the correlation SCE, the MSE performance is constant for each IFDMA symbol within the TDMA slot. However, for the subspace SCE, the time variability influences the



(a)



(b)

Figure 4.15. MSE as a function of (a)  $E_B/N_0$  in dB and (b) the IFDMA symbol index  $k$  with the user velocity  $v$  as parameter assuming that  $L_C = Q = 8$ ,  $K = 30$ ,  $U = 1$  and  $I = 2$ .

MSE of the channel estimates. The higher the velocity  $v$ , the higher the MSE of the subspace SCE. For each investigated velocity, the best performance is achieved for the estimate corresponding to the IFDMA symbol with index  $k = 0$ . This is accounted for the transmission of the pilot symbols within the IFDMA symbol with index  $k = 0$ . With an increasing time duration between the IFDMA symbol with index  $k = 0$  and an IFDMA symbol with index  $k$ , the information about the channel that is provided due to pilot symbol transmission is outdated. Therefore, the performance degradation increases with increasing IFDMA symbol index  $k$  and increasing velocity  $v$  of the mobile terminal.

In the following, the performance of the proposed correlation SCE+DDCE+WF and the subspace SCE+DDCE+WF is investigated. In Figure 4.16(a), the MSE is given as a function of  $E_B/N_0$  in dB with the user velocity  $v$  as parameter. For the simulations, the following parameters have been used:

- The WINNER SCM urban macro-cell channel is considered.
- For the iterative Wiener filtering,  $V = 6$  filter coefficients are applied.
- In order to observe the influence of the time variability of the channel independently from the influences introduced by multiple users in the system, the results are presented for  $U = 1$  user in the system.

It can be seen that for correlation SCE+DDCE+WF, the MSE is slightly decreased in comparison to the MSE of correlation SCE for the WINNER SCM urban macro-cell channel shown in Figure 4.12. Moreover, the performance remains unaffected by the increasing velocity of the mobile terminal. Nevertheless, the estimation performance of correlation SCE+DDCE+WF is very poor. In contrast to this, the performance of subspace SCE+DDCE+WF exhibits a significantly better performance. Comparing the result for  $v = 0$  km/h with the result for subspace SCE shown in Figure 4.12, it reveals that the application of DDCE+WF considerably improves the estimation performance. For an example, the improvement is approximately 15 dB for  $MSE = 10^{-2}$ . This shows that the application of DDCE+WF for the estimation of time domain channel variations mitigates estimation errors that occur due to an erroneous estimation of the frequency domain channel variations. Due to symbol detection, updating channel estimation and subsequent Wiener filtering in each iteration step for DDCE+WF, the propagation of the estimation error caused by the initializing estimate is strongly mitigated. As the performance improvement of subspace SCE+DDCE+WF compared to subspace SCE is clearly better than for correlation SCE+DDCE+WF, it can be



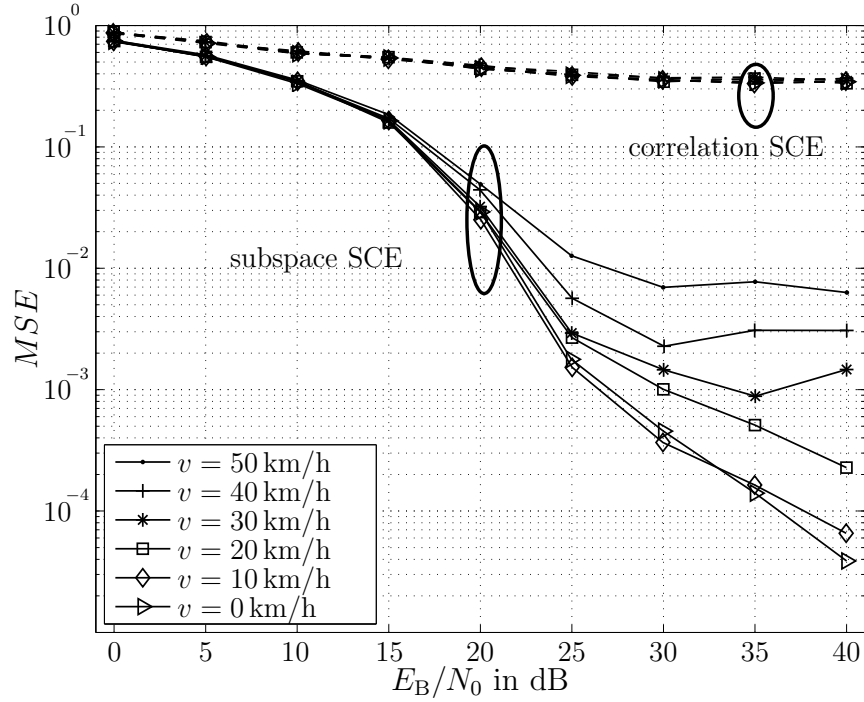
deduced that the proposed DDCE+WF requires a certain quality of its initializing estimate to develop its error mitigating property. Obviously, for the initialization with the correlation SCE, the estimation performance is insufficient and cannot be improved noticeably by the application of DDCE+WF. On the contrary, for the initialization with the subspace SCE, the initializing estimate provides a satisfying performance for  $E_B/N_0 > 5$  dB and, thus, the performance can be improved significantly. Nevertheless, for an increasing velocity  $v$ , the MSE of subspace SCE+DDCE+WF exhibits an increasing error floor for large SNR values. The increasing error floor can be explained by an error propagation due to the time varying channel conditions. The error propagation is reduced by the iterative Wiener filtering but cannot be completely avoided.

In Figure 4.16(b), the performance of the proposed subspace SCE+DDCE+WF is compared to the case where pure pilot assisted channel estimation represented by symbolwise LS is used for the initialization of the DDCE+WF.

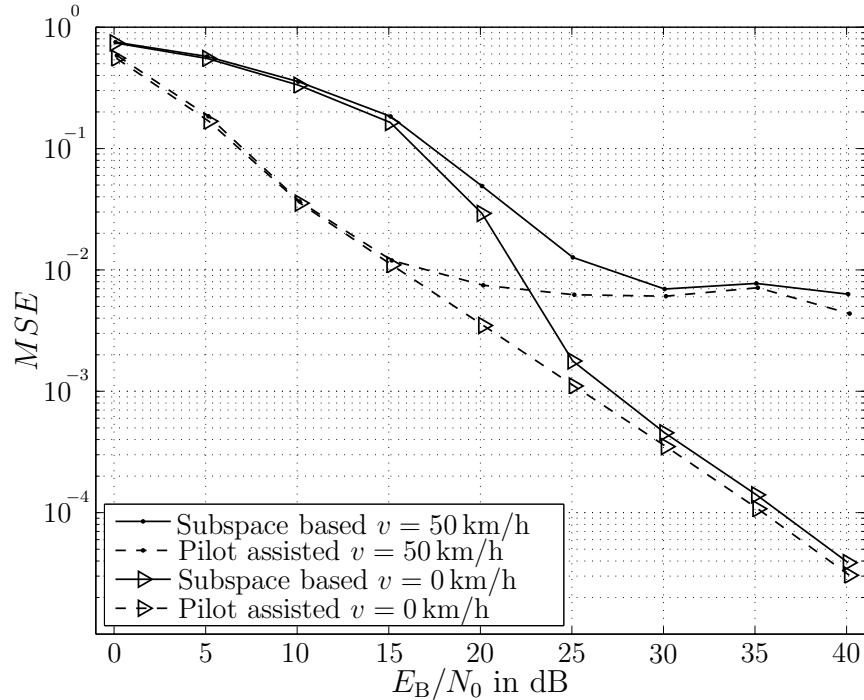
The initialization with correlation SCE is not considered for this comparison due to its unsatisfying results that have been shown in Figure 4.16(a). The results in Figure 4.16(b) are valid for the same assumptions as in Figure 4.16(a). As the pure pilot assisted initialization consumes twice as much pilot symbols as the subspace SCE initialization, the pilot symbol overhead is included in the MSE results as an SNR degradation according to Eq. (3.52).

Figure 4.16(b) shows that for  $E_B/N_0 < 25$  dB, the DDCE+WF with symbolwise LS initialization exhibits a clearly better performance than the subspace SCE+DDCE+WF. This can be attributed to the fact that the symbolwise LS provides better estimation performances for  $E_B/N_0 < 25$  dB than the subspace SCE. The high quality of the symbolwise LS initializing estimate leads to a strong performance improvement while applying DDCE+WF. Nevertheless, for  $E_B/N_0 \geq 25$  dB, the subspace SCE+DDCE+WF exhibits the same performance as DDCE+WF with symbolwise LS initialization. This result is remarkable as the subspace SCE initializing estimate requires half the number of pilot symbols than the symbolwise LS initializing estimate and provides satisfying estimation performance for a pilot allocation where a pure pilot assisted initialization fails to estimate the channel at all. Moreover, it can be stated that the performance gain due to the application of DDCE+WF is significantly larger for the subspace SCE than for the symbolwise LS.

In the following, the influence of multiple users in the system is investigated for subspace SCE+DDCE+WF. In Figure 4.17, the MSE is given as a function of  $E_B/N_0$  in dB with the number  $U$  of users as parameter. Further parameters are as follows:



(a) Comparison of correlation and subspace based semibind channel estimation with interpolation depth  $I = 2$  as initialization for DDCE+WF



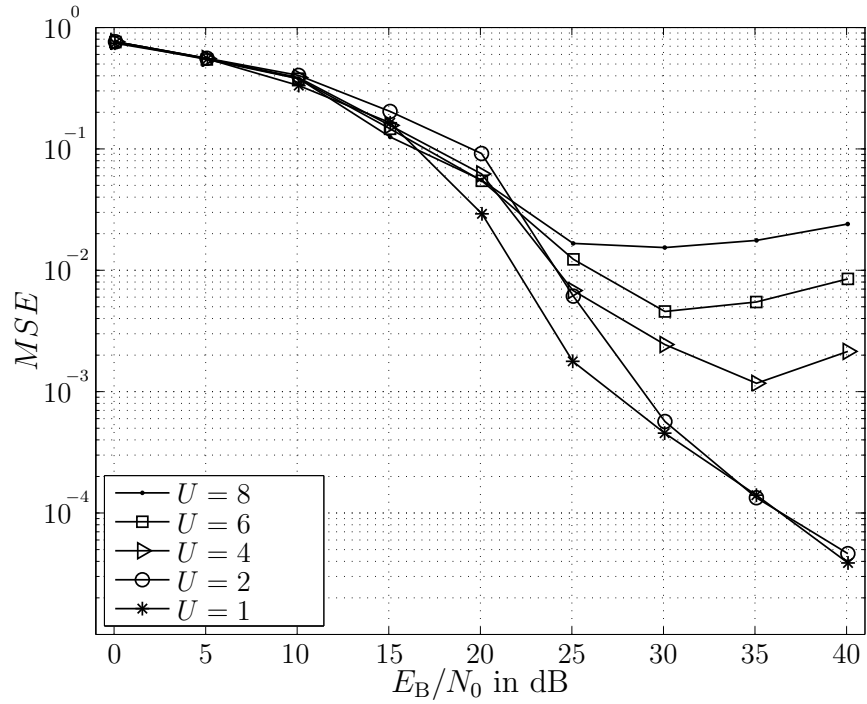
(b) Comparison of subspace based semibind channel estimation with interpolation depth  $I = 2$  and pilot assisted channel estimation with  $I = 1$  as initialize for DDCE+WF

Figure 4.16. MSE as a function of  $E_B/N_0$  in dB with the velocity  $v$  as parameter for the WINNER SCM urban macro-cell channel and assuming that  $Q = 8$ ,  $K = 30$ ,  $U = 1$ .

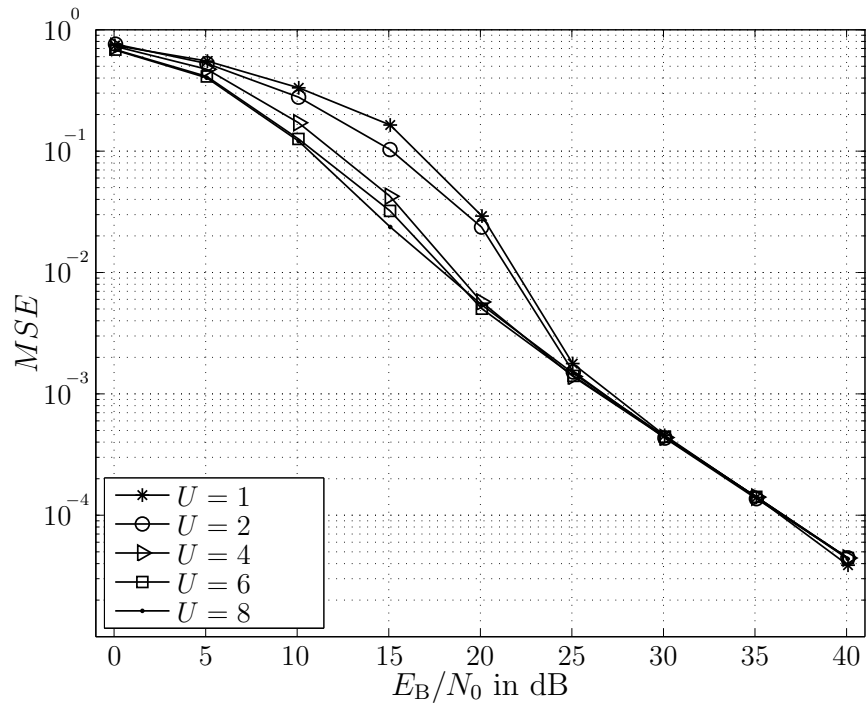
- The WINNER SCM urban macro-cell channel is used.
- For the iterative Wiener filtering,  $V = 6$  filter coefficients are applied.
- In order to observe the influence of numbers of users independently from the influences introduced by time varying channel, the results are presented for a velocity of  $v = 0$  km/h.

In Figure 4.17(a), results are presented for the case of an uplink transmission. It can be seen that the MSE performance exhibits an increasing error floor with increasing number  $U$  of users in the system. For  $U = 2$  and  $E_B/N_0 \geq 30$  dB, the performance of the initializing subspace SCE is sufficient for the error mitigation probability of the DDCE+WF and the MSE is equal to the case with  $U = 1$  user in the system. For  $U = 4$ , the initializing estimate provides insufficient performance and the application of DDCE+WF fails to mitigate the estimation errors.

Figure 4.17(b) shows results for the same assumptions as in Figure 4.17(b) but for the case of downlink transmission. It can be seen that the estimation performance is improved significantly for  $E_B/N_0 \leq 25$  dB due to the transmission of multiple users in the system. The largest performance gain is achieved if the number  $U$  of users is increased from  $U = 2$  to  $U = 4$ . Obviously, for  $U = 4$ , the performance of the initializing subspace SCE exceeds a threshold at which the DDCE+WF copes better with initializing estimation errors. Moreover, it can be seen that the error floor which has been observed for the MSE of subspace SCE in Figure 4.14 for  $U \geq 6$ , is mitigated by the DDCE+WF and does not occur in Figure 4.17(b). For  $E_B/N_0 > 25$  dB, the estimation performance is identical if the signals of  $U = 1, 2, 4, 6, 8$  users are transmitted in the system.



(a) Uplink



(b) Downlink

Figure 4.17. MSE as a function of  $E_B/N_0$  in dB with the number  $U$  of users as parameter for the WINNER SCM urban macro-cell channel and assuming that  $Q = 8$ ,  $K = 30$  and  $v = 0$  km/h.

#### 4.4.4 Complexity

In this section, the correlation SCE+DDCE+WF and the subspace SCE+DDCE+WF are investigated in terms of their computational complexity.

According to Section 3.4.5, the computational complexity is measured based on the required number of complex multiplications. In the following, the assumptions introduced in Section 3.4.5 are valid. In Table 4.3, the number of complex multiplications is given for the respective estimation algorithm. It is again assumed that the  $Q \times Q$  DFT and IDFT operations can be implemented by FFT and IFFT operations according to [KK98] with  $Q \cdot \log_2(Q)$  complex multiplications each.

Table 4.3. Number of complex multiplications

Algorithm	Complex multiplications
correlation SCE+DDCE+WF	$(Q + 1) \cdot L_U \cdot K + 2 \cdot Q + Q \cdot \log_2(Q) + Q_P + (K - 1) \cdot (Q \cdot (V + 2) + 2 \cdot Q \cdot \log_2(Q))$
subspace SCE+DDCE+WF	$8Q^4 + \mathcal{O}(45Q^3) + (9L_U K + 2) \cdot Q^2 + (Q_P + \log_2(Q))Q + Q_P + (K - 1) \cdot (Q \cdot (V + 2) + 2 \cdot Q \cdot \log_2(Q))$

For each semiblind estimation algorithm, the second line given by  $K \cdot (Q \cdot (V + 2) + 2 \cdot Q \cdot \log_2(Q) + \mathcal{O}(\text{decoding}))$  is identical as it refers to the number of complex multiplications for the DDCE+WF. In each of the  $K - 1$  iteration steps, there are  $2 \cdot Q \cdot \log_2(Q)$  multiplications for the FFT and IFFT operations applied to the estimated data symbols,  $Q$  multiplications for the LS estimation,  $Q$  multiplication for the equalization and  $V \cdot Q$  multiplications for the Wiener filtering. The multiplications for the coding and decoding process in each iteration step are neglected at this point, as the coding and decoding processes do not represent the crucial part of the algorithms in terms of complexity. The number of multiplications strongly depends on the coding and decoding algorithms and their implementation and, thus, varies for different coding and decoding algorithms. The initialization of DDCE+WF with correlation SCE consumes  $Q_P$  multiplications for the LS estimates of the pilot carrying subcarriers,  $(Q + 1) \cdot L_U \cdot K + Q$  multiplications for the evaluation of Eq. (4.15),  $Q \cdot \log_2(Q)$  multiplications for the FFT operation and  $Q$  multiplications for the calculation and resolving of the factor of ambiguity. It can be stated that initialization with the correlation based semiblind channel

estimation exhibits a clearly lower computational complexity than initialization with the subspace based semiblind channel estimation. For subspace SCE, there are again  $Q_P$  multiplications for the LS estimates of the pilot carrying subcarriers. The calculation of the  $3Q \times 3Q$  autocorrelation matrix consumes  $L_U \cdot K \cdot (3 \cdot Q)^2$  multiplications. The complexity order of the eigenvalue decomposition of an  $L \times L$  matrix has been presented in, e.g., [GvL96, Sil08] and equals  $\mathcal{O}(\frac{5}{3}L^3)$ . For  $L = 3Q$ , the eigenvalue decomposition of the  $3Q \times 3Q$  autocorrelation matrix entails a large number of complex multiplications and leads to a complexity order  $\mathcal{O}(45Q^3)$ . Finally, the calculation of Eq. (4.74) utilizes  $8 \cdot Q^4 + 2 \cdot Q^2 + Q \cdot Q_P$  multiplications and the FFT operation in order to obtain the channel transfer factors utilizes  $Q \cdot \log_2(Q)$  multiplications. For subspace SCE, the critical part in terms of the computational complexity is the computation of  $\sum_{q=0}^{Q-1} \hat{\mathbf{g}}_q^{(u)} \cdot \hat{\mathbf{g}}_q^{(u)H}$  which leads to  $8Q^4$  complex multiplications.

## 4.5 Conclusions

In this chapter, two second order statistics based semiblind channel estimation approaches have been introduced for the application to IFDMA in order to estimate the channel variations in frequency domain. The application of these two second order statistics based semiblind channel estimation approaches opens up the possibility to extend the sampling theorem in frequency domain and allows to reduce the number of pilot symbols in frequency domain in comparison to pure pilot assisted channel estimation. The second order statistics based semiblind channel estimation approaches have been adapted to estimate channels with large delay spreads and investigated in terms of the influence of multiple users in the system. Additionally, these second order statistics based semiblind channel estimation approaches have been combined with decision directed channel estimation in order to estimate the channel variations in time domain. By doing so, the sampling theorem in time domain can be extended and the number of pilot symbols in time domain is reduced compared to pure pilot assisted channel estimation. The decision directed channel estimation has been extended by an iterative Wiener filtering process to combat the error propagating character of decision directed estimation approaches. The introduced semiblind channel estimation algorithms have been investigated in terms of their pilot symbol overhead consumption, their MSE performance and their computational complexity. The main conclusions of this chapter can be summarized as follows:

- The comparison of the two second order based semiblind channel estimation approaches for the estimation of frequency domain channel variations reveals

that the subspace SCE provides a clearly better estimation performance than the correlation SCE. Due to the estimation principle of subspace SCE by separation of signal and noise subspace, a channel estimate is obtained for large SNR values which is close to the optimum channel estimate. The correlation SCE represents a biased estimator and the estimation performance exhibits large error floors.

- Due to the extension of the second order based semiblind channel estimation approaches to channels with large delay spreads, the channel transfer factors corresponding to the  $Q$  allocated subcarriers can be estimated utilizing  $Q_P = Q/2$  pilot carrying subcarriers independent of the number  $L_C$  of channel delay taps.
- For typical urban propagation scenarios, channels with large delay spreads are estimated with a slight performance degradation in comparison to channels with small delay spreads. For rural area propagation scenarios, the estimation of channels with large and small delay spreads reveals identical performances.
- The correlation SCE remains unaffected by multiple users in the system. In contrast to this, the performance of subspace SCE is degraded if the signals of multiple users are transmitted within the same TDMA slot during uplink transmission. However, during downlink transmission, the transmission of multiple users within the same TDMA slot leads to a significant performance improvement, especially in the low SNR region.
- The combination of DDCE+WF with correlation SCE produces a channel estimate with slight performance improvements compared to the results for correlation SCE only.
- The combination of DDCE+WF with subspace SCE produces a channel estimate with significant performance improvements compared to the results for subspace SCE only. The performance improvements can be attributed to error mitigating properties of DDCE+WF which are based on the iterative Wiener filtering process. As the combination of DDCE+WF with subspace SCE produces a clearly stronger performance improvement than the combination with correlation SCE, it can be stated that the error mitigating property of DDCE+WF is effective if the initializing estimate provides a certain quality of the estimates.
- For large SNR values, the subspace SCE+DDCE+WF provides comparable estimation performance as DDCE+WF with symbolwise LS as initialization which consumes twice as much pilot symbols as the subspace SCE initialization.
- For IFDMA, the time varying channel transfer factors can be estimated although the distance between the inserted pilot symbols violates the sampling theorem in

frequency and time domain. That means, the application of semiblind channel estimation to IFDMA allows a noticeable reduction of the pilot symbol overhead while providing satisfying estimation performance. The sampling theorem in frequency and time domain is extended at the expense of an increased computational complexity.



## Chapter 5

# Channel Estimation for Block-IFDMA

### 5.1 Introduction

In this chapter, channel estimation for B-IFDMA is addressed. The B-IFDMA scheme can be described as DFT precoded OFDMA where blocks of  $K_F$  neighboring subcarriers are equidistantly distributed over the available bandwidth. Thus, it can be seen as generalization of IFDMA where each block consists of  $K_F > 1$  subcarrier. On the one hand, channel estimation for B-IFDMA comprises similarities to the channel estimation for IFDMA. On the other hand, for B-IFDMA, new aspects arise compared to IFDMA due to the blockwise allocation of subcarriers in frequency domain. In the following, selected topics concerning the pilot assisted and semiblind channel estimation algorithms presented for IFDMA in Chapter 3 and Chapter 4 are introduced with regard to the application to B-IFDMA. Parts of this chapter have been originally published by the author in [SK07, SFK07, SK09a, SK10].

In Section 5.2, a system model is presented for B-IFDMA which is based on the IFDMA signal generation in frequency domain introduced in Section 2.2.2. Section 5.3 addresses the pilot assisted channel estimation for B-IFDMA and the differences compared to pilot assisted channel estimation for IFDMA. In Section 5.4, semiblind channel estimation is introduced for B-IFDMA and, again, the differences compared to semiblind channel estimation for IFDMA are elaborated. Section 5.5 gives the main conclusions of this chapter.

### 5.2 System Model

In this section, a system model for a mobile communication system utilizing B-IFDMA as multiple access scheme is presented. The considered system is identical to the one introduced in Chapter 2 for IFDMA except the subcarrier allocation. Thus, in this section, the B-IFDMA signal generation and demodulation is explained based on the description of IFDMA signal generation and demodulation in frequency domain described in Section 2.2.2 and Section 2.4, respectively. In the following, the focus is on the distinction of B-IFDMA and IFDMA. Therefore, the B-IFDMA subcarrier

allocation is of central interest and the parts in signal generation and demodulation that are identical to IFDMA are referred to Section 2.2.2 and Section 2.4, respectively.

For B-IFDMA signal generation, data bits that are transmitted by a user with index  $u$ ,  $u = 0, \dots, U-1$ , are channel coded, interleaved and mapped according to a bit mapping scheme like PSK or QAM. The resulting data symbols are fed into the B-IFDMA signal generator where blocks  $\mathbf{d}_k^{(u)}$ ,  $k = 0, \dots, K-1$ , consisting of  $Q$  data symbols that are transmitted at data symbol rate  $1/T_S$  by a user with index  $u$  are processed simultaneously. A DFT precoding is applied to the block  $\mathbf{d}_k^{(u)}$  of data symbols according to Eq. (2.3) and the output of the precoder is denoted by  $\bar{\mathbf{d}}_k^{(u)} = [\bar{d}_{k,0}^{(u)}, \dots, \bar{d}_{k,Q-1}^{(u)}]^T$ . For B-IFDMA, the elements  $\bar{d}_{k,q}^{(u)}$  are transmitted on  $Q/K_F$  blocks each consisting of  $K_F$  neighboring subcarriers that are distributed over the total number  $N$  of subcarriers in the system. The block-interleaved subcarrier allocation is depicted exemplarily in Figure 5.1 for a user with index  $u = 0$  and a user with index  $u = 1$ . For B-IFDMA, the assignment of the elements  $\bar{d}_{k,q}^{(u)}$  to the user specific set of  $Q$  subcarriers can be described by an  $N \times Q$  mapping matrix  $\mathbf{M}_B^{(u)}$ . The mapping matrix  $\mathbf{M}_B^{(u)}$  is characterized by its elements  $[\mathbf{M}_B^{(u)}]_{n,q}$ , with  $n = 0, \dots, N-1$  and  $q = 0, \dots, Q-1$  that are given by

$$[\mathbf{M}_B^{(u)}]_{n,q} = \begin{cases} 1 & \text{for } n = \left\lfloor \frac{q}{K_F} \right\rfloor \cdot K_F \left( \frac{N}{Q} - 1 \right) + q + u \cdot K_F, \\ 0 & \text{else.} \end{cases} \quad (5.1)$$

After allocating the elements of  $\bar{\mathbf{d}}_k^{(u)}$  to the specific set of subcarriers, an  $N$ -point IDFT operation is applied in order to get a time domain signal vector at the output of the B-IFDMA signal generator. The  $k^{\text{th}}$  B-IFDMA symbol of a user with index  $u$  with the elements  $x_{k,n}^{(u)}$ ,  $n = 0, \dots, N-1$ , transmitted at chip rate  $1/T_C = L_U/T_S$  is represented by

$$\mathbf{x}_k^{(u)} = \mathbf{F}_N^H \cdot \mathbf{M}_B^{(u)} \cdot \mathbf{F}_Q \cdot \mathbf{d}_k^{(u)} = [x_{k,0}^{(u)}, \dots, x_{k,N-1}^{(u)}]^T \quad (5.2)$$

[SFF<sup>+</sup>07]. The elements  $x_{k,n}^{(u)}$ ,  $n = 0, \dots, N-1$ , will be denoted as chips in the following. In order to avoid intersymbol and intercarrier interference due to transmission over a multipath channel, a cyclic prefix consisting of  $N_G = L_G \cdot Q$  elements is inserted in-between successive B-IFDMA symbols. The  $k^{\text{th}}$  B-IFDMA symbol with cyclic prefix is denoted by  $\tilde{\mathbf{x}}_k^{(u)}$  and has a duration of  $T = (N_G + N) \cdot T_C$ .

Finally,  $K$  successive B-IFDMA symbols  $\tilde{\mathbf{x}}_k^{(u)}$  with cyclic prefix with indices  $k = 0, \dots, K-1$  are summarized in a TDMA slot and transmitted over the mobile radio channel which is represented by the impulse response vector  $\mathbf{h}_k^{(u)}$ . Further on,  $\tilde{\mathbf{x}}_k^{(u)}$  is distorted by AWGN represented by the vector  $\tilde{\mathbf{v}}_k^{(u)} = [\nu_{k,0}^{(u)}, \dots, \nu_{k,N+N_G-1}^{(u)}]$  whose elements have the average power  $\sigma_v^2$ . The interference between successively transmitted

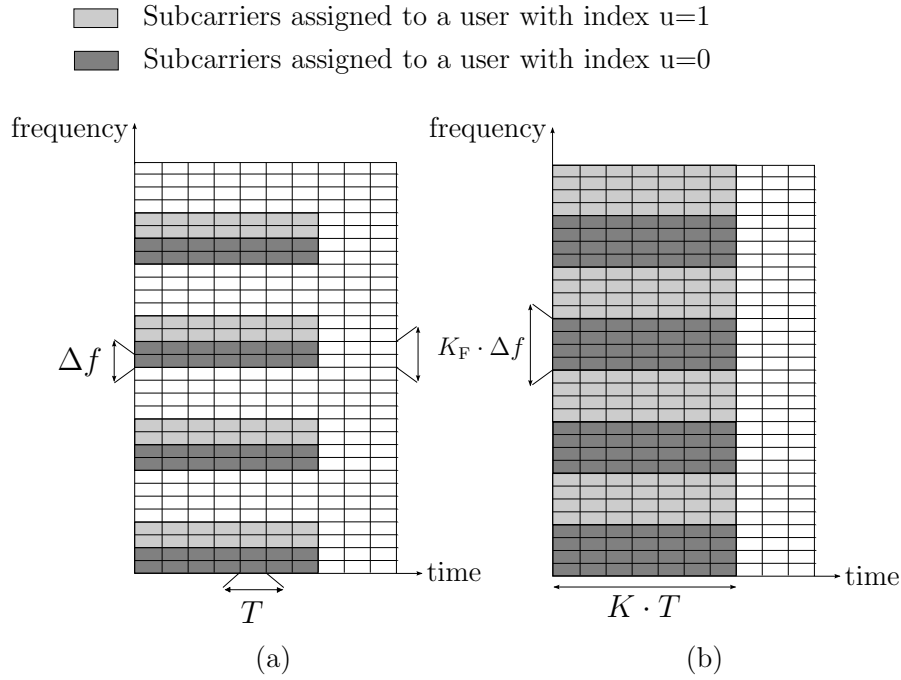


Figure 5.1. B-IFDMA subcarrier allocation for (a)  $Q = 8$ ,  $K_F = 2$  and (b)  $Q = 16$ ,  $K_F = 4$ .

B-IFDMA symbols is avoided due to cyclic prefix insertion and the transmission over the channel can be explained for a single B-IFDMA symbol with index  $k$  independently from the other B-IFDMA symbols. At the receiver, the cyclic prefix part of each B-IFDMA symbol is discarded and the received B-IFDMA symbol without cyclic prefix can be described according to Eq. (2.34) as a function of the transmitted B-IFDMA symbol  $\mathbf{x}_k^{(u)}$ , the  $N \times N$  circulant matrix  $\mathbf{H}_k^{(u)}$  having  $\mathbf{h}_k^{(u)}$  as its first column and the AWGN vector  $\boldsymbol{\nu}_k^{(u)} = [\nu_{k,N_G}^{(u)}, \dots, \nu_{k,N+N_G-1}^{(u)}]^T$  by

$$\mathbf{r}_k^{(u)} = \mathbf{H}_k^{(u)} \cdot \mathbf{x}_k^{(u)} + \boldsymbol{\nu}_k^{(u)}. \quad (5.3)$$

The derivations in Section 2.4 show that for IFDMA, the interference between different subcarriers is avoided due to cyclic prefix insertion. This is also valid for B-IFDMA as it has been shown in [FKCK06]. Therefore, the transmission of an B-IFDMA symbol over a multipath channel can be described in frequency domain by the multiplication of the DFT elements  $\bar{d}_{k,q}$ ,  $q = 0, \dots, Q-1$ , transmitted on each allocated subcarrier with one complex channel coefficient  $\bar{c}_{k,q}^{(u)}$  which is denoted as the  $q^{\text{th}}$  channel transfer factor corresponding to the subcarrier with index  $\left\lfloor \frac{q}{K_F} \right\rfloor \cdot K_F \left( \frac{N}{Q} - 1 \right) + q + u \cdot K_F$  and the B-IFDMA symbol with index  $k$  in the following.  $\bar{c}_{k,q}^{(u)}$  is specified according to

$$\bar{c}_{k,q}^{(u)} = \bar{h}_{k, \left\lfloor \frac{q}{K_F} \right\rfloor \cdot K_F \left( \frac{N}{Q} - 1 \right) + q + u \cdot K_F}^{(u)}, \quad q = 0, \dots, Q-1. \quad (5.4)$$

With Eqs. (3.7), (3.8), the vector  $\bar{\mathbf{c}}_k^{(u)} = [\bar{c}_{k,0}^{(u)}, \dots, \bar{c}_{k,Q-1}^{(u)}]^T$  and the vector  $\bar{\mathbf{v}}_k^{(u)} =$

$[\bar{v}_{k,0}^{(u)}, \dots, \bar{v}_{k,Q-1}^{(u)}]^T$  containing the AWGN corresponding to the  $Q$  subcarriers that are allocated to a user with index  $u$  in the B-IFDMA symbol with index  $k$ , the received values on the  $Q$  allocated subcarriers in frequency domain can be described by

$$\bar{\mathbf{y}}_k^{(u)} = \mathbf{M}_B^{(u)T} \cdot \mathbf{F}_N \cdot \mathbf{r}_k^{(u)} = \text{diag}\{\bar{\mathbf{c}}_k^{(u)}\} \cdot \bar{\mathbf{d}}_k^{(u)} + \bar{\mathbf{v}}_k^{(u)}. \quad (5.5)$$

## 5.3 Pilot Assisted Channel Estimation for Block-IFDMA

### 5.3.1 Introduction

In this Section 5.3, the pilot assisted channel estimation algorithms introduced for IFDMA in Chapter 3 are elaborated with respect to their application to B-IFDMA. In the following, the pilot insertion methods and estimation algorithms of pilot assisted channel estimation are considered which contain new aspects compared to the IFDMA case. Table 5.1 gives an overview of the aspects of pilot assisted channel estimation for B-IFDMA which exhibit new features compared to IFDMA and, thus, are considered in the following sections.

Table 5.1. Pilot assisted channel estimation for B-IFDMA in comparison to IFDMA

ESTIMATION APPROACH FOR FREQUENCY DOMAIN CHANNEL VARIATIONS	symbolwise	same principle as for IFDMA
	subcarrierwise	new pilot allocation pattern + new interpolation method
	chipwise	new possibility of pilot insertion + new estimation algorithm
ESTIMATION APPROACH FOR TIME DOMAIN CHANNEL VARIATIONS	multiple B-IFDMA symbols	same principle as for IFDMA

The application of symbolwise LS follows the same principle that has been explained for IFDMA in Section 3.2.2. Accordingly, the symbolwise LS is not explained in this section as its application to B-IFDMA is analogous to the symbolwise LS for IFDMA.

For subcarrierwise pilot insertion, B-IFDMA in contrast to IFDMA supports the application of an additional pilot symbol allocation pattern in frequency domain due to the blockwise subcarrier allocation. Furthermore, the blocks of  $K_F$  neighboring subcarriers allow interpolation at least within these blocks of subcarriers and, thus, new aspects arise in terms of the interpolation in frequency domain for subcarrierwise pilot insertion. Therefore, in Section 5.3.2, the subcarrierwise pilot insertion and the corresponding estimation algorithm is introduced for B-IFDMA. For B-IFDMA in contrast to IFDMA, the application of a third pilot insertion method is possible as a result of the blockwise allocation of subcarriers. For this third pilot insertion method,  $Q_P \cdot L_U$  chips of the pilot carrying B-IFDMA symbol are used for pilot transmission. At the receiver, the channel transfer function is estimated by solving a system of equations for a certain number of channel transfer factors. The remaining channel transfer factors are evaluated under the assumption of small channel variations in frequency domain within each block of  $K_F$  neighboring subcarriers. In the following, this pilot insertion method will be referred to as chipwise pilot insertion and is introduced in Section 5.3.3. In analogy to the explanations in Section 3.3 for IFDMA, the symbolwise, subcarrierwise and chipwise pilot insertion method are used to transmit pilot symbols within multiple pilot carrying B-IFDMA symbols. The interpolation in time domain is then performed by a Wiener interpolation. Again, the principle of interpolation in time domain is equivalent to IFDMA and, thus, it will not be considered in this section. In Section 5.3.4, the pilot assisted channel estimation algorithms are investigated in terms of their influence on the PAPR of the transmit signal, their pilot symbol overhead consumption, their MSE estimation performance and their computational complexity.

## 5.3.2 Subcarrierwise Pilot Insertion

### 5.3.2.1 Signal Generation

In this section, the B-IFDMA signal generation is presented for the subcarrierwise pilot insertion with two different pilot allocation patterns.

According to the subcarrierwise pilot insertion for IFDMA explained in Section 3.2.3, a subset of  $Q_P$  subcarriers out of the total number  $Q$  of subcarriers allocated to a certain user in the B-IFDMA symbol with index  $k = \kappa$  is utilized for pilot transmission. The remaining  $Q_D = Q - Q_P$  subcarriers are exploited by transmitting data symbols within the  $\kappa^{\text{th}}$  B-IFDMA symbol. As defined in Eq. (3.13),  $\bar{\rho}^{(u)} = [\bar{\rho}_0^{(u)}, \dots, \bar{\rho}_{Q_P-1}^{(u)}]^T$  denotes the sequence of pilot symbols in frequency domain. The sequence of data symbols in frequency domain has been defined in Eq. (3.17) and is denoted by  $\bar{\delta}_\kappa^{(u)} =$

$[\bar{d}_{\kappa,0}^{(u)}, \dots, \bar{d}_{\kappa,Q_D-1}^{(u)}]^T$ . The elements  $\bar{\rho}_{q_P}^{(u)}$ ,  $q_P = 0, \dots, Q_P - 1$ , are mapped onto a subset consisting of  $Q_P$  subcarriers out of the total number  $Q$  of subcarriers allocated to the user. The elements  $\bar{d}_{\kappa,q_D}^{(u)}$ ,  $q_D = 0, \dots, Q_D - 1$ , are transmitted on the remaining  $Q_D$  non-pilot carrying subcarriers. In the following, the pilot and non-pilot carrying subcarriers are defined for two different pilot allocation patterns.

**Equidistant allocation** For the equidistant pilot allocation pattern, the pilot carrying subcarriers are equidistantly distributed within each block of  $K_F$  subcarriers and every  $I^{\text{th}}$  subcarrier is used for pilot transmission. Thus, the number  $Q_P$  of subcarriers that are used for pilot transmission is calculated by  $Q_P = \frac{Q}{I}$ , where  $I$  is chosen such that  $Q_P \in \mathbb{Z}$ . The elements  $\bar{\rho}_{q_P}^{(u)}$ ,  $q_P = 0, \dots, Q_P - 1$ , are transmitted on the pilot carrying subcarriers with indices

$$\eta(q_P) = \left\lfloor \frac{q_P \cdot I}{K_F} \right\rfloor \cdot K_F \cdot \left( \frac{N}{Q} - 1 \right) + q_P \cdot I + u \cdot K_F. \quad (5.6)$$

The elements  $\bar{d}_{\kappa,q_D}^{(u)}$ ,  $q_D = 0, \dots, Q_D - 1$ , are transmitted on the non-pilot carrying subcarriers with indices

$$\zeta(q_D) = \left\lfloor \frac{q_D \cdot I}{(I-1) \cdot K_F} \right\rfloor \cdot K_F \cdot \left( \frac{N}{Q} - 1 \right) + q_D + \left\lfloor \frac{q_D}{I-1} \right\rfloor + u \cdot K_F + 1. \quad (5.7)$$

In Figure 5.2 (a), the equidistant pilot allocation pattern is sketched for  $I = 2$ .

**Marginal allocation** For the marginal pilot allocation pattern, the two subcarriers at the margin of each block of  $K_F$  subcarriers are used for pilot transmission. Thus, the number  $Q_P$  of subcarriers that are used for pilot transmission is calculated by

$$Q_P = \frac{2 \cdot Q}{K_F}. \quad (5.8)$$

With mod denoting the modulo operator, the elements  $\bar{\rho}_{q_P}^{(u)}$ ,  $q_P = 0, \dots, Q_P - 1$ , are transmitted on the pilot carrying subcarriers with indices

$$\eta(q_P) = \left\lfloor \frac{q_P}{2} \right\rfloor \cdot \frac{K_F \cdot N}{Q} + (q_P \bmod 2) \cdot (K_F - 1) + u \cdot K_F. \quad (5.9)$$

The elements  $\bar{d}_{\kappa,q_D}^{(u)}$ ,  $q_D = 0, \dots, Q_D - 1$ , are transmitted on the non-pilot carrying subcarriers with indices

$$\zeta(q_D) = \left\lfloor \frac{q_D}{K_F - 2} \right\rfloor \cdot \frac{K_F \cdot N}{Q} + (q_D \bmod (K_F - 2)) + 1 + u \cdot K_F. \quad (5.10)$$

The marginal pilot allocation is sketched in Figure 5.2 (b).

The allocation of the elements  $\bar{\rho}_{q_P}^{(u)}$ ,  $q_P = 0, \dots, Q_P - 1$ , to the pilot carrying subcarriers is performed by the application of the pilot mapping matrix  $\mathbf{M}_{BP}^{(u)}$  whose elements  $[\mathbf{M}_{BP}^{(u)}]_{n,q_P}$  for  $n = 0, \dots, N - 1$  and  $q_P = 0, \dots, Q_P - 1$  are given by

$$[\mathbf{M}_{BP}^{(u)}]_{n,q_P} = \begin{cases} 1 & \text{for } n = \eta(q_P), \\ 0 & \text{else.} \end{cases} \quad (5.11)$$

The allocation of the elements  $\bar{d}_{\kappa,q_D}^{(u)}$ ,  $q_D = 0, \dots, Q_D - 1$ , to the non-pilot carrying subcarriers is realized by a data mapping matrix  $\mathbf{M}_{BD}^{(u)}$ . The elements  $[\mathbf{M}_{BD}^{(u)}]_{n,q_D}$  for  $n = 0, \dots, N - 1$  and  $q_D = 0, \dots, Q_D - 1$  of the data mapping matrix  $\mathbf{M}_{BD}^{(u)}$  are given by

$$[\mathbf{M}_{BD}^{(u)}]_{n,q_D} = \begin{cases} 1 & \text{for } n = \zeta(q_D), \\ 0 & \text{else.} \end{cases} \quad (5.12)$$

The superposition of the mapped pilot and mapped data symbols is multiplied by an  $N \times N$  IDFT matrix  $\mathbf{F}_N^H$  and the B-IFDMA symbol  $\mathbf{x}_\kappa^{(u)}$  containing pilot and data symbols is given by

$$\mathbf{x}_\kappa^{(u)} = \mathbf{F}_N^H \cdot \left( \mathbf{M}_{BP}^{(u)} \cdot \mathbf{F}_{Q_P} \cdot \boldsymbol{\rho}^{(u)} + \mathbf{M}_{BD}^{(u)} \cdot \mathbf{F}_{Q_D} \cdot \boldsymbol{\delta}_\kappa^{(u)} \right). \quad (5.13)$$

Finally,  $\mathbf{x}_\kappa^{(u)}$  is expanded by a cyclic prefix with  $N_G$  elements and the resulting B-IFDMA symbol  $\tilde{\mathbf{x}}_\kappa^{(u)}$  with cyclic prefix is transmitted over the mobile radio channel.

### 5.3.2.2 Estimation Algorithm

In this section, the channel estimation algorithm is explained for the subcarrierwise pilot insertion method.

At the receiver, the cyclic prefix is discarded and the received B-IFDMA symbol  $\mathbf{r}_\kappa^{(u)}$  is analyzed at the pilot carrying subcarriers. Therefore,  $\mathbf{r}_\kappa^{(u)}$  is transformed into frequency domain by multiplication with the  $N \times N$  DFT matrix  $\mathbf{F}_N$  and multiplied by the transpose  $\mathbf{M}_{BP}^{(u)T}$  of the pilot mapping matrix. Then, according to Eq. (3.25), an estimate of the channel transfer factors of the pilot carrying subcarriers with indices  $\eta(q_P)$ ,  $q_P = 0, \dots, Q_P - 1$ , in the B-IFDMA symbol with index  $\kappa$  is determined by a LS estimation and given by

$$\left[ \hat{c}_{\kappa,0}^{(u)}, \dots, \hat{c}_{\kappa,Q_P-1}^{(u)} \right]^T = \text{diag} \{ \bar{\mathbf{p}}^{(u)} \}^{-1} \cdot \mathbf{M}_{BP}^{(u)T} \cdot \mathbf{F}_N \cdot \mathbf{r}_\kappa^{(u)} \quad (5.14)$$

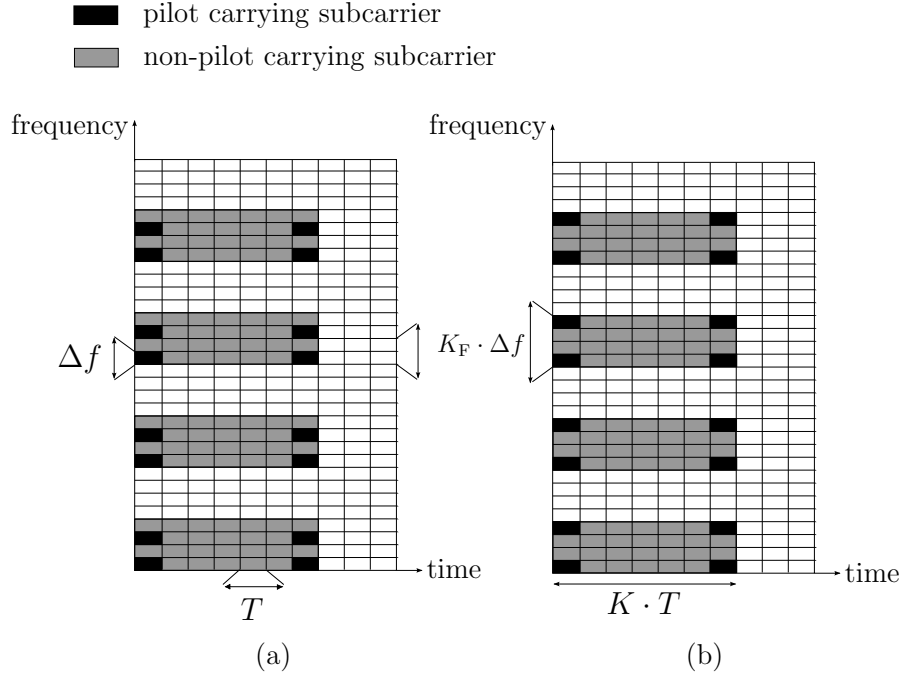


Figure 5.2. Pilot and non-pilot carrying subcarriers for (a) equidistant pilot allocation and (b) marginal pilot allocation in case of two pilot carrying B-IFDMA symbols.

[Kay93]. According to [Kay93], Eq. (5.14) represents the MVU estimate of the vector  $[\bar{c}_{\kappa,0}^{(u)}, \dots, \bar{c}_{\kappa,Q_P-1}^{(u)}]^T$ . The LS estimates  $\hat{\bar{c}}_{\kappa,q_P}^{(u)}$ ,  $q_P = 0, \dots, Q_P - 1$ , are exploited to get estimates  $\hat{\bar{c}}_{\kappa,q_D}^{(u)}$ ,  $q_D = 0, \dots, Q_D - 1$  of the channel transfer factors of the remaining, non-pilot carrying subcarriers with indices  $\zeta(q_D)$ . For this purpose, three different interpolation methods are proposed that are explained in the following.

**Wiener interpolation** The application of Wiener interpolation filtering in frequency domain to B-IFDMA follows the same principle as the application to IFDMA. Therefore, Section 3.2.3 can serve as a reference. For each non-pilot carrying subcarrier with index  $\zeta(q_d)$ ,  $q_d = 0, \dots, Q_D - 1$ , the channel transfer factor is calculated by the Wiener interpolation. Finally, the LS estimates of the pilot carrying subcarriers and the Wiener filter estimates of the non-pilot carrying subcarriers are combined in the vector  $\hat{\bar{\mathbf{c}}}_{\kappa}^{(u)}$ .

**DFT interpolation** The DFT interpolation is applied for the case that the number  $Q_P$  of pilot carrying subcarriers is larger than or equal to the number  $L_C$  of channel delay taps. Then, the DFT interpolation can be applied according to Section 3.2.3 where it is explained for IFDMA.



**Repetition** For the case that the distance between neighboring blocks of subcarriers is larger than the coherence bandwidth of the channel and that there is only one pilot carrying subcarrier per block of  $K_F$  subcarriers, i.e.,  $Q_P = \frac{Q}{K_F}$ , the application of an interpolation filter is not feasible. Then, the LS-estimate of the nearest pilot carrying subcarrier is used for equalization of the non-pilot carrying subcarriers within the same block of  $K_F$  subcarriers. Thus, the vector  $\hat{\mathbf{c}}_\kappa^{(u)}$  containing the channel estimates for each allocated subcarrier within the B-IFDMA symbol with index  $\kappa$  is given by

$$\hat{\mathbf{c}}_\kappa^{(u)} = \underbrace{[\hat{c}_{\kappa,0}^{(u)}, \hat{c}_{\kappa,0}^{(u)}, \dots, \dots]}_{K_F\text{-times}} \underbrace{[\hat{c}_{\kappa,Q_P-1}^{(u)}, \hat{c}_{\kappa,Q_P-1}^{(u)}, \dots]}_{K_F\text{-times}}^T. \quad (5.15)$$

In the following, subcarrierwise pilot insertion with repetition is shortly denoted as subcarrierwise repetition.

### 5.3.3 Chipwise Pilot Insertion

#### 5.3.3.1 Signal Generation

In this section, the signal generation is presented for chipwise pilot insertion.

For chipwise pilot insertion, a subset of  $Q_P \cdot L_U$  chips out of the total number  $Q \cdot L_U$  of chips in the B-IFDMA symbol with index  $k = \kappa$  is utilized for pilot transmission. The remaining  $Q_D \cdot L_U = (Q - Q_P) \cdot L_U$  chips are used for the transmission of data symbols within the  $\kappa^{\text{th}}$  B-IFDMA symbol. That means, pilot and data symbols are multiplexed within the B-IFDMA symbol with index  $k = \kappa$ .

For  $k = \kappa$ , the  $Q \times 1$  vector  $\boldsymbol{\rho}^{(u)} = [0, \dots, 0, \rho_0^{(u)}, \dots, \rho_{Q_P-1}^{(u)}]^T$  of  $Q_P$  pilot symbols with  $E\{|\rho_q^{(u)}|^2\} = \sigma_P^2$  and the  $Q \times 1$  vector  $\boldsymbol{\delta}_\kappa^{(u)} = [d_{\kappa,0}^{(u)}, \dots, d_{\kappa,Q_D-1}^{(u)}, 0, \dots, 0]^T$  of data symbols with  $E\{|d_{\kappa,q}^{(u)}|^2\} = \sigma_D^2$  are processed in parallel. The superposition  $\boldsymbol{\rho}^{(u)} + \boldsymbol{\delta}_\kappa^{(u)}$  of both vectors is multiplied by the  $Q \times Q$  DFT matrix  $\mathbf{F}_Q$ . The elements of the resulting vector are mapped onto the  $Q$  block-interleaved subcarriers in frequency domain and transformed in time domain via the  $N \times N$  IDFT matrix  $\mathbf{F}_N^H$ . Thus, the sequence  $\mathbf{x}_\kappa^{(u)}$  containing multiplexed pilot and data symbols is calculated by

$$\mathbf{x}_\kappa^{(u)} = \mathbf{F}_N^H \cdot \mathbf{M}_B^{(u)} \cdot \mathbf{F}_Q \cdot (\boldsymbol{\rho}^{(u)} + \boldsymbol{\delta}_\kappa^{(u)}). \quad (5.16)$$

That means, on each allocated subcarrier, a superposition of pilot and data symbols in frequency domain is transmitted. Due to the chipwise pilot insertion, pilot and data symbols are not orthogonal in frequency domain.

Finally,  $\mathbf{x}_\kappa^{(u)}$  is expanded by a cyclic prefix with  $N_G$  elements and the resulting B-IFDMA symbol  $\tilde{\mathbf{x}}_\kappa^{(u)}$  with cyclic prefix is transmitted over the mobile radio channel.

### 5.3.3.2 Estimation Algorithm

In this section, the channel estimation algorithm is explained for the chipwise pilot insertion method.

For that purpose, the received symbol  $\mathbf{r}_\kappa^{(u)}$  with index  $\kappa$  is considered after removal of the cyclic prefix.  $\mathbf{r}_\kappa^{(u)}$  is transformed into frequency domain by multiplication with the  $N \times N$  DFT matrix  $\mathbf{F}_N$  and multiplied by the transpose  $\mathbf{M}_B^{(u)T}$  of the mapping matrix which leads to the vector  $\bar{\mathbf{y}}_\kappa^{(u)}$  in frequency domain that is given by

$$\begin{aligned}\bar{\mathbf{y}}_\kappa^{(u)} &= \mathbf{M}_B^{(u)T} \cdot \mathbf{F}_N \cdot \mathbf{r}_\kappa^{(u)} \\ &= \text{diag}\{\bar{\mathbf{c}}_\kappa^{(u)}\} \cdot \mathbf{F}_Q \cdot \left(\boldsymbol{\rho}^{(u)} + \boldsymbol{\delta}_\kappa^{(u)}\right) + \bar{\mathbf{v}}_\kappa^{(u)}.\end{aligned}\quad (5.17)$$

In the following, let  $[\mathbf{z}]_e$  denote a vector containing the elements with even indices of a vector  $\mathbf{z}$ , i.e.,  $[\mathbf{z}]_e = [[\mathbf{z}]_0, [\mathbf{z}]_2, \dots, [\mathbf{z}]_{\text{end}-2}]^T$  and let  $[\mathbf{z}]_o$  denote a vector containing the elements with odd indices of a vector  $\mathbf{z}$ , i.e.,  $[\mathbf{z}]_o = [[\mathbf{z}]_1, [\mathbf{z}]_3, \dots, [\mathbf{z}]_{\text{end}-1}]^T$ . Further, let  $[\mathbf{F}_Q]_{e,1:Q}$  address the rows with even indices and the  $Q$  columns,  $[\mathbf{F}_Q]_{e,Q_D+1:Q}$  the rows with even indices and the last  $Q_P$  columns and  $[\mathbf{F}_Q]_{e,1:Q_D}$  the rows with even indices and the first  $Q_D$  columns of the  $Q \times Q$  DFT matrix  $\mathbf{F}_Q$ .

Then, the vector  $\bar{\mathbf{y}}_\kappa^{(u)}$  can be separated into a vector  $[\bar{\mathbf{y}}_\kappa^{(u)}]_e$  containing the elements corresponding to the subcarriers with even indices according to

$$\begin{aligned}[\bar{\mathbf{y}}_\kappa^{(u)}]_e &= \text{diag}\left\{[\bar{\mathbf{c}}_\kappa^{(u)}]_e\right\} \cdot [\mathbf{F}_Q]_{e,1:Q} \cdot \left(\boldsymbol{\rho}^{(u)} + \boldsymbol{\delta}_\kappa^{(u)}\right) + [\bar{\mathbf{v}}_\kappa^{(u)}]_e \\ &= \text{diag}\left\{[\bar{\mathbf{c}}_\kappa^{(u)}]_e\right\} \cdot \left([\mathbf{F}_Q]_{e,Q_D+1:Q} \cdot [\rho_0^{(u)}, \dots, \rho_{Q_P-1}^{(u)}]^T\right. \\ &\quad \left.+ [\mathbf{F}_Q]_{e,1:Q_D} \cdot [d_{\kappa,0}^{(u)}, \dots, d_{\kappa,Q_D-1}^{(u)}]^T\right) + [\bar{\mathbf{v}}_\kappa^{(u)}]_e\end{aligned}\quad (5.18)$$

and into a vector  $[\bar{\mathbf{y}}_\kappa^{(u)}]_o$  containing the elements corresponding to the subcarriers with odd indices according to

$$\begin{aligned}[\bar{\mathbf{y}}_\kappa^{(u)}]_o &= \text{diag}\left\{[\bar{\mathbf{c}}_\kappa^{(u)}]_o\right\} \cdot [\mathbf{F}_Q]_{o,1:Q} \cdot \left(\boldsymbol{\rho}^{(u)} + \boldsymbol{\delta}_\kappa^{(u)}\right) + [\bar{\mathbf{v}}_\kappa^{(u)}]_o \\ &= \text{diag}\left\{[\bar{\mathbf{c}}_\kappa^{(u)}]_o\right\} \cdot \left([\mathbf{F}_Q]_{o,Q_D+1:Q} \cdot [\rho_0^{(u)}, \dots, \rho_{Q_P-1}^{(u)}]^T\right. \\ &\quad \left.+ [\mathbf{F}_Q]_{o,1:Q_D} \cdot [d_{\kappa,0}^{(u)}, \dots, d_{\kappa,Q_D-1}^{(u)}]^T\right) + [\bar{\mathbf{v}}_\kappa^{(u)}]_o.\end{aligned}\quad (5.19)$$

It can be seen that both vectors are dependent on the same unknown data vector  $[d_{\kappa,0}^{(u)}, \dots, d_{\kappa,Q_D-1}^{(u)}]^T$  and the matrices  $\text{diag}\{[\bar{\mathbf{c}}_{\kappa}^{(u)}]_e\}$  and  $\text{diag}\{[\bar{\mathbf{c}}_{\kappa}^{(u)}]_o\}$  containing the unknown channel transfer factors. For the case that at least  $K_F = 2$  subcarriers per block are available and under the assumption that there is only slight variation between channel transfer factors corresponding to neighboring subcarriers, the vector  $[\bar{\mathbf{c}}_{\kappa}^{(u)}]_e$  corresponding to the subcarriers with even indices is approximately equal to the vector  $[\bar{\mathbf{c}}_{\kappa}^{(u)}]_o$  corresponding to the subcarriers with odd indices, i.e.,  $[\bar{\mathbf{c}}_{\kappa}^{(u)}]_e \approx [\bar{\mathbf{c}}_{\kappa}^{(u)}]_o$ . An estimate  $[\hat{\bar{\mathbf{c}}}_{\kappa}^{(u)}]_e$  can be found by solving Eq. (5.18) and (5.19) for  $\text{diag}\{[\bar{\mathbf{c}}_{\kappa}^{(u)}]_e\}$ . Thus, Eq. (5.18) and (5.19) can be combined in one equation where the data vector  $[d_{\kappa,0}^{(u)}, \dots, d_{\kappa,Q_D-1}^{(u)}]^T$  is eliminated.

Under the assumption of negligible AWGN, the solution of Eq. (5.18) and (5.19) for  $\text{diag}\{[\bar{\mathbf{c}}_{\kappa}^{(u)}]_e\} \approx \text{diag}\{[\bar{\mathbf{c}}_{\kappa}^{(u)}]_o\}$  yields

$$\begin{aligned} \text{diag}\left\{[\bar{\mathbf{c}}_{\kappa}^{(u)}]_e\right\} &= \text{diag}\left\{\left(\left([\mathbf{F}_Q]_{e,1:Q_D}\right)^H \cdot \text{diag}\left\{[\bar{\mathbf{y}}_{\kappa}^{(u)}]_e\right\}\right.\right. \\ &\quad \left.\left.- \left([\mathbf{F}_Q]_{o,1:Q_D}\right)^H \cdot \text{diag}\left\{[\bar{\mathbf{y}}_{\kappa}^{(u)}]_o\right\}\right)^{-1} \cdot \begin{bmatrix} \rho_0^{(u)} \\ \vdots \\ \rho_{Q_P-1}^{(u)} \end{bmatrix}\right\}^{-1}. \end{aligned} \quad (5.20)$$

A detailed derivation of Eq. (5.20) is presented in Appendix A.5. In the following, the chipwise pilot insertion with the solution of the system of equations is shortly denoted as chipwise SoE.

### 5.3.4 Performance and Complexity Analysis

#### 5.3.4.1 Analysis Assumptions

In this Section 5.3.4, the pilot insertion methods and the corresponding channel estimation approaches presented in Section 5.3 are analyzed in terms of their influence on the PAPR of the transmit signal, their pilot symbol overhead consumption, their MSE performance and their computational complexity. The results are obtained by computer simulations and are valid for the simulation parameters that have been introduced in Section 3.4.1 and summarized in Table 3.1.

#### 5.3.4.2 Peak-to-Average Power Ratio

In this section, the subcarrierwise and chipwise pilot insertion are investigated in terms of their respective influence on the PAPR of the pilot carrying B-IFDMA symbols. The

PAPR in case of symbolwise pilot insertion serves as a reference because it exhibits the PAPR of the B-IFDMA symbol without pilot insertion. In accordance with Section 3.4.2, the investigations are carried out based on the definition of the PAPR that is given by Eq. (3.44) and on the simulation results obtained from 1000 Monte-Carlo runs. In the following, the CDF of the PAPR per pilot carrying B-IFDMA symbol is presented. It is assumed that interpolation between the blocks consisting of  $K_F = 8$  subcarriers is not feasible and, thus, for subcarrierwise pilot insertion with equidistant pilot allocation, the interpolation depths to be investigated have to fulfill  $I \leq K_F$ . For subcarrierwise pilot insertion with marginal pilot allocation, one subcarrier at the two margins of the block consisting of  $K_F$  subcarriers is used for pilot transmission.

In Figure 5.3, the CDF of the PAPR in dB is presented for the case of symbolwise, subcarrierwise and chipwise pilot insertion for  $Q = 512$  allocated subcarriers per user and  $K_F = 8$  subcarriers per block. Figure 5.3 shows that symbolwise and chipwise pilot insertion exhibit the same PAPR which is the lowest as it equals the PAPR of the B-IFDMA itself without pilot transmission. For subcarrierwise pilot insertion with equidistant pilot allocation, the PAPR is the lowest for  $I = 8$ . For  $I = 8$ , there is one pilot carrying subcarrier per block of  $K_F$  subcarriers. For an increasing number of pilot carrying subcarriers per block, i.e., for a decreasing interpolation depth  $I$ , the PAPR of the transmit signal increases. The increasing PAPR can be explained by the fact that for a small interpolation depth  $I$ , the pilot allocation in frequency domain differs noticeably from an equidistant distribution in frequency domain. For  $I = 8$ , one pilot carrying subcarrier per block is utilized and, thus, the  $Q_P$  pilot carrying subcarriers are equidistantly distributed over the total bandwidth. For  $I = 4$ , two pilot carrying subcarriers per block are utilized and, thus, the  $Q_P$  pilot carrying subcarriers lose their equidistant allocation over the total bandwidth. In Section 3.4.2 it has been shown that a signal with an equidistant subcarrier allocation in frequency domain exhibits a low PAPR in time domain. As the subcarrierwise pilot allocation comprises a superposition of the modulated data and pilot sequence, the PAPR of the B-IFDMA transmit signal is less degraded if the superposed pilot sequence exhibits an equidistant allocation of subcarriers in frequency domain. For subcarrierwise pilot insertion with marginal pilot allocation, two pilot carrying subcarriers are utilized per block and the PAPR is comparable to the PAPR for equidistant pilot allocation with  $I = 4$ .

In Figure 5.4, the CDF of the PAPR in dB is shown for the case of symbolwise, subcarrierwise and chipwise pilot insertion for  $Q = 512$  allocated subcarriers per user and  $K_F = 4$  and  $K_F = 2$  subcarriers per block. For  $K_F = 4$ , it can again be seen that the symbolwise and chipwise pilot insertion exhibit the lowest PAPR. For subcarrierwise pilot insertion with equidistant pilot allocation, the maximum interpolation depth  $I = 4$  provides the lowest PAPR as there is only one pilot carrying subcarrier per block.

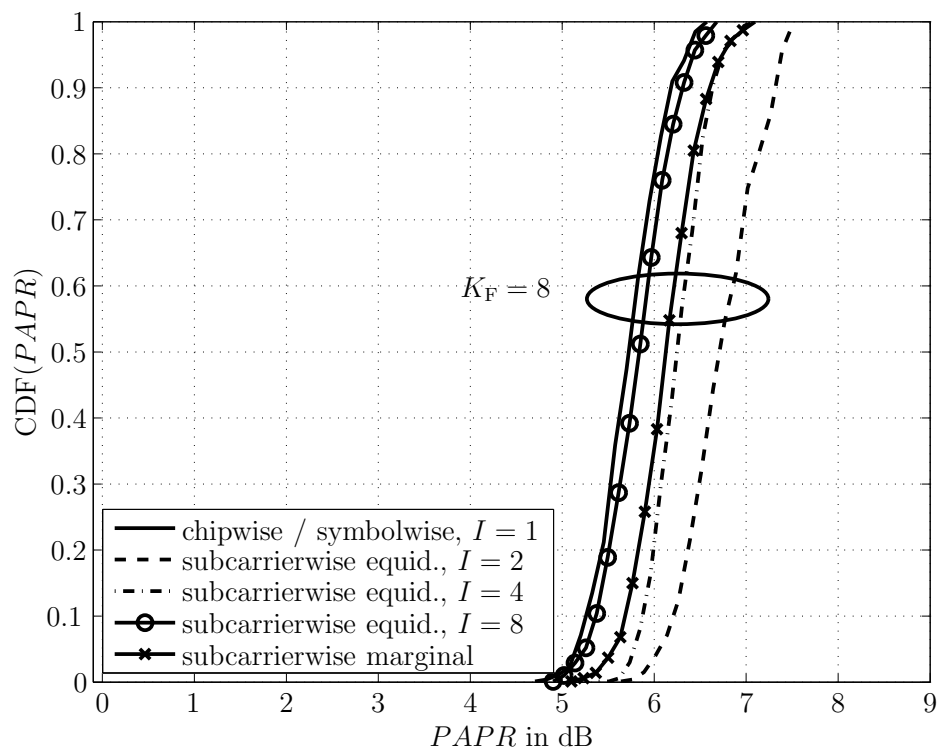


Figure 5.3. CDF of the PAPR in dB in case of chipwise and subcarrierwise pilot insertion for  $Q = 512$  with  $K_F = 8$  subcarriers per block.

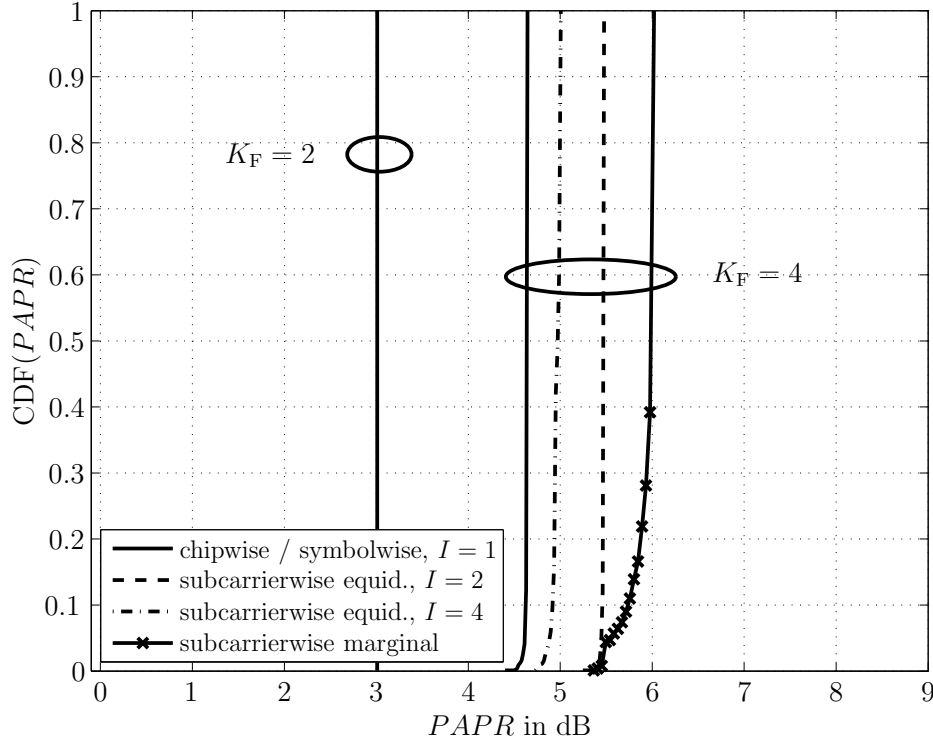


Figure 5.4. CDF of the PAPR in dB in case of chipwise and subcarrierwise pilot insertion for  $Q = 512$  with  $K_F = 4$  and  $K_F = 2$  subcarriers per block.

However, in contrast to  $K_F = 8$ , the subcarrierwise pilot insertion with marginal pilot allocation shows the most degrading PAPR as for  $K_F = 4$ , the marginal pilot allocation differs the most from an equidistant subcarrier allocation in frequency domain. For  $K_F = 2$ , only symbolwise, chipwise and subcarrierwise pilot insertion with equidistant pilot allocation for  $I = 2$  is applicable. Figure 5.4 shows that all three pilot insertion methods exhibit the same PAPR. As for subcarrierwise pilot insertion with equidistant pilot allocation for  $I = 2$ , the signal generation can be taken as two superimposed IFDMA signals and the symbolwise and chipwise pilot allocation represent the PAPR of the B-IFDMA symbol without pilot transmission, it can be stated that for  $K_F = 2$ , the PAPR of the B-IFDMA signal is equivalent to the PAPR of two superimposed IFDMA signals.

### 5.3.4.3 Pilot Symbol Overhead

In this section, the subcarrierwise and chipwise pilot insertion and their corresponding channel estimation algorithms are investigated in terms of their respective pilot symbol overhead consumption.

For subcarrierwise pilot insertion, the distance between neighboring pilot carrying subcarriers has to fulfill the sampling theorem in frequency domain. Therefore, in order to estimate the channel variations in frequency domain, at least one pilot carrying subcarrier per coherence bandwidth  $B_{\text{coh}}$  is required and the pilot distance  $D_F$  in frequency domain corresponds to the pilot distance for IFDMA that has been defined in Eq. (3.45). Accordingly, the estimation performance can be improved by choosing  $D_F$  under consideration of an oversampling factor  $O_F$  in frequency domain.

For B-IFDMA, each user is allocated to blocks of  $K_F$  adjacent subcarriers with a distance  $L_U \cdot K_F$  between neighboring blocks of subcarriers. Interpolation in-between neighboring blocks of subcarriers is feasible if

$$D_F \geq 2 \cdot K_F \cdot L_U . \quad (5.21)$$

For  $D_F < 2 \cdot K_F \cdot L_U$ , every allocated block of subcarriers has to be used for pilot transmission. For this case, interpolation is only possible within each block of  $K_F$  subcarriers and, thus, the pilot distance  $D_F$  is equivalent to the pilot distance within each of these blocks of subcarriers. The interpolation depth  $I$  is chosen under consideration of the pilot distance within each block of  $K_F$  subcarriers and is calculated according to

$$I = \lfloor D_F \rfloor . \quad (5.22)$$

With the aforementioned considerations and for  $D_F \geq 2 \cdot K_F \cdot L_U$ , i.e., the case where interpolation in-between the blocks is feasible, the number  $Q_P$  of pilot carrying subcarriers is given by

$$Q_P = \left\lceil \frac{Q}{K_F} \cdot \left( \left\lfloor \frac{D_F}{K_F \cdot L_U} \right\rfloor \right)^{-1} \right\rceil . \quad (5.23)$$

For  $D_F < 2 \cdot K_F \cdot L_U$ , i.e., the case where interpolation in-between the blocks is not feasible, the number  $Q_P$  of pilot carrying subcarriers is given by

$$Q_P = \left\lceil \frac{K_F}{D_F} \right\rceil \cdot \frac{Q}{K_F} . \quad (5.24)$$

For chipwise pilot insertion,  $Q_P \cdot L_U$  chips with  $Q_P = Q/2$  are used for pilot transmission. The estimation algorithm for chipwise pilot insertion is operating with an equal number of pilot and data symbols per pilot carrying B-IFDMA symbol because it is assumed that interpolation between two neighboring subcarriers in frequency domain is practically feasible. Therefore, the number  $Q_P$  of pilot symbols per pilot carrying B-IFDMA symbol is independent of the channel characteristic and, thus, independent of  $D_F$ .

The number  $P$  of pilot carrying B-IFDMA symbols for the estimation of the channel variations in time domain by Wiener interpolation is calculated according to the IFDMA case as explained in Section 3.4.3.

With Eq. (3.52), the pilot symbol overhead  $\Lambda$  can be calculated for B-IFDMA while applying the introduced pilot insertion methods and their respective estimation algorithms. For B-IFDMA, the pilot symbol overhead is independent on the number  $Q$  of allocated subcarriers per user but depends on the number  $K_F$  of subcarriers per block.

In Figure 5.5, the overhead  $\Lambda$  is depicted as a function of the number  $K_F$  of subcarriers per block for the case of symbolwise pilot insertion serving as a reference curve, subcarrierwise pilot insertion with the oversampling factor  $O_F$  in frequency domain as parameter and chipwise pilot insertion. It is assumed that interpolation in-between blocks of subcarriers is not possible. As for this case, the pilot symbol overhead is independent on the number  $Q$  of allocated subcarriers, the results are identical for each value of  $Q < 2 \cdot O_F \cdot L_C \cdot K_F$ . Further on, the results are valid for  $K = 30$  successively transmitted B-IFDMA symbols and a velocity of  $v = 50$  km/h which corresponds to the case where  $K < D_T$ . Therefore,  $P = 2$  pilot carrying IFDMA symbols are utilized for channel estimation which complies with the application of an oversampling factor of  $O_T \approx 3$  in time domain.

In Figure 5.5(a), the pilot symbol overhead is calculated for a channel with  $L_C = 128$  delay taps and, thus, a coherence bandwidth of  $B_{\text{coh}} = 8 \cdot \Delta f$ . The number  $K_F$  of subcarriers per block is increased from 1 to 16. For  $K_F = 1$ , the B-IFDMA scheme is equivalent to IFDMA and the pilot symbol overhead is equivalent to the pilot symbol overhead for IFDMA. The results in Figure 5.5(a) show that for subcarrierwise pilot insertion with  $O_F = 4$  and for  $K_F > 1$  subcarriers per block, the pilot symbol overhead is reduced by a factor 2 compared to the symbolwise pilot insertion. For  $O_F = 4$ , every second subcarrier within each block is used for pilot transmission. Therefore, the pilot symbol overhead of chipwise pilot insertion is equivalent to subcarrierwise pilot insertion with  $O_F = 4$  as  $Q_P = Q/2$  pilot symbols are transmitted per pilot carrying B-IFDMA symbol in this case. For subcarrierwise pilot insertion with  $O_F = 2$ , every 4<sup>th</sup> subcarrier is used for pilot transmission and, thus, the pilot symbol overhead decreases for  $K_F \geq 4$ . Accordingly, for subcarrierwise pilot insertion with  $O_F = 1$ , every 8<sup>th</sup> subcarrier is used for pilot transmission and, thus, the pilot symbol overhead decreases for  $K_F \geq 8$ . In Figure 5.5(b), the pilot symbol overhead is calculated for a channel with  $L_C = 8$  delay taps and, thus, a coherence bandwidth of  $B_{\text{coh}} = 128 \cdot \Delta f$ . Again, the number  $K_F$  of subcarriers per block is increased from 1 to 16. The results in Figure 5.5(b) show that for this small channel delay spread, the pilot symbol overhead can be reduced by increasing the number  $K_F$  of subcarriers per block in frequency



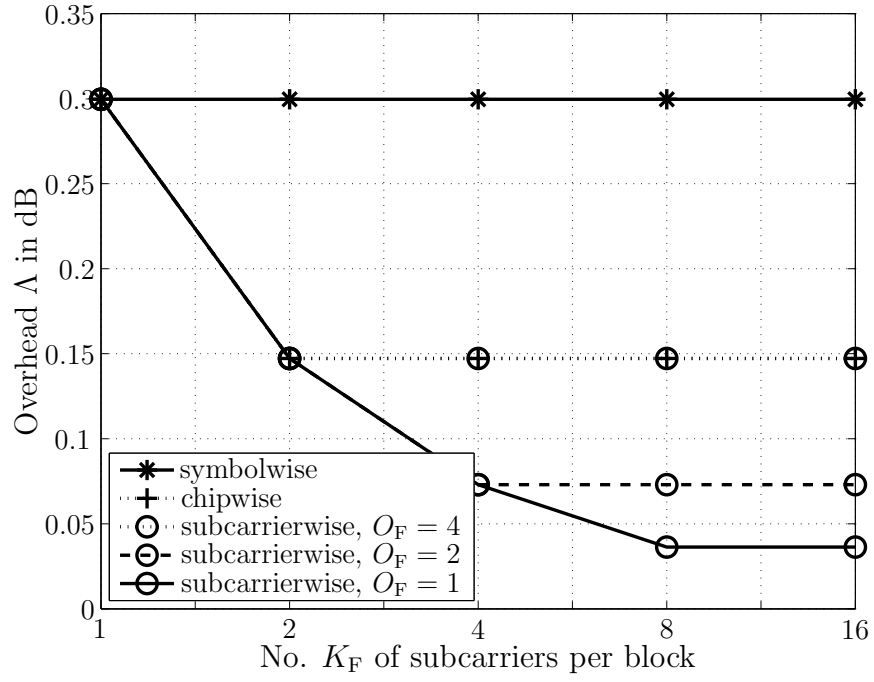
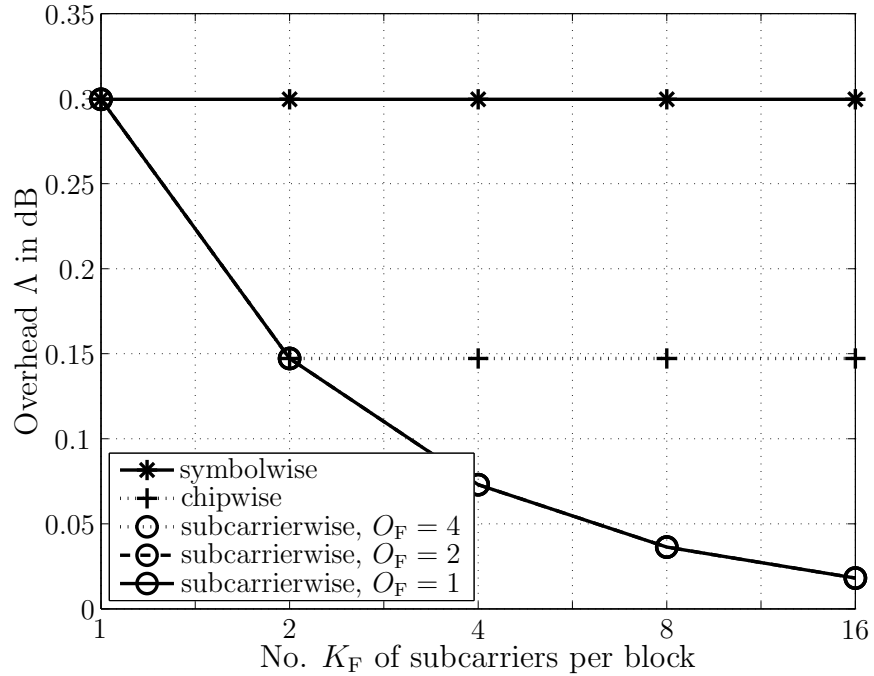
(a)  $L_C = 128$ (b)  $L_C = 8$ 

Figure 5.5. Overhead  $\Lambda$  as a function of the number  $K_F$  of subcarriers per block with the oversampling factor  $O_F = 1, 2, 4$  as parameter and a velocity of  $v = 50$  km/h.

domain. Due to the assumption that interpolation between neighboring blocks in frequency domain is not feasible, one pilot carrying subcarrier is utilized per block of  $K_F$  subcarriers and, thus, the pilot symbol overhead increases with increasing number of blocks, i.e., decreasing  $K_F$  for a fixed number  $Q$  of allocated subcarriers.

#### 5.3.4.4 Mean Square Error

In this section, the performances of the estimation algorithms introduced in Section 5.3 are investigated in terms of their MSE performance. In accordance to the preceding chapters, the MSE is again defined by Eq. (3.54).

In Figures 5.6-5.7, the MSE is presented in dependency of the SNR which is given as a logarithmic value of the ratio between the energy  $E_B$  that is spent per useful data bit and the noise power  $N_0$ . The calculation of the SNR takes into account the SNR degradation due the overhead that is caused by channel coding, cyclic prefix insertion and pilot symbol insertion according to Section 5.3.4.3. The presented curves are obtained from Monte-Carlo simulations whose results are averaged over 1000 simulation runs and are valid for the WINNER SCM urban macro-cell channel which exhibits a coherence bandwidth  $B_{\text{coh}} \leq 8 \cdot \Delta f$ , cf. Section 3.4.1. For the MSE performance analysis, the following parameters are utilized:

- For subcarrierwise pilot insertion, an interpolation depth  $I = 2$  is applied. Thus, there are  $Q_P = Q/2$  pilot carrying subcarriers and every second allocated subcarrier is utilized for pilot transmission.
- The time domain channel variations are estimated by two pilot carrying B-IFDMA or IFDMA symbols with indices  $k = 0$  and  $k = 29$  and Wiener interpolation with  $V = 2$  filter coefficients.
- Results are shown for velocities of  $v = 28 \text{ km/h}$  and  $v = 84 \text{ km/h}$  of the mobile station. As the channel is estimated for a single TDMA slot consisting of  $K = 30$  B-IFDMA or IFDMA symbols, the considered velocities are equivalent to oversampling factors  $O_T = 6$  and  $O_T = 2$  in time domain.
- In the following, results for symbolwise LS are shown as reference curves.

In the following, the performance of DFT interpolation in frequency domain which is applied to B-IFDMA is investigated and compared to the application of DFT interpolation in frequency domain to IFDMA. As DFT interpolation is only feasible if the

number  $Q_P$  of pilot carrying subcarriers is larger than or equal to the number  $L_C$  of channel delay taps, the number  $Q$  of allocated subcarriers is chosen as  $Q = 512$ . For B-IFDMA, the number of subcarriers per block is  $K_F = 2$ . In Figure 5.6, the frequency domain channel variations are estimated for B-IFDMA and IFDMA by subcarrierwise pilot insertion with DFT interpolation.

Figure 5.6 shows that the application of DFT interpolation in frequency domain to B-IFDMA leads to a clearly worse performance than its application to IFDMA. For  $O_T = 2$ , the result for B-IFDMA exhibits an error floor for  $E_B/N_0 > 15$  dB whereas the result for IFDMA shows good performance and differs only slightly from the result of symbolwise pilot insertion for  $E_B/N_0 \leq 25$  dB. For  $O_T = 6$ , the performance difference between DFT interpolation for B-IFDMA and IFDMA is smaller than for  $O_T = 2$ , but shows still a significant degradation for B-IFDMA. For IFDMA, the performance of DFT interpolation is comparable to the performance of symbolwise LS. The performance difference of the DFT interpolation for B-IFDMA and IFDMA can be explained by the difference in the subcarrier allocation in frequency domain. For IFDMA, the non-pilot carrying subcarriers exhibit a distance of  $L_U \cdot \Delta f$  to the nearest neighboring pilot carrying subcarrier. For B-IFDMA, the distance between a non-pilot carrying subcarrier and its nearest neighboring pilot carrying subcarrier is  $\Delta f$ . The DFT interpolation calculates the channel impulse response with the help of the channel transfer factors corresponding to the pilot carrying subcarriers and utilizes this intermediate calculation to determine the channel transfer factors corresponding to the non-pilot carrying subcarriers. This estimation procedure entails a limited resolution of the estimate in frequency domain and, thus, the channel transfer factors corresponding to the non-pilot carrying subcarriers which exhibit a larger distance to the pilot carrying subcarriers are estimated with a higher accuracy.

It has been shown that the application of DFT interpolation in frequency domain to B-IFDMA is feasible if  $Q_P \geq L_C$ . However, the DFT interpolation provides only poor performance while applied to B-IFDMA. Nevertheless, for B-IFDMA, interpolation in frequency domain is possible if  $Q_P < L_C$  due to the  $K_F$  neighboring subcarriers in frequency domain. In the following, different pilot insertion methods and their corresponding estimation algorithms which have been introduced in Section 5.3.2 and Section 5.3.3 for the estimation of frequency domain channel variations are investigated and compared for the case of a small number  $Q$  of allocated subcarriers and for the case  $Q_P < L_C$ .

In Figure 5.7(a), results are shown for B-IFDMA with  $Q = 8$  allocated subcarriers and  $K_F = 2$  subcarriers per block in frequency domain. The channel variations in frequency domain are estimated by chipwise SoE, subcarrierwise repetition and symbolwise LS.

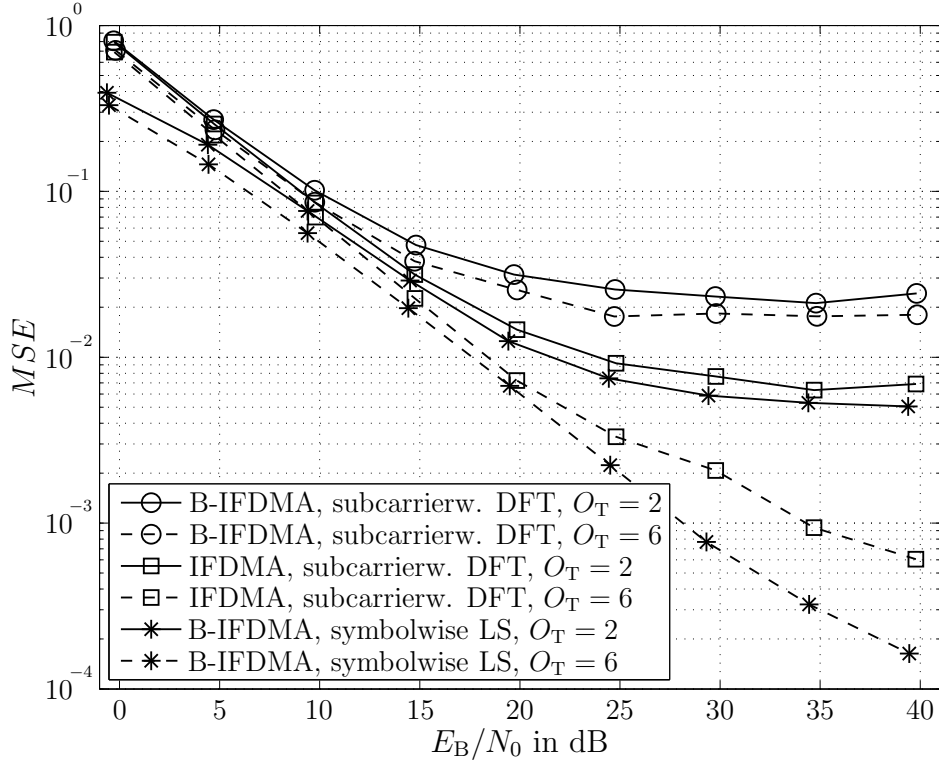


Figure 5.6. MSE as a function of  $E_B/N_0$  in dB with the oversampling factor  $O_T$  in time domain as parameter for subcarrierwise DFT for B-IFDMA and IFDMA and for symbolwise LS for B-IFDMA with  $Q = 512$  allocated subcarriers.

For subcarrierwise pilot insertion with  $I = 2$ , Wiener interpolation is not feasible as  $K_F = 2$  and the distance between neighboring blocks is larger than the coherence bandwidth of the WINNER SCM urban macro-cell channel.

It can be seen that the performance of chipwise SoE is poor, especially for low to moderate SNR values. The reason for that can be found in the double inversion in Eq. (5.20). If the matrices that shall be inverted are ill-conditioned, the solution of the system of equations loses precision. The MSE for subcarrierwise repetition exhibits an error floor for  $E_B/N_0 > 20$  dB due to the occurrence of interpolation errors in frequency domain which can be reduced to the basic interpolation technique which is applied if there is only one pilot carrying subcarrier available per block. For  $O_T = 6$  and  $E_B/N_0 > 15$  dB, the subcarrierwise repetition provides a clearly worse performance than the symbolwise LS. Nevertheless, for  $O_T = 2$ , the performance difference is reduced significantly which shows that the interpolation errors due to the time variability of the channel exceed the erroneous interpolation in frequency domain for subcarrierwise repetition and that the interpolation errors in time domain contribute most to the overall estimation errors. Moreover, based on the comparison to Figure 5.6, it can be stated that

subcarrierwise repetition provides better estimation performance than subcarrierwise DFT and is applicable for the case  $Q_P < L_C$ .

In Figure 5.7(b), results are shown for B-IFDMA with  $Q = 8$  allocated subcarriers and  $K_F = 4$  subcarriers per block in frequency domain. For subcarrierwise pilot insertion, the interpolation depth  $I = 2$  is applied in frequency domain. As there are two pilot carrying subcarriers per block, Wiener interpolation within each block of  $K_F$  subcarriers is feasible. In the following, the influence of the pilot positions in frequency domain shall be investigated and, thus, results for subcarrierwise Wiener with equidistant and marginal pilot allocation are compared. The performance of symbolwise LS serves as a reference.

It can be seen that for  $O_T = 6$ , the marginal pilot allocation shows better performance than the equidistant pilot allocation although the distance between neighboring pilots is smaller for the equidistant pilot allocation than for the marginal allocation. For  $O_T = 2$ , i.e., higher velocity, there is only a slight performance gain of the marginal pilot allocation as in this case the interpolation errors in time domain are predominant and have a stronger influence on the overall estimation performance. For  $E_B/N_0 < 18$  dB, subcarrierwise Wiener performs better than symbolwise LS for both, the marginal and the equidistant pilot allocation. For  $E_B/N_0 \geq 18$  dB and  $O_T = 2$ , subcarrierwise Wiener shows the same performance as symbolwise LS. This can be reduced to the noise mitigating property of the Wiener interpolation which has been mentioned already in Section 3.4.4. For  $E_B/N_0 \geq 18$  dB and  $O_T = 6$ , subcarrierwise Wiener exhibits performance degradations in comparison to symbolwise LS due to interpolation errors in frequency domain which occur for both, the marginal and the equidistant pilot allocation.

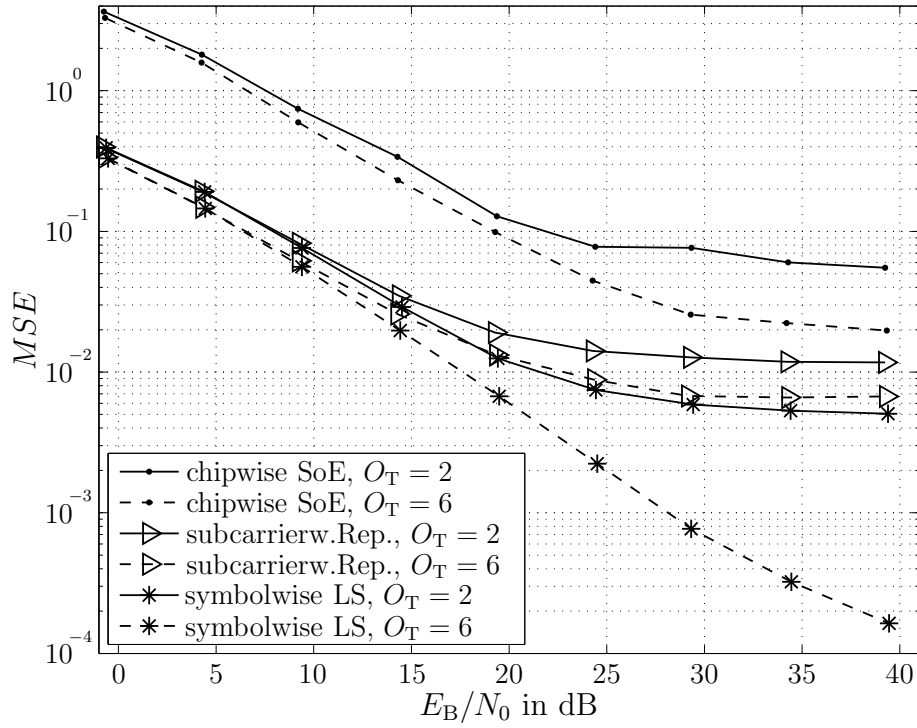
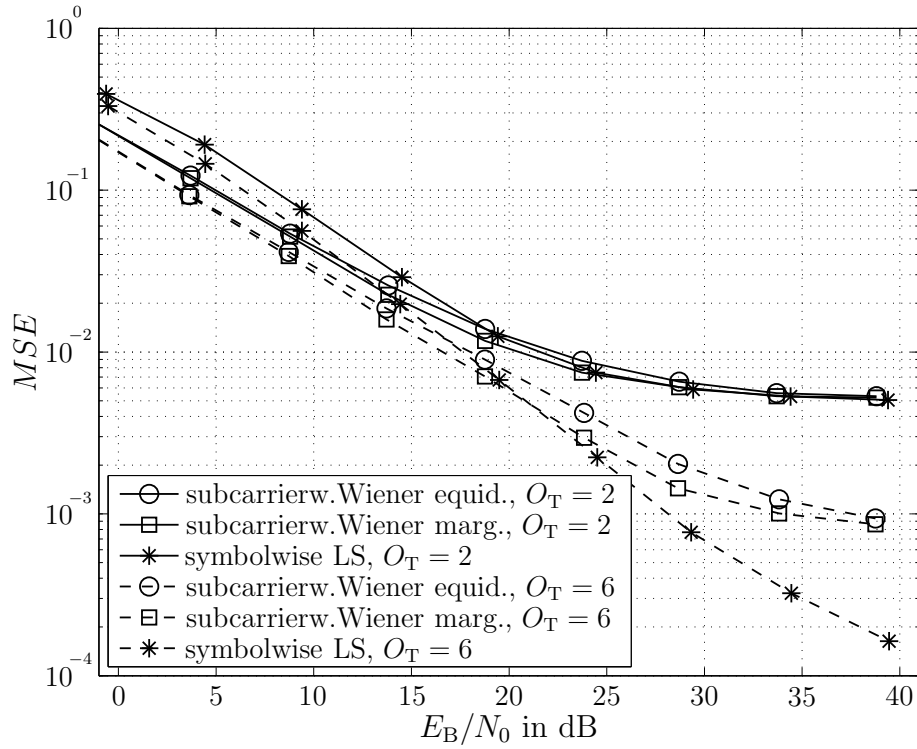
(a)  $K_F = 2$ (b)  $K_F = 4$ 

Figure 5.7. MSE as a function of  $E_B/N_0$  in dB for the estimation of channel variations in frequency and time domain under consideration of an oversampling factor  $O_T = 2$  and  $O_T = 6$  in time domain for  $Q = 8$  allocated subcarriers.

### 5.3.4.5 Complexity

In this section, the pilot assisted channel estimation algorithms introduced in Section 5.3 for B-IFDMA are investigated in terms of their computational complexity which is measured based on the required number of complex multiplications. The results are shown in Table 5.2 and are valid for the same assumptions as in Section 3.4.5.

Table 5.2. Number of complex multiplications

Algorithm	Complex multiplications
symbolwise LS	$P \cdot Q + (K - P) \cdot Q \cdot V$
subcarrierwise Wiener	$P \cdot (Q_P + Q_D \cdot W) + (K - P) \cdot Q \cdot V$
subcarrierwise DFT	$P \cdot (Q_P + Q_P \log_2(Q_P) + Q \log_2(Q)) + (K - P) \cdot Q \cdot V$
subcarrierwise repetition	$P \cdot Q_P + (K - P) \cdot Q \cdot V$
chipwise SoE	$P \cdot \left( \left( \frac{Q}{2} \right)^3 + 3 \cdot \left( \frac{Q}{2} \right)^2 + \frac{Q}{2} \right) + (K - P) \cdot Q \cdot V$

As already explained in Section 3.4.5, the second part of the number of multiplications is equal for each of the considered channel estimation approaches as it contributes to the Wiener interpolation in time domain. The first part of the number of multiplications contributes to the estimation of the channel variations in frequency domain. The symbolwise LS, the subcarrierwise Wiener and the subcarrierwise DFT exhibit the same computational complexity as for IFDMA. It can be seen that the subcarrierwise repetition requires least number of complex multiplications as the  $Q_P$  LS estimates are simply repeated for the neighboring non-pilot carrying subcarriers. The chipwise SoE exhibits the highest computational complexity. The matrix inversion in Eq. (5.20) consumes  $(Q/2)^3$  complex multiplications and, thus, represents the most critical part in

terms of complexity for chipwise SoE. As already explained for IFDMA, for symbolwise LS and subcarrierwise Wiener, the second part representing the Wiener interpolation in time domain is the dominating part in terms of complexity under the assumption of practical parameters. This is also true for subcarrierwise repetition and, thus, the complexity of the three algorithms is comparable as it is mainly determined by the Wiener interpolation in time domain. For subcarrierwise DFT, the number of multiplications due to the estimation of frequency domain channel variations is smaller than the number of multiplications due to the estimation of time domain channel variations but still cannot be neglected for practical parameters. For chipwise SoE, the first part representing the estimation of frequency domain channel variations contributes noticeably to the overall computational complexity.

## 5.4 Semiblind Channel Estimation for Block-IFDMA

### 5.4.1 Introduction

In this Section 5.4, semiblind channel estimation is introduced for B-IFDMA. Although the B-IFDMA signal generation cannot be represented by compression and repetition in time domain like the signal generation for IFDMA, the B-IFDMA signal still contains redundancy due to the DFT precoding. Therefore, the second order statistics based semiblind channel estimation approaches for the estimation of frequency domain channel variations are also applicable to B-IFDMA. In the following, the parts of the semiblind channel estimation algorithms introduced for IFDMA in Chapter 4 containing new aspects for the application to B-IFDMA are emphasized and elaborated. Table 5.3 gives an overview of the aspects of semiblind channel estimation for B-IFDMA which are considered in the following section.

The application of correlation SCE is realizable by adapting the algorithm explained for IFDMA to the block interleaved subcarrier allocation. Section 4.4 has shown that the correlation SCE provides only poor estimation performance and, thus, for B-IFDMA, the correlation SCE is not considered. For subspace SCE, the redundancy that is inherent to each B-IFDMA symbol due to the DFT precoding is exploited. By doing so, the block interleaved subcarrier allocation is considered in particular. The subspace SCE for B-IFDMA is introduced in Section 5.4. The estimation of the channel variations in time domain by the application of DDCE+WF to B-IFDMA follows the same principle as the application to IFDMA and does not exhibit new aspects compared to



the explanations in Section 4.3. In Section 5.4.3, the subspace SCE is investigated in terms of the MSE performance. The analysis of the semiblind channel estimation for B-IFDMA in terms of pilot symbol overhead consumption and computational complexity is omitted as it does not reveal new findings compared to the performance analysis of semiblind channel estimation for IFDMA in Section 4.4.

Table 5.3. Semiblind channel estimation for B-IFDMA in comparison to IFDMA

ESTIMATION APPROACH FOR FREQUENCY DOMAIN CHANNEL VARIATIONS	correlation SCE	not considered
	subspace SCE	generalization of algorithm used for IFDMA
ESTIMATION APPROACH FOR TIME DOMAIN CHANNEL VARIATIONS	DDCE+WF	same principle as for IFDMA

### 5.4.2 Subspace Based Semiblind Channel Estimation

In this section, the subspace SCE is introduced for B-IFDMA. The estimation principle is explained for the case of channels with small delay spreads, i.e., for the case that  $L_C \leq Q$ . The following derivations shall emphasize the difference to subspace SCE for IFDMA and are based on the derivations in Section 4.2.3.

According to Section 4.2.3, the subspace SCE comprises a combination of pilot assisted channel estimation and subspace based channel estimation. For pilot assisted channel estimation, the subcarrierwise pilot insertion is applied according to Section 5.3.2.1 and the LS estimates  $\hat{c}_{\kappa, q_P}^{(u)}$ ,  $q_P = 0, \dots, Q_P - 1$ , of the channel transfer factors corresponding to the  $Q_P$  pilot carrying subcarriers are obtained. The estimates of the channel transfer factors corresponding to the non-pilot carrying subcarriers are obtained by the subspace SCE.

It is again assumed that there are only small channel variations in time domain, implying that the matrices  $\mathbf{H}_{k,0}^{(u)}$  and  $\mathbf{H}_{k,1}^{(u)}$  defined in Eq. (4.3) and (4.4) are approximately constant for the B-IFDMA symbols with indices  $k = 0, \dots, K - 1$  as defined in Eq. (4.39). For IFDMA, it is obvious that each received IFDMA symbol contains redundancy due to the signal generation that can be explained by compression, repetition and phase shifting. Although the B-IFDMA signal generation cannot be

explained by compression, repetition and phase shifting, each B-IFDMA symbol exhibits redundancy due to the DFT precoding. That means, each B-IFDMA symbol consists of  $(L_U + L_G)Q$  chips but contains only  $Q$  data symbols. Let the vector  $\tilde{\mathbf{x}}_k^{(u)}$  which contains the transmitted B-IFDMA symbol including cyclic prefix be split into  $L = L_U + L_G$  blocks  $\mathbf{x}_{k,j}^{(u)} = [x_{k,jQ}^{(u)}, \dots, x_{k,jQ+Q-1}^{(u)}]^T$ ,  $j = 0, \dots, L-1$ , each consisting of  $Q$  elements. Further, let the received vector  $\tilde{\mathbf{r}}_k^{(u)}$  be split into  $L = L_U + L_G$  blocks  $\mathbf{r}_{k,j}^{(u)} = [r_{k,jQ}^{(u)}, \dots, r_{k,jQ+Q-1}^{(u)}]^T$ ,  $j = 0, \dots, L-1$ , each consisting of  $Q$  elements. In analogy to Section 4.2.3, for the application of subspace SCE to B-IFDMA, three blocks of length  $Q$  of the received signal are considered. The last block  $\mathbf{r}_{k-1,L-1}^{(u)}$  of the B-IFDMA symbol with index  $k-1$  and the first two blocks  $\mathbf{r}_{k,0}^{(u)}$  and  $\mathbf{r}_{k,1}^{(u)}$  of the B-IFDMA symbol with index  $k$  are comprised in one vector. With  $\boldsymbol{\nu}_{k,j}^{(u)} = [\nu_{k,jQ}^{(u)}, \dots, \nu_{k,jQ+Q-1}^{(u)}]^T$ ,  $j = 0, \dots, L-1$ , the vector of length  $3Q$  containing the three received B-IFDMA blocks  $\mathbf{r}_{k-1,L-1}^{(u)}$ ,  $\mathbf{r}_{k,0}^{(u)}$  and  $\mathbf{r}_{k,1}^{(u)}$  is represented by

$$\begin{bmatrix} \mathbf{r}_{k-1,L-1}^{(u)} \\ \mathbf{r}_{k,0}^{(u)} \\ \mathbf{r}_{k,1}^{(u)} \end{bmatrix} = \begin{bmatrix} \mathbf{H}_1^{(u)} & \mathbf{H}_0^{(u)} & \mathbf{0}_Q & \mathbf{0}_Q \\ \mathbf{0}_Q & \mathbf{H}_1^{(u)} & \mathbf{H}_0^{(u)} & \mathbf{0}_Q \\ \mathbf{0}_Q & \mathbf{0}_Q & \mathbf{H}_1^{(u)} & \mathbf{H}_0^{(u)} \end{bmatrix} \cdot \begin{bmatrix} \mathbf{x}_{k-1,L-1}^{(u)} \\ \mathbf{x}_{k-1,L-1}^{(u)} \\ \mathbf{x}_{k,0}^{(u)} \\ \mathbf{x}_{k,1}^{(u)} \end{bmatrix} + \begin{bmatrix} \boldsymbol{\nu}_{k-1,L-1}^{(u)} \\ \boldsymbol{\nu}_{k,0}^{(u)} \\ \boldsymbol{\nu}_{k,1}^{(u)} \end{bmatrix}. \quad (5.25)$$

With the  $4Q \times 2Q$  matrix  $\boldsymbol{\Gamma}^{(u)}$  defined by

$$\boldsymbol{\Gamma}^{(u)} = \begin{bmatrix} [\mathbf{F}_N^H]_{(L_U-2)Q:(L_U-1)Q-1,:} & \mathbf{0}_{1 \times N} \\ [\mathbf{F}_N^H]_{(L_U-1)Q:L_UQ-1,:} & \mathbf{0}_{1 \times N} \\ \mathbf{0}_{1 \times N} & [\mathbf{F}_N^H]_{(L_U-1)Q:L_UQ-1,:} \\ \mathbf{0}_{1 \times N} & [\mathbf{F}_N^H]_{0:Q-1,:} \end{bmatrix} \cdot \begin{bmatrix} \mathbf{M}_B^{(u)} & \mathbf{0}_{N \times Q} \\ \mathbf{0}_{N \times Q} & \mathbf{M}_B^{(u)} \end{bmatrix} \cdot \begin{bmatrix} \mathbf{F}_Q & \mathbf{0}_Q \\ \mathbf{0}_Q & \mathbf{F}_Q \end{bmatrix}, \quad (5.26)$$

Eq. (5.25) can be rewritten according to

$$\begin{bmatrix} \mathbf{r}_{k-1,L-1}^{(u)} \\ \mathbf{r}_{k,0}^{(u)} \\ \mathbf{r}_{k,1}^{(u)} \end{bmatrix} = \mathbf{H}_{\text{sub}}^{(u)} \cdot \boldsymbol{\Gamma}^{(u)} \cdot \begin{bmatrix} \mathbf{w}_{k-1}^{(u)} \\ \mathbf{w}_k^{(u)} \end{bmatrix} + \begin{bmatrix} \boldsymbol{\nu}_{k-1,L-1}^{(u)} \\ \boldsymbol{\nu}_{k,0}^{(u)} \\ \boldsymbol{\nu}_{k,1}^{(u)} \end{bmatrix}. \quad (5.27)$$

The  $3Q \times 3Q$  autocorrelation matrix of the vector defined in Eq. (5.27) is given by

$$\begin{aligned} \mathcal{A}^{(u)} &= \mathbb{E} \left\{ \begin{bmatrix} \mathbf{r}_{k-1,L-1}^{(u)} \\ \mathbf{r}_{k,0}^{(u)} \\ \mathbf{r}_{k,1}^{(u)} \end{bmatrix} \cdot \begin{bmatrix} \mathbf{r}_{k-1,L-1}^{(u)} \\ \mathbf{r}_{k,0}^{(u)} \\ \mathbf{r}_{k,1}^{(u)} \end{bmatrix}^H \right\} \\ &= \mathbf{H}_{\text{sub}}^{(u)} \cdot \boldsymbol{\Gamma}^{(u)} \cdot \sigma_W^2 \cdot \mathbf{I}_{2Q} \cdot \boldsymbol{\Gamma}^{(u)H} \cdot \mathbf{H}_{\text{sub}}^{(u)H} + \sigma_\nu^2 \cdot \mathbf{I}_{3Q}. \end{aligned} \quad (5.28)$$

Based on the derivations in Section 4.2.3, it can be deduced that the signal subspace is spanned by its eigenvectors which are the columns of the matrix  $\mathbf{H}_{\text{sub}}^{(u)} \cdot \mathbf{\Gamma}^{(u)}$ . The eigenvalue decomposition of matrix  $\mathcal{A}^{(u)}$  leads to  $3Q$  eigenvectors and their corresponding eigenvalues. Again, it is assumed that the  $Q$  eigenvectors corresponding to the  $Q$  smallest eigenvalues span the noise subspace. Let  $\mathbf{g}_0^{(u)}, \dots, \mathbf{g}_{Q-1}^{(u)}$  denote the eigenvectors corresponding to the  $Q$  smallest eigenvalues that span the noise subspace. Then, due to orthogonality between signal and noise subspace, the constraint

$$\mathbf{g}_q^{(u)\text{H}} \cdot \mathbf{H}_{\text{sub}}^{(u)} \cdot \mathbf{\Gamma}^{(u)} = \mathbf{0}_{1 \times 2Q}, \quad 0 \leq q \leq Q-1 \quad (5.29)$$

must hold. For practical implementations, the autocorrelation matrix  $\mathcal{A}^{(u)}$  is estimated by the arithmetic mean over  $K$  received B-IFDMA symbols according to

$$\hat{\mathcal{A}}^{(u)} = \frac{1}{K} \sum_{k=0}^{K-1} \begin{bmatrix} \mathbf{r}_{k-1,L-1}^{(u)} \\ \mathbf{r}_{k,0}^{(u)} \\ \mathbf{r}_{k,1}^{(u)} \end{bmatrix} \cdot \begin{bmatrix} \mathbf{r}_{k-1,L-1}^{(u)} \\ \mathbf{r}_{k,0}^{(u)} \\ \mathbf{r}_{k,1}^{(u)} \end{bmatrix}^{\text{H}}. \quad (5.30)$$

Thus, the estimates  $\hat{\mathbf{g}}_q^{(u)}$ ,  $q = 0, \dots, Q-1$ , of the noise subspace eigenvectors  $\mathbf{g}_q^{(u)}$  are available for the solution of the orthogonality constraint in Eq. (5.29). In order to explicitly represent the orthogonality constraint as a function of the vector  $[h_0^{(u)}, \dots, h_{L_C-1}^{(u)}, 0, \dots, 0]$ , the estimated noise subspace eigenvectors  $\hat{\mathbf{g}}_q^{(u)}$  are transformed into the  $Q \times 4Q$  matrices  $\hat{\mathcal{G}}_q^{(u)}$  according to Eq. (4.49) and the orthogonality constraint can be rewritten according to

$$[h_0^{(u)}, \dots, h_{L_C-1}^{(u)}, 0, \dots, 0]^* \cdot \hat{\mathcal{G}}_q^{(u)} \cdot \mathbf{\Gamma}^{(u)} = \mathbf{0}_{1 \times 2Q}, \quad 0 \leq q \leq Q-1. \quad (5.31)$$

The combination of Eq. (5.31) and the pilot assisted channel estimates in a system of equations in order to get an estimate of the vector  $[h_0^{(u)}, \dots, h_{L_C-1}^{(u)}, 0, \dots, 0]$  is identical to Section 4.2.3 and, therefore, not considered in this section.

### 5.4.3 Performance Analysis

#### 5.4.3.1 Analysis Assumptions

In this Section 5.4.3, the subspace based semiblind estimation of frequency domain channel variations for B-IFDMA is investigated with respect to the MSE performance. The results are obtained by computer simulations and are again valid for the simulation parameters that have been introduced in Section 3.4.1 and summarized in Table 3.1. In accordance to the performance analysis of semiblind channel estimation for IFDMA

in Section 4.4, the Typical Urban VarDelay channel is used for the simulations as it offers the possibility to adjust the number of channel delay taps. The analysis with regard to the PAPR of the B-IFDMA transmit signal is omitted as the PAPR influence of subcarrierwise pilot insertion has been presented in Section 5.3.4.2.

### 5.4.3.2 Mean Square Error

The MSE is again defined according to Eq. (3.54) and is depicted in dependency of  $E_B/N_0$  in dB. The results are valid for the following parameters:

- There are  $Q = 8$  subcarriers allocated to the user under consideration.
- The Typical Urban VarDelay channel with  $L_C = 8$  channel delay taps is used in the simulations. That means the channel exhibits a coherence bandwidth of  $B_{\text{coh}} = 128 \cdot \Delta f$  which is equal to the distance between neighboring allocated subcarriers for the case  $K_F = 1$ .

In Figure 5.8, the subcarrier allocation and pilot allocation for B-IFDMA with different block sizes is depicted exemplarily on a grid in frequency and time domain. The case with  $K_F = 1$  subcarrier per block is equal to the IFDMA subcarrier allocation. In the example, the coherence bandwidth of the channel is chosen to be equal to the distance between neighboring allocated subcarriers for the case  $K_F = 1$ . Thus, the depicted example represents the simulated parameter set. Figure 5.8(a) presents the case where every second allocated subcarrier is used for pilot transmission. It can be seen that for  $K_F = 1$  and  $K_F = 2$ , the positions of the pilot carrying subcarriers are identical and the sampling theorem in frequency domain is extended by factor 2. In Figure 5.8(b), every 4<sup>th</sup> subcarrier is used for pilot transmission and, again, the positions of the pilot carrying subcarriers are identical for the block sizes  $K_F = 1$ ,  $K_F = 2$  and  $K_F = 4$ . Here, the sampling theorem in frequency domain is extended by factor 4.

In Figure 5.9, the MSE is depicted for the cases which are represented by the examples illustrated in Figure 5.8. Figure 5.9(a) shows the results for the case that every second allocated subcarrier is used for pilot transmission and, thus, corresponds to Figure 5.8(a). The number  $K_F$  of subcarriers per block is chosen as parameter. Figure 5.9(a) shows that for  $E_B/N_0 > 13$  dB, the performance for  $K_F = 2$  is clearly better than for  $K_F = 1$ . This can be explained with the help of the graphical illustration in Figure 5.8(a) as follows. For  $K_F = 2$ , each block of subcarriers contains a pilot carrying subcarrier. Neighboring blocks exhibit a distance of  $2 \cdot B_{\text{coh}}$ . In contrast to  $K_F = 1$ ,

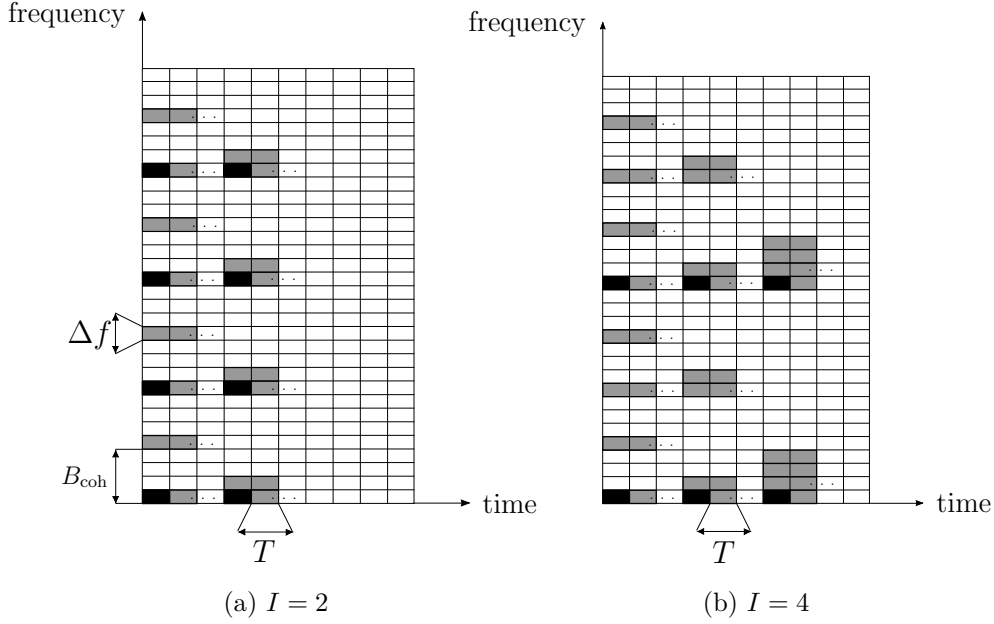


Figure 5.8. Pilot and non-pilot carrying subcarriers for different number  $K_F$  of subcarriers per block and interpolation depths  $I$ .

there is no non-pilot carrying block in-between whose channel transfer factors have to be estimated. Therefore, the calculation of the channel transfer factors corresponding to the non-pilot carrying subcarrier exhibits a better performance for  $K_F = 2$  as the non-pilot carrying subcarriers are adjacent to a pilot carrying subcarrier.

In the following, the performance of subspace SCE is investigated for the case that there exists a non-pilot carrying block of  $K_F = 2$  subcarriers. Figure 5.9(b) presents the results for the case that every 4<sup>th</sup> allocated subcarrier is used for pilot transmission and, thus, corresponds to Figure 5.8(b). It shows that for  $E_B/N_0 < 17$  dB, the results for  $K_F = 1$  exhibit the best performance. For  $17 \text{ dB} \leq E_B/N_0 < 33 \text{ dB}$ , the performance improves with increasing block size. However, the improvement is less for increasing the number of subcarriers per block from  $K_F = 2$  to  $K_F = 4$  than for the increase from  $K_F = 1$  to  $K_F = 2$ . For  $E_B/N_0 \geq 33 \text{ dB}$ , the results for  $K_F = 2$  exhibit the best performance. Figure 5.9(b) shows that the results for  $K_F = 2$  again provide a clearly better performance than for  $K_F = 1$  if the SNR reaches a certain threshold. This can also be substantiated by the differing number of non-pilot carrying blocks of subcarriers. For  $K_F = 1$ , there are three non-pilot carrying blocks whereas for  $K_F = 2$ , there is only one non-pilot carrying block of subcarriers in-between the blocks with pilots. Nevertheless, for  $K_F = 4$ , the performance improvement is less compared to  $K_F = 2$  and even degrades for high SNR values, although there is no non-pilot carrying

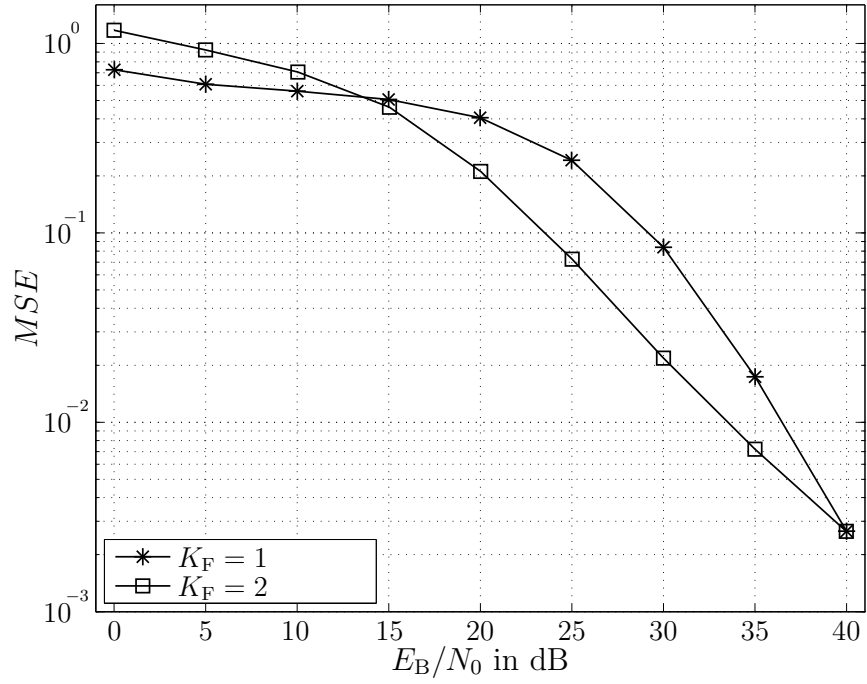
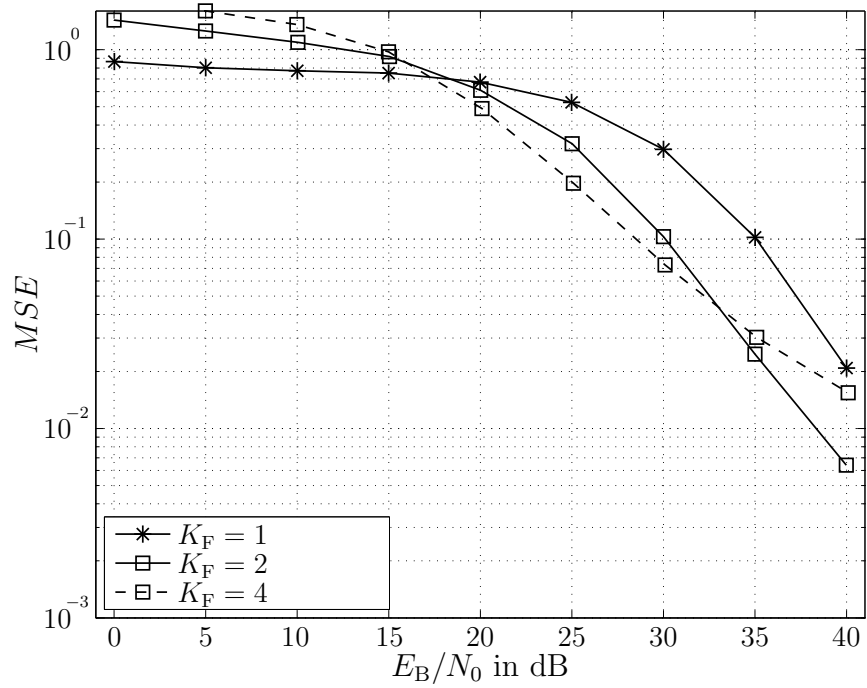
(a)  $I = 2$ (b)  $I = 4$ 

Figure 5.9. MSE as a function of  $E_B/N_0$  in dB for subspace SCE applied to B-IFDMA with different number  $K_F$  of subcarriers per block and interpolation depths  $I$  for  $Q = 8$  and  $L_C = 8$ .

block of subcarriers. This can be explained as follows. For  $K_F = 4$ , the distance between neighboring blocks equals  $4 \cdot B_{\text{coh}}$ . Due to this large distance, the received B-IFDMA signal which is analyzed for the subspace SCE exhibits less information about the channel variations in frequency domain than the received B-IFDMA signal for  $K_F = 2$ . As the subspace SCE calculates the channel impulse response first, some information about the channel variations in frequency domain is necessary in order to deduce the channel delay taps. This information in the received B-IFDMA signal reduces with increasing block sizes and, thus, the estimation performances degrades for an increasing block size.

It has been shown that the application of subspace based semiblind channel estimation allows to violate the sampling theorem in frequency domain by factor two, at least. However, for the case considered in Figure 5.9 and  $K_F > 2$ , extending the sampling theorem by factor two implies that a pilot carrying subcarrier is utilized within each block of subcarriers due to the distance of  $L_U \cdot K_F \cdot \Delta f$  between neighboring blocks. For block sizes  $K_F > 2$ , interpolation can be applied within the blocks of subcarriers and pilot assisted estimation of the frequency domain channel variations is feasible with identical number of pilot symbols in frequency domain. Therefore, in Figure 5.10, the estimation of frequency domain channel variations is compared for subcarrierwise repetition and subspace SCE for the case  $K_F = 2$  and  $I = 2$  meaning that there is one pilot carrying subcarrier per block. The velocity  $v$  of the mobile terminal is chosen as parameter. An algorithm for the estimation of channel variations in time domain is not applied in the following.

It can be seen that the subspace SCE is clearly outperformed by subcarrierwise repetition. Solely, for  $E_B/N_0 > 35$  dB and a velocity of  $v = 20$  km/h, the subspace SCE performs slightly better than subcarrier repetition. These results show that pilot assisted estimation of channel variations in frequency domain is preferable to the subspace SCE if there is at least one pilot carrying subcarrier per block.

## 5.5 Conclusions

In this chapter, pilot assisted and semiblind channel estimation have been presented for B-IFDMA. The similarities and differences compared to pilot assisted and semiblind channel estimation for IFDMA have been elaborated and new algorithms exploiting the block-interleaved subcarrier allocation of B-IFDMA have been introduced for pilot assisted as well as for semiblind channel estimation. The introduced estimation algorithms have been investigated in terms of the PAPR of the transmit signal, the pilot

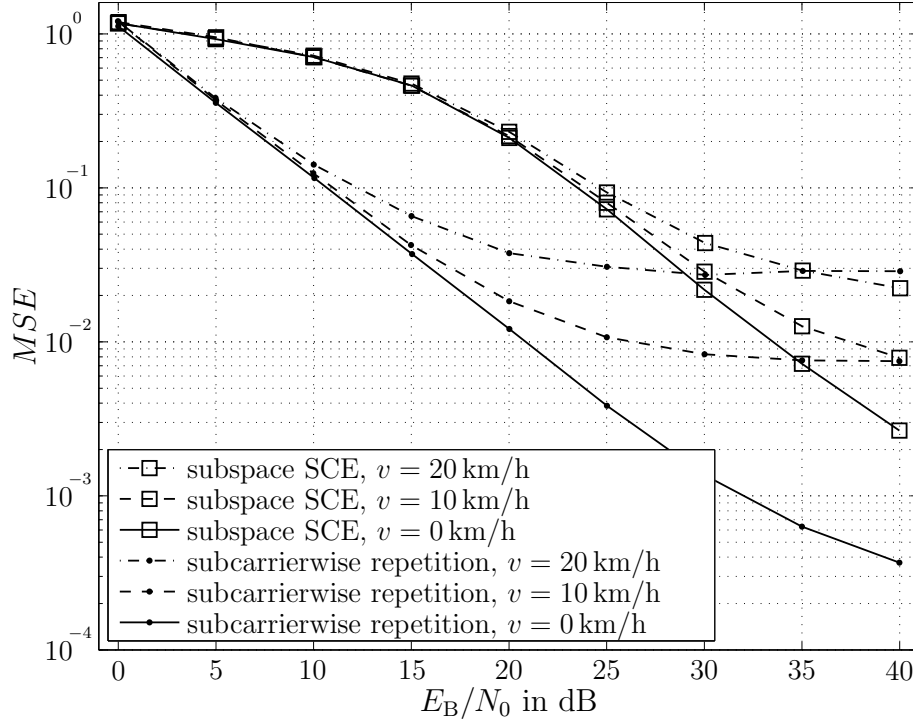


Figure 5.10. MSE as a function of  $E_B/N_0$  in dB for the estimation of frequency domain channel variations with subspace SCE and subcarrier repetition for  $Q = 8$ ,  $K_F = 2$  and  $L_C = 8$ .

symbol overhead consumption, the MSE performance and the computational complexity. The main conclusions of this chapter can be summarized as follows:

- Concerning pilot assisted channel estimation for B-IFDMA, advantage can be taken of the block interleaved subcarrier allocation by applying interpolation within each block of subcarriers in frequency domain.
- The DFT interpolation in frequency domain is applicable only for the case that the number  $L_C$  of channel delay taps is smaller than or equal to the number  $Q_P$  of pilot carrying subcarriers. For  $K_F > 1$  and  $Q_P \geq L_C$ , the pilot allocation in frequency domain does not represent an ideal sampling and, thus, the DFT interpolation provides only poor performance.
- The chipwise pilot insertion exhibits a lower PAPR compared to subcarrierwise pilot insertion. However, the MSE performance of the chipwise SoE is poor.
- For  $K_F = 2$ , the best trade-off between pilot symbol overhead and MSE performance is provided by subcarrierwise repetition.



- For  $K_F = 4$ , subcarrierwise Wiener with marginal pilot allocation shows slight performance improvement compared to subcarrierwise Wiener with equidistant pilot allocation.
- Subspace SCE is applicable to B-IFDMA and provides good estimation performance for a block size of  $K_F = 2$ . The application of subspace SCE allows to extend the sampling theorem in frequency domain. However, pure pilot assisted channel estimation with a reduced number of subcarriers is applicable for B-IFDMA as interpolation within each block of subcarriers is always feasible and the interpolation in-between neighboring blocks of subcarriers is not necessary. Due to this, the subspace SCE is only beneficial in terms of pilot symbol overhead if pilot symbols are transmitted within every second block of subcarriers.
- The results of subspace SCE provide a better performance for  $K_F = 2$  subcarriers per block compared to  $K_F = 1$  subcarrier per block. This is reduced to the smaller number of non-pilot carrying blocks for  $K_F = 2$ .
- For  $K_F = 4$ , the MSE performance degrades compared to  $K_F = 2$  as the received signal contains less information about the channel variations in frequency domain.



# Chapter 6

## Conclusions

This thesis deals with channel estimation for IFDMA and B-IFDMA. Due to the DFT precoding of the data symbols and the interleaved and block-interleaved subcarrier allocations, new aspects arise for the IFDMA and B-IFDMA channel estimation. These new aspects have been elaborated in Chapter 1. It is explained that the application of a certain channel estimation algorithm shall have small influence on the PAPR of the transmit signal and shall provide reliable estimation performance while consuming low pilot symbol overhead. For IFDMA, it is revealed that the distributed allocation of subcarriers makes the application of interpolation filters in frequency domain difficult and may lead to an increased pilot symbol overhead. For B-IFDMA, advantage shall be taken of the possibility to apply interpolation within each block of neighboring subcarriers in frequency domain.

First, the focus is on the IFDMA scheme and a system model for IFDMA transmission is presented in Chapter 2. It is shown that the received IFDMA signal after transmission over a mobile radio channel experiences a flat fading channel on each allocated subcarrier in frequency domain. Thus, in order to describe the channel influence on each received IFDMA symbol, the knowledge of the channel transfer factors corresponding to the allocated subcarriers is sufficient.

In Chapter 3, the symbolwise pilot insertion method is introduced which maintains the advantageous low PAPR of the IFDMA signal after pilot multiplexing. For the symbolwise pilot insertion, pilot symbols are transmitted on each allocated subcarrier and the channel transfer factors are estimated by an LS estimator applied on each subcarrier. This estimation approach provides a good estimation performance but prevents the transmission of data symbols within the pilot carrying IFDMA symbol. Therefore, the subcarrierwise pilot insertion method is introduced which uses a subset of the allocated subcarriers for pilot transmission and, thus, exhibits a smaller pilot symbol overhead than the symbolwise pilot insertion method. The reduction of pilot symbol overhead comes at the expense of a slightly increased PAPR of the transmit signal. For the subcarrierwise pilot insertion, interpolation filters are used to estimate the channel transfer factors corresponding to the non-pilot carrying subcarriers. This implies that the distance between neighboring pilot carrying subcarriers is smaller than the coherence bandwidth of the channel. The evaluation of simulation results reveals that reliable channel estimation performance is obtained if two pilot carrying subcarriers are used per coherence bandwidth. For IFDMA, the subcarriers allocated to a

certain user are equidistantly distributed over the bandwidth and, thus, the application of subcarrierwise pilot insertion with interpolation filters is only possible if the number of allocated subcarriers is larger than or equal to two times the number of channel delay taps. Chapter 3 shows that interpolation in frequency domain is applicable to IFDMA in some special cases and that, apart from these, the reduction of pilot symbol overhead in frequency domain is not feasible.

In Chapter 4, the pilot symbol overhead for IFDMA channel estimation is reduced by the introduction of semiblind channel estimation algorithms. For the estimation of channel variations in frequency domain two algorithms are derived, both exploiting the knowledge about the cyclostationarity which is inherent to the received IFDMA signal. The first introduced algorithm is the correlation based semiblind channel estimation which gains information about the channel variations in frequency domain by analyzing the estimated autocorrelation matrix of the received IFDMA signal. Although the algorithm utilizes the cyclic prefix parts of each received IFDMA symbol which are not mutually orthogonal for different users, the correlation based semiblind channel estimation is not influenced by multiple users in the system because the parts of the autocorrelation matrix are evaluated that are not influenced by the signals of other users. However, the correlation based semiblind channel estimation provides only poor estimation performance and the estimate exhibits a large error floor. The second introduced algorithm for the semiblind estimation of the frequency domain channel variations is the subspace based semiblind channel estimation which is based on the separation of the signal and noise subspace of the received IFDMA signal. This algorithm provides good estimation performance, especially for high SNR values. However, the performance of the subspace based semiblind channel estimation is strongly influenced by multiple users in the system. During uplink transmission, the performance is degraded with increasing number of users in the system. In contrast to this, the performance is improved with an increasing number of users during downlink transmission which can be explained by the increase of the received signal power. Both semiblind algorithms for the estimation of frequency domain channel variations are combined with a decision directed channel estimation in order to estimate the time domain channel variations. The decision directed channel estimation approach is extended by an iterative Wiener filtering process in order to mitigate the error propagation in time domain. The performance of subspace based semiblind channel estimation with decision directed channel estimation provides good performance results while consuming lower pilot symbol overhead in frequency and time domain than pilot assisted channel estimation.

Chapter 5 addresses channel estimation for B-IFDMA. The introduced pilot assisted and semiblind channel estimation algorithms for IFDMA are investigated with respect

to their application to B-IFDMA. It is revealed that for pilot assisted channel estimation, the distributed blocks of subcarriers can be exploited by applying interpolation in frequency domain within each block. By doing so, the pilot symbol overhead in frequency domain can be reduced and at the same time reliable channel estimates can be obtained. The blockwise subcarrier allocation opens up the possibility to introduce a new possibility of pilot insertion compared to IFDMA. For the chipwise pilot insertion method, a certain number of chips per B-IFDMA symbol is used for pilot transmission and the channel transfer factors are estimated by solving a system of equations. The chipwise pilot insertion exhibits a low PAPR, but provides only poor estimation performance. For B-IFDMA, the channel variations in frequency domain can also be estimated with the help of semiblind channel estimation. Although the performance of subspace based semiblind channel estimation for B-IFDMA is good, the semiblind estimation of frequency domain channel variations is not mandatory for the reduction of the pilot symbol overhead as the number of pilot symbols can also be reduced while applying pilot assisted channel estimation to B-IFDMA.

To summarize, it can be stated that the presented pilot assisted channel estimation algorithms provide most reliable channel estimates for nearly all SNR values in case of IFDMA as well as B-IFDMA. For IFDMA, the reduction of pilot symbols in frequency domain entails the usage of the introduced semiblind channel estimation approaches. The subspace based semiblind channel estimation exhibits satisfying estimation performance for large SNR values. However, the reduction of pilot symbols comes at the expense of an increased computational complexity. For B-IFDMA, the application of pilot assisted channel estimation is reasonable as the number of pilot symbols in frequency domain can be reduced due to the blockwise subcarrier allocation. However, while applying the presented subspace based semiblind channel estimation to B-IFDMA, the pilot symbol overhead in frequency domain can be further reduced.



# Appendix

## A.1 Derivation of Eq. (4.27) in Section 4.2.2.2

In the following, Eq. (4.27) representing the relation between the vector  $\tilde{\mathbf{r}}_k^{(u)}$  containing the inverse phase shifted received blocks  $\tilde{\mathbf{r}}_{k,j}^{(u)}$ ,  $j = 0, \dots, L-1$ , and the matrix  $\mathcal{H}^{(u)}$  containing the cyclic channel impulse response is derived for the correlation based semiblind channel estimation for large delay spreads.

The calculation of the received vector  $\tilde{\mathbf{r}}_k^{(u)}$  which has been defined in Eq. (4.25) leads to

$$\tilde{\mathbf{r}}_k^{(u)} = \begin{bmatrix} \square & & \mathbf{H}_{k,0}^{(u)} \cdot \Phi_{L_U-L_G}^{(u)} & & \\ \square & & \square & & \\ \vdots & & \vdots & & \\ \square & & \square & & \\ \mathbf{0}_Q & \mathbf{H}_{k,L_G}^{(u)} \cdot \Phi_{L_U-L_G}^{(u)} + \dots + \mathbf{H}_{k,1}^{(u)} \cdot \Phi_{L_U-1}^{(u)} + \mathbf{H}_{k,0}^{(u)} \cdot \Phi_0^{(u)} & & & \\ \vdots & & \vdots & & \\ \mathbf{0}_Q & \mathbf{H}_{k,L_G}^{(u)} \cdot \Phi_{L_U-1}^{(u)} + \mathbf{H}_{k,L_G-1}^{(u)} \cdot \Phi_0^{(u)} + \dots + \mathbf{H}_{k,0}^{(u)} \cdot \Phi_{L_G-1}^{(u)} & & & \\ \mathbf{0}_Q & \mathbf{H}_{k,L_G}^{(u)} \cdot \Phi_0^{(u)} + \dots + \mathbf{H}_{k,0}^{(u)} \cdot \Phi_{L_G}^{(u)} & & & \\ \vdots & & \vdots & & \\ \mathbf{0}_Q & \mathbf{H}_{k,L_G}^{(u)} \cdot \Phi_{L_U-L_G-1}^{(u)} + \dots + \mathbf{H}_{k,0}^{(u)} \cdot \Phi_{L_U-1}^{(u)} & & & \end{bmatrix} \cdot \begin{bmatrix} \mathbf{w}_{k-1}^{(u)} \\ \mathbf{w}_k^{(u)} \end{bmatrix} + \tilde{\mathbf{v}}_k^{(u)} . \quad (\text{A.1})$$

The multiplication of Eq. (A.1) with the matrix containing the inverse phase shift

according to Eq. (4.26) leads to the vector  $\check{\mathbf{r}}_k^{(u)}$  that is given by

$$\check{\mathbf{r}}_k^{(u)} = \begin{bmatrix} \square & \Phi_{L_U-L_G}^{(u)H} \cdot \mathbf{H}_{k,0}^{(u)} \cdot \Phi_{L_U-L_G}^{(u)} \\ \square & \square \\ \vdots & \vdots \\ \square & \square \\ \mathbf{0}_Q & \Phi_{L_U-1}^{(u)H} \cdot \left( \mathbf{H}_{k,L_G}^{(u)} \cdot \Phi_{L_U-L_G}^{(u)} + \cdots + \mathbf{H}_{k,1}^{(u)} \cdot \Phi_{L_U-1}^{(u)} + \mathbf{H}_{k,0}^{(u)} \cdot \Phi_0^{(u)} \right) \\ \vdots & \vdots \\ \mathbf{0}_Q & \Phi_{L_G-1}^{(u)H} \cdot \left( \mathbf{H}_{k,L_G}^{(u)} \cdot \Phi_{L_U-1}^{(u)} + \mathbf{H}_{k,L_G-1}^{(u)} \cdot \Phi_0^{(u)} + \cdots + \mathbf{H}_{k,0}^{(u)} \cdot \Phi_{L_G-1}^{(u)} \right) \\ \mathbf{0}_Q & \Phi_{L_G}^{(u)H} \cdot \left( \mathbf{H}_{k,L_G}^{(u)} \cdot \Phi_0^{(u)} + \cdots + \mathbf{H}_{k,0}^{(u)} \cdot \Phi_{L_G}^{(u)} \right) \\ \vdots & \vdots \\ \mathbf{0}_Q & \Phi_{L_U-L_G-1}^{(u)H} \cdot \left( \mathbf{H}_{k,L_G}^{(u)} \cdot \Phi_{L_U-L_G-1}^{(u)} + \cdots + \mathbf{H}_{k,0}^{(u)} \cdot \Phi_{L_U-1}^{(u)} \right) \end{bmatrix} \cdot \begin{bmatrix} \mathbf{w}_{k-1}^{(u)} \\ \mathbf{w}_k^{(u)} \end{bmatrix} + \begin{bmatrix} \Phi_{L_U-L_G}^{(u)H} & 0 & \cdots & 0 \\ 0 & \ddots & 0 & 0 \\ & 0 & \Phi_{L_U-1}^{(u)H} & 0 & \cdots & 0 \\ \vdots & & 0 & \Phi_0^{(u)H} & 0 & \vdots \\ & & & \ddots & 0 & \\ 0 & \cdots & & 0 & \Phi_{L_U-1}^{(u)H} \end{bmatrix} \cdot \check{\mathbf{v}}_k^{(u)}. \quad (\text{A.2})$$

For  $x = 0, \dots, L_G - 1$ , the matrices  $\Phi_x^{(u)H} \cdot (\mathbf{H}_{k,L_G}^{(u)} \cdot \Phi_{L_U-L_G+x}^{(u)} + \cdots + \mathbf{H}_{k,x+1}^{(u)} \cdot \Phi_{L_U-1}^{(u)} + \mathbf{H}_{k,x}^{(u)} \cdot \Phi_0^{(u)} + \cdots + \mathbf{H}_{k,0}^{(u)} \cdot \Phi_x^{(u)})$  are calculated according to

$$\begin{aligned} & \Phi_x^{(u)H} \cdot \left( \mathbf{H}_{k,L_G}^{(u)} \cdot \Phi_{L_U-L_G+x}^{(u)} + \cdots + \mathbf{H}_{k,x+1}^{(u)} \cdot \Phi_{L_U-1}^{(u)} + \mathbf{H}_{k,x}^{(u)} \cdot \Phi_0^{(u)} + \cdots + \mathbf{H}_{k,0}^{(u)} \cdot \Phi_x^{(u)} \right) \\ &= \begin{bmatrix} e^{j \cdot x \cdot \varphi^{(u)}} & 0 & \cdots & 0 \\ 0 & \ddots & & \vdots \\ \vdots & & & 0 \\ 0 & \cdots & 0 & e^{j \cdot ((x+1)Q-1) \cdot \varphi^{(u)}} \end{bmatrix}. \end{aligned}$$



$$\begin{aligned}
& \left( \begin{bmatrix} h_{k,L_G Q}^{(u)} & \cdots & \cdots & h_{k,(L_G-1)Q+1}^{(u)} \\ \vdots & & \ddots & \vdots \\ 0 & \cdots & 0 & h_{k,L_G Q}^{(u)} \end{bmatrix} \right. \\
& \quad \cdot \begin{bmatrix} e^{-j \cdot (L_U - L_G + x) \cdot Q \cdot \varphi^{(u)}} & 0 & \cdots & 0 \\ 0 & \ddots & & \vdots \\ \vdots & & & 0 \\ 0 & \cdots & 0 & e^{-j \cdot ((L_U - L_G + x + 1) \cdot Q - 1) \cdot \varphi^{(u)}} \end{bmatrix} \\
& \quad + \cdots + \begin{bmatrix} h_{k,(x+1)Q}^{(u)} & \cdots & h_{k,xQ+1}^{(u)} \\ \vdots & & \ddots \\ h_{k,(x+2)Q-1}^{(u)} & \cdots & h_{k,(x+1)Q}^{(u)} \end{bmatrix} \cdot \begin{bmatrix} e^{-j \cdot (L_U - 1) \cdot Q \cdot \varphi^{(u)}} & 0 & \cdots & 0 \\ 0 & \ddots & & \vdots \\ \vdots & & & 0 \\ 0 & \cdots & 0 & e^{-j \cdot (L_U \cdot Q - 1) \cdot \varphi^{(u)}} \end{bmatrix} \\
& \quad + \begin{bmatrix} h_{k,xQ}^{(u)} & \cdots & h_{k,(x-1)Q+1}^{(u)} \\ \vdots & & \ddots \\ h_{k,(x+1)Q-1}^{(u)} & \cdots & h_{k,xQ}^{(u)} \end{bmatrix} \cdot \begin{bmatrix} e^{-j \cdot 0 \cdot Q \cdot \varphi^{(u)}} & 0 & \cdots & 0 \\ 0 & \ddots & & \vdots \\ \vdots & & & 0 \\ 0 & \cdots & 0 & e^{-j \cdot (Q-1) \cdot \varphi^{(u)}} \end{bmatrix} \\
& \quad + \cdots + \begin{bmatrix} h_{k,0}^{(u)} & 0 & \cdots & \cdots & 0 \\ h_{k,1}^{(u)} & h_{k,0}^{(u)} & 0 & \cdots & \vdots \\ \vdots & & \ddots & & 0 \\ h_{k,Q-1}^{(u)} & \cdots & & h_{k,0}^{(u)} \end{bmatrix} \cdot \begin{bmatrix} e^{-j \cdot x \cdot Q \cdot \varphi^{(u)}} & 0 & \cdots & 0 \\ 0 & \ddots & & \vdots \\ \vdots & & & 0 \\ 0 & \cdots & 0 & e^{-j \cdot ((x+1)Q-1) \cdot \varphi^{(u)}} \end{bmatrix} \Bigg) \\
\end{aligned} \tag{A.3}$$

It is known that with  $\varphi^{(u)} = 2\pi u/N$  and  $z \in \mathbb{R}$

$$\begin{aligned}
e^{j \cdot (z \pm L_U) \cdot Q \cdot \varphi^{(u)}} &= e^{j \cdot (z \cdot Q \cdot \frac{2\pi}{N} \cdot u \pm L_U \cdot Q \cdot \frac{2\pi}{N} \cdot u)} \\
&= e^{j \cdot (z \cdot Q \cdot \frac{2\pi}{N} \cdot u \pm 2\pi \cdot u)} \\
&= e^{j \cdot z \cdot Q \cdot \varphi^{(u)}}.
\end{aligned} \tag{A.4}$$

Then, Eq. (A.3) becomes

$$\Phi_x^{(u)H} \cdot \left( \mathbf{H}_{k,L_G}^{(u)} \cdot \Phi_{L_U - L_G + x}^{(u)} + \cdots + \mathbf{H}_{k,x+1}^{(u)} \cdot \Phi_{L_U - 1}^{(u)} + \mathbf{H}_{k,x}^{(u)} \cdot \Phi_0^{(u)} + \cdots + \mathbf{H}_{k,0}^{(u)} \cdot \Phi_x^{(u)} \right)$$

$$\begin{aligned}
&= \begin{bmatrix} h_{k,L_G Q}^{(u)} \cdot e^{j \cdot (L_U - L_G) \cdot Q \cdot \varphi^{(u)}} & \dots & \dots & h_{k,(L_G-1)Q+1}^{(u)} \cdot e^{j \cdot ((L_U - L_G - 1) \cdot Q + 1) \cdot \varphi^{(u)}} \\ \vdots & & \ddots & \vdots \\ 0 & \dots & 0 & h_{k,L_G Q}^{(u)} \cdot e^{j \cdot (L_U - L_G) \cdot Q \cdot \varphi^{(u)}} \end{bmatrix} \\
&+ \dots + \begin{bmatrix} h_{k,(x+1)Q}^{(u)} \cdot e^{j \cdot (x+1-L_U) \cdot Q \cdot \varphi^{(u)}} & \dots & h_{k,xQ+1}^{(u)} \cdot e^{j \cdot ((x-L_U) \cdot Q + 1) \cdot \varphi^{(u)}} \\ \vdots & & \ddots \\ h_{k,(x+2)Q-1}^{(u)} \cdot e^{j \cdot ((x+2-L_U)Q-1) \cdot \varphi^{(u)}} & \dots & h_{k,(x+1)Q}^{(u)} \cdot e^{j \cdot (x+1-L_U) \cdot Q \cdot \varphi^{(u)}} \end{bmatrix} \\
&+ \begin{bmatrix} h_{k,xQ}^{(u)} \cdot e^{j \cdot x \cdot Q \cdot \varphi^{(u)}} & \dots & h_{k,(x-1)Q+1}^{(u)} \cdot e^{j \cdot ((x-1) \cdot Q + 1) \cdot \varphi^{(u)}} \\ \vdots & & \ddots \\ h_{k,(x+1)Q-1}^{(u)} \cdot e^{j \cdot ((x+1)Q-1) \cdot \varphi^{(u)}} & \dots & h_{k,xQ}^{(u)} \cdot e^{j \cdot x \cdot Q \cdot \varphi^{(u)}} \end{bmatrix} \\
&+ \dots + \begin{bmatrix} h_{k,0}^{(u)} & 0 & \dots & \dots & 0 \\ h_{k,1}^{(u)} \cdot e^{j \cdot \varphi^{(u)}} & h_0^{(u)} & 0 & \dots & \vdots \\ \vdots & & \ddots & & 0 \\ h_{k,Q-1}^{(u)} \cdot e^{j \cdot (Q-1) \cdot \varphi^{(u)}} & \dots & h_{k,0}^{(u)} \end{bmatrix} = \mathcal{H}_k^{(u)} \tag{A.5}
\end{aligned}$$

For  $x = L_G, \dots, L_U - 1$ , the matrices  $\Phi_x^{(u)H} \cdot (\mathbf{H}_{k,L_G}^{(u)} \cdot \Phi_{x-L_G}^{(u)} + \dots + \mathbf{H}_{k,0}^{(u)} \cdot \Phi_x^{(u)})$  are calculated according to

$$\begin{aligned}
&\Phi_x^{(u)H} \cdot (\mathbf{H}_{k,L_G}^{(u)} \cdot \Phi_{x-L_G}^{(u)} + \dots + \mathbf{H}_{k,0}^{(u)} \cdot \Phi_x^{(u)}) \\
&= \begin{bmatrix} e^{j \cdot x \cdot \varphi^{(u)}} & 0 & \dots & 0 \\ 0 & \ddots & & \vdots \\ \vdots & & 0 & \\ 0 & \dots & 0 & e^{j \cdot ((x+1)Q-1) \cdot \varphi^{(u)}} \end{bmatrix} \cdot \left( \begin{bmatrix} h_{k,L_G Q}^{(u)} & \dots & \dots & h_{k,(L_G-1)Q+1}^{(u)} \\ \vdots & & \ddots & \vdots \\ 0 & \dots & 0 & h_{k,L_G Q}^{(u)} \end{bmatrix} \right. \\
&\quad \left. \begin{bmatrix} e^{-j \cdot (x-L_G) \cdot Q \cdot \varphi^{(u)}} & 0 & \dots & 0 \\ 0 & \ddots & & \vdots \\ \vdots & & 0 & \\ 0 & \dots & 0 & e^{-j \cdot ((x-L_G+1) \cdot Q - 1) \cdot \varphi^{(u)}} \end{bmatrix} \right)
\end{aligned}$$

$$\begin{aligned}
& + \dots + \left[ \begin{array}{cccccc} h_{k,0}^{(u)} & 0 & \dots & \dots & 0 \\ h_{k,1}^{(u)} & h_{k,0}^{(u)} & 0 & \dots & \vdots \\ \vdots & & \ddots & & 0 \\ h_{k,Q-1}^{(u)} & \dots & & h_{k,0}^{(u)} \end{array} \right] \cdot \left[ \begin{array}{cccccc} e^{-j \cdot x \cdot Q \cdot \varphi^{(u)}} & 0 & \dots & & 0 \\ 0 & \ddots & & & \vdots \\ \vdots & & & & 0 \\ 0 & \dots & 0 & e^{-j \cdot ((x+1)Q-1) \cdot \varphi^{(u)}} \end{array} \right] \Bigg) \\
& = \left[ \begin{array}{cccccc} h_{k,L_G Q}^{(u)} \cdot e^{j \cdot L_G \cdot Q \cdot \varphi^{(u)}} & \dots & \dots & h_{k,(L_G-1)Q+1}^{(u)} \cdot e^{j \cdot ((L_G-1) \cdot Q + 1) \cdot \varphi^{(u)}} \\ \vdots & & \ddots & \ddots & \vdots \\ 0 & \dots & 0 & h_{k,L_G Q}^{(u)} \cdot e^{j \cdot L_G \cdot Q \cdot \varphi^{(u)}} \end{array} \right] \\
& + \dots + \left[ \begin{array}{cccccc} h_{k,0}^{(u)} & 0 & \dots & \dots & 0 \\ h_{k,1}^{(u)} \cdot e^{j \cdot \varphi^{(u)}} & h_{k,0}^{(u)} & 0 & \dots & \vdots \\ \vdots & & \ddots & & 0 \\ h_{k,Q-1}^{(u)} \cdot e^{j \cdot (Q-1) \cdot \varphi^{(u)}} & \dots & & h_{k,0}^{(u)} \end{array} \right] = \mathcal{H}_k^{(u)}
\end{aligned} \tag{A.6}$$

With Eq. (A.5) and (A.6), Eq. (A.2) is represented by

$$\begin{aligned}
\tilde{\mathbf{r}}_k^{(u)} & = \left\{ \begin{array}{l} L_G \\ L_U \end{array} \right\} \cdot \left[ \begin{array}{cc} \square & \Phi_{L_U-L_G}^{(u)H} \cdot \mathbf{H}_{k,0}^{(u)} \cdot \Phi_{L_U-L_G}^{(u)} \\ \vdots & \square \\ & \vdots \\ \square & \square \\ \mathbf{0}_Q & \mathcal{H}_k^{(u)} \\ \vdots & \vdots \\ \mathbf{0}_Q & \mathcal{H}_k^{(u)} \end{array} \right] \cdot \left[ \begin{array}{c} \mathbf{w}_{k-1}^{(u)} \\ \mathbf{w}_k^{(u)} \end{array} \right] \\
& + \left[ \begin{array}{cccccc} \Phi_{L_U-L_G}^{(u)H} & 0 & \dots & 0 \\ 0 & \ddots & 0 & 0 \\ & 0 & \Phi_{L_U-1}^{(u)H} & 0 & \dots & 0 \\ \vdots & & 0 & \Phi_0^{(u)H} & 0 & \vdots \\ & & & \ddots & 0 \\ 0 & \dots & & 0 & \Phi_{L_U-1}^{(u)H} \end{array} \right] \cdot \tilde{\mathbf{v}}_k^{(u)}.
\end{aligned} \tag{A.7}$$

## A.2 Derivation of the matrices $\mathcal{G}_0^{(u)}, \dots, \mathcal{G}_{Q-1}^{(u)}$ in Eq. (4.49)

In the following, the transformation of the noise subspace eigenvectors  $\mathbf{g}_q^{(u)}$  into the matrices  $\mathcal{G}_q^{(u)}$ ,  $q = 0, \dots, Q-1$ , according to Eq. (4.49) is derived for the case of channels with small delay spreads. In Section 4.2.3.1, the matrices  $\mathcal{G}_q^{(u)}$  are utilized to represent Eq. (4.45) explicitly as a function of the  $1 \times Q$  vector  $[h_0^{(u)}, \dots, h_{L_C-1}^{(u)}, 0 \dots, 0]^*$  which contains the delay taps of the channel. With the  $Q \times 1$  vectors  $\mathbf{g}_{q,j}^{(u)}$ ,  $j = 0, 1, 2$ , according to Eq. (4.46), Eq. (4.45) can be rewritten according to

$$\begin{aligned} \mathbf{g}_q^{(u)H} \cdot \mathbf{H}_{\text{sub}}^{(u)} &= \begin{bmatrix} \mathbf{g}_{q,0}^{(u)H} & \mathbf{g}_{q,1}^{(u)H} & \mathbf{g}_{q,2}^{(u)H} \end{bmatrix} \cdot \begin{bmatrix} \mathbf{H}_1^{(u)} & \mathbf{H}_0^{(u)} & \mathbf{0}_Q & \mathbf{0}_Q \\ \mathbf{0}_Q & \mathbf{H}_1^{(u)} & \mathbf{H}_0^{(u)} & \mathbf{0}_Q \\ \mathbf{0}_Q & \mathbf{0}_Q & \mathbf{H}_1^{(u)} & \mathbf{H}_0^{(u)} \end{bmatrix} \\ &= \begin{bmatrix} \mathbf{g}_{q,0}^{(u)H} \cdot \mathbf{H}_1^{(u)} & \mathbf{g}_{q,0}^{(u)H} \cdot \mathbf{H}_0^{(u)} + \mathbf{g}_{q,1}^{(u)H} \cdot \mathbf{H}_1^{(u)} & \mathbf{g}_{q,1}^{(u)H} \cdot \mathbf{H}_0^{(u)} + \mathbf{g}_{q,2}^{(u)H} \cdot \mathbf{H}_1^{(u)} & \mathbf{g}_{q,2}^{(u)H} \cdot \mathbf{H}_0^{(u)} \end{bmatrix}. \end{aligned} \quad (\text{A.8})$$

With  $\mathbf{A}_{q,j}^{(u)}$  the  $Q \times Q$  matrix that is defined by Eq. (4.47) and  $\mathbf{B}_{q,j}^{(u)}$  the  $Q \times Q$  matrix that is given by Eq. (4.48), the multiplication of the partial noise subspace eigenvector  $\mathbf{g}_{q,j}^{(u)}$  with the matrix  $\mathbf{H}_1^{(u)}$  and the matrix  $\mathbf{H}_0^{(u)}$  can be rewritten according to

$$\mathbf{g}_{q,j}^{(u)H} \cdot \mathbf{H}_1^{(u)} = [h_0^{(u)}, \dots, h_{L_C-1}^{(u)}, 0 \dots, 0]^* \cdot \mathbf{A}_{q,j}^{(u)} \quad (\text{A.9})$$

and

$$\mathbf{g}_{q,j}^{(u)H} \cdot \mathbf{H}_0^{(u)} = [h_0^{(u)}, \dots, h_{L_C-1}^{(u)}, 0 \dots, 0]^* \cdot \mathbf{B}_{q,j}^{(u)}, \quad (\text{A.10})$$

respectively.

With Eq. (A.9) and (A.10), Eq. (A.8) can be expressed with the help of the matrices  $\mathbf{A}_{q,j}^{(u)}$  and  $\mathbf{B}_{q,j}^{(u)}$  by

$$\begin{aligned} &\begin{bmatrix} \mathbf{g}_{q,0}^{(u)H} \cdot \mathbf{H}_1^{(u)} & \mathbf{g}_{q,0}^{(u)H} \cdot \mathbf{H}_0^{(u)} + \mathbf{g}_{q,1}^{(u)H} \cdot \mathbf{H}_1^{(u)} & \mathbf{g}_{q,1}^{(u)H} \cdot \mathbf{H}_0^{(u)} + \mathbf{g}_{q,2}^{(u)H} \cdot \mathbf{H}_1^{(u)} & \mathbf{g}_{q,2}^{(u)H} \cdot \mathbf{H}_0^{(u)} \end{bmatrix} \\ &= [h_0^{(u)}, \dots, h_{L_C-1}^{(u)}, 0 \dots, 0]^* \cdot \begin{bmatrix} \mathbf{A}_{q,0}^{(u)} & \mathbf{B}_{q,0}^{(u)} + \mathbf{A}_{q,1}^{(u)} & \mathbf{B}_{q,1}^{(u)} + \mathbf{A}_{q,2}^{(u)} & \mathbf{B}_{q,2}^{(u)} \end{bmatrix}. \end{aligned} \quad (\text{A.11})$$

Thus, the  $Q \times 4Q$  matrices  $\mathcal{G}_q^{(u)}$ ,  $q = 0, \dots, Q-1$ , are given by

$$\mathcal{G}_q^{(u)} = \begin{bmatrix} \mathbf{A}_{q,0}^{(u)} & \mathbf{B}_{q,0}^{(u)} + \mathbf{A}_{q,1}^{(u)} & \mathbf{B}_{q,1}^{(u)} + \mathbf{A}_{q,2}^{(u)} & \mathbf{B}_{q,2}^{(u)} \end{bmatrix}. \quad (\text{A.12})$$

### A.3 Derivation of Eq. (4.61) in Section 4.2.3.2

In the following, the relation between the vector containing the inverse phase shifted received blocks  $\tilde{\mathbf{r}}_{k-1,L-1}^{(u)}$ ,  $\tilde{\mathbf{r}}_{k,0}^{(u)}$ ,  $\tilde{\mathbf{r}}_{k,L_G}^{(u)}$  and the matrix  $\mathcal{H}^{(u)}$  containing the cyclic channel impulse response according to Eq. (4.61) is derived. After some calculation and under consideration of Eq. (4.60), Eq. (4.61) is represented by

$$\begin{aligned}
 \begin{bmatrix} \tilde{\mathbf{r}}_{k-1,L-1}^{(u)} \\ \tilde{\mathbf{r}}_{k,0}^{(u)} \\ \tilde{\mathbf{r}}_{k,L_G}^{(u)} \end{bmatrix} &= \begin{bmatrix} \Phi_{L_U-1}^{(u)H} & \mathbf{0}_Q & \mathbf{0}_Q \\ \mathbf{0}_Q & \Phi_0^{(u)H} & \mathbf{0}_Q \\ \mathbf{0}_Q & \mathbf{0}_Q & \Phi_0^{(u)H} \end{bmatrix} \cdot \begin{bmatrix} \mathbf{r}_{k-1,L-1}^{(u)} \\ \mathbf{r}_{k,0}^{(u)} \\ \mathbf{r}_{k,L_G}^{(u)} \end{bmatrix} = \\
 &\begin{bmatrix} \Phi_{L_U-1}^{(u)H} \left( \mathbf{H}_{L_G}^{(u)} \cdot \Phi_{L_U-L_G-1}^{(u)} + \dots + \mathbf{H}_0^{(u)} \cdot \Phi_{L_U-1}^{(u)} \right) & \mathbf{0}_Q \\ \Phi_0^{(u)H} \left( \mathbf{H}_{L_G}^{(u)} \cdot \Phi_{L_U-L_G}^{(u)} + \dots + \mathbf{H}_1^{(u)} \cdot \Phi_{L_U-1}^{(u)} \right) & \Phi_0^{(u)H} \cdot \mathbf{H}_0^{(u)} \cdot \Phi_{L_U-L_G}^{(u)} \\ \mathbf{0}_Q & \Phi_0^{(u)H} \left( \mathbf{H}_{L_G}^{(u)} \cdot \Phi_{L_U-L_G}^{(u)} + \dots + \mathbf{H}_1^{(u)} \cdot \Phi_{L_U-1}^{(u)} + \mathbf{H}_0^{(u)} \cdot \Phi_0^{(u)} \right) \end{bmatrix} \\
 &+ \begin{bmatrix} \Phi_{L_U-1}^{(u)H} & \mathbf{0}_Q & \mathbf{0}_Q \\ \mathbf{0}_Q & \Phi_0^{(u)H} & \mathbf{0}_Q \\ \mathbf{0}_Q & \mathbf{0}_Q & \Phi_0^{(u)H} \end{bmatrix} \cdot \begin{bmatrix} \nu_{k-1,L-1}^{(u)} \\ \nu_{k,0}^{(u)} \\ \nu_{k,L_G}^{(u)} \end{bmatrix}. \tag{A.13}
 \end{aligned}$$

In the following, it is assumed for the sake of simplicity that the number  $L_C$  of channel delay taps is equal to the elements transmitted within the cyclic prefix part of each IFDMA symbol, i.e.,  $L_C = L_G \cdot Q$ . Nevertheless, the subsequent derivations are valid for an arbitrary number  $L_C$  of channel delay taps. Then, the matrix  $\Phi_{L_U-1}^{(u)H} \cdot \left( \mathbf{H}_{L_G}^{(u)} \cdot \Phi_{L_U-L_G-1}^{(u)} + \dots + \mathbf{H}_0^{(u)} \cdot \Phi_{L_U-1}^{(u)} \right)$  can be calculated by

$$\begin{aligned}
 &\Phi_{L_U-1}^{(u)H} \cdot \left( \mathbf{H}_{L_G}^{(u)} \cdot \Phi_{L_U-L_G-1}^{(u)} + \dots + \mathbf{H}_0^{(u)} \cdot \Phi_{L_U-1}^{(u)} \right) \\
 &= \begin{bmatrix} e^{j \cdot (L_U-1) \cdot Q \cdot \varphi^{(u)}} & 0 & \dots & 0 \\ 0 & \ddots & & \vdots \\ \vdots & & & 0 \\ 0 & \dots & 0 & e^{j \cdot (L_U \cdot Q - 1) \cdot \varphi^{(u)}} \end{bmatrix} \cdot \\
 &\left( \begin{bmatrix} h_{L_G Q}^{(u)} & \dots & \dots & h_{(L_G-1)Q+1}^{(u)} \\ \vdots & \ddots & \ddots & \vdots \\ 0 & \dots & 0 & h_{L_G Q}^{(u)} \end{bmatrix} \cdot \begin{bmatrix} e^{-j \cdot (L_U-L_G-1) \cdot Q \cdot \varphi^{(u)}} & 0 & \dots & 0 \\ 0 & \ddots & & \vdots \\ \vdots & & & 0 \\ 0 & \dots & 0 & e^{-j \cdot ((L_U-L_G) \cdot Q - 1) \cdot \varphi^{(u)}} \end{bmatrix} \right)
 \end{aligned}$$

$$\begin{aligned}
& + \cdots + \begin{bmatrix} h_0^{(u)} & 0 & \cdots & \cdots & 0 \\ h_1^{(u)} & h_0^{(u)} & 0 & \cdots & \vdots \\ \vdots & & \ddots & & 0 \\ h_{Q-1}^{(u)} & \cdots & & h_0^{(u)} \end{bmatrix} \cdot \begin{bmatrix} e^{-j \cdot (L_U - 1) \cdot Q \cdot \varphi^{(u)}} & 0 & \cdots & 0 \\ 0 & \ddots & & \vdots \\ \vdots & & & 0 \\ 0 & \cdots & 0 & e^{-j \cdot (L_U \cdot Q - 1) \cdot \varphi^{(u)}} \end{bmatrix} \Bigg) \\
& = \begin{bmatrix} h_{L_G Q}^{(u)} \cdot e^{j \cdot L_G \cdot Q \cdot \varphi^{(u)}} & \cdots & \cdots & h_{(L_G - 1)Q + 1}^{(u)} \cdot e^{j \cdot ((L_G - 1) \cdot Q + 1) \cdot \varphi^{(u)}} \\ \vdots & & \ddots & \vdots \\ 0 & \cdots & 0 & h_{L_G Q}^{(u)} \cdot e^{j \cdot L_G \cdot Q \cdot \varphi^{(u)}} \end{bmatrix} \\
& + \cdots + \begin{bmatrix} h_0^{(u)} & 0 & \cdots & \cdots & 0 \\ h_1^{(u)} \cdot e^{j \cdot \varphi^{(u)}} & h_0^{(u)} & 0 & \cdots & \vdots \\ \vdots & & \ddots & & 0 \\ h_{Q-1}^{(u)} \cdot e^{j \cdot (Q-1) \cdot \varphi^{(u)}} & \cdots & & h_0^{(u)} \end{bmatrix} = \mathcal{H}^{(u)}
\end{aligned} \tag{A.14}$$

It is known that with  $\varphi^{(u)} = 2\pi u/N$  and  $z \in \mathbb{R}$

$$\begin{aligned}
e^{j \cdot (z \pm L_U) \cdot Q \cdot \varphi^{(u)}} &= e^{j \cdot (z \cdot Q \cdot \frac{2\pi}{N} \cdot u \pm L_U \cdot Q \cdot \frac{2\pi}{N} \cdot u)} \\
&= e^{j \cdot (z \cdot Q \cdot \frac{2\pi}{N} \cdot u \pm 2\pi \cdot u)} \\
&= e^{j \cdot z \cdot Q \cdot \varphi^{(u)}}.
\end{aligned} \tag{A.15}$$

Then, the matrix  $\Phi_0^{(u)H} \cdot \left( \mathbf{H}_{L_G}^{(u)} \cdot \Phi_{L_U - L_G}^{(u)} + \cdots + \mathbf{H}_1^{(u)} \cdot \Phi_{L_U - 1}^{(u)} + \mathbf{H}_0^{(u)} \cdot \Phi_0^{(u)} \right)$  can be calculated by

$$\begin{aligned}
& \Phi_0^{(u)H} \cdot \left( \mathbf{H}_{L_G}^{(u)} \cdot \Phi_{L_U - L_G}^{(u)} + \cdots + \mathbf{H}_1^{(u)} \cdot \Phi_{L_U - 1}^{(u)} + \mathbf{H}_0^{(u)} \cdot \Phi_0^{(u)} \right) \\
& = \begin{bmatrix} e^{j \cdot 0 \cdot \varphi^{(u)}} & 0 & \cdots & 0 \\ 0 & \ddots & & \vdots \\ \vdots & & & 0 \\ 0 & \cdots & 0 & e^{j \cdot (Q-1) \cdot \varphi^{(u)}} \end{bmatrix} \cdot \\
& \left( \begin{bmatrix} h_{L_G Q}^{(u)} & \cdots & \cdots & h_{(L_G - 1)Q + 1}^{(u)} \\ \vdots & \ddots & \ddots & \vdots \\ 0 & \cdots & 0 & h_{L_G Q}^{(u)} \end{bmatrix} \cdot \begin{bmatrix} e^{-j \cdot (L_U - L_G) \cdot Q \cdot \varphi^{(u)}} & 0 & \cdots & 0 \\ 0 & \ddots & & \vdots \\ \vdots & & & 0 \\ 0 & \cdots & 0 & e^{-j \cdot ((L_U - L_G + 1) \cdot Q - 1) \cdot \varphi^{(u)}} \end{bmatrix} \right)
\end{aligned}$$

$$\begin{aligned}
& + \dots + \begin{bmatrix} h_Q^{(u)} & \dots & h_1^{(u)} \\ \vdots & & \ddots \\ h_{2Q-1}^{(u)} & \dots & h_Q^{(u)} \end{bmatrix} \cdot \begin{bmatrix} e^{-j \cdot (L_U - 1) \cdot Q \cdot \varphi^{(u)}} & 0 & \dots & 0 \\ 0 & \ddots & & \vdots \\ \vdots & & & 0 \\ 0 & \dots & 0 & e^{-j \cdot (L_U \cdot Q - 1) \cdot \varphi^{(u)}} \end{bmatrix} \\
& + \begin{bmatrix} h_0^{(u)} & 0 & \dots & \dots & 0 \\ h_1^{(u)} & h_0^{(u)} & 0 & \dots & \vdots \\ \vdots & & \ddots & & 0 \\ h_{Q-1}^{(u)} & \dots & & h_0^{(u)} \end{bmatrix} \cdot \begin{bmatrix} e^{-j \cdot 0 \cdot Q \cdot \varphi^{(u)}} & 0 & \dots & 0 \\ 0 & \ddots & & \vdots \\ \vdots & & & 0 \\ 0 & \dots & 0 & e^{-j \cdot (Q-1) \cdot \varphi^{(u)}} \end{bmatrix} \Bigg) \\
& = \begin{bmatrix} h_{L_G Q}^{(u)} \cdot e^{j \cdot L_G \cdot Q \cdot \varphi^{(u)}} & \dots & \dots & h_{(L_G - 1)Q + 1}^{(u)} \cdot e^{j \cdot ((L_G - 1) \cdot Q + 1) \cdot \varphi^{(u)}} \\ \vdots & & \ddots & \vdots \\ 0 & \dots & 0 & h_{L_G Q}^{(u)} \cdot e^{j \cdot L_G \cdot Q \cdot \varphi^{(u)}} \end{bmatrix} \\
& + \dots + \begin{bmatrix} h_Q^{(u)} \cdot e^{j \cdot Q \cdot \varphi^{(u)}} & \dots & h_1^{(u)} \cdot e^{j \cdot \varphi^{(u)}} \\ \vdots & & \ddots \\ h_{2Q-1}^{(u)} \cdot e^{j \cdot (2Q-1) \cdot \varphi^{(u)}} & \dots & h_Q^{(u)} \cdot e^{j \cdot Q \cdot \varphi^{(u)}} \end{bmatrix} + \begin{bmatrix} h_0^{(u)} & 0 & \dots & \dots & 0 \\ h_1^{(u)} \cdot e^{j \cdot \varphi^{(u)}} & h_0^{(u)} & 0 & \dots & \vdots \\ \vdots & & \ddots & & 0 \\ h_{Q-1}^{(u)} \cdot e^{j \cdot (Q-1) \cdot \varphi^{(u)}} & \dots & & h_0^{(u)} \end{bmatrix} \\
& = \mathcal{H}^{(u)}
\end{aligned} \tag{A.16}$$

With the previous derivations, it can be deduced that the matrix  $\Phi_0^{(u)H} \cdot (\mathbf{H}_{L_G}^{(u)} \cdot \Phi_{L_U - L_G}^{(u)} + \dots + \mathbf{H}_1^{(u)} \cdot \Phi_{L_U - 1}^{(u)})$  can be represented by

$$\Phi_0^{(u)H} \cdot (\mathbf{H}_{L_G}^{(u)} \cdot \Phi_{L_U - L_G}^{(u)} + \dots + \mathbf{H}_1^{(u)} \cdot \Phi_{L_U - 1}^{(u)}) = \mathcal{H}^{(u)} - \Phi_0^{(u)H} \cdot \mathbf{H}_0^{(u)} \cdot \Phi_0^{(u)}. \tag{A.17}$$

## A.4 Derivation of the matrices $\hat{\mathcal{G}}_0^{(u)}, \dots, \hat{\mathcal{G}}_{Q-1}^{(u)}$ in Eq. (4.69)

In the following, the transformation of the noise subspace eigenvectors  $\hat{\mathbf{g}}_q^{(u)}$  into the matrices  $\hat{\mathcal{G}}_q^{(u)}$  for  $q = 0, \dots, Q - 1$ , according to Eq. (4.69) is explained for the case of channels with large delay spreads. In Section 4.2.3.2, the matrices  $\hat{\mathcal{G}}_q^{(u)}$

are utilized to represent Eq. (4.65) explicitly as a function of the  $1 \times 2Q$  vector  $[c_0^{(u)}, \dots, c_{Q-1}^{(u)}, h_0^{(u)}, \dots, h_{Q-1}^{(u)}]^*$ . The  $3Q \times 1$  vector  $\hat{\mathbf{g}}_q^{(u)}$  is split up in three  $Q \times 1$  vectors  $\hat{\mathbf{g}}_{q,j}^{(u)}$ ,  $j = 0, 1, 2$ , according to the definition for  $\mathbf{g}_{q,j}^{(u)}$ ,  $j = 0, 1, 2$ , in Eq. (4.46).

With this, Eq. (4.65) can be rewritten according to

$$\begin{aligned} & \hat{\mathbf{g}}_q^{(u)H} \cdot \begin{bmatrix} \mathcal{H}^{(u)} & \mathbf{0}_Q \\ \left( \mathcal{H}^{(u)} - \Phi_0^{(u)H} \cdot \mathbf{H}_0^{(u)} \cdot \Phi_0^{(u)} \right) & \left( \Phi_0^{(u)H} \cdot \mathbf{H}_0^{(u)} \cdot \Phi_{L_U-L_G}^{(u)} \right) \\ \mathbf{0}_Q & \mathcal{H}^{(u)} \end{bmatrix} \\ &= \left[ \hat{\mathbf{g}}_{q,0}^{(u)H} \cdot \mathcal{H}^{(u)} + \hat{\mathbf{g}}_{q,1}^{(u)H} \cdot \mathcal{H}^{(u)} - \hat{\mathbf{g}}_{q,1}^{(u)H} \cdot \Phi_0^{(u)H} \cdot \mathbf{H}_0^{(u)} \cdot \Phi_0^{(u)}, \right. \\ & \quad \left. \hat{\mathbf{g}}_{q,1}^{(u)H} \cdot \Phi_0^{(u)H} \cdot \mathbf{H}_0^{(u)} \cdot \Phi_{L_U-L_G}^{(u)} + \hat{\mathbf{g}}_{q,2}^{(u)H} \cdot \mathcal{H}^{(u)} \right]. \end{aligned} \quad (\text{A.18})$$

With  $\mathbf{C}_{q,j}^{(u)}$ ,  $\mathbf{D}_{q,j}^{(u)}$  and  $\mathbf{E}_{q,j}^{(u)}$  the  $Q \times Q$  matrices that is defined by Eqs. (4.66), (4.67) and (4.68), the multiplication of the partial noise subspace eigenvector  $\hat{\mathbf{g}}_{q,j}^{(u)}$  with the matrix  $\mathcal{H}^{(u)}$  and the matrix  $\mathbf{H}_0^{(u)}$  can be rewritten according to

$$\hat{\mathbf{g}}_{q,j}^{(u)H} \cdot \Phi_0^{(u)H} \cdot \mathbf{H}_0^{(u)} \cdot \Phi_0^{(u)} = [c_0^{(u)}, \dots, c_{Q-1}^{(u)}, h_0^{(u)}, \dots, h_{Q-1}^{(u)}]^* \cdot \mathbf{C}_{q,j}^{(u)}, \quad (\text{A.19})$$

$$\hat{\mathbf{g}}_{q,j}^{(u)H} \cdot \mathcal{H}^{(u)} = [c_0^{(u)}, \dots, c_{Q-1}^{(u)}, h_0^{(u)}, \dots, h_{Q-1}^{(u)}]^* \cdot \mathbf{D}_{q,j}^{(u)} \quad (\text{A.20})$$

and

$$\hat{\mathbf{g}}_{q,1}^{(u)H} \cdot \Phi_0^{(u)H} \cdot \mathbf{H}_0^{(u)} \cdot \Phi_{L_U-L_G}^{(u)} = [c_0^{(u)}, \dots, c_{Q-1}^{(u)}, h_0^{(u)}, \dots, h_{Q-1}^{(u)}]^* \cdot \mathbf{E}_{q,j}^{(u)}, \quad (\text{A.21})$$

respectively.

With Eqs. (A.19), (A.20) and (A.21), Eq. (A.18) can be expressed with the help of the matrices  $\mathbf{C}_{q,j}^{(u)}$ ,  $\mathbf{D}_{q,j}^{(u)}$  and  $\mathbf{E}_{q,j}^{(u)}$  by

$$\begin{aligned} & \left[ \hat{\mathbf{g}}_{q,0}^{(u)H} \cdot \mathcal{H}^{(u)} + \hat{\mathbf{g}}_{q,1}^{(u)H} \cdot \mathcal{H}^{(u)} - \hat{\mathbf{g}}_{q,1}^{(u)H} \cdot \Phi_0^{(u)H} \cdot \mathbf{H}_0^{(u)} \cdot \Phi_0^{(u)}, \right. \\ & \quad \left. \hat{\mathbf{g}}_{q,1}^{(u)H} \cdot \Phi_0^{(u)H} \cdot \mathbf{H}_0^{(u)} \cdot \Phi_{L_U-L_G}^{(u)} + \hat{\mathbf{g}}_{q,2}^{(u)H} \cdot \mathcal{H}^{(u)} \right] \\ &= [c_0^{(u)}, \dots, c_{Q-1}^{(u)}, h_0^{(u)}, \dots, h_{Q-1}^{(u)}]^* \cdot \left[ \mathbf{D}_{q,0}^{(u)} + \mathbf{D}_{q,1}^{(u)} - \mathbf{C}_{q,1}^{(u)}, \mathbf{E}_{q,1}^{(u)} + \mathbf{D}_{q,2}^{(u)} \right]. \end{aligned} \quad (\text{A.22})$$

Thus, the  $2Q \times 2Q$  matrices  $\hat{\mathcal{G}}_q^{(u)}$ ,  $q = 0, \dots, Q-1$ , are given by

$$\hat{\mathcal{G}}_q^{(u)} = \left[ \mathbf{D}_{q,0}^{(u)} + \mathbf{D}_{q,1}^{(u)} - \mathbf{C}_{q,1}^{(u)}, \mathbf{E}_{q,1}^{(u)} + \mathbf{D}_{q,2}^{(u)} \right]. \quad (\text{A.23})$$



## A.5 Derivation of Eq. (5.20) in Section 5.3.3

In the following, the derivation of Eq. (5.20) with the help of Eq. (5.18) and (5.19) is presented.

First, Eq. (5.18) and (5.19) are solved for the data vector  $[d_{\kappa,0}^{(u)}, \dots, d_{\kappa,Q_D-1}^{(u)}]^T$  which leads to

$$\begin{aligned} & [d_{\kappa,0}^{(u)}, \dots, d_{\kappa,Q_D-1}^{(u)}]^T \\ &= \left( [\mathbf{F}_Q]_{e,1:Q_D} \right)^H \cdot \left( \text{diag} \left\{ [\bar{\mathbf{c}}_{\kappa}^{(u)}]_e \right\}^{-1} \cdot [\bar{\mathbf{y}}_{\kappa}^{(u)}]_e - [\mathbf{F}_Q]_{e,Q_D+1:Q} \cdot [\rho_0^{(u)}, \dots, \rho_{Q_P-1}^{(u)}]^T \right) \end{aligned} \quad (\text{A.24})$$

and

$$\begin{aligned} & [d_{\kappa,0}^{(u)}, \dots, d_{\kappa,Q_D-1}^{(u)}]^T \\ &= \left( [\mathbf{F}_Q]_{o,1:Q_D} \right)^H \cdot \left( \text{diag} \left\{ [\bar{\mathbf{c}}_{\kappa}^{(u)}]_o \right\}^{-1} \cdot [\bar{\mathbf{y}}_{\kappa}^{(u)}]_o - [\mathbf{F}_Q]_{o,Q_D+1:Q} \cdot [\rho_0^{(u)}, \dots, \rho_{Q_P-1}^{(u)}]^T \right), \end{aligned} \quad (\text{A.25})$$

respectively.

The data vector in Eq. (A.24) can be substituted by Eq. (A.25) which leads to

$$\begin{aligned} & \left( [\mathbf{F}_Q]_{e,1:Q_D} \right)^H \cdot \left( \text{diag} \left\{ [\bar{\mathbf{c}}_{\kappa}^{(u)}]_e \right\}^{-1} \cdot [\bar{\mathbf{y}}_{\kappa}^{(u)}]_e - [\mathbf{F}_Q]_{e,Q_D+1:Q} \cdot [\rho_0^{(u)}, \dots, \rho_{Q_P-1}^{(u)}]^T \right) \\ &= \left( [\mathbf{F}_Q]_{o,1:Q_D} \right)^H \cdot \left( \text{diag} \left\{ [\bar{\mathbf{c}}_{\kappa}^{(u)}]_o \right\}^{-1} \cdot [\bar{\mathbf{y}}_{\kappa}^{(u)}]_o - [\mathbf{F}_Q]_{o,Q_D+1:Q} \cdot [\rho_0^{(u)}, \dots, \rho_{Q_P-1}^{(u)}]^T \right). \end{aligned} \quad (\text{A.26})$$

After some calculation, Eq. (A.26) can be represented by

$$\begin{aligned} & \left( [\mathbf{F}_Q]_{e,1:Q_D} \right)^H \cdot \text{diag} \left\{ [\bar{\mathbf{c}}_{\kappa}^{(u)}]_e \right\}^{-1} \cdot [\bar{\mathbf{y}}_{\kappa}^{(u)}]_e - \left( [\mathbf{F}_Q]_{o,1:Q_D} \right)^H \cdot \text{diag} \left\{ [\bar{\mathbf{c}}_{\kappa}^{(u)}]_o \right\}^{-1} \cdot [\bar{\mathbf{y}}_{\kappa}^{(u)}]_o \\ &= \left( \left( [\mathbf{F}_Q]_{e,1:Q_D} \right)^H \cdot [\mathbf{F}_Q]_{e,Q_D+1:Q} - \left( [\mathbf{F}_Q]_{o,1:Q_D} \right)^H \cdot [\mathbf{F}_Q]_{o,Q_D+1:Q} \right) \cdot [\rho_0^{(u)}, \dots, \rho_{Q_P-1}^{(u)}]^T \end{aligned} \quad (\text{A.27})$$

which is equal to

$$\begin{aligned} & \left( [\mathbf{F}_Q]_{e,1:Q_D} \right)^H \cdot \text{diag} \left\{ \left[ \bar{\mathbf{c}}_\kappa^{(u)} \right]_e \right\}^{-1} \cdot \left[ \bar{\mathbf{y}}_\kappa^{(u)} \right]_e - \left( [\mathbf{F}_Q]_{o,1:Q_D} \right)^H \cdot \text{diag} \left\{ \left[ \bar{\mathbf{c}}_\kappa^{(u)} \right]_o \right\}^{-1} \cdot \left[ \bar{\mathbf{y}}_\kappa^{(u)} \right]_o \\ &= \left[ \rho_0^{(u)}, \dots, \rho_{Q_P-1}^{(u)} \right]^T. \end{aligned} \quad (\text{A.28})$$

With  $[\bar{\mathbf{c}}_\kappa^{(u)}]_e = [\bar{c}_{\kappa,0}^{(u)}, \bar{c}_{\kappa,2}^{(u)}, \dots, \bar{c}_{\kappa,Q-2}^{(u)}]^T$  and  $[\bar{\mathbf{c}}_\kappa^{(u)}]_e \approx [\bar{\mathbf{c}}_\kappa^{(u)}]_o$ , Eq. (A.28) can be rewritten according to

$$\left( \left( [\mathbf{F}_Q]_{e,1:Q_D} \right)^H \cdot \text{diag} \left\{ \left[ \bar{\mathbf{y}}_\kappa^{(u)} \right]_e \right\} - \left( [\mathbf{F}_Q]_{o,1:Q_D} \right)^H \cdot \text{diag} \left\{ \left[ \bar{\mathbf{y}}_\kappa^{(u)} \right]_o \right\} \right) \cdot \begin{bmatrix} \bar{c}_{\kappa,0}^{(u)-1} \\ \bar{c}_{\kappa,2}^{(u)-1} \\ \vdots \\ \bar{c}_{\kappa,Q-2}^{(u)-1} \end{bmatrix} = \begin{bmatrix} \rho_0^{(u)} \\ \vdots \\ \rho_{Q_P-1}^{(u)} \end{bmatrix}. \quad (\text{A.29})$$

Then, a solution for  $[\bar{c}_{\kappa,0}^{(u)-1}, \bar{c}_{\kappa,2}^{(u)-1}, \dots, \bar{c}_{\kappa,Q-2}^{(u)-1}]^T$  is given by

$$\begin{bmatrix} \bar{c}_{\kappa,0}^{(u)-1} \\ \bar{c}_{\kappa,2}^{(u)-1} \\ \vdots \\ \bar{c}_{\kappa,Q-2}^{(u)-1} \end{bmatrix} = \left( \left( [\mathbf{F}_Q]_{e,1:Q_D} \right)^H \cdot \text{diag} \left\{ \left[ \bar{\mathbf{y}}_\kappa^{(u)} \right]_e \right\} - \left( [\mathbf{F}_Q]_{o,1:Q_D} \right)^H \cdot \text{diag} \left\{ \left[ \bar{\mathbf{y}}_\kappa^{(u)} \right]_o \right\} \right)^{-1} \cdot \begin{bmatrix} \rho_0^{(u)} \\ \vdots \\ \rho_{Q_P-1}^{(u)} \end{bmatrix} \quad (\text{A.30})$$

and a solution for  $\text{diag}\{[\bar{\mathbf{c}}_\kappa^{(u)}]_e\}$  is given by

$$\begin{aligned} & \text{diag} \left\{ \left[ \bar{\mathbf{c}}_\kappa^{(u)} \right]_e \right\} \\ &= \text{diag} \left\{ \left( \left( [\mathbf{F}_Q]_{e,1:Q_D} \right)^H \cdot \text{diag} \left\{ \left[ \bar{\mathbf{y}}_\kappa^{(u)} \right]_e \right\} - \left( [\mathbf{F}_Q]_{o,1:Q_D} \right)^H \cdot \text{diag} \left\{ \left[ \bar{\mathbf{y}}_\kappa^{(u)} \right]_o \right\} \right)^{-1} \cdot \begin{bmatrix} \rho_0^{(u)} \\ \vdots \\ \rho_{Q_P-1}^{(u)} \end{bmatrix} \right\}^{-1}. \end{aligned} \quad (\text{A.31})$$

## List of Acronyms

<b>AWGN</b>	Additive White Gaussian Noise
<b>BER</b>	Bit Error Rate
<b>B-IFDMA</b>	Block-Interleaved Frequency Division Multiple Access
<b>CAZAC</b>	Constant Amplitude Zero Autocorrelation
<b>CDF</b>	Cumulative Distribution Function
<b>CP</b>	Cyclic Prefix
<b>DFT</b>	Discrete Fourier Transform
<b>DDCE+WF</b>	Decision Directed Channel Estimation with iterative Wiener Filtering
<b>FD</b>	Frequency Domain
<b>FDE</b>	Frequency Domain Equalizer
<b>FFT</b>	Fast Fourier Transform
<b>FIR</b>	Finite Impulse Response
<b>IDFT</b>	Inverse Discrete Fourier Transform
<b>IFDMA</b>	Interleaved Frequency Division Multiple Access
<b>IFFT</b>	Inverse Fast Fourier Transform
<b>LFDMA</b>	Localized Frequency Division Multiple Access
<b>LS</b>	Least Square
<b>MMSE</b>	Minimum Mean Square Error
<b>MSE</b>	Mean Square Error
<b>MVU</b>	Minimum Variance Unbiased
<b>OFDM</b>	Orthogonal Frequency Division Multiplexing
<b>OFDMA</b>	Orthogonal Frequency Division Multiple Access
<b>PAPR</b>	Peak-to-Average Power Ratio

<b>PSK</b>	Phase Shift Keying
<b>QAM</b>	Quadrature Amplitude Modulation
<b>SC-FDMA</b>	Single Carrier Frequency Division Multiple Access
<b>SNR</b>	Signal-to-Noise Ratio
<b>TD</b>	Time Domain
<b>TDMA</b>	Time Division Multiple Access
<b>WINNER</b>	Wireless World Initiative New Radio
<b>WSSUS</b>	Wide-Sense Stationary Uncorrelated Scattering

# Notation

$A_{i,j}$	Element of matrix $\mathbf{A}$
$\alpha$	Angle between moving direction of mobile terminal and direction of arrival
$\mathbf{a}_k$	Vector containing $V$ Wiener filter coefficients in frequency domain
$a_{k,0}, \dots, a_{k,V-1}$	Elements of vector $\mathbf{a}_k$
$\mathcal{A}^{(u)}$	$3Q \times 3Q$ autocorrelation matrix for subspace based semiblind channel estimation
$B_{\text{coh}}$	Coherence bandwidth of channel
$\mathbf{b}_{qD}$	Vector containing $W$ Wiener filter coefficients in frequency domain
$b_{qD,0}, \dots, b_{qD,W-1}$	Elements of vector $\mathbf{b}_{qD}$
$c$	Speed of light
$\mathbf{c}_k^{(u)}$	Vector containing the cyclic channel impulse response of a user with index $u$
$c_{k,q}^{(u)}$	$q^{\text{th}}$ element of vector $\mathbf{c}_k^{(u)}$
$\bar{\mathbf{c}}_k^{(u)}$	Frequency domain representation of $\mathbf{c}_k^{(u)}$
$\bar{c}_{k,q}^{(u)}$	$q^{\text{th}}$ element of vector $\bar{\mathbf{c}}_k^{(u)}$
$\mathbf{d}_k^{(u)}$	Vector containing the data symbols of the $k$ th IFDMA symbol transmitted by the user with index $u$
$\bar{\mathbf{d}}_k^{(u)}$	Frequency domain representation of $\mathbf{d}_k^{(u)}$
$d_{k,q}^{(u)}$	$q$ th element of the vector $\mathbf{d}_k^{(u)}$
$\bar{d}_{k,q}^{(u)}$	$q$ th element of the vector $\bar{\mathbf{d}}_k^{(u)}$
$\boldsymbol{\delta}_\kappa^{(u)}$	Vector containing the $Q_D$ data symbols of user $u$ in the pilot carrying IFDMA symbol with index $\kappa$
$\delta$	Delta-distribution
$\Delta f$	Subcarrier spacing
$D_F$	Distance between pilot carrying subcarriers in frequency domain
$D_T$	Distance between pilot carrying IFDMA symbol in time domain
$E\{\cdot\}$	Expectation operator
$\eta(q_P)$	Index of pilot carrying subcarrier
$f_D$	Doppler shift
$f_{D,\text{max}}$	Maximum Doppler shift
$f_0$	Carrier frequency
$\mathbf{F}_N$	$N \times N$ DFT matrix

$\mathbf{F}_N^H$	$N \times N$ IDFT matrix
$\mathbf{F}_Q$	$Q \times Q$ DFT matrix
$\mathbf{F}_Q^H$	$Q \times Q$ IDFT matrix
$\mathbf{F}_{Q_D}$	$Q_D \times Q_D$ DFT matrix
$\mathbf{F}_{Q_D}^H$	$Q_D \times Q_D$ IDFT matrix
$\mathbf{F}_{Q_P}$	$Q_P \times Q_P$ DFT matrix
$\mathbf{F}_{Q_P}^H$	$Q_P \times Q_P$ IDFT matrix
$\mathbf{g}_q^{(u)}$	$q^{\text{th}}$ noise subspace eigenvector of matrix $\mathcal{A}^{(u)}$
$\mathbf{g}_{q,j}^{(u)}$	$j^{\text{th}}$ block containing $Q$ elements of the vector $\mathbf{g}_q^{(u)}$
$\hat{\mathbf{g}}_q^{(u)}$	Estimate of the vector $\mathbf{g}_q^{(u)}$
$\mathcal{G}_q^{(u)}$	$q^{\text{th}}$ transformed matrix containing the vector $\mathbf{g}_q^{(u)}$
$\hat{\mathcal{G}}_q^{(u)}$	Estimate of the matrix $\mathcal{G}_q^{(u)}$
$\mathbf{\Gamma}^{(u)}$	$4Q \times 2Q$ matrix for subspace based semiblind channel estimation for B-IFDMA
$h(t, \tau)^{(u)}$	Time continuous channel impulse response of the mobile radio channel
$\bar{h}(t, f)^{(u)}$	Fourier transform of $h(t, \tau)^{(u)}$ with respect to $\tau$
$\mathbf{h}_k^{(u)}$	Vector containing the $L_C$ channel delay taps $h_{k,l}(u)$
$h_{k,l}(u)$	$l^{\text{th}}$ channel delay tap of the discrete-time channel impulse response at time index $k$ for a user with index $u$
$\bar{\mathbf{h}}_k^{(u)}$	Frequency domain representation of $\mathbf{h}_k^{(u)}$
$\bar{h}_{k,n}^{(u)}$	Channel transfer factor of subcarrier with index $n$ at time index $k$ for a user with index $u$
$\mathbf{H}_k^{(u)}$	$N \times N$ right circulant channel matrix
$\mathcal{H}_k^{(u)}$	$Q \times Q$ right circulant channel matrix
$\bar{\mathcal{H}}_k^{(u)}$	$Q \times Q$ diagonal matrix having the channel transfer factors as its main diagonal
$\mathbf{H}_{k,0}^{(u)}, \dots, \mathbf{H}_{k,L_G}^{(u)}$	$Q \times Q$ Toeplitz matrices containing parts of the channel impulse response
$\mathbf{H}_{k,\text{corr}}^{(u)}$	$LQ \times (L+1)Q$ channel matrix of user $u$ for correlation based semiblind channel estimation
$\mathbf{H}_{\text{sub}}^{(u)}$	$3Q \times 4Q$ channel matrix of user $u$ for subspace based semiblind channel estimation
$I$	Interleaving depth in frequency domain
$J_0(\cdot)$	$0^{\text{th}}$ order Bessel function of first kind
$K$	Number of IFDMA symbols per TDMA slot
$k$	Index of IFDMA symbol

---

$K_F$	Number of subcarriers per block for B-IFDMA
$\kappa$	Index of pilot carrying IFDMA symbol
$L$	Repetition factor for IFDMA symbols with cyclic prefix
$L_C$	Number of channel delay taps of the discrete-time channel impulse response
$L_U$	Repetition/compression factor for IFDMA symbols
$L_G$	Repetition factor for cyclic prefix
$\mathcal{L}$	Number of delay paths of the time continuous channel impulse response
$l$	Index of channel delay tap of the discrete-time channel impulse response
$\Lambda$	Pilot symbol overhead in dB
$\mathbf{M}^{(u)}$	IFDMA mapping matrix for the allocation of subcarriers
$\mathbf{M}_P^{(u)}$	IFDMA mapping matrix for the allocation of pilot carrying subcarriers
$\mathbf{M}_D^{(u)}$	IFDMA mapping matrix for the allocation of data carrying subcarriers
$\mathbf{M}_B^{(u)}$	B-IFDMA mapping matrix for the allocation of subcarriers
$\mathbf{M}_{BP}^{(u)}$	B-IFDMA mapping matrix for the allocation of pilot carrying subcarriers
$\mathbf{M}_{BD}^{(u)}$	B-IFDMA mapping matrix for the allocation of data carrying subcarriers
$MSE$	Mean square error
$N$	Number of available subcarriers in the system
$n$	Subcarrier index
$N_G$	Number of cyclic prefix elements
$N_0$	Noise power
$O_F$	Oversampling factor in frequency domain
$O_T$	Oversampling factor in time domain
$PAPR_k$	Peak-to-Average power ratio per IFDMA symbol
$\varphi^{(u)}$	User dependent phase
$\Phi_i^{(u)}$	User dependent phase shift matrix with index $i$
$\mathbf{p}^{(u)}$	Vector containing the modulated pilot symbols of user $u$ in time domain
$p_n^{(u)}$	$n^{\text{th}}$ element of vector $\mathbf{p}^{(u)}$
$\bar{\mathbf{p}}^{(u)}$	Vector containing the modulated pilot symbols of user $u$ in frequency domain

$\bar{p}_n^{(u)}$	$n^{\text{th}}$ element of vector $\bar{\mathbf{p}}^{(u)}$
$P$	Number of pilot carrying IFDMA symbols
$Q$	Number of data symbols per IFDMA symbol
$q$	Index of data symbol per IFDMA symbol
$Q_P$	Number of pilot symbols per pilot carrying IFDMA symbol
$q_P$	Index of pilot symbol within a pilot carrying IFDMA symbol
$Q_D$	Number of data symbols per pilot carrying IFDMA symbol
$q_D$	Index of data symbol within a pilot carrying IFDMA symbol
$R_{\bar{h}}(t', f')^{(u)}$	Autocorrelation function of $\bar{h}(t, f)^{(u)}$ with respect to $t'$ and $f'$
$R_{\bar{h},t}(t')^{(u)}$	Time correlation function
$R_{\bar{h},f}(f')^{(u)}$	Frequency correlation function
$\tilde{\mathbf{r}}_k^{(u)}$	Received $k^{\text{th}}$ IFDMA symbol of user with index $u$ with cyclic prefix
$\mathbf{r}_k^{(u)}$	Received $k^{\text{th}}$ IFDMA symbol of user with index $u$
$r_{k,n}^{(u)}$	$n^{\text{th}}$ element of the vector $\tilde{\mathbf{r}}_k^{(u)}$ or the vector $\mathbf{r}_k^{(u)}$
$\mathbf{r}_{k,j}^{(u)}$	Vector containing $Q$ elements of the $j^{\text{th}}$ block of the vector $\tilde{\mathbf{r}}_k^{(u)}$
$\tilde{\mathbf{r}}_k^{(u)}$	Received $k^{\text{th}}$ inverse phase shifted IFDMA symbol of user $u$ with cyclic prefix
$\boldsymbol{\rho}^{(u)}$	Vector containing the $Q_P$ pilot symbols of user $u$ in time domain
$\rho_{q_P}^{(u)}$	$q_P^{\text{th}}$ element of vector $\boldsymbol{\rho}^{(u)}$
$\bar{\boldsymbol{\rho}}^{(u)}$	Vector containing the $Q_P$ pilot symbols of user $u$ in frequency domain
$\bar{\rho}_{q_P}^{(u)}$	$q_P^{\text{th}}$ element of vector $\bar{\boldsymbol{\rho}}^{(u)}$
$S_{f_D}(f_D)^{(u)}$	Doppler power spectral density
$S_{\tau}(\tau)^{(u)}$	Delay power spectral density
$\sigma_D^2$	Average power of data symbols
$\sigma_P^2$	Average power of pilot symbols
$\sigma_W^2$	Average power of compressed data symbols
$\sigma_v^2$	Average power of AWGN
$\varsigma(q_D)$	Index of non-pilot carrying subcarrier
$t$	Absolute time
$T$	Time duration of an IFDMA symbol with cyclic prefix
$T_{\text{coh}}$	Coherence time of channel
$T_C$	Time duration of a compressed data symbol
$T_S$	Time duration of a data symbol
$\tau$	Relative path delay time



---

$\tau_{\max}$	Maximum path delay time
$\tau_{\text{rms}}$	Root mean square width of the path delay time
$\tau_{\iota}$	Path delay time of $\iota^{\text{th}}$ path
$\Theta_{\text{corr}}^{(u)}$	$(L+1)Q \times 2Q$ phase shift matrix of user $u$ for correlation based semiblink channel estimation
$\Theta_{\text{sub}}^{(u)}$	$4Q \times 2Q$ phase shift matrix of user $u$ for subspace based semiblink channel estimation
$U$	Number of users
$u$	User index
$v$	Velocity of mobile terminal
$V$	Number of Wiener filter coefficients for filtering in time domain
$\tilde{\mathbf{v}}_k^{(u)}$	AWGN vector of the IFDMA symbol with index $k$ and user $u$ plus cyclic prefix
$\mathbf{v}_k^{(u)}$	AWGN vector of the IFDMA symbol with index $k$ and user $u$
$\nu_{k,n}^{(u)}$	$n^{\text{th}}$ element of the vector $\tilde{\mathbf{v}}_k^{(u)}$ or the vector $\mathbf{v}_k^{(u)}$
$\mathbf{w}_k^{(u)}$	Vector containing the compressed version of $\mathbf{d}_k^{(u)}$
$w_{k,q}^{(u)}$	$q^{\text{th}}$ element of the vector $\mathbf{w}_k^{(u)}$
$W$	Number of Wiener filter coefficients for filtering in frequency domain
$\mathbf{x}_k^{(u)}$	$k^{\text{th}}$ IFDMA symbol transmitted by the user with index $u$
$\tilde{\mathbf{x}}_k^{(u)}$	$k^{\text{th}}$ IFDMA symbol with cyclic prefix transmitted by the user with index $u$
$\mathbf{y}_k^{(u)}$	Vector containing the demodulated IFDMA symbol with index $k$ of user $u$
$\bar{\mathbf{y}}_k^{(u)}$	Frequency domain representation of $\mathbf{y}_k^{(u)}$
$\mathbf{0}_{a \times b}$	$a \times b$ matrix containing all zero elements
$\mathbf{0}_a$	$a \times a$ matrix containing all zero elements
$\mathbf{I}_a$	$a \times a$ identity matrix
$\square$	Matrix or vector entries with no relevance for the remainder
$\text{diag}\{\cdot\}$	Diagonal matrix with the vector elements as its main diagonal
$(\cdot)^{\text{T}}$	Transpose of a vector or matrix
$(\cdot)^{\text{H}}$	Conjugate transpose of a vector or matrix
$(\cdot)^*$	Conjugate of a scalar, vector, or matrix
$(\cdot)^{-1}$	Inverse of a square matrix
$ \cdot $	Absolute value of a scalar
$\ \cdot\ _2$	Euclidean norm or 2-norm of a vector
$\lceil z \rceil$	Nearest integer larger than or equal to $z$

---

$\lfloor z \rfloor$	Nearest integer smaller than or equal to $z$
$[\cdot]_{a,b}$	Element in the $a^{\text{th}}$ row and $b^{\text{th}}$ column of a matrix
$[\mathbf{z}]_{\text{e}}$	Vector containing the even indices of vector $\mathbf{z}$
$[\mathbf{z}]_{\text{o}}$	Vector containing the odd indices of vector $\mathbf{z}$
$[\mathbf{Z}]_{a:b,c:d}$	Matrix containing the rows with indices $a, \dots, b$ and columns with indices $c, \dots, d$ of a matrix $\mathbf{Z}$

# Bibliography

- [3GP06] 3GPP, “Physical Layer Aspects for Evolved Universal Terrestrial Radio Access,” Technical Specification Group Radio Access Network, Tech. Rep. Technical Report TR 25.814 v7.1.0, Oct. 2006.
- [BC02] N. Benvenuto and G. Cherubini, *Algorithms for Communications Systems and their Applications*. John Wiley & Sons Ltd., 2002.
- [Bel63] P. Bello, “Characterization of Randomly Time-Variant Linear Channels,” *IEEE Transactions on Communications Systems*, vol. 11, no. 4, pp. 360–393, Dec. 1963.
- [BRN08] I. Budiarjo, I. Rashad, and H. Nikookar, “On The Use of Virtual Pilots with Decision Directed Method in OFDM Based Cognitive Radio Channel Estimation Using 2x1-D Wiener Filter,” in *Proc. IEEE International Conference on Communications*, Beijing, China, May 2008, pp. 703–707.
- [CSLG00] A. Chevreuil, E. Serpedin, P. Loubaton, and G. Giannakis, “Blind Channel Identification and Equalization Using Periodic Modulation Precoders: Performance Analysis,” *IEEE Transactions on Signal Processing*, vol. 48, no. 6, pp. 1570–1586, Jun. 2000.
- [DeB04] I. DeBroeck, “Interleaved Frequency-Division Multiple Access: Systembeschreibung sowie Analyse und Optimierung des Übertragungsverhaltens im Mobilfunkkanal,” Ph.D. dissertation, Technische Universität Darmstadt, D17 Darmstädter Dissertationen, Jan. 2004.
- [DLF08] R. Dinis, C.-T. Lam, and D. Falconer, “Joint Frequency-Domain Equalization and Channel Estimation Using Superimposed Pilots,” in *Proc. IEEE Wireless Communications and Networking Conference*, Las Vegas, USA, Apr. 2008, pp. 447–452.
- [DMO09] M. Döttling, W. Mohr, and A. Osseiran, *Radio Technologies and Concepts for IMT-Advanced*, 1st ed. John Wiley & Sons, 2009.
- [FCS04] A. Filippi, E. Costa, and E. Schulz, “Low Complexity Interleaved Subcarrier Allocation in OFDM Multiple Access Systems,” in *Proc. IEEE Vehicular Technology Conference*, Los Angeles, California, USA, September 2004, pp. 1890–1893.
- [FK03] K. Fazel and S. Kaiser, *Multi-Carrier and Spread Spectrum Systems*, 1st ed. John Wiley & Sons Ltd, 2003.
- [FKCK06] T. Frank, A. Klein, E. Costa, and A. Kuehne, “Low Complexity and Power Efficient Space-Time-Frequency Coding for OFDMA,” in *Proc. IST Mobile & Wireless Communications Summit*, Mykonos, Greece, Jun. 2006.
- [FKCS04] T. Frank, A. Klein, E. Costa, and E. Schulz, “Robustness of IFDMA as Air Interface Candidate for Future Mobile Radio Systems,” in *Advances*

- in *Radio Science, Kleinheubacher Berichte 2004*, Miltenberg, Germany, Oct. 2004, pp. 261–270.
- [FKCS05a] ———, “IFDMA - A Promising Multiple Access Scheme for Future Mobile Radio Systems,” in *Proc. IEEE 16th International Symposium on Personal, Indoor and Mobile Radio Communications*, vol. 2, Berlin, Germany, Sept. 2005, pp. 1214–1218 Vol. 2.
- [FKCS05b] ———, “Low Complexity Equalization With and Without Decision Feedback and its Application to IFDMA,” in *IEEE 16th International Symposium on Personal, Indoor and Mobile Radio Communications*, vol. 2, Berlin, Germany, Sept. 2005, pp. 1219–1223.
- [FKH08] T. Frank, A. Klein, and T. Haustein, “A Survey on the Envelope Fluctuations of DFT Precoded OFDMA Signals,” in *Proc. IEEE International Conference on Communications*, Beijing, China, May 2008, pp. 3495–3500.
- [FS99] P. Frenger and A. Svensson, “Decision Directed Coherent Detection in Multicarrier Systems on Rayleigh Fading Channels,” *IEEE Transactions on Vehicular Technology*, vol. 48, no. 2, pp. 490–498, Mar. 1999.
- [GEPB06] M. García, O. Edfors, and J. Paez-Borrallo, “Peak Power Reduction for OFDM systems with Orthogonal Pilots Sequences,” *IEEE Transactions on Wireless Communications*, vol. 5, no. 1, pp. 47–51, Jan. 2006.
- [GG08] A. Guha and K. Giridhar, “Enhanced Channel Estimation and Tracking for Single Carrier Uplink Transmission Scheme,” in *Proc. of National Conference on Communications*, Mumbai, India, 2008.
- [GN07] F. Gao and A. Nallanathan, “Blind Channel Estimation for OFDM Systems via a Generalized Precoding,” *IEEE Transactions on Vehicular Technology*, vol. 56, no. 3, pp. 1155–1164, May 2007.
- [GRC<sup>+</sup>02] D. Galda, H. Rohling, E. Costa, H. Haas, and E. Schulz, “A Low Complexity Transmitter Structure for OFDM-FDMA Uplink Systems,” in *Proc. IEEE Vehicular Technology Conference*, Birmingham, United Kingdom, May 2002, pp. 1737–1741 vol.4.
- [GvL96] G. H. Golub and C. F. van Loan, *Matrix Computations*, 3rd ed. The John Hopkins University Press, 1996.
- [Hän01] E. Hänsler, *Statistische Signale*, 3rd ed., ser. Grundlagen und Anwendungen. Springer-Verlag, 2001.
- [Hay96] M. H. Hayes, *Statistical Digital Signal Processing and Modeling*, 1st ed. John Wiley & Son, Inc., 1996.
- [HFBC01] C. K. Ho, B. Farhang-Boroujeny, and F. Chin, “Added Pilot Semi-blind Channel Estimation Scheme for OFDM in Fading Channels,” in *Proc. IEEE Global Telecommunications Conference*, vol. 5, San Antonio, USA, Nov. 2001, pp. 3075–3079.

- [HG99] J. Heath, R.W. and G. Giannakis, "Exploiting Input Cyclostationarity for Blind Channel Identification in OFDM Systems," *IEEE Transactions on Signal Processing*, vol. 47, no. 3, pp. 848–856, Mar. 1999.
- [HKR97a] P. Hoeher, S. Kaiser, and P. Robertson, "Pilot-Symbol-Aided Channel Estimation in Time and Frequency," in *Proc. IEEE Global Telecommunications Conference*, Phoenix, USA, Nov. 1997.
- [HKR97b] —, "Two-Dimensional Pilot-Symbol-Aided Channel Estimation by Wiener Filtering," in *IEEE International Conference on Acoustics, Speech, and Signal Processing*, vol. 3, Munich, Germany, Apr. 1997, pp. 1845–1848 vol.3.
- [Hoe92] P. Hoeher, "A Statistical Discrete-Time Model for the WSSUS Multipath Channel," *IEEE Transactions on Vehicular Technology*, vol. 41, no. 4, pp. 461–468, Nov. 1992.
- [HP03] S. Hara and R. Prasad, *Multicarrier Techniques for 4G Mobile Communications*. Artech House, 2003.
- [HWG04] J. He, Z. Wu, and G. Gu, "Semiblind Tracking and Equalization of Time-varying Multipath Channels," in *Proc. IEEE Wireless Communications and Networking Conference*, vol. 4, Mar. 2004, pp. 2444–2449.
- [Kan05] G. Kang, "Time and Frequency Domain Joint Channel Estimation in Multi-Carrier Multi-Branch Systems," Ph.D. dissertation, Technische Universität Kaiserslautern, 2005.
- [Kay93] S. Kay, *Fundamentals of Statistical Signal Processing*, ser. Estimation Theory. New Jersey, USA: Prentice Hall PTR, 1993.
- [KB90] W. Koch and A. Baier, "Optimum and Sub-Optimum Detection of Coded Data Disturbed by Time-Varying Intersymbol Interference [Applicable to Digital Mobile Radio Receivers]," in *Proc. IEEE Global Telecommunications Conference*, Dec. 1990, pp. 1679–1684 vol.3.
- [KK98] K. D. Kammeyer and K. Kroschel, *Digitale Signalverarbeitung - Filterung und Spektralanalyse*, 4th ed. B.G. Teubner, Stuttgart, 1998.
- [LFDL07a] C.-T. Lam, D. Falconer, and F. Danilo-Lemoine, "A Low Complexity Frequency Domain Iterative Decision-Directed Channel Estimation Technique for Single-Carrier Systems," in *Proc. IEEE Vehicular Technology Conference*, Dublin, Ireland, Apr. 2007, pp. 1966–1970.
- [LFDL07b] —, "PAPR Reduction using Frequency Domain Multiplexed Pilot Sequences," in *Proc. IEEE Wireless Communications and Networking Conference*, Mar. 2007, pp. 1428–1432.
- [LFDL08] —, "Iterative Frequency Domain Channel Estimation for DFT-precoded OFDM Systems using in-band Pilots," *IEEE Journal on Selected Areas in Communications*, vol. 26, no. 2, pp. 348–358, Feb. 2008.

- [LFDLD06] C.-T. Lam, D. Falconer, F. Danilo-Lemoine, and R. Dinis, "Channel Estimation for SC-FDE Systems Using Frequency Domain Multiplexed Pilots," in *Proc. IEEE Vehicular Technology Conference*, Sept. 2006, pp. 1–5.
- [LIC] D.-H. Lee, S.-B. Im, and H.-J. Choi, in *Proc. Asia-Pacific Conference on Communications*.
- [LMG06] J. Lim, H. G. Myung, and D. J. Goodman, "Proportional Fair Scheduling of Uplink Single-Carrier FDMA Systems," in *Proc. 17th International Symposium on Personal, Indoor and Mobile Radio Communications*, Helsinki, Finland, September 2006.
- [LP05] R. Lin and A. Petropulu, "Linear Precoding Assisted Blind Channel Estimation for OFDM Systems," *IEEE Transactions on Vehicular Technology*, vol. 54, no. 3, pp. 983–995, May 2005.
- [LTAN08] W. Li, O. Takyu, K. Adachi, and M. Nakagawa, "Performance Evaluation of Decision Directed Channel Estimation for Single User IFDMA," in *Proc. IEEE Radio and Wireless Symposium*, Orlando, USA, Jan. 2008, pp. 659–662.
- [MdC99] B. Muquet and M. de Courville, "Blind and Semi-blind Channel Identification Methods Using Second Order Statistics for OFDM Systems," in *Proc. IEEE International Conference on Acoustics, Speech, and Signal Processing*, vol. 5, Phoenix, USA, Mar. 1999, pp. 2745–2748.
- [MdCD02] B. Muquet, M. de Courville, and P. Duhamel, "Subspace-Based Blind and Semi-Blind Channel Estimation for OFDM Systems," *IEEE Transactions on Signal Processing*, vol. 50, no. 7, pp. 1699–1712, Jul. 2002.
- [MdCDB99] B. Muquet, M. de Courville, P. Duhamel, and V. Buzenac, "A Subspace Based Blind and Semi-Blind Channel Identification Method for OFDM Systems," in *IEEE Workshop on Signal Processing Advances in Wireless Communications*, Annapolis, USA, May 1999, pp. 170–173.
- [MDCM95] E. Moulines, P. Duhamel, J.-F. Cardoso, and S. Mayrargue, "Subspace Methods for the Blind Identification of Multichannel FIR Filters," *IEEE Transactions on Signal Processing*, vol. 43, no. 2, pp. 516–525, Feb. 1995.
- [MG08] H. G. Myung and D. J. Goodman, *Single Carrier FDMA - A New Air Interface for Long Term Evolution*, 1st ed. John Wiley & Sons, Ltd., 2008.
- [MMF98] H. Meyr, M. Moeneclaey, and S. A. Fechtel, *Digital Communication Receivers: Synchronization, Channel Estimation and Signal Processing*. John Wiley & Sons, Inc., 1998.
- [Mol05] A. F. Molisch, *Wireless Communications*, 1st ed. John Wiley & Sons, Ltd, 2005.

- [Pae02] M. Paetzold, *Mobile Fading Channels*, 1st ed. John Wiley & Sons, Ltd, 2002.
- [Pap84] A. Papoulis, *Probability, Random Variables, and Stochastic Processes*, 2nd ed., ser. 2. McGraw-Hill, Inc., 1984.
- [Pop92] B. M. Popovic, "Generalized Chirp-like Polyphase Sequences with Optimal Correlation Properties," *IEEE Transactions on Information Theory*, vol. 38, pp. 1406–1409, Jul. 1992.
- [Pro01] J. Proakis, *Digital Communications*, 4th ed. McGraw-Hill Book Company, New York, 2001.
- [Rap02] T. S. Rappaport, *Wireless Communications - Principles and Practice*, 2nd ed. Upper Saddle River, NJ: Prentice Hall PTR, 2002.
- [RGR<sup>+</sup>03] J. Ran, R. Grunheid, H. Rohling, E. Bolin, and R. Kern, "Decision-Directed Channel Estimation Method for OFDM Systems with High Velocities," in *Proc. IEEE Vehicular Technology Conference*, vol. 4, Jeju, Korea, Apr. 2003, pp. 2358 – 2361.
- [RVH95] P. Robertson, E. Villebrun, and P. Hoeher, "A Comparison of Optimal and Sub-Optimal MAP Decoding Algorithms Operating in the Log Domain," in *Proc. IEEE International Conference on Communications*, vol. 2, Seattle, USA, Jun. 1995, pp. 1009 –1013 vol.2.
- [San03] F. Sanzi, "Kanalschätzverfahren für Mobilfunksysteme mit Mehrträgermodulation OFDM," Ph.D. dissertation, Institut für Nachrichtenübertragung, University of Stuttgart, Feb. 2003.
- [SDB98] M. Schnell and I. De Broeck, "Application of IFDMA to Mobile Radio Transmission," in *Proc. IEEE International Conference on Universal Personal Communications*, vol. 2, Florence, Italy, Oct. 1998, pp. 1267 –1272.
- [SDBS98] U. Sorger, I. De Broeck, and M. Schnell, "IFDMA - A New Spread-Spectrum Multiple-Access Scheme," in *Proc. of International Conference on Communications*, Atlanta, Georgia, USA, Jun. 1998, pp. 1013–1017.
- [SE96] M. Sandell and O. Edfors, "A Comparative Study of Pilot-Based Channel Estimation for Wireless OFDM," Division of Signal Processing, Luleå University of Technology, Tech. Rep. Research Report TULEA 1996:19, Sep. 1996.
- [SFE<sup>+</sup>09] T. Svensson, T. Frank, T. Eriksson, D. Aronsson, M. Sternad, and A. Klein, "Block Interleaved Frequency Division Multiple Access for Power Efficiency, Robustness, Flexibility and Scalability," *EURASIP Journal on Wireless Communications and Networks*, vol. Volume 2009, no. Article ID 720973, 2009.

- [SFF<sup>+</sup>07] T. Svensson, T. Frank, D. Falconer, M. Sternad, E. Costa, and A. Klein, "B-IFDMA - A Power Efficient Multiple Access Scheme for Non-Frequency-Adaptive Transmission," in *Proc. 16th IST Mobile and Wireless Communications Summit*, Budapest, Hungary, July 2007, pp. 1–5.
- [SFK06] A. Sohl, T. Frank, and A. Klein, "Channel Estimation for DFT Precoded OFDMA with Blockwise and Interleaved Subcarrier Allocation," in *Proc. International OFDM Workshop*, Hamburg, Germany, 2006.
- [SFK07] —, "Channel Estimation for Block-IFDMA," in *Proc. International Multi-Carrier Spread Spectrum Workshop*, Herrsching, Germany, May 2007, pp. 347–356.
- [SG98] E. Serpedin and G. Giannakis, "Blind Channel Identification and Equalization with Modulation-induced Cyclostationarity," *IEEE Transactions on Signal Processing*, vol. 46, no. 7, pp. 1930–1944, Jul. 1998.
- [Sil08] Y. C. B. Silva, "Adaptive Beamforming and Power Allocation in Multi-Carrier Multicast Wireless Networks," Ph.D. dissertation, Technische Universität Darmstadt, Mar. 2008.
- [SK07] A. Sohl and A. Klein, "Comparison of Localized, Interleaved and Block-Interleaved FDMA in Terms of Pilot Multiplexing and Channel Estimation," in *Proc. 15th European Signal Processing Conference*, Poznan, Poland, Sept. 2007.
- [SK08] —, "Blind Channel Estimation Based on Second Order Statistics for IFDMA," in *Proc. 19th International Symposium on Personal, Indoor and Mobile Radio Communications*, Cannes, France, Sept. 2008.
- [SK09a] —, "Block-IFDMA – Iterative Channel Estimation versus Estimation with Interpolation Filters," in *Proc. International Multi-Carrier Systems & Solutions Workshop*, Herrsching, Germany, May 2009, pp. 123–132.
- [SK09b] —, "Channel Estimation for IFDMA - Comparison of Semiblind Channel Estimation Approaches and Estimation with Interpolation Filtering," in *Proc. 20th International Symposium on Personal, Indoor and Mobile Radio Communications*, Tokyo, Japan, 2009, pp. 441 – 445.
- [SK10] —, "Comparison of Different Channel Estimation Approaches for Block-IFDMA," *European Transactions on Telecommunications*, no. 5, 2010.
- [SKJ94] H. Sari, G. Karam, and I. Jeanclaude, "Frequency-Domain Equalization of Mobile Radio and Terrestrial Broadcast Channels," in *Proc. IEEE Global Telecommunications Conference*, San Francisco, USA, Nov./Dec. 1994, pp. 1–5 vol.1.
- [SL05] H. Schulze and C. Lüders, *Theory and Application of OFDM and CDMA*, 1st ed. John Wiley & Sons Ltd, 2005.



- [SV07a] B. Su and P. Vaidyanathan, "A Semi-Blind Pilot-Assisted Channel Estimation Algorithm in OFDM Systems," in *Proc. Asilomar Conference on Signals, Systems and Computers*, Pacific Grove, USA, Nov. 2007, pp. 1763–1767.
- [SV07b] —, "Subspace-Based Blind Channel Identification for Cyclic Prefix Systems Using Few Received Blocks," *IEEE Transactions on Signal Processing*, vol. 55, no. 10, pp. 4979–4993, Oct. 2007.
- [TG97] M. K. Tsatsanis and G. B. Giannakis, "Transmitter Induced Cyclostationarity for Blind Channel Equalization," *IEEE Trans. on Signal Processing*, vol. 45, no. 7, pp. 1785–1794, Jul. 1997.
- [TM97] F. Tufvesson and T. Maseng, "Pilot Assisted Channel Estimation for OFDM in Mobile Cellular Systems," in *Proc. IEEE Vehicular Technology Conference*, Phoenix, USA, May 1997, pp. 1639–1643.
- [TXK94] L. Tong, G. Xu, and T. Kailath, "Blind Identification and Equalization Based on Second Order Statistics: A Time Domain Approach," *IEEE Trans. on Information Theory*, vol. 40, no. 2, pp. 340–349, March 1994.
- [TYU09] O. Takyu, T. Yamasaki, and Y. Umeda, "Scattered pilot assisted channel estimation for IFDMA," in *Proc. International Conference on Wireless Communication, Vehicular Technology, Information Theory and Aerospace Electronic Systems Technology*, Aalborg, Denmark, May 2009, pp. 832–836.
- [vdBES<sup>+</sup>95] J. J. van de Beek, O. Edfors, M. Sandell, S. K. Wilson, and P. O. Björjesson, "On Channel Estimation in OFDM Systems," in *Proc. IEEE International Vehicular Technology Conference*, Rosemont, USA, Jul. 1995, pp. 715–719.
- [vNP00] R. van Nee and R. Prasad, *OFDM for Wireless Multimedia Communications*, 1st ed. Artech House, 2000.
- [WG00] Z. Wang and G. Giannakis, "Wireless Multicarrier Communications," *IEEE Signal Processing Magazine*, vol. 17, no. 3, pp. 29–48, May 2000.
- [WINDf] WINNER, "Final Report on Identified RI Key Technologies, System Concept, and their Assessment," Tech. Rep. D2.10 v. 1.0, Dec. 2005, viewed 14.04.2010, [www.ist-winner.org/deliverables/D2.10.pdf](http://www.ist-winner.org/deliverables/D2.10.pdf).
- [WINDf] WINNERII, "The WINNER II Air Interface: Refined Multiple Access Concepts," IST-4-027756, Tech. Rep. D4.6.1, Nov. 2006, viewed 09.02.2010, [www.ist-winner.org/deliverables/D4.6.1.pdf](http://www.ist-winner.org/deliverables/D4.6.1.pdf).
- [WINDf] —, "WINNER II Channel Models, Part I Channel Models," Tech. Rep. D1.1.2, v1.2, February 2008, viewed 09.02.2010, [www.ist-winner.org/deliverables/D1.1.2.pdf](http://www.ist-winner.org/deliverables/D1.1.2.pdf).

- [XZG03] P. Xia, S. Zhou, and G. Giannakis, “Bandwidth- and Power-Efficient Multicarrier Multiple Access,” *IEEE Transactions on Communications*, vol. 51, pp. 1828–1837, Nov. 2003.

# Lebenslauf

Name: Anja Sohl  
Anschrift: Heidelbergerstraße 38  
64285 Darmstadt  
Geburtsdatum: 28. November 1979  
Geburtsort: Limburg an der Lahn  
Familienstand: ledig

## Schulausbildung

1986-1990 Grundschole MPS Goldener Grund  
in Selters Taunus  
1990-1999 Gymnasium Marienschule  
in Limburg an der Lahn

## Studium

10/1999-2001 Studium der Elektrotechnik an der  
Technischen Universität Darmstadt,  
Studienabschluss: Vordiplom  
2001-04/2005 Studium der Elektrotechnik an der  
Technischen Universität Darmstadt,  
Studienabschluss: Diplom

## Berufstätigkeit

seit Mai 2005 wissenschaftliche Mitarbeiterin am  
Fachgebiet Kommunikationstechnik,  
Institut für Nachrichtentechnik,  
Technische Universität Darmstadt

Darmstadt, den 25. Mai 2010



## Erklärung laut §9 der Promotionsordnung

Ich versichere hiermit, dass ich die vorliegende Dissertation allein und nur unter Verwendung der angegebenen Literatur verfasst habe. Die Arbeit hat bisher noch nicht zu Prüfungszwecken gedient.

Darmstadt, 25. Mai 2010,

